Final Review

TU Delft AI Satellite

AE3200: Design Synthesis Exercise

DSE 01

Delft University of Technology

TU Delft

Final Review

TU Delft AI Satellite

by

DSE 01

Student Name	Student Number
Canosa Ybarra, David	4839277
Janisch, Katharina-Inés	4658035
Kalis, Nicolas	4537130
Lentschig, Dennis	4658116
Lopez Rivera, Antonio	4877985
Manieri, Matteo	4565207
Regnery, Kim	4644239
van der Wal, Tinka	4868803

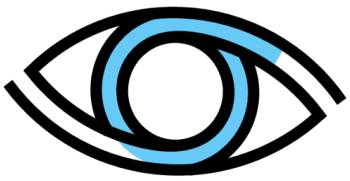

SigmaSat

Instructor:	Ir. Melkert, Joris
Tutor:	Dr. Menicucci, Alessandra
Coaches:	González Saiz, Gabriel
	Yüksel, Onur
Teaching Assistant:	Mottinelli, Lorenza
Institution:	Delft University of Technology
Place:	Faculty of Aerospace Engineering, Delft
Project Duration:	November, 2021 - January, 2022

TU Delft

Contents

Nomenclature

Abbreviations

Abbreviation	Definition
AI	Artificial Intelligence
ADCS	Attitude Determination and Control System
ALU	Arithmetic logic unit
BCR	Battery Conditioning Unit
BER	Bit Error Rate
CDHS	Command and Data Handling System
CH4	Methane
COMMS	Communications System
CO2	Carbon Dioxide
COTS	Commercial Off the Shelf
CPU	Central Processing Unit
CU	Control Unit
DOT	Design Option Tree
EbN0	Energy per Bit to Noise Power Spectral Density Ratio
ELSSI	Elaborate Life-cycle Space Sustainability Indicator
EM	Electro-Magnetic
EMR	Electromagnetic Radiation
EO/RS	Earth observation and Remote Sensing
EO	Earth observation
EOL	End of Life
EPS	Electrical Power System
ERSS	Earth-Repeat Sun-Synchronous
ESA	European Space Agency
fov	Field of view
FBS	Functional Breakdown Structure
FFD	Functional Flow Diagram
GC	Ground Control
GCS	Ground Control Segment
GMAT	General Mission Analysis Tool
GMSK	Gaussian Minimum Shift Keying
GS	Ground Segment
GSaaS	Ground Segment as a Service
HPGP	High Power Green Propellant
H2O	Water
HKD	House Keeping Data
ISA	International Standard Atmosphere
LEO	Low Earth Orbit
MNS	Mission Need Statement
MOC	Missions Operation Center
MPC	Model Predictive Controllers
OBC	On Board Computer
OS	Operating System
OTS	Off-the-shelf Component
PCM	Power Conditioning Module

Abbreviation	Definition
PDU	Power Distribution Circuit
POS	Project Objective Statement
PROP	Propulsion System
QPSK	Quadrature Phase Shift Keying
RF	Radio Frequency
RGB	Red Green Blue
RTC	Real-Time Clock
ROM	Read Only Memory
SC	Space Craft
SEE	Single Event Error
SEL	Single Event Latchup
SEU	Single Event Upset
TB	Thermal Budget
tbd	to be determined
TML	Total Mass Loss
TRL	Technology Readiness Level
TT&C	Telemetry, Tracking and Control
TO	Topology Optimization
UHF	Ultra High Frequency
VLEO	Very Low Earth Orbit
VHF	Very High Frequency
WFD	Work Flow Diagram

Symbols

Symbol	Definition	Unit
a	Semi-major axis	[km]
A	Area	[m^2]
a_{alb}	mean albedo effect	[-]
A_{alb}	Area accounting for the albedo effect	[m^2]
A_{IR}	Area accounting for the Earth's irradiation	[m^2]
a_{rev}	Orbital height per revolution	[km]
A_{sun}	Projected area towards the sun	[m^2]
A_{total}	Total Satellite Area	[m^2]
C_D	Drag coefficient	[-]
$Data_{useful}$	Useful data	[bits]
e	eccentricity	[-]
E	Elastic modulus	[Pa]
$\bar{e_\alpha}$	Median pointing accuracy	[arcsec]
$\bar{e_{loc}}$	Median positioning error	[m]
f_E	Eclipse Fraction	
$f_{nat\ lat}$	Natural frequency latitudinal	[Hz]
$f_{nat\ long}$	Natural frequency longitudinal	[Hz]
F	Visibility factor	[-]
F_D	Force of Drag	[N]
h	Orbit height	[km]
$\bar{H}_{cap}$	Median momentum storage capacity	[Nms]
I_{sp}	Specific Impluse	[s]

Symbol	Definition	Unit
I	Second moment of area	[m^4]
j	Number of orbits	[-]
J	Total Impulse	[Ns]
J_a	Intensity of the albedo radiation	[W/m^2]
J_p	Intensity of Earth's radiation	[W/m^2]
J_s	Solar irradiance	[W/m^2]
J_2	Gravity Field Coefficient	[-]
k	Number of days	[-]
L	Length	[m]
m	Mass	[kg]
$\bar{m}$	Median mass	[kg]
m_B	Mass of beam	[kg]
m_p	Mass of propellant	[kg]
N_{bits}	Number of bits	[-]
N_{pixels}	Number of pixels	[-]
$N_{spectralbands}$	Number of spectral bands	[-]
$N_{totalbands}$	Total number of spectral bands	[-]
$N_{totalbits}$	Number of bits in total	[-]
$N_{usefulbands}$	Number of useful spectral bands	[-]
P	Orbital Period	[min]
P_E	Earth rotational period	[s]
P_{ES}	Earth rotational period around sun	[s]
P_0	Critical Buckling Load	[N]
$\bar{P}$	Median power consumption	[W]
$\bar{P}_{peak}$	Median peak power consumption	[W]
$\dot{Q}_{env}$	Power due to the space environment	[W]
$\dot{Q}_{int}$	Internal power dissipation	[W]
$\dot{Q}_{out}$	Total infrared power dissipation of the satellite	[W]
R_{orbit}	Radius of Orbit	[m]
R_E	Radius of Earth	[km]
$t_{imaging}$	imaging time	[s]
T	Thrust	[N]
T_m	Mission Life-time	[s]
$\bar{T}_{peak}$	Median peak torque	[Nm]
$t_{processing}$	Processing time	[s]
$t_{startup}$	Startup time	[s]
V	Velocity	[m/s]
$\bar{V}$	Median volume	[m^3]
$W_{refinery}$	Width of refinery	[km]
$W_{imaging}$	Imaging power	[W]
$W_{processing}$	Processing power	[W]
$W_{readout}$	Readout power	[W]
$W_{startup}$	Startup power	[W]
YD	Yearly Degradation of Solar Cell	[-]
YM	Mission Duration	[years]
y	Distance from neutral axis	[m]
α	Solar absorptance	[-]
β	angle between the orbit plane and the incoming vector from the sun	[°]

Symbol	Definition	Unit
Δ	Change	[-]
Δ_{eq}	Equatorial spacing	[km]
ε	Infrared emittance	[-]
η	Efficiency	[-]
μ	Gravitational parameter	[km^{3}s]
$\bar{\mu}_{peak}$	Median peak dipole	[Am^2]
ρ	Density	[kg/m^3]
σ	Stefan-Boltzmann constant	[W/m^2K^4]
σ_y	Yield stress	[Pa]
Ω	Longitude of the ascending node	[deg]
☢$_{tol}$	Total Ionizing dose	[krad]

1 Executive Overview

Solutions for reducing greenhouse gas emissions are paramount under the current environmental circumstances. With methane and carbon dioxide being the most critical emission gasses, SigmaSat set out to find a way to reduce these emissions and simultaneously fulfill its scientific mission. While executing the scientific mission of designing a small satellite mission to demonstrate the latest advances in artificial intelligence, SigmaSat managed to devise a design that allows players in the energy production industry (such as refineries) to drastically reduce their methane and CO2 emissions.

The scientific mission of this DSE is demonstrating the abilities of AI in space, which translates to the following mission statement: ”To demonstrate the latest advances in AI with an Earth Observation (EO) CubeSat mission”. The SigmaSat team has been given 10 weeks to complete the design which is presented in this report. The project objective statement is: ”Develop a design for an Earth Observation CubeSat mission to demonstrate applications of AI in space within a budget of 5 Million Euros, by 8 students in 10 weeks time”. Through these mission and project object statements and the top level requirements set by the costumer, the SigmaSat team has designed a CubeSat

As a result of an initial market analysis, a better understanding of the requirements set by the market was achieved. From the satellite mission market analysis, it was determined that the EO/RS (Earth Observation and Remote Sensing) is a very lucrative market with a numerous players. Additionally, CubeSats and nanosatellites are extremely popular and are gaining popularity due to their ease of engineering and low initial investment. In other words, the first three segments this mission falls in have positive market trends and are very popular. This poses the problem of competition. Being a singular stand alone CubeSat, it requires either a very specific tailored mission to allow the satellite to be competitive in the market, or, an application of on-board AI, which sets it apart from the competition. The last segment the mission falls in is in fact also the most niché segment. There are only a hand full of satellites with on-board AI. It is important to distinguish on-board AI from AI applied to gathered data. As removing on-board usage of AI from the mission broadens the market in such a way that remaining competitive will be a very challenging task. Adding on to everything the fact that AI is the next considerable advancement in the space industry, and that it will allow companies to cut costs, adds to the importance and viability of the mission. Summing up, being able to combine the most lucrative and popular markets with a cutting edge, extremely innovative and vital new piece of technology will allow this mission to over cut the competition and set a new standard.

When considering the payload mission it was determined the mission will focus on carbon dioxide and methane fugitive emissions. It will focus on fugitive emissions with material impact created by the energy production industry through the production of oil (eg. refineries and oil wells). Besides the possible reduction of losses due to the fugitive emissions, there is also a great push from governments to reduce emissions and therefore the payload mission has potential to be quite lucrative. Especially if the mission can achieve rapid response times, allowing customers to greatly reduce their response time in cases of very big leaks. When considering the competition, the biggest threat comes from other satellites with similar missions, such as GHGSat and Sentinell-5P. Ensuring SigmaSat’s accuracy is greater than that of GHGSat and Sentinell-5P makes the mission stand out from the competition. Ensuring a reduced budget enables SigmaSat to compete with alternatives such as usage of drones and Long-Range Laser Networks.

Operational modes for the satellite have been established to cover all possible tasks the satellite performs. The satellite has 5 operational modes, where the main one is the nominal mode. Within the nominal mode there are a variety of tasks that the satellite will perform. These tasks have been presented in an orbital diagram. Transition conditions have also been developed for autonomous state transition. To increase the level of autonomy for the safe mode transition, a transition protocol has been developed. Using the operational modes, the lowest satellite target has been determined.

The satellite payload is based on the Chameleon camera to obtain hyperspectral data. This data will be preprocessed in order to reduce the noise. After this step clouded scenes will be filtered and the data is ready for the AI that will recognise methane and carbon dioxide leaks. For this the Myriad 2 chip will be used as processor allowing for a quick and low power consuming processing. The use of AI on board combined with

the payload processor allow for a quick response mission with smaller amounts of downlink data. Without the AI this would not have been possible.

The satellite will fly in an Earth-repeat and Sun-synchronous, Very Low Earth Orbit (VLEO). The $\triangle V$ was calculated for the orbital maintenance and given to the propulsion department. The satellite will de-orbit naturally if propulsion runs out as End-of-Life (EOL) maneuver. RAAN optimisation would be the next step in the orbit determination.

The main outputs from the ground segment analysis are the communication medium, ground segment provider, ground stations locations, customer data streams and overall ground segment cost. For this mission radio frequencies were chosen as communications medium. It was decided to make use of a ground segment provider to allow access to ground stations all over Earth at a fraction of the cost of building and manning a ground station. The chosen ground segment provider is KSAT, while using their ground stations in Troll and Svalbard. The creation of a fugitive emissions database and platform have been explored to overcome complications present today in costumer data streams. Additionally, a possible revenue model has been discussed for the proposed database and platform. The overall costs of the ground segment provider will be in the range of €13,025 to €43,417.

While a propulsion system was initially deemed not necessary, a new orbit configuration brought it back. The propulsion system had to be electric since it has to constantly provide thrust to compensate for drag. The Enpulsion NANO propulsion system was selected after a trade-off as it can compensate for drag and is the most efficient for the mission. A HPGP propulsion solution was deemed infeasible and ”less green” since the thrust of this propulsion system is too high and it uses almost 24 times as much propellant.

The communications on the satellite are separated into two systems, one for TT&C (tracking, telemetry, and control) in UHF and one for the payload data in S-Band. This is because UHF antennas are omni-directional and highly reliable, in combination with reduced data downlink requirements from TT&C, it makes it the best solution for telemetry data. S-Band was chosen for the data downlink as a higher data rate was required. Having decided the communication streams and frequency bands the link budgets for both communication systems have been determined. Using the ground stations determined in the ground segment section, a very high and stable communication link can be established. The main reasons for this are the excellent ground station gain and size.

For the selection of the On-board Computer (OBC) over 20 possible OBCs were compared and 5 potential candidates were selected based on applicability of AI algorithms on the subsystem. From here, a more in depth analysis has been performed with the help of experts. The Antelope by KP Labs was found to be the best choice, and together with the additional services provided by KP labs and the payload processor from Ubotica, a CDHS integrated setup has been created. The six different implementations for AI on the CDH system, namely FDIR, predictive maintenance, telemetry correlation, autonomous re-targeting, planning and picture processing have been analysed and elaborated upon. Through a more in-depth analysis of the compatible electrical interfaces a block diagram has been created that shows the connections between all subsystems of the satellite.

After determining a sensor and actuator suit, the approach for ADCS was taken to search first for integrated ADCS units, and only if one could not be found to suit the needs of the satellite, purchase and integrate separate components. A search of the CubeSat integrated ADCS unit market followed. 12 units were traded off on the grounds of four overarching criteria: precision and reliability, volume and mass, power and data interface, and cost. After conducting a sensitivity analysis, the Hyperion Technologies iADCS400-50 was chosen, with attitude determination and control accuracies of 30 and 360 arcseconds respectively and high specific maximum torque and momentum storage capacity. Its lack of an integrated ADCS receiver prompted a similar search and trade-off, resulting in the choice for the Hyperion Technologies GNSS200 GPS receiver and the ISISPACE ISIS-GAPA-DSH-0001 antenna. Integration of the GPS receiver and antenna into the iADCS400-50 was discussed with a Hyperion Technologies representatives and positively assessed. The choice for an integrated ADCS unit, and for the integration of the GPS receiver and antenna in it offloads significant design, integration and testing effort to a company with extensive expertise and facilities, increasing the reliability of the final assembly and reducing engineering and logistics costs for the mission. Target acquisition algorithm was discussed afterwards. Thanks to the on-board controller of the iADCS400-50 and the target acquisition algorithm, SigmaSat is capable of independently identifying, planning and executing all possible target acquisition manoeuvres, in each and every orbit, enabling it to fulfill its Earth observation mission.

Using the established modes of operation and determining the busiest orbit, the power required during the eclipse and the sunlit period could be determined. Using this, the solar panels could be sized using the time spent in the sun, and the battery size using the time spent in the eclipse. Because the satellite operates in

a Sun-synchronous orbit, it can use one degree of freedom on the solar panels to enable maximum power generation throughout the charge cycle. The required solar array size is 8x2U, or 4x2U on both sides. Due to the high solar power input, large batteries are needed, which have more capacity than required.

The structure of a CubeSat is a fundamental part of the spacecraft and requires extensive amount of time to design fully due to the fact is that a conventional Off-the-shelf (OTS) solution would not be possible considering the fundamentally different design of the satellite. One of the aspects that makes this satellite so different to others in its class is the abnormally high power requirement, resulting in an 8U CubeSat structure. From the final CAD of the spacecraft it was found that there is a 2U column in the structure that is empty, although this is not necessarily a drawback it does mean that the spacecraft could be changed into a 6U satellite or more components could be added to improve the mission.

The design of the thermal control system comprises of 2 main analyses: a single and multi-node thermal model. Due to the stringent power budget, all active systems were disregarded for the detailed design. Within the passive systems, the focal point was directed to surface finishes and coatings. With a thermal model developed in ESATAN, a software package to predict temperature and heat flows, several radiative cases were analysed. However, due to time constraint and licensing issues, the boundary conditions stemming from the power dissipation of the subsystems were unable to be included in the analyses. Instead a smaller evaluation of the highest resulting temperature from the component's' dissipating heat was performed yielding the necessity for insulation. From this, a black epoxy paint was chosen for the side panels of the satellite while a trade-off on different OTS MLI options was executed. For future work, the inclusion of the components in the ESATAN thermal case is important while applying the chosen clean MLI by RUAG.

From the start of the design phase, it was vital for SigmaSat to ensure this mission is as sustainable as possible. Especially today, creating sustainable products is as important as ever. Sustainability is a very difficult concept to judge quantitatively, however to properly analyse the level of sustainability of a mission, a quantitative approach is required. To quantitatively analyse sustainability, SigmaSat made use of the ELSSI. The ELSSI is an easy to use indicator that determines the level of sustainability in a satellite mission. The ELSSI indicator was developed in corporation with experts in the field. SigmaSat has made use of this indicator throughout the design phase, ensuring a sustainability immersion throughout the design. Incorporating ELSSI also allowed sustainability evaluations throughout the process of the design rather than at the end when making changes is more difficult. At the end of the design phase, the satellite was once again subjected to the ELSII and given a final score. This score is 4.05 out of 5, which is a very good result and ensures that SigmaSat can call its mission sustainable.

Overall the mission is projected to cost from €2,766,000 to €3,224,000. Where the materials and parts costs add up to roughly €1,130,000 and the man-hours add up to roughly €1,682,000. The projected total mission cost is far below the requirement of €5 million, and therefore allows room for unexpected costs. Especially at this stage of the design the accuracy of the cost breakdown is not high. There are still a lot of uncertainties when it comes to man-hour calculations and unexpected costs that fall within the MISC category. It should be noted that any possible income is not mentioned in this section and report. Post-DSE project planning has been evaluated and presented in the report including a risk analysis.

It is the combination of innovative, never before flown AI applications that enable SigmaSat to call itself the smartest in the class. As a result of the before mentioned groundbreaking innovations, the space industry is one step closer to Space 4.0. The above-mentioned technological innovations and decisions lead to a sustainable, 8U, LEO, emission monitoring CubeSat. The result of this design is a class-smartest, competition outperforming, budget-friendly emission detection solution, with potential to revolutionize the emission leak detection industry and help save the planet.

2 Introduction

The following chapters will outline the steps taken to develop a final Design for SigmaSat. The SigmaSat is an Earth observation CubeSat making use of a hyperspectral camera. A market analysis follows, which outlines the needs for these types of CubeSats and explores the market to determine similar payload missions. Following the market analysis, a functional analysis is given. The functional analysis outlines the tasks that SigmaSat has to perform when in orbit. This gives an overview of the requirements for each subsystem. After the functional analysis, an overview of the operational modes is gives an impression of the actions that the satellite has to take during the course of the mission. This includes an explanation of the sequence of events that occur during the mission where the satellite is imaging, processing, and transmitting the payload data.

Following explanations regarding the general satellite functionality, the satellite's subsystems are addressed. Chapters 6 to 15 discuss the design process for each subsystem, trade-offs, design choices and an evaluation of the feasibility. The order is as follows: Chapter 6 Payload, Chapter 7 Astrodynamics, Chapter 8 Ground Segment, Chapter 9 Propulsion, Chapter 10 Communications, Chapter 11 Command and Data Handling, Chapter 7 Attitude Determination and Control, Chapter 13 Electrical Power System, Chapter 14 Structures, and Chapter 15 Thermal Control. Following this, Chapter 16 talks about verification and validation which summarizes the steps taken to verify and validate the methods used during the design phase.

Lastly, the report discusses the sustainability of the project and uses the previously established ELSSI method to assess the sustainability of the project. This is followed by the risk assessment and the risk map overview of the project as well as a cost analysis of the project until launch. Indications for the necessary phases to complete the project until launch are also given.

3 Market Analysis

Two market analyses have been performed. The first investigates the need for an Earth observation CubeSat, while the second explores the market with respect to the satellites payload mission. This chapter is based on the market analyses performed in (Canosa et al., 2021a) and (Canosa et al., 2021b)

3.1. Satellite Mission Market Analysis

The Mission Needs Statement (MNS) and Project Objective Statement (POS) define the mission from a top level perspective and decide the market segments this mission will be in. first of all, it is important to analyse the mission from a market segment point of view and create a market definition. The mission can be divided in the following segments:

- Low Earth Orbit Satellite
- Earth Observation Satellite
- CubeSat (Nanosatellite)
- Satellite with (on-board) Artificial Intelligence capabilities

The market analysis will be conducted looking at these market segments individually, but also as combination.

3.1.1. Market Size

As of the 30th of March 2021, the number of active and defunct LEO satellites circling the earth has increased to 5000, which is a 50% increase from the amount two years prior (Boley & Byers, 2021) Over the period of 2015 to 2019 there have been 875 nanosatellite (1-10kg) launches (Spaceworks, 2020) Of these launches, 51% was related to Earth Observation and Remote Sensing, which is the biggest proportion compared to other purposes. Technology (29%), scientific (12%), Communications (7%) and Novel missions (1%), make up the rest of the missions. While Earth Observation and Remote Sensing represents a large part of the nanosatellite's missions, EO/RS by nanosatellites only represents a small proportion of all of the EO/RS missions.

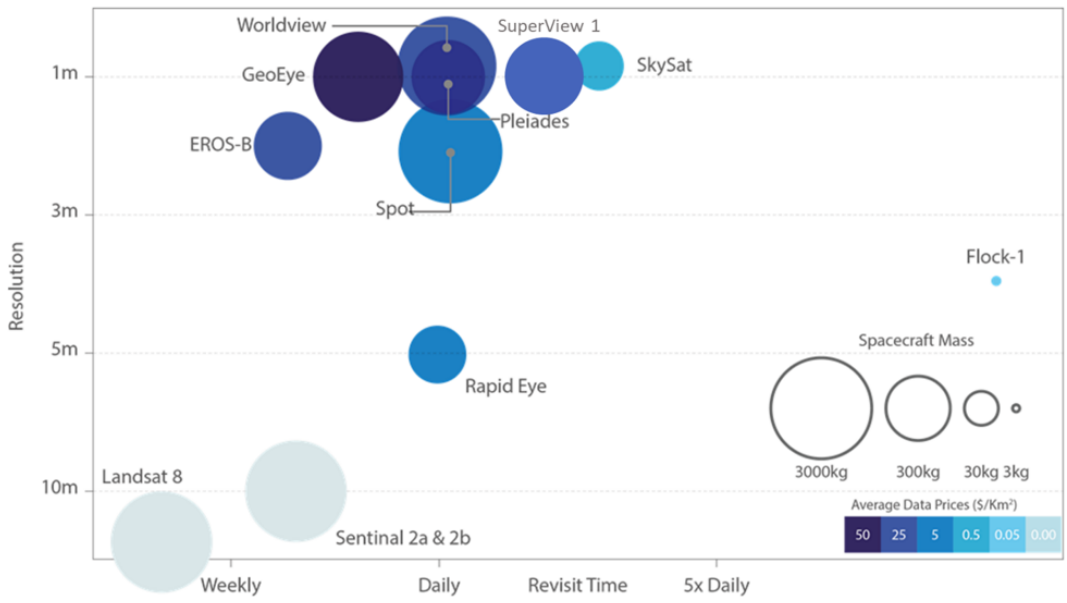

Figure 3.1: Earth Observation Satellites Fleet

When looking at Figure Figure 3.1 (ESA, 2020), one can clearly see that the only nanosatellite mission mentioned within their fleet is the Flock-1. From the figure it is also very visible that the Flock-1 mission is in a

league of its own, this is mainly due to the high revisit time, but also due to the high resolution to cost ratio. It should be noted however that this chart does not indicate quantity of missions or customer usage. If one looks outside of ESA and to smaller companies and educational institutions, one quickly notices that the opposite is true. While for big agencies like ESA, nanosatellites only play a small role within their entire EO/RS fleet, for smaller companies nanosatellites are the way to go due to their small initial investment and their ability (due to the small investment) to focus on very specific missions. Pair this with being able to have a complete constellation for a fraction of the cost of constellations such as GPS and Galileo, and private companies can and will insert themselves within the space industry.

3.1.2. Market Dynamics

For the period 2020-2024 an expected 1900 Nanosatellites will be launched of which 45% are expected to be in the Earth Observation/Remote Sensing segment (Spaceworks, 2020). While the percentage of EO/RS will be in decline from 51% to 45%, the absolute number of EO/RS nanosatellites will go up. This trend is also shared outside the field of nanosatellites. The Earth observation data sale market has been steadily growing since 2015 and is projected to continue growing (Intelligence, 2020).

The same is to be said about satellites in a LEO orbit. As mentioned before the amount of satellites in LEO orbit has increased to 5000, and if large constellations such as Starlink will be successful this number will rise at an incredible pace (Starlink alone is projected to add 11 000 satellites in LEO orbit) (Boley & Byers, 2021). This does have a cost attached to it, which is the cluttering of the orbit. As the amount of satellites increases, efforts to avoid said satellites or obtain a desired path not yet taken by another satellite increase. This might in the future lead to extra regulations regarding the use of LEO orbits.

While AI has made leaps forwards on Earth, in the space industry the usage of AI has been limited and slow. Most AI usages in regard to space missions have been regarding on-Earth processing of “space data”. This is not to say that it is not needed. Gianluca Furano, an on-board computer and AI expert working for ESA, once said: “We desperately need AI in space” (Hamilton, 2020) indicating that AI used on-board a satellite is the next big thing and is necessary to advance satellite technology to the next level. His quote also shows how important a demonstrator CubeSat is to advance this industry. Adding on to this, while (especially private) companies and agencies have an everlasting goal of cutting costs wherever they can, they are desperately looking for ways to do so in one of the most expensive industries. If AI is able to cut personnel, communication or any other type of cost, it allows the industry to take a step forward.

Up until now, the application of AI on-board has been slow, this is mainly due to the conservative nature of the space industry. The conservativeness with regards to AI implementation mainly comes from high risks involved with applying new cutting-edge technologies and difficulties with radiation and processors in space. This is also apparent when looking at processor speeds used in satellites today (without AI). As seen in Figure 3.2 (Arechiga et al., 2018) processor speeds are lacking greatly, but steadily improving at the same linear rate as on-Earth.

3.1.3. Competition

A CubeSat on a LEO orbit that is used for Earth Observation with the use of AI is a niche market. However, besides the AI every other sub-segment is not a niche market. Instead, they are over-saturated markets with a lot of competition.

With regards to Earth observation, there are not many missions that incorporate on-board AI. Most of the Earth Observation missions make us of AI by analyzing the gathered data on Earth using AI. In general, successful Earth observation missions have a higher level of investment and high masses. This allows the creators to design and launch more complex and advanced systems. A nanosatellite is quite opposite in the sense that initial investment is low, amount of investors that you have to please are low and the mass is low. This allows nanosatellites to innovate more radically than the successful larger missions. The catch being: nanosatellites have to be more innovative and unique by design, otherwise they do not stand a chance in the market compared to the more sophisticated, more expensive, larger missions. Combing Earth observation with on-board AI ensures innovation and uniqueness, allowing the nanosatellite or CubeSat to compete with larger Earth observation missions.

As mentioned before, nanosatellites (and therefore also CubeSats) are gaining momentum and the number of launched nanosatellites is projected to grow to 460 for the year 2024 (270% increase compared to the year 2019) (Spaceworks, 2020). In other words, the nanosatellite market contains quite a few competitors. However, just like with the segment of Earth Observation, once you add AI to the equation, the market becomes a lot less oversaturated to the point that there are only a handful of competitors.

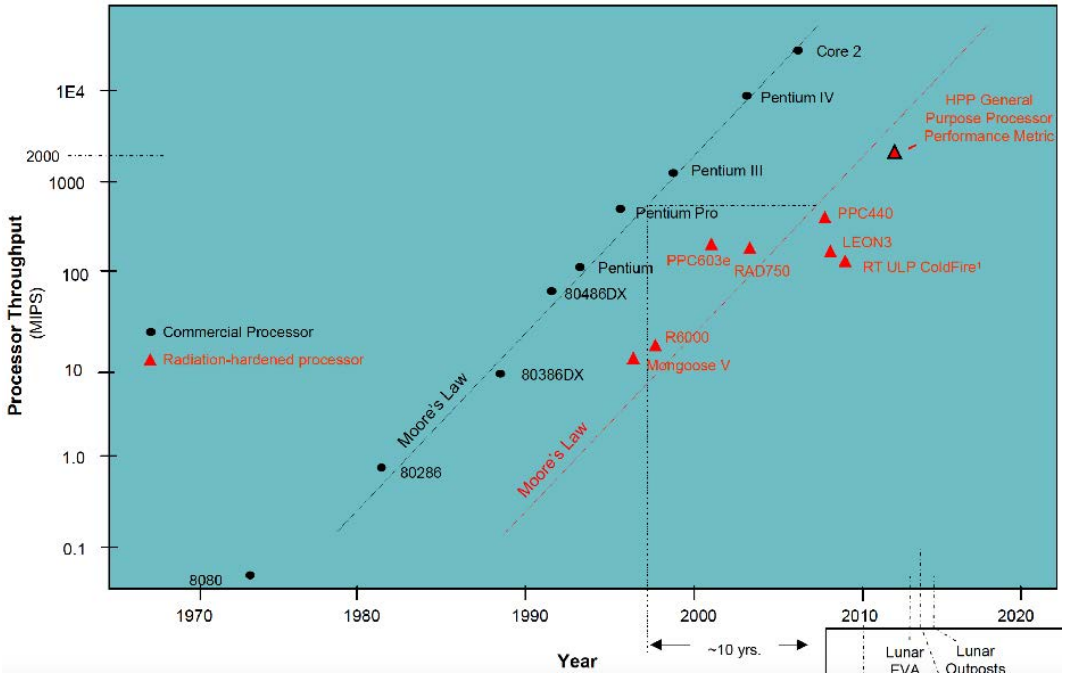

Figure 3.2: Radiation-Hardened Processor Progress

While a CubeSat, on a LEO orbit, that is used for Earth Observation with the use of AI is located in an extremely niche market with only a few direct competitors, it is vital to ensure that the AI is used at full potential to set the mission aside from other markets that are extremely over-saturated and where a small, low investment mission will not make a significant impact.

3.1.4. Customer

Besides our stakeholders it is also interesting to investigate who else could be a possible customer, other than the TU Delft and ESA. Satellite Earth Observation data sales is a very lucrative market. Throughout the years of 2018 and 2026 this market is expected to have a compound annual growth rate of 8.3% (Intelligence, 2020). Global Commercial EO Data Sales from Enterprise and Defense accounted for 1.65 Billion Euros in 2015, and grew to 3.35 billion (105% increase). While North America holds the largest market share, the highest regional growth rates are found in Asia. As mentioned before the market is extremely competitive and moving toward a fragmented stage. This is mainly due to there being more and more suppliers of Earth observation satellites.

So while our main customer are our stakeholders, there is a great potential of other customers within the (steadily) growing market. One should however, be aware of the large amount of competition.

3.1.5. Stakeholders & Competitor Analysis

In this project there are multiple stakeholders, but our primary active stakeholder is Dr. Menicucci, Alessandra who proposed this assignment to research key areas where AI would be beneficial in EO satellites. There are also multiple passive stakeholders who would like access to the data that the satellite would collect as well as stakeholders who would benefit from a proof of concept of AI in the subsystems of the satellites.

When it come to how this SC compares to others, the Cubesat will use AI to get an edge over the satellites in its class. Being a larger CubeSat will allow it to benefit from the advantages of being a standard for CubeSat but at the same time having significantly more power.

3.2. Payload Mission Market Analysis

From other missions including Sentinel 5P (Observations, n.d.) and PRISMA (Guanter et al., 2021) one can see that with hyperspectral cameras it is possible to, amongst other things, monitor emissions such as Methane (CH4), Carbon Dioxide (CO2), and Nitrous Oxide (N2O). A small research, and conversations with experts in the field such as Michael Rast (Senior Advisor Earth Observation Programmes, ESA) and Filippo Lodice (Earth Observation Engineer, Telespazio) revealed the need for additional research in the field of fugitive emissions. Fugitive emissions make up a non-negligible part in global and emissions, where the most

important pollutants are methane and CO2. Methane has the greatest impact on global warming however (Shell, n.d.).

Seeing as the main focus point of this mission relates to methane emissions it is important to assess the market needs with regards to this emitter. This means defining important concepts, identifying possible customers, assessing the financial prospects within this market, assessing the necessity of rapid response, and identifying the competition. From each segment mission guidelines will be established that will be used throughout the trade-off process.

3.2.1. Important Concepts

Within the field of fugitive emissions there are two important concepts that relate to our mission. Emission leaks can be classified as having a material impact or negligible impact. According to Nunez-Lopez (Nuñez-Lopez et al., 2019), “leakages of greater than a specified mass of CO2 or brine across a specified physical space (e.g. out of a storage complex or from the subsurface into atmosphere and/or aqueous environments) are defined as a material impact”. In other words, leakages that leaks more than a certain amount of CO2 (or methane) are defined to be of material impact. Leaks of negligible impact are defined to be of smaller amounts or slower speeds.

Seeing as our mission focuses on rapid response and considering that we are investigating fugitive emissions from space and thus have limited available resolution it is important to focus our mission on leaks with material impact, as these will be easier to spot and because a rapid response has the biggest impact when applied to a leak of material impact.

Mission Guideline MG-01: Focus on leaks with material impact.

3.2.2. Identifying Possible Costumers

As of the 29th of December 2017, there are 536 oil refineries around the world according to FracTracker (Auch, 2017). All of the 536 refineries are shown on the map in Figure 3.3. These refineries produce a rough total of 79,000,000 barrels of oil per day. These estimates might be skewed due to the reluctance of countries to share rates of individual refineries. Through the production of the oil, 1.2-1.3 BMT of methane are produced (Auch, 2017). Through the refinery, transmission, and distribution of gas, 14,832 kt (kilotons) of methane were produced in 2020, of which 9,554 kt (64.4 %) (IEA, 2021) are fugitive. This emphasizes the gravity and importance of the issue, but most importantly, indicates that refineries all over the world must do an effort to reduce these numbers.

Mission Guideline MG-02: Tailor mission to satisfy at least one of the many available costumers.

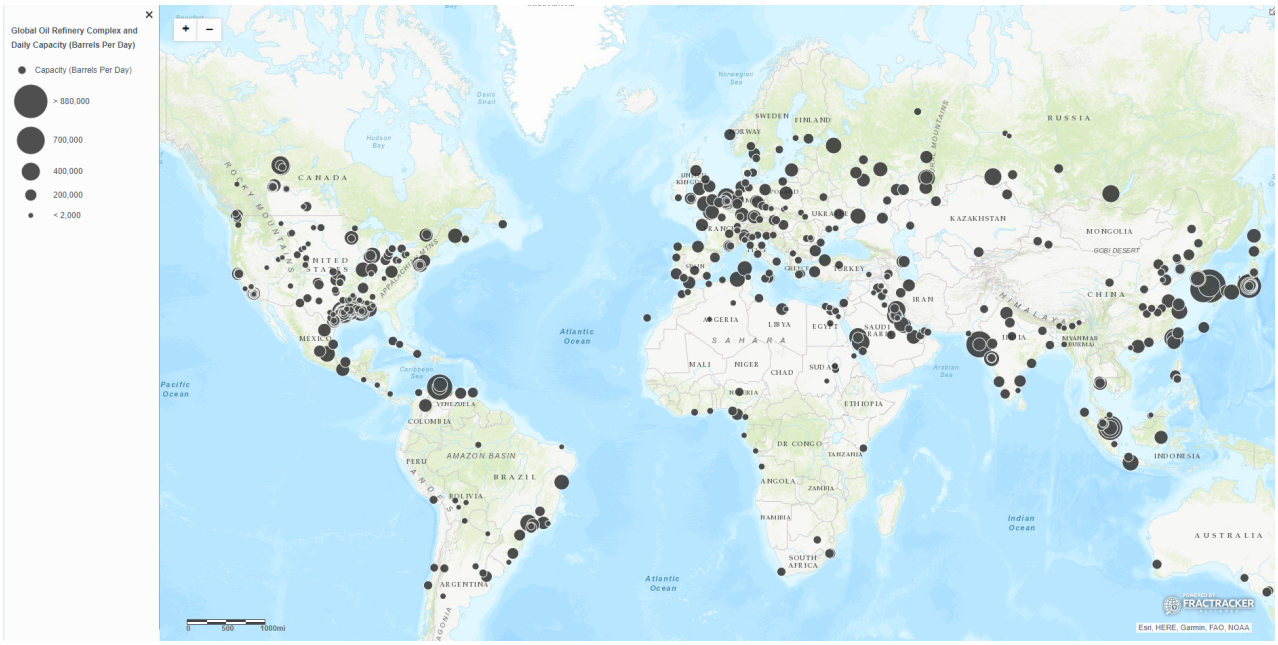

Figure 3.3: Oil refinery locations in the world

3.2.3. Assessing Financial Prospects

According to Jonathan Mingle (Mingle, 2019), in the United States alone, fugitive emissions from the oil and gas industry total an estimated 13 million metric tons per year, amounting to $2 billion in lost revenue; globally, the value of leaking gas is $30 billion. These figures only refer to the financial value of the lost material and do not include the social cost of the emissions. Within the United States methane is the second largest source of greenhouse gas emissions. This warming effect is reflected in the social cost of emitted methane, which during the Obama Administration was set to $1,400 per metric ton (Heikkinen, 2017). "The social cost is an estimate of the economic costs, or damages, of emitting one additional ton of carbon dioxide into the atmosphere, and thus the benefits of reducing emissions" (Rennert et al., 2021). Governmental Budgets also reflect the need and financial prosperity for methane reducing measures. The European Union proposed a draft budget in 2020, including a budget of 13.1 billion EUR for research and innovation for the reduction of methane (IEA, 2021).

Mission Guideline MG-03: Ensure mission covers the necessary aspects to enjoy the financial prospects in this market.

3.2.4. Assessing Necessity of Rapid Response

As our mission is a rapid response mission it is important to identify the need for rapid response within methane emissions. To do this one can assess possible leak "speeds" and add a financial value (social cost and financial burden) to the amount of methane leaked. To get an idea of the leak speeds, a leak west of Basrah (Iraq) is used as a case study. Through Kayross SAS (a geoanalytics firm) the leak was detected using satellite data. Due to the low revisiting time, only one satellite image could be used to find and analyse the leak. At the moment the image was taken the leak released methane at a rate of 73 tons an hour, but experts estimate the figure during the full duration of the leak could be 180 tons an hour. To give an indication of the gravity of the leak: a leak releasing 180 tons of methane an hour, lasting for 24 hours results in the same environmental impact as the average emissions of 200,000 cars in one year (Timmermans, 2021).

To add a financial value to this leak, two figures are calculated: social cost and financial cost. The social cost, using the $1,400 per metric ton set by the Obama Administration would mount up to $252,000 per hour. The financial cost would add up to $378,000 per hour (using the average price of methane on Nov 29, 2021) (GlobalPetrolPrices, 2021). Considering these values one can easily conclude that when it comes to methane leaks with material impact, every hour counts. Which translates to a mission objective of finding, identifying and notifying about a leak as quick as possible. When purely considering the financial prospects of the mission, being able to save a company 3 hours for 5 leaks would completely pay back the mission and generate a marginal profit.

Mission Guideline MG-04: Ensure the satellite is able to provide data in the timeliest fashion possible.

3.2.5. Identifying the Competition

Due to the gravity of methane leaks and the financial losses associated with it, there are already many methods companies can use to find and identify these leaks. The main methods used for this are:

- Foot inspection with gas imaging cameras
- Usage of drones with laser methane gas detectors
- Usage of Long-Range Laser Networks
- Usage of satellite data

Foot inspection with gas imaging cameras is the most old-fashioned method of detecting gas leaks, and is, as one might imagine, time consuming and costly for the refinery. The most common and most used (besides foot inspection) method of detecting gas leaks in refineries is the usage of drones. Drones are ideal as they are able to carry a high sensitivity laser methane gas detector (with an accuracy from 1 to 50,000 parts per million per square meter). While drones are able to transfer data to the operator with a range of up to 5km, their flight time (25 minutes) and flying height (30 meters) make them less than ideal to cover refineries that have a greater surface area (UGCS, n.d.). On average Shell refineries in Europe and North America have a surface area of 4.6km2 (with a standard deviation of 1.9) (Shell, n.d.), this poses challenges to drones that only have a flight time of 25 minutes. The usage of Long-Range Laser Networks might be beneficial for such large refineries, as they work best at refineries with more large open spaces. The purchase cost of $150,000 per device, their limited range of maximum 1 km, intensive labor efforts and need for tall vantage points make them less than ideal for most refineries, however.

Having investigated foot inspection, drones and the usage of long-range laser networks, leaves the usage of satellite data. As of today, the main satellite data used for methane leak detection is that of GHGSat and Sentinel 5P. The benefit of using the sentinel 5P data is that there is more data available than just methane leak data. Tropomi (the instrument on board of the satellite) monitors the following products (Observations, n.d.):

- UV Aerosol Index
- Aerosol Layer Height
- Carbon Monoxide (CO)
- Cloud
- Formaldehyde
- Methane (CH4)
- Nitrogen Dioxide (NO2)
- Ozone Profiles
- Sulphur Dioxide (SO2)
- Ozone (O3)
- Tropospheric Ozone (O3)
- UV

As one might imagine that is a lot more than can be achieved by a small CubeSat mission. There is a catch however. Sentinels revisit times are less than ideal and are not enough to qualify for fast response. GHGSat is able to gather more specific methane leak related data and in a more timely fashion (revisit time for GHGSat is about two weeks) (Varon et al., 2020). Therefore, GHGSat is the real main competitor for our mission. The drawback of GHGSat is that as of right now, whilst they can see methane concentrations, they are not able to use the data to identify specific sources of methane. This is because the data is based on rolling monthly averages and does not consider winds that move methane through the atmosphere.

Mission Guideline MG-05: Ensure mission edges out the competition by: covering a wider range, being less labor intense and faster than foot inspection, the usage of drones or Long-Range Laser Network, and having a higher resolution and being faster than GHGSat and Sentinel-5P.

3.3. Additional Research

Throughout the design process, multiple experts from different fields have been asked for input on the mission. The business idea was reviewed and additional input was given. From experts in the energy production industry the feedback was given to widen the focus from only looking at refineries to also including oil wells, pipelines and decommissioned oil wells, as these locations tend to leak often and have less supervision than refineries, increasing the impact of the mission. Additionally, the experts stressed the importance of ground resolution. As of right now, the researchers using the currently available data have difficulties determining the exact location of leaks due to low ground resolution. This leads to longer computation times, which impedes rapid response. A higher ground resolution would help resolve this issue. This feedback was communicated to the payload engineer, and incorporated in the design.

Additional feedback received during these talks revealed the lack of one direct communications between data creators and data user. In other words, a direct link between satellite companies and energy producers is missing. This results in energy producers having to gather and analyse data themselves. This requires a lot of investments and efforts from companies that are primarily focused on the creation of oil. Section 8 further analyses this problem and proposes a solution.

3.4. Market Analysis Conclusions

As a result of the market analysis, a better understanding of the requirements set by the market was achieved. From the satellite mission market analysis, it was determined that the EO/RS is a very lucrative market with a numerous players. Additionally, CubeSats and nanosatellites are extremely popular and are gaining popularity due to their ease of engineering and low initial investment. In other words, the first three segments this mission falls in have positive market trends and are very popular. This poses the problem of competition. Being

a singular stand alone CubeSat requires either a very specific tailored mission to allow the satellite to be competitive in the market, or, an application of on-board AI, which sets it apart from the competition. The last segment the mission falls in is in fact also the most niche segment. There are only a hand full of satellites with on-board AI. It is important to distinguish on-board AI from AI applied to gathered data. As removing on-board usage of AI from the mission broadens the market in such a way that remaining competitive will be a very challenging task. Adding on to everything the fact that AI is the next considerable advancement in the space industry, and that it will allow companies to cut costs, adds to the importance and viability of the mission. Summing up, being able to combine the most lucrative and popular markets with a cutting edge, extremely innovative and vital new piece of technology will allow this mission to over cut the competition and set a new standard.

When considering the payload mission it was determined the mission will focus on carbon dioxide and methane fugitive emissions. It will focus on fugitive emissions with material impact created by the energy production industry through the production of oil (eg. refineries and oil wells). Besides the possible reduction of losses due to the fugitive emissions, there is also a great push from governments to reduce emissions and therefore the payload mission has potential to be quite lucrative. Especially if the mission can achieve rapid response times, allowing customers to greatly reduce their response time in cases of very big leaks. When considering the competition, the biggest threat comes from other satellites with similar missions, such as GHGSat and Sentinell-5P. Ensuring SigmaSat's accuracy is greater than that of GHGSat and Sentinell-5P makes the mission stand out from the competition. Ensuring a reduced budget enables SigmaSat to compete with alternatives such as usage of drones and Long-Range Laser Networks.

4 Functional Analysis

In this chapter a preliminary functional analysis of the mission will be presented. The Functional Flow Diagram (FFD) and Functional Breakdown Structure (FBS) of the mission can be seen in the pages after this introduction.

The FBS is a summary of all the functions that the satellite will be able to do or will need to execute during it's mission. The FFD then takes these functions and shows how they would be performed in-sync. The aforementioned diagrams can be seen below.

- 1.1 Detailed Design
- 1.2 Production and Functional Tests
- 1.3 Environmental Tests
- 1.4 Launch Preparations and Launch
  - 1.4.1 Incoming task data
  - 1.4.2 Withstand launch loads
  - 1.4.3 Provide protection to the subsystems
    - 1.4.3.1 Protect from radiation
    - 1.4.3.2 Protect from temperature
    - 1.4.3.3 Protect from EMF
- 1.5 Operations
  - 1.5.1 Enter Initialization mode
    - 1.5.1.1 Operational mode
    - 1.5.1.2 Charge EPS
    - 1.5.1.3 Start OBC boot
    - 1.5.1.4 Activate startup timer
    - 1.5.1.5 Start OBC safe mode
    - 1.5.1.6 Start OBC antenna deployment
  - 1.5.2 Enter Safe mode
    - 1.5.2.1 EPS
      - 1.5.2.2 Measure power consumption of satellite bus
      - 1.5.2.3 Generate power from energy gen. source
      - 1.5.2.4 Receive power from energy storage
        - 1.5.2.4.1 Monitoring of thermal sensors
        - 1.5.2.4.2 Conversion of data
        - 1.5.2.4.3 Handling of failure
        - 1.5.2.4.4 Reporting to CDHS
      - 1.5.2.5 Regulate input voltages
      - 1.5.2.6 Receive OBC power distribution command
      - 1.5.2.7 Regulate output voltages
      - 1.5.2.8 Distribute power to satellite bus
      - 1.5.2.9 Report to OBC
      - 1.5.2.10 Store excess power into energy storage
    - 1.5.2.2 Comunicate with GS
      - 1.5.2.2.1 Compute orbit propagation
      - 1.5.2.2.2 Generate mission database
      - 1.5.2.2.3 Generate mission planning tools
      - 1.5.2.2.4 Perform TT&C management & analysis
      - 1.5.2.2.6 Combine in MOC server
        - 1.5.2.2.5 Connect to mission terminals
        - 1.5.2.2.7 Transaction from user segment
      - 1.5.2.2.8 Obtain command from GS server
      - 1.5.2.2.9 Pass signal through software defined radio transceiver
      - 1.5.2.2.10 Modulate signal
      - 1.5.2.2.11 Amplify signal through low noise amplifiers
      - 1.5.2.2.12 Pass signal through polarization switch
      - 1.5.2.2.14 Send signal to and through transceiver
    - 1.5.2.3 Power off non-essential systems
    - 1.5.2.6 Reset supply lines
  - 1.5.3 Enter Operational mode
    - 1.5.3.1 Receive instructions
      - 1.5.3.1.1 Generate signal
      - 1.5.3.1.2 Prepare signal
      - 1.5.3.1.3 Send signal
      - 1.5.3.1.4 Recieve signal from GS
      - 1.5.3.1.5 Amplify signal using low noise amplifier
      - 1.5.3.1.6 Demodulate signal
      - 1.5.3.1.7 Decode signal
      - 1.5.3.1.8 Send signal to CDHS
    - 1.5.3.2 Perform scheduled items (CDHS)
      - 1.5.3.2.1 OBC Waiting
      - 1.5.3.2.2 Incoming task data
      - 1.5.3.2.3 Move task to execute list
      - 1.5.3.2.4 Identify next task in queue
      - 1.5.3.2.5 Execute task
      - 1.5.3.2.6 Task completion
      - 1.5.3.2.7 Task failure
      - 1.5.3.2.8 Remove task from execute list
      - 1.5.3.2.9 Store/ communicate data
      - 1.5.3.2.10 Log error / communicate to mission control
    - 1.5.3.4 Housekeeping
      - 1.5.3.4.1 OBC pings subsystem
      - 1.5.3.4.2 log error
      - 1.5.3.4.3 Aks subsystem for houskeeping data
      - 1.5.3.4.4 Receive house keeping data
      - 1.5.3.4.6 Use error detecting code to see bitflips / errors
    - 1.5.3.5 ADCS
      - 1.5.3.5.1 Generate trajectory
      - 1.5.3.5.2 Run control algorithm
      - 1.5.3.5.3 Generate actuator commands
      - 1.5.3.5.4 Engage angular actuators
      - 1.5.3.5.5 PROP
        - 1.5.3.5.5.1 Fire thrusters
        - 1.5.3.5.5.2 Disable thrusters
      - 1.5.3.5.6 Sense spacecraft state
    - 1.5.3.6 PAYLOAD
      - 1.5.3.6.1 Obtain command from CDHS
      - 1.5.3.6.2 Capture image of the subject
      - 1.5.3.6.3 Collect data
      - 1.5.3.6.4 Process data
      - 1.5.3.6.5 Inform CDHS that the data is collected
      - 1.5.3.6.6 Forward data to COMMS
    - 1.5.3.7 Communicate with mission control
      - 1.5.3.7.1 Receive data from CDHS
      - 1.5.3.7.2 Encode signal
      - 1.5.3.7.3 Modulate signal
      - 1.5.3.7.4 Amplify signal
      - 1.5.3.7.5 Transite data to GS
      - 1.5.3.7.6 Receive data
      - 1.5.3.7.7 Process data
      - 1.5.3.7.8 Store data
    - 1.5.3.8 Schedule items
  - 1.5.4 Enter Idle mode
    - 1.5.4.1 Recharge batteries
  - 1.5.5 Enter Recovery mode
    - 1.5.5.1 Monitor State
    - 1.5.5.2 Excessive tumbling rate detected
    - 1.5.5.3 Execessive temperature rate detected
    - 1.5.5.4 Excessive bus voltage rate detected
    - 1.5.5.5 EPS
      - 1.5.5.5.1 Measure power consumotion of satellite bus
      - 1.5.5.5.2 Recieve power from energy storage source
      - 1.5.5.5.3 Regulate input voltages
      - 1.5.5.5.4 Recieve OBC power distribution command
      - 1.5.5.5.5 Regulate output voltages
      - 1.5.5.5.6 Report to OBC
      - 1.5.5.5.7 Distribute power to satellite bus
    - 1.5.5.6 Conduct temperature mitigation
    - 1.5.5.7 Conduct power mititgation
    - 1.5.5.8 Conduct detumbling manoeuvre
- 1.6 End of Life
  - 1.6.1 Decommisioning
  - 1.6.2 Deorbiting

SIDE NOTE:
Tasks such as ADCS, EPS, TC, STRUC & CDHS are constanlty running. Location only indicates when they FIRST start

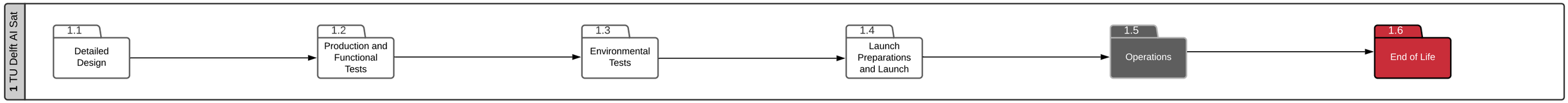
1 TU Delft AI Sat
1.1
Detailed Design
1.2
Production and Functional Tests
1.3
Environmental Tests
1.4
Launch Preparations and Launch
1.5
Operations
1.6
End of Life

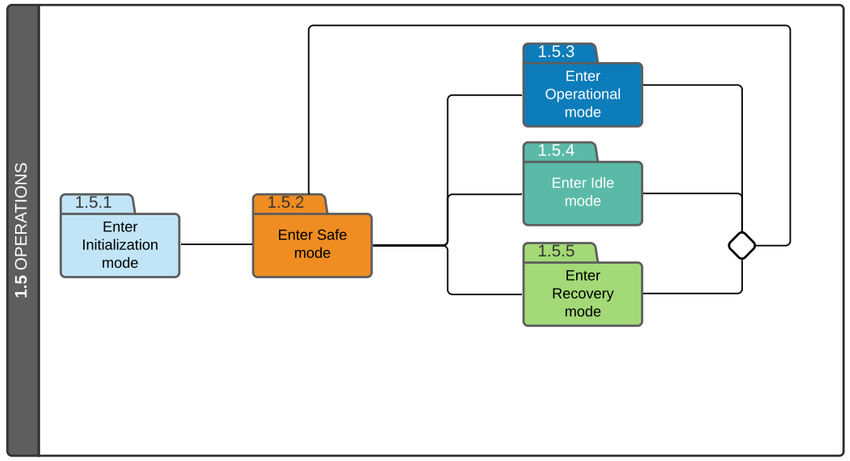
1.5 OPERATIONS
1.5.1
Enter Initialization mode
1.5.2
Enter Safe mode
1.5.3
Enter Operational mode
1.5.4
Enter Idle mode
1.5.5
Enter Recovery mode

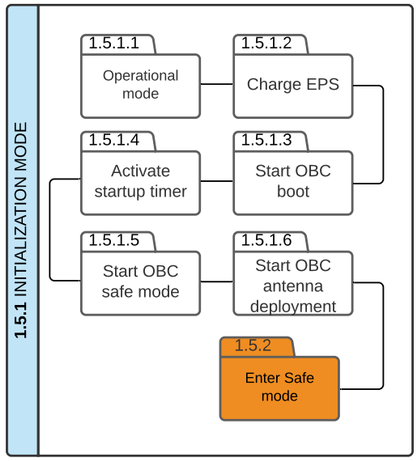
1.5.1 INITIALIZATION MODE
1.5.1.1
Operational mode
1.5.1.2
Charge EPS
1.5.1.3
Start OBC boot
1.5.1.4
Activate startup timer
1.5.1.5
Start OBC safe mode
1.5.1.6
Start OBC antenna deployment
1.5.2
Enter Safe mode

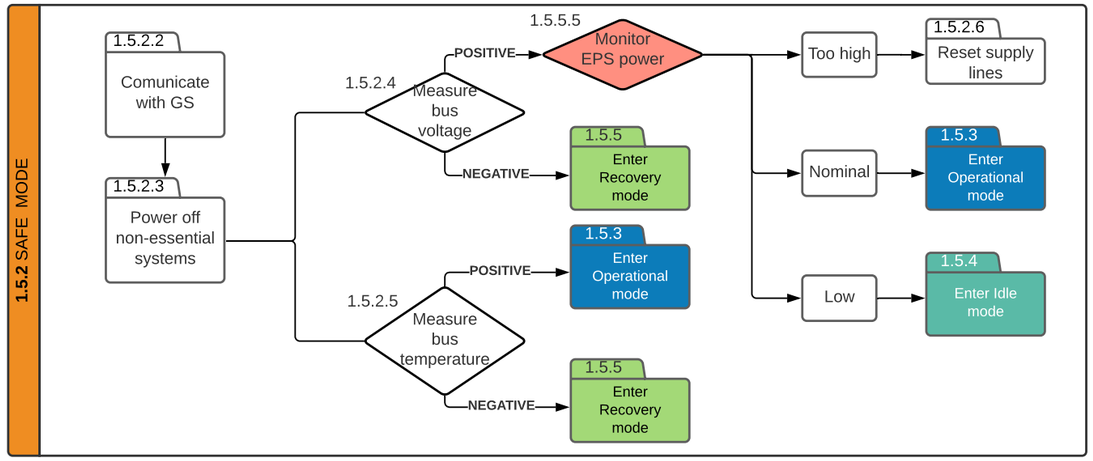
1.5.2 SAFE MODE
1.5.2.2
Comunicate with GS
1.5.2.3
Power off non-essential systems
1.5.2.4
Measure bus voltage
1.5.2.5
Measure bus temperature
POSITIVE
NEGATIVE
1.5.5.5
Monitor EPS power
1.5.5
Enter Recovery mode
1.5.3
Enter Operational mode
Too high
Nominal
Low
1.5.2.6
Reset supply lines
1.5.3
Enter Operational mode
1.5.4
Enter Idle mode

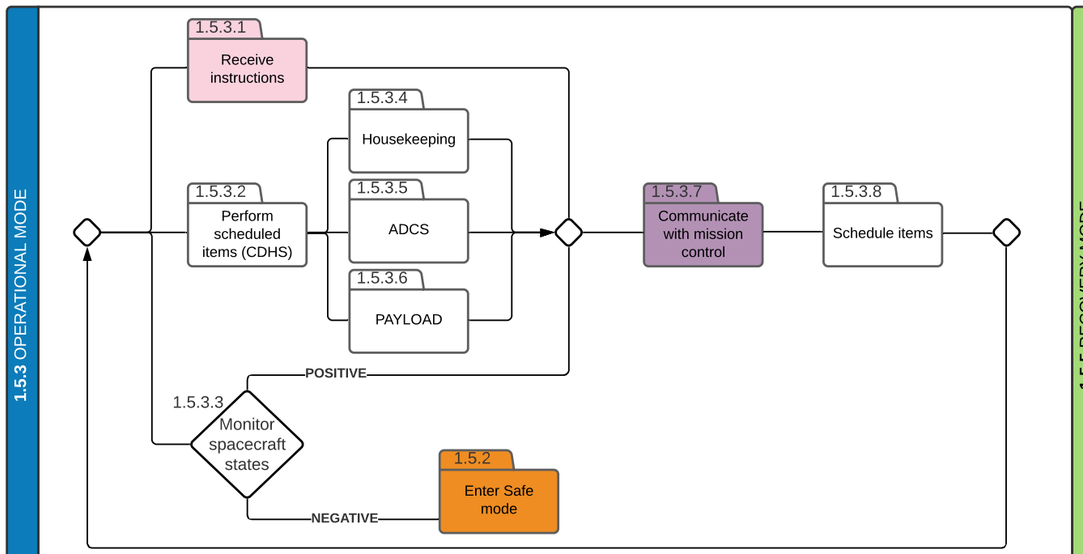
1.5.3 OPERATIONAL MODE
1.5.3.1
Receive instructions
1.5.3.2
Perform scheduled items (CDHS)
1.5.3.3
Monitor spacecraft states
1.5.3.4
Housekeeping
1.5.3.5
ADCS
1.5.3.6
PAYLOAD
1.5.3.7
Communicate with mission control
1.5.3.8
Schedule items
POSITIVE
NEGATIVE
1.5.2
Enter Safe mode

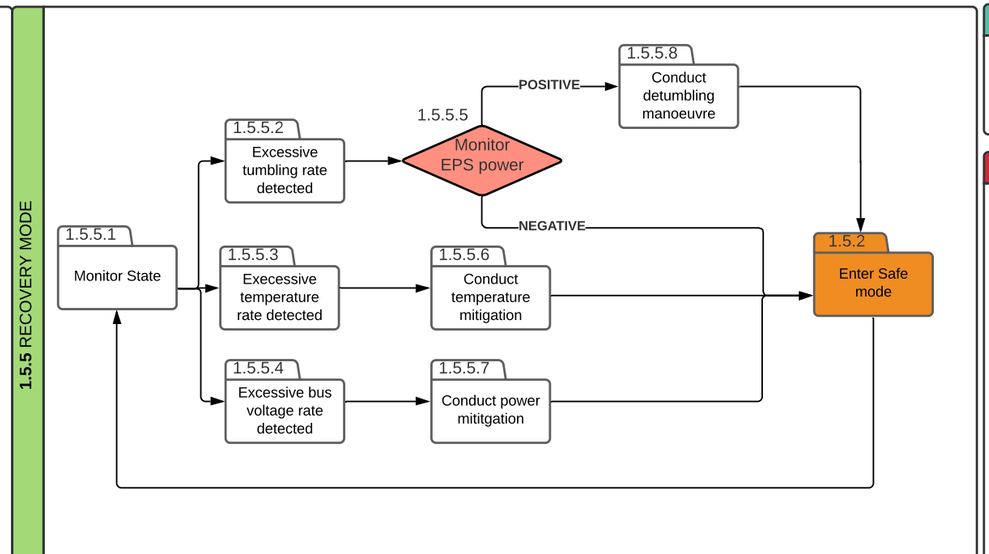
1.5.5 RECOVERY MODE
1.5.5.1
Monitor State
1.5.5.2
Excessive tumbling rate detected
1.5.5.3
Execessive temperature rate detected
1.5.5.4
Excessive bus voltage rate detected
1.5.5.5
Monitor EPS power
1.5.5.6
Conduct temperature mitigation
1.5.5.7
Conduct power mititgation
1.5.5.8
Conduct detumbling manoeuvre
POSITIVE
NEGATIVE
1.5.2
Enter Safe mode

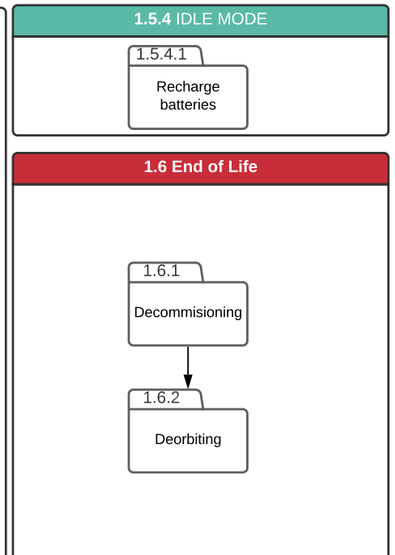
1.5.4 IDLE MODE
1.5.4.1
Recharge batteries
1.6 End of Life
1.6.1
Decommisioning
1.6.2
Deorbiting

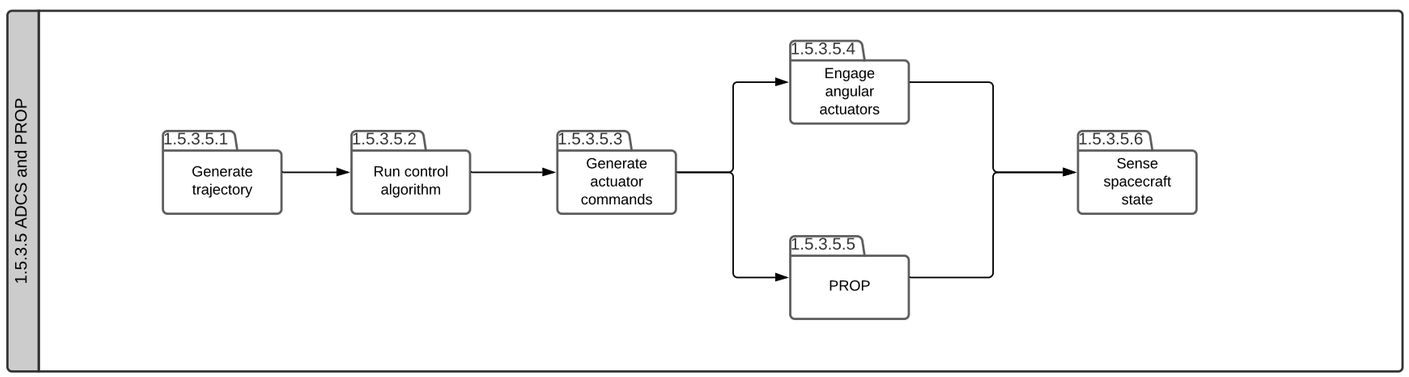
1.5.3.5 ADCS and PROP
1.5.3.5.1
Generate trajectory
1.5.3.5.2
Run control algorithm
1.5.3.5.3
Generate actuator commands
1.5.3.5.4
Engage angular actuators
1.5.3.5.5
PROP
1.5.3.5.6
Sense spacecraft state

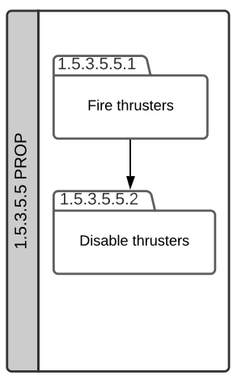
1.5.3.5.5 PROP
1.5.3.5.5.1
Fire thrusters
1.5.3.5.5.2
Disable thrusters

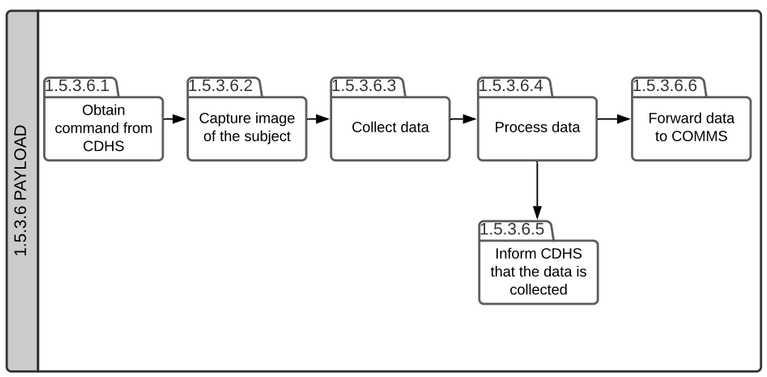
1.5.3.6 PAYLOAD
1.5.3.6.1
Obtain command from CDHS
1.5.3.6.2
Capture image of the subject
1.5.3.6.3
Collect data
1.5.3.6.4
Process data
1.5.3.6.5
Inform CDHS that the data is collected
1.5.3.6.6
Forward data to COMMS

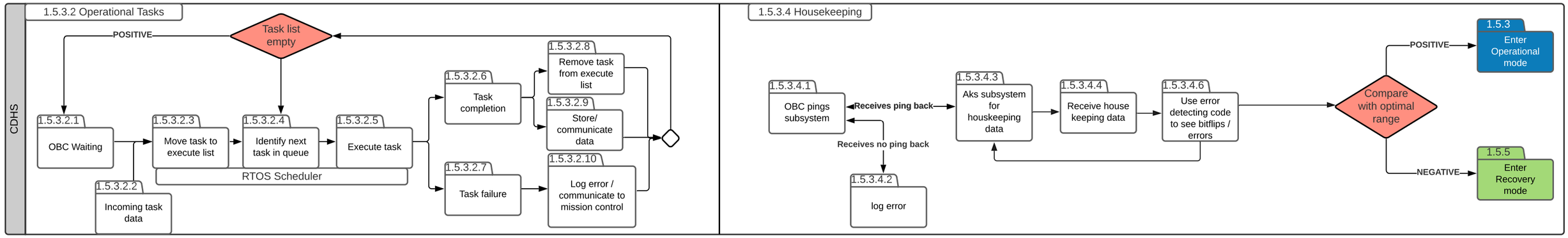
CDHS
1.5.3.2 Operational Tasks
Task list empty
POSITIVE
1.5.3.2.1
OBC Waiting
1.5.3.2.2
Incoming task data
1.5.3.2.3
Move task to execute list
1.5.3.2.4
Identify next task in queue
1.5.3.2.5
Execute task
RTOS Scheduler
1.5.3.2.6
Task completion
1.5.3.2.7
Task failure
1.5.3.2.8
Remove task from execute list
1.5.3.2.9
Store/ communicate data
1.5.3.2.10
Log error / communicate to mission control
1.5.3.4 Housekeeping
1.5.3.4.1
OBC pings subsystem
Receives ping back
Receives no ping back
1.5.3.4.2
log error
1.5.3.4.3
Aks subsystem for houskeeping data
1.5.3.4.4
Receive house keeping data
1.5.3.4.6
Use error detecting code to see bitflips / errors
Compare with optimal range
POSITIVE
1.5.3
Enter Operational mode
NEGATIVE
1.5.5
Enter Recovery mode

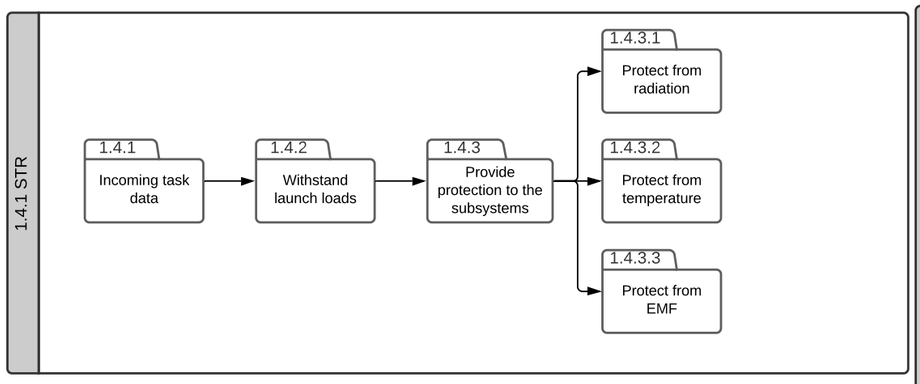
1.4.1 STR
1.4.1
Incoming task data
1.4.2
Withstand launch loads
1.4.3
Provide protection to the subsystems
1.4.3.1
Protect from radiation
1.4.3.2
Protect from temperature
1.4.3.3
Protect from EMF

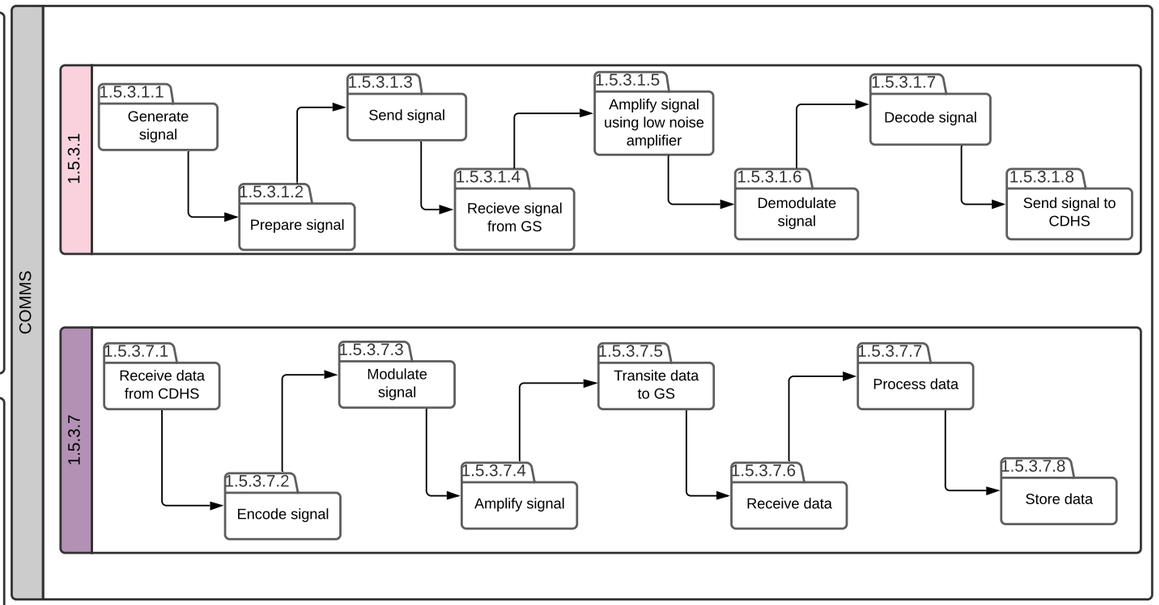
COMMS
1.5.3.1
1.5.3.1.1
Generate signal
1.5.3.1.2
Prepare signal
1.5.3.1.3
Send signal
1.5.3.1.4
Recieve signal from GS
1.5.3.1.5
Amplify signal using low noise amplifier
1.5.3.1.6
Demodulate signal
1.5.3.1.7
Decode signal
1.5.3.1.8
Send signal to CDHS
1.5.3.7
1.5.3.7.1
Receive data from CDHS
1.5.3.7.2
Encode signal
1.5.3.7.3
Modulate signal
1.5.3.7.4
Amplify signal
1.5.3.7.5
Transite data to GS
1.5.3.7.6
Receive data
1.5.3.7.7
Process data
1.5.3.7.8
Store data

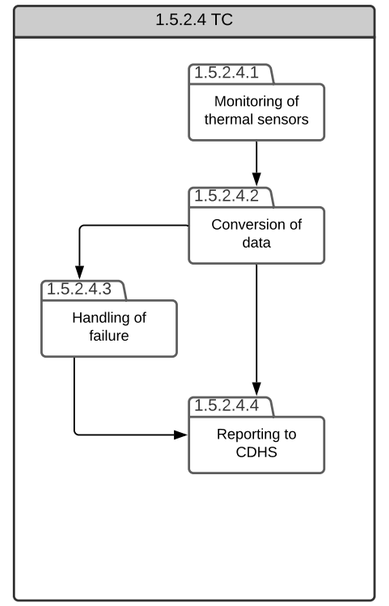
1.5.2.4 TC
1.5.2.4.1
Monitoring of thermal sensors
1.5.2.4.2
Conversion of data
1.5.2.4.3
Handling of failure
1.5.2.4.4
Reporting to CDHS

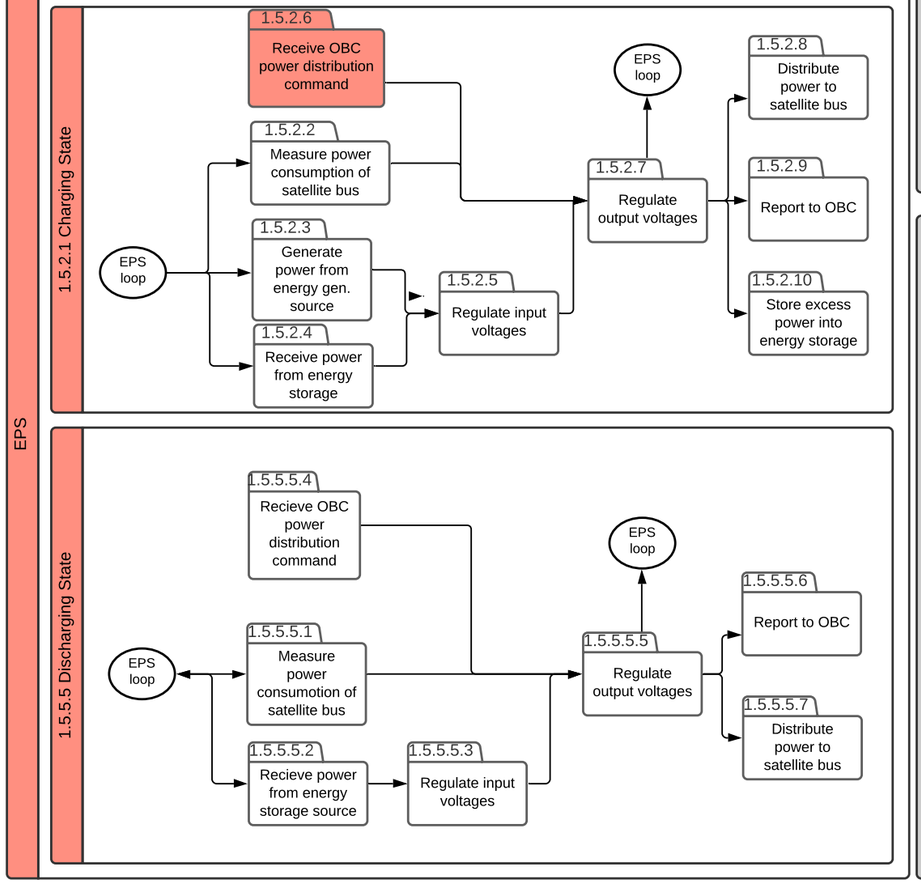
EPS
1.5.2.1 Charging State
1.5.2.6
Receive OBC power distribution command
1.5.2.2
Measure power consumption of satellite bus
1.5.2.3
Generate power from energy gen. source
1.5.2.4
Receive power from energy storage
EPS loop
1.5.2.5
Regulate input voltages
1.5.2.7
Regulate output voltages
EPS loop
1.5.2.8
Distribute power to satellite bus
1.5.2.9
Report to OBC
1.5.2.10
Store excess power into energy storage
1.5.5.5 Discharging State
1.5.5.5.4
Recieve OBC power distribution command
1.5.5.5.1
Measure power consumption of satellite bus
1.5.5.5.2
Recieve power from energy storage source
EPS loop
1.5.5.5.3
Regulate input voltages
1.5.5.5.5
Regulate output voltages
EPS loop
1.5.5.5.6
Report to OBC
1.5.5.5.7
Distribute power to satellite bus

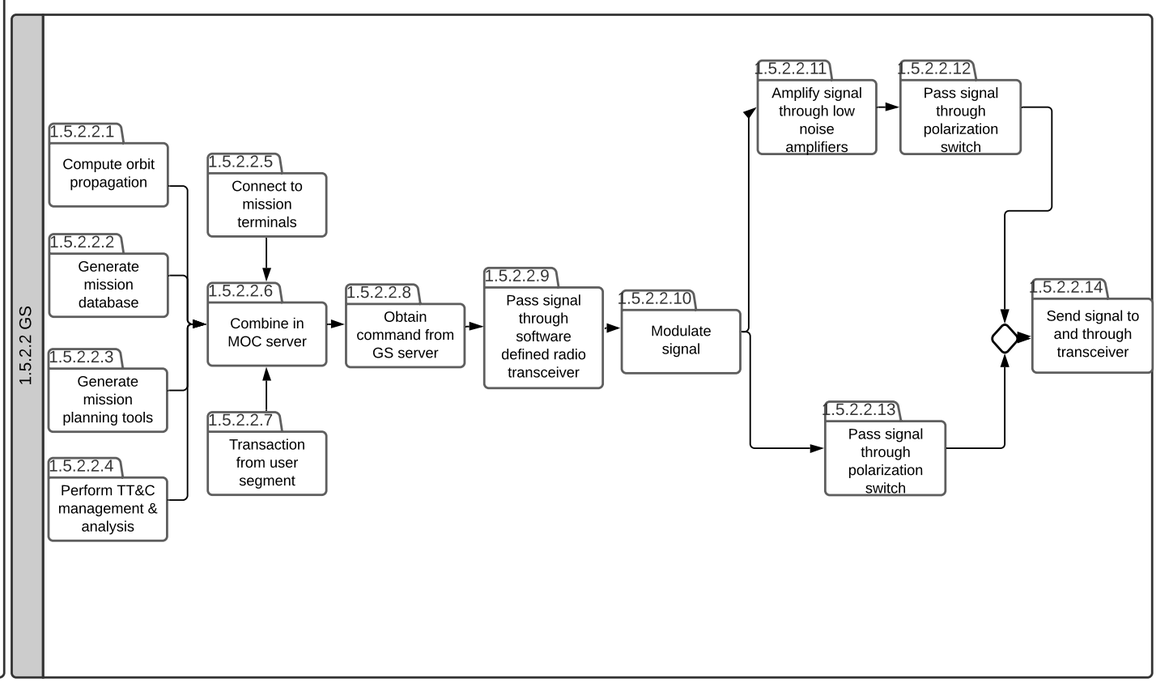
1.5.2.2 GS
1.5.2.2.1
Compute orbit propagation
1.5.2.2.2
Generate mission database
1.5.2.2.3
Generate mission planning tools
1.5.2.2.4
Perform TT&C management & analysis
1.5.2.2.5
Connect to mission terminals
1.5.2.2.6
Combine in MOC server
1.5.2.2.7
Transaction from user segment
1.5.2.2.8
Obtain command from GS server
1.5.2.2.9
Pass signal through software defined radio transceiver
1.5.2.2.10
Modulate signal
1.5.2.2.11
Amplify signal through low noise amplifiers
1.5.2.2.12
Pass signal through polarization switch
1.5.2.2.13
Pass signal through polarization switch
1.5.2.2.14
Send signal to and through transceiver

5 Modes of Operations

To properly design the space mission, operational modes have to be established. These operational modes have to address the entire satellite mission, from orbit insertion to decommission. Along with covering the entire mission operational modes need to cover all possible actions a satellite takes. This section will outline the operational modes established for this mission and how the satellite transitions from mode to mode.

5.1. Operational Modes

The SigmaSat satellite is, compared to the average CubeSat, rather complex. This is mainly due to the addition of AI on the satellite, but also due to it having a propulsion system and dual antennas. Generally, simpler CubeSats have a reduced number of operational modes as there are few operations that have to be performed. SigmaSat however, can not evade an increase in operational modes. Five operational modes were chosen for SigmaSat, starting with the Initialization Mode, this mode handles all operations related to the initialization of the space mission and the activation of the satellite. This mode will only be used in the initial phases of the space mission. If everything goes well, the satellite will transition to Nominal Mode. In this mode all the regular activities pertaining to the mission will occur. This operational mode is divided up into a collection of tasks which will be described later on. The satellite also has a Safe Mode, which it will transition into whenever things are not going as planned or errors are found. Detumble Mode is the operational mode that has as objective to detumble the satellite, which means taking control over the orientation of the satellite. At the end of the mission the satellite will transition into Decommission Mode where the satellite will be prepared for end of life. Decommission Mode is more a phase than a mode, but was added for the sake of completeness.

The correlations between the different modes are visualized in Figure 5.1. The modes were established in such a way that the satellite can never be in multiple modes at the same time. Additionally, as shown in Figure 5.1, the satellite can not go from a mode to any other mode. It can only transition into the modes the current mode is connected with through an arrow, and only in the direction of the arrow. There are a few other rules regarding mode transitions, including: the satellite can not return to Initialization Mode when it has successfully gone from Initialization Mode to Nominal Mode (faults with the initialization mode will be fixed in Safe Mode), the satellite can enter Decommission Mode only once and ground station can override mode transitions at any point (satellite will continually listen to UHF ground commands).

Every mode contains a list of tasks that the satellite can and will perform. These tasks have a sequence corresponding to them that will be followed whenever the satellite is performing this task. Figure 5.6, shows all the tasks pertaining to the different modes. As visible from the table, nominal mode has tasks sorted together in groupings. Due to the high number of tasks pertaining to nominal mode, tasks have been grouped to increase clarity. These groups are: payload, charging, housekeeping and communication. The payload grouping includes the tasks: payload execution task and image processing task which combined cover all the actions necessary for the payload. Charging is a grouping that includes only one task: charge optimization, which optimizes the satellite orientation for charging. The housekeeping grouping includes all Nominal Mode tasks that focus on the day-to-day operation of the satellite, such as a pointing task, and momentum dumping task. The communication grouping, groups all tasks related to data link, such as the payload downlink task and the alert task. A detailed description of all the tasks is given in Figure 5.6, while the Nominal Mode Operations Section describes and illustrates the task division for Nominal Mode

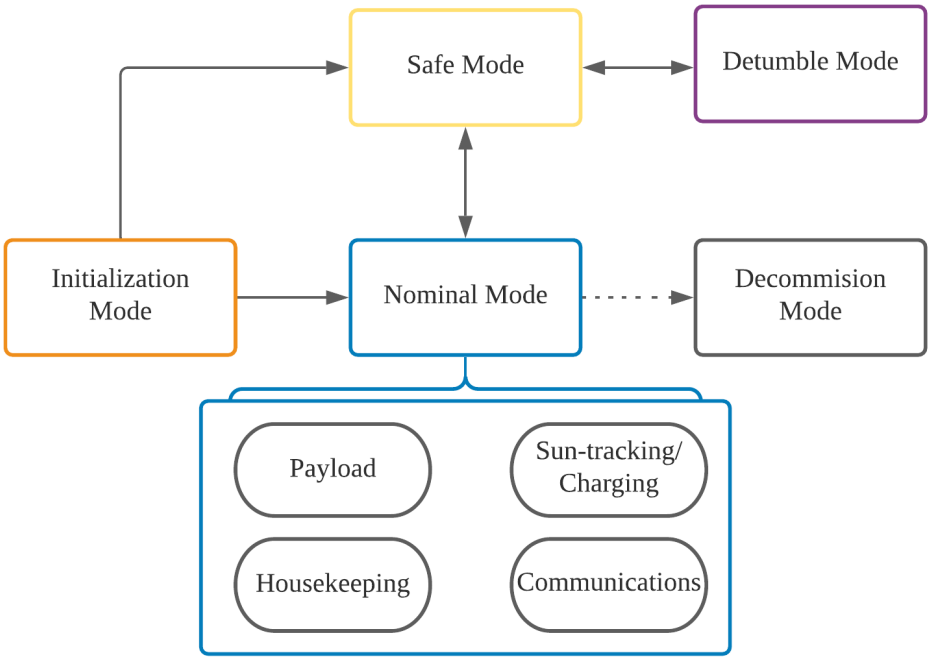

Figure 5.1: Operational Modes

5.2. Transition Conditions

Having determined the modes of the satellite, its important to understand how these correlate with each other. To optimize mode correlations, transition conditions have been determined/established for every mode transition. Transition conditions are a set of conditions that are constantly monitored and determine when and if a mode transition will occur. While in a mode, the satellite will constantly monitor telemetry data, this telemetry data is used to determine if the satellite is functioning as expected. Examples of monitored telemetry data are: voltage, power, temperature and rotational velocities. Every monitored property corresponds to a transition condition/indicator, and every transition condition/indicator has an acceptable range of values in which this property must lay. These values will be determined at a later stage and are designated as ”XX-XX [Unit]” or ”Pass/Fail”, for now. For every mode these transition conditions are different, as different things are important. Transition conditions are also task dependent, as one might imagine that satellite power usage will be higher during the payload execution task compared to the Alert task.

The transition conditions are shown in Figure 5.2 and will be discussed in more detail below.

As mentioned before, there are 4 modes, each with different transition conditions/indicators. The first mode the satellite will be in is the initialization mode. From this mode, the satellite can go into nominal or safe mode. The transition conditions from initialization to safe mode and their value ranges are described in Table 5.1.

Initialization Mode - Safe Mode

Note: the Initialization Mode is the mode in which most of the subsystems will be powered on for the first time and antennas and solar panels are deployed. Some of the transition conditions only apply once the relevant subsystem has been turned on/ activated/ deployed according to the initialization sequence. For example: if according to initialization sequence, the ACDS subsystems has not yet been turned on, the Missing Subsystem Pings transition condition will disregard the missing pings from the ACDS subsystem.

Table 5.1: Transition Conditions from Initialization Mode to Safe Mode

Transition Condition	Description	Value Range / Binary conditions
Voltage	Measure of the voltage throughout the satellite, which might suggest a voltage surge or lack of power e.g.	XX – XX [Unit]
Current	Measure of the current throughout the satellite, which might suggest a latch-up or lack of power e.g.	XX – XX [Unit]
Power	Measure of power in EPS subsystem, which is critical to ensure proper operations in non-charging tasks.	XX – XX [Unit]
Power Generation	Rate of charging of the satellite through the solar panels.	XX – XX [Unit]
Temperature	Measure of the temperature throughout the satellite, which is important to ensure all subsystems operate in their intended temperature ranges.	XX – XX [Unit]
Rotational Velocity	Measure of the rotational velocities of the satellite, that might indicate tumbling.	XX – XX [Unit]
Processing Power	Measure of power drawn by processor.	XX – XX [Unit]
Missing Subsystem Pings	Detection of pings given out by subsystems. Missing pings could indicate a malfunctioning subsystem or a shut down subsystem.	Pass / Fail
Presence of System Alerts	Detection of alerts given by the various subsystems, indicating incorrect operation of subsystem.	Pass/Fail
Antenna Deployment Status	Detection of antenna status with respect to deployment.	Pass/Fail
Solar Panel Deployment Status	Detection of solar panel status with respect to deployment.	Pass/Fail
Watchdogs	Detection of watchdog intervention	Pass/Fail
Ground Station Input	Detection of ground station command (through UHF), resulting in premature Safe Mode transition.	Pass/Fail

Initialization Mode - Nominal Mode

Note: As initialization mode has a very rigid sequence of events, these transition indicators apply at the end of this sequence. In other words, if at the end of the initialization sequence the transition conditions below are all within their acceptable ranges and all pass, the satellite will transition into Nominal Mode.

Table 5.2: Transition Conditions from Initialization Mode to Nominal Mode

Transition Condition	Description	Value Range / Binary conditions
Antenna Deployment Status	Detection of antenna status with respect to deployment.	Pass/Fail
Solar Panel Deployment Status	Detection of solar panel status with respect to deployment.	Pass/Fail
Subsystem Status		
Power	Measure of power in EPS subsystem, which is critical to ensure proper operations in non-charging tasks.	XX - XX [Unit]

Nominal Mode - Safe Mode

Table 5.3: Transition Conditions for the transition Initialization Mode - Safe Mode

Transition Condition	Description	Value Range / Binary conditions
Voltage	Measure of the voltage throughout the satellite, which might suggest a voltage surge or lack of power e.g.	XX – XX [Unit]
Current	Measure of the current throughout the satellite, which might suggest a latch-up or lack of power e.g.	XX – XX [Unit]
Power	Measure of power in EPS subsystem, which is critical to ensure proper operations in non-charging tasks.	XX – XX [Unit]
Power Generation	Rate of charging of the satellite through the solar panels.	XX – XX [Unit]
Temperature	Measure of the temperature throughout the satellite, which is important to ensure all subsystems operate in their intended temperature ranges.	XX – XX [Unit]
Rotational Velocity	Measure of the rotational velocities of the satellite, that might indicate tumbling.	XX – XX [Unit]
Processing Power	Measure of power drawn by processor.	XX – XX [Unit]
Missing Subsystem Pings	Detection of pings given out by subsystems. Missing pings could indicate a malfunctioning subsystem or a shut down subsystem.	Pass / Fail
Presence of System Alerts	Detection of alerts given by the various subsystems, indicating incorrect operation of subsystem.	Pass/Fail
Antenna Deployment Status	Detection of antenna status with respect to deployment.	Pass/Fail
Solar Panel Deployment Status	Detection of solar panel status with respect to deployment.	Pass/Fail
Watchdogs	Detection of watchdog intervention	Pass/Fail
Ground Station Input	Detection of ground station command (through UHF), resulting in premature Safe Mode transition.	Pass/Fail

Nominal Mode - Decommission Mode

Table 5.4: Transition Conditions from Nominal Mode to Decommission Mode

Transition Condition	Description	Value Range/ Binary conditions
Mission Phase	The phase of the mission is the main determinant for this transition.	Pass/Fail
Ground Station Input	In extraordinary situations, ground station can order the premature transition to Decommission Mode	Pass/Fail

Safe Mode - Detumble Mode

Table 5.5: Transition Conditions for the transition Safe Mode - Detumble Mode

Transition Condition	Description	Value Range/ Binary conditions
Rotational Velocities	Measure of the rotational velocities of the satellite, that might indicate tumbling.	XX - XX [Unit]

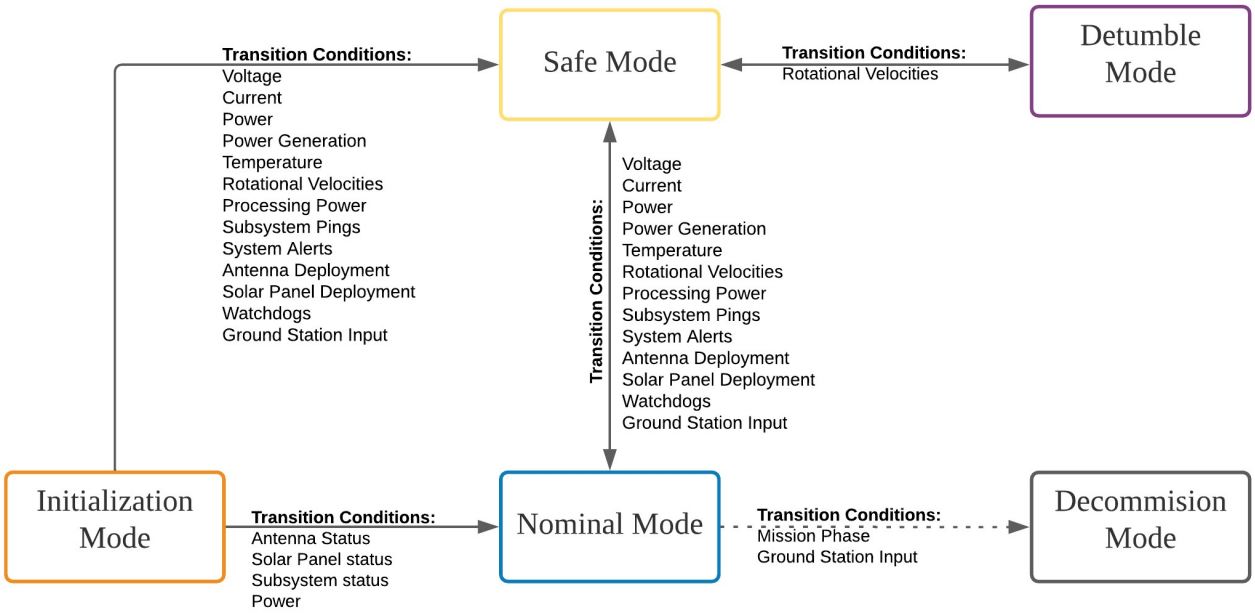

Figure 5.2: Transition Conditions

5.3. Transition Protocol

For a preliminary Fault Detection, Isolation and Recovery (FDIR) analysis, transition protocols are set up detailing the switch from Nominal Mode to Safe Mode. Through FDIR, the satellite would be able to detect faults, isolate faults and recover from them in an autonomously manner. The suggested transition protocols ensure a method of on-board fault isolation and recovery. While not all faults can be recovered autonomously, this method would allow recovery for the faults with the highest chance of occurrence.

The transition from nominal to safe mode is very critical. A failure in this transition could lead to a mission failure. Due to the critically of this transition, protocols are set up to ensure smooth, consistent and proper operation. These protocols are also going to be created for the other transitions, however, in this chapter only the transition from nominal mode to safe mode is explored in more detail.

As mentioned before there are a variety of transition conditions. These are monitored throughout the lifespan of the mission. If there are no failures, all the transition indicators pass. Transition indicators are judged on a pass/fail basis, depending on their value within the pre-determined boundaries of said indicator. Figure 5.3 shows the transition from nominal mode to safe mode in more detail. Stage I in Figure 5.3 shows operational nominal mode without any failures or faults. All condition indicators are set to Pass. In Stage II the satellite is still in nominal mode, however, not all the transition conditions are set to pass. This could have been due to an event or discovered during routine service checks. Once a failed transition condition is discovered the satellite will transition from the nominal mode to the safe mode. Within the safe mode (Stage III), the failed transition conditions are investigated and given a corresponding error code. The error code will lead to a Safe Mode protocol which will be executed in Stage IV. Pre-flight all possible errors (based on the transition conditions) will have been examined and a protocol will have been written for each one. This enables a more autonomous operation of the satellite with less input from the ground stations.

Safe Mode protocols are a step by step guide that the satellite will follow to, hopefully, remove the transition condition errors and resume nominal operation. These steps could include remedies such as the rebooting of systems, changing solar panel orientation, modifying the orbit. Certain protocols will include actions that require the satellite to acquire all telemetry data, send it down to a ground station and let the ground segment develop a remedy to the problem. In case the combination of transition condition errors does not result in a known error and known Safe Mode Protocol, telemetry will be sent down and ground segment will create a protocol. Additionally, ground control can at any time, override the Safe Mode protocol and implement it's own protocol. In general, any time the satellite changes mode, the ground segment will be notified.

Once the protocol has been followed and transition conditions are set to Pass, the satellite will go from Safe Mode to Nominal Mode (Stage V & VI). In case there are still errors after the protocol has been followed, the satellite will wait for input from the ground segment.

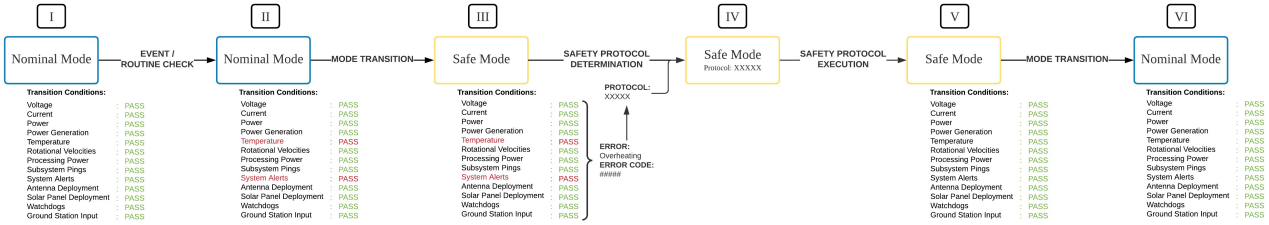

Figure 5.3: Transition Protocol (from Nominal Mode to Safe Mode)

5.4. Nominal Mode Operations

Nominal Mode is quite repetitive for SigmaSat. While many of tasks are performed during each orbit, there is not a lot of variation of tasks performed for the different orbits. Essentially there are two types of orbits SigmaSat flies, a non-busy orbit, that includes charging tasks and housekeeping tasks and a busy orbit, that adds payload and communication tasks to the orbit. For clarification, the busy orbit is called the payload orbit and the non-busy orbit is the non-payload orbit. These orbits are illustrated in Figure 5.4 and Figure 5.5. Starting with the non-payload orbit (as seen in Figure 5.5), we can see that the orbit is quite simple. Starting from the North and going anti-clockwise the satellite is performing a telemetry link task, after which a pointing task will ensure it can charge while being in stand-by. Arriving at the South Pole ground station, a pointing task will be performed to ensure the telemetry link task can be performed. Once this is done, the satellite remains in standby, unless a momentum dumping task or orbital maintenance task has to be performed before arriving at the North Pole. Once the satellite arrived at the North Pole and pointed itself to the ground station, this orbit and its tasks will be repeated unless it is entering a payload orbit. Figure 5.4 illustrates this orbit.

In Canosa et al., 2021a we have established that the SigmaSat mission is a fast response mission. Considering this mission property and the conclusions from the market analysis in Canosa et al., 2021b, it is critical to ensure the right data and alert are send as quick as possible after they have been gathered. From a mission design aspect this meant having to investigate the bottlenecks in the downlink of the data and alert. Besides the obvious bottleneck which is the reduced flexibility in payload execution (the image has to be taken at a very specific moment in time), the main bottlenecks are processing speed, downlink speed and ground station network. Having looked at all possible ranges of values, a conclusion was drawn necessitating all payload related tasks and data downlink to be performed in one singular orbit.

Seeing as the satellite has to perform the payload execution, data processing and data downlink in one orbit, this orbit (the payload orbit) is extremely crowded with tasks. The orbit shown in Figure 5.4, assumes a payload target on the Northern Hemisphere. Starting from the North and moving counter-clockwise, we see that after the communication task, the satellite points itself to the sun for charging, charges, and points itself to the target to perform the payload execution task. After which the satellite will charge and process the data simultaneously. At the South Pole ground station the satellite is not expected to have already finished processing and compressing the data, therefore there will be no payload data downlink at the South Pole. Depending on processing speeds and the results of the data, an emissions alert might be ready to downlink, however. In that case the alert can be downlinked to the South Pole using UHF. The remainder of the orbit the satellite is tasked with data processing and some housekeeping tasks. If the satellite finishes these all before reaching the North Pole ground station, it will perform the stand-by task. At the North Pole all processed emissions data will be downlinked.

5.4.1. Target Determination

From Canosa et al., 2021b and the market analysis it has been established that the SigmaSat mission will focus on at least one main target, the Shell Refinery in Moerdijk. More payload targets are possible and strongly encouraged as they increase the global relevance of the mission and possible revenue. One main target was chosen to scale the orbit. This means that the orbit was created with the intention to pass over the main target, any other possible target has to be on the same ground track. While on the same ground track however, SigmaSat is free to investigate any target. From a satellite operations point of view, targets are not limited to refineries or oil wells and thus can also be points of interests such as pipelines, storage locations or factories.

Depending on the location of the other targets, the satellite might not have enough time to perform all of it's orbital tasks. Therefore some variables were established that indicate the amount of time between tasks. The variables can been seen in Figure 5.4. The imaging time ($t_{imaging}$) was determined to be 1s as found in Chapter 6. The processing time ($t_{processing}$) was determined to be 189s, as explained later in Section 6.11.1,

and finally the average downlink times were determined to be 180.2s for the North Station and 185.1s for the South Station (Section 10.3.2). Through these values one can determine the minimum height of the target from the south pole, in order to process all the data on time for the orbit. This minimum height that the lowest possible target the SigmaSat can analyse is at 53° S.

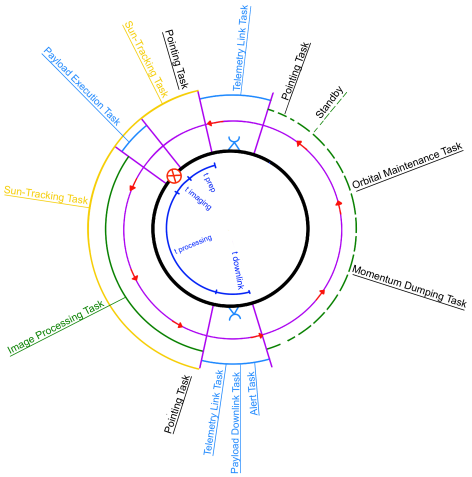

Figure 5.4: Nominal Mode - Payload Orbital Tasks

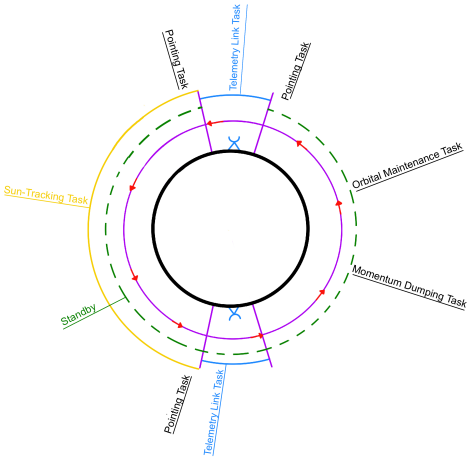

Figure 5.5: Nominal Mode - Non-Payload Orbital Tasks

Modes	Grouping	Tasks	Description
Aquisition Mode			
		Initialization Task	EPS gets turned on and starts its basic functionality
		Boot up sequence Task	Boot of OBC by the EPS
		Deploy Antennas	
		Deploy solar panels	
		Idle State	Mode in which TTC begins its basic functionalities. All subsystems of the satellite are functioning at a basic level.
Nominal			
	Payload	Payload Execution Task	Task in which satellite takes the image
		Image Processing Task	Task in which satellite processes the data from image
	Charging	Charge optimization	The task in which the satellite tracks the sun in a way that the maximises sun exposure and charges the satellite. [Can be combined with other tasks]
	Housekeeping	Stand-by	State in which subsystems [besides PL & Comms] perform basic functions
		Pointing Task	Task in which satellite is made to point in the required direction
		Orbital Maintenance Task	Main task: perfoem propulsive manouvres
		Momentum Dumping Task	Momentum gets dumped after a critical level is reached.
		Perform GS Tasks	Satellite performs non-nominal tasks given by ground station
	Communication	Payload Downlink Task	Satellites downlinks payload data to ground station
		Alert Task	Satellites downlinks UHF alert to ground station
		Telemetry Downlink Task	Satellites downlinks and receives telemetry data
Safe Mode			
		Unpower non-essential systems	To preserve power and isolate the fault, all non-essential subsystems are turned o
		Recharge	The satellite will recharge itself
		Gather Telemetry (internal)	The satellite will gather internal telemetry data
		Downlink Telemetry	The satellate will donwlink gathered internal telemetry data
		Receive Telemetry (listening mode)	The satellite will listen to ground station commands
		Reboot	The satellite will reboot systems for fault determination
		Enter Nominal Mode	If conditions are met, satelliet will transition to Nominal Mode
Detumbling Mode			
		Check Power Levels	Satellite will check power levels of satellite
		Detumble	Satellite will perform manuevres to detumble
		Enter Safe Mode	Satellite will transition to Safe Mode
Service Routines	Housekeeping		
		Check Voltages	
		Check Current	
		Check Power	
		Check Power Generation	
		Check Temperatures	
		Check Rotational Velocities	
		Check Processing Power	
		Check for Missing Subsystem Pings	
		Check for Presence of System Alerts	
		Check Antenna Deployment Status	
		Check Solar Panel Deployment Status	
		Check Watchdogs	
		Check for Ground Station Input	

Figure 5.6: Operational Tasks

6 Payload

In this chapter the payload will be discussed. The Payload instrument itself was already chosen in (Canosa et al., 2021b). The chosen camera is the Chameleon imager from SCS Space. Therefore this chapter will mainly focus on the handling of the data obtained by the imager. First the requirements and functional flow diagram will be discussed. These allow for further research into the payload and heavily influence the structure of this chapter. After those topics are fully discussed the chapter will move on to discuss the methods and the conclusions. Think of the type of algorithms, the training data and the required time and power budgets.

6.1. Requirements

The requirements related to the payload subsystem are stated in Table 6.1.

Table 6.1: Payload Requirements

Identification	Parent	Requirement
AIS-PL-REQ-01	AIS-TL-REQ-08	The payload shall have a minimun swathwidth of 10 km.
AIS-PL-REQ-02	AIS-TL-REQ-08	The payload shall have a spectral range between 1630-1675 nm or 1800-2500 nm.
AIS-PL-REQ-03	AIS-TL-REQ-08	The payload shall provide images with a resolution of max 30 m^2 per pixel.
AIS-PL-REQ-04	AIS-TL-REQ-08	The payload shall provide images with a spectral resolution better than 20 nm.
AIS-PL-REQ-05	AIS-TL-REQ-08	The payload shall remain operable between 10 and 30 degrees Celcius.
AIS-PL-REQ-06	AIS-TL-REQ-08	The payload processor will have a maximum processing time of 15 min.

6.2. Functional Flow Diagram

In this section the functional flow diagram will be discussed. It is shown in Figure 6.1. The layout of this chapter is largely influenced by this diagram.

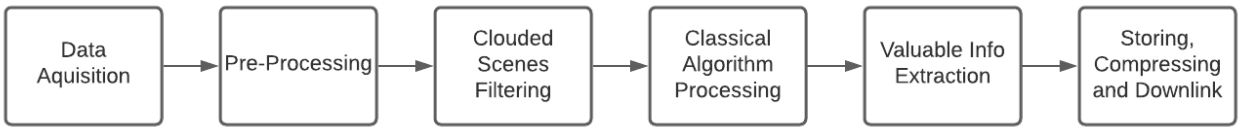

Figure 6.1: WFD Payload Data

The data acquisition section talks about the specifications of the obtained hyperspectral cubes. Then the data will be preprocessed during which errors and noise will be accounted for. After this the data will be checked for clouded scenes where images with unmanageable noise levels will be removed. The classical algorithm processing entails all the processes needed to extract useful information from the data, for example methods of detecting the needed atmospheric gasses. This information will move onto the valuable info extraction, where the conclusions are summarized to a compact signal. This is also the moment when all the redundant data (such as data not containing the refinery) will be removed. The rest of the raw data will move on to storing, compressing and downlink.

6.3. Data Acquisition

Like stated before, the Chameleon Imager is the chosen payload for this mission. Given an orbital height of 6656.1 km the values stated in Table 6.2 can be derived.

Spatial resolution	Swath
10.5 m	11.03 km

Table 6.2: Chameleon Imager Specs

The spatial resolution is what will set this mission apart from competitors. GHGsat for example has a spatial resolution of 50 m. Meaning that the SigmaSat will be able to find leaks in a more precise manner.

At the given orbital altitude the satellite will be traveling at a speed of 7.738 kms^{-1} resulting in a ground velocity of 2.6 kms^{-1}. Assuming a refinery area of 7 km^2, this would result in the camera recording data for 2.69 seconds, this number will be rounded to 2.7 seconds. Given the amount of data the hyperspetral imager produces (480 Mbps) this results in a datacube of 1296 Mb worth of data.

6.4. Pre-Processing

The obtained data is affected by various factors which can effect the quality of the images. For this reason preprocessing of the data is required. The aim of this process is to correct for these factors thus creating a more valuable data set.

6.4.1. Geo Referencing

Preprocessing might be needed for geo-referencing, geo-referencing is necessary in order to take pictures of the refineries themselves instead of for example the land next to it. Artificial Intelligence can be used for this. However, this might not be needed due to an accurate ADCS system. First the requirements for the pointing accuracy will be determined.

The main requirement is self explanatory: the entirety of the refinery needs to be visible in the hyperspectral scan. Given an altitude of 400 km, a fov of 2.3 ° and a refinery width of 7 km, a needed pointing accuracy 1587 arcsec. This requirement is met by the ADCS sytem and will be further elaborated on in Chapter 12. For this reason there is no need for the usage of AI with regards to geo-referencing.

6.4.2. Radiometric Correction

Radiometric correction has the aim to remove noise caused by inconsistencies in image brightness values (**radiometriccofrrection**). This can be caused by a multitude of factors. For example: cloud coverage or scene illumination. The cloud coverage problem will be solved by using a cloud detection AI that removes all data severely effected by clouds. This research can be found in Section 6.5. A big part of scene illumination depends on the angle between the sun, earth and satellite. This can be accounted for by looking at the date and time of the image acquisition and changing the data accordingly.

6.4.3. Radiometric Sensor Correction

There are a multitude of problems to be looked at with regards to radiometric sensor correction:

- Shot noise
- line or column drop-outs
- line or column striping

Shot noise

Shot noise occurs in the case of a random bad pixel. This pixel can be removed in 3 steps: identify missing pixel, record the 8 pixels around it, and calculate the average.

Line or column drop-outs

Line or column dropouts occur when an entire line containing no spectral information is produces. This could happen when one of the detector lines fails. There are two methods to fixing this problem: taking the average values of the pixels above and below or using another picture to fill in the missing values [1]. Since we are dealing with a methane emission problem the first option is preferred, since the usage of old images will not contain that information.

[1] https://www.nrcan.gc.ca/maps-tools-and-publications/satellite-imagery-and-air-photos/tutorial-fundamentals-remote-sensing/image-interpretation-analysis/pre-processing/9403

Line or column striping
Line or column striping are far more common than drop-outs. The most popular solution is histogram matching. [2] For this method a standard value is picked. This is done by looking at the values generated by one specific row, then for every other row the gain and relative shift of the mean are determined. Knowing this information allows for proper reconstruction of the values.

6.4.4. Correcting Geometric Distortion
There are two types of geometric distortion [3]:

- Non-systematic distortions
- Systematic distortions

Nonsystematic distortion includes all distortions caused by variations of the spacecrafts attitude, velocity and altitude. These are all non predictable and thus need data from the ADCS system to be accounted for. Systematic distortion are predictable distortions caused by the flight path [4]. For example: when taking pictures at an angle to the Earth, the image will seem compressed, or when flying at high speeds the image may seem stretched. This should also be accounted for.

6.5. Clouded Scenes filtering
In this section various methods will be discussed to get rid of useless data before having to process it fully. This is beneficial for both the quality of the mission and the power and link budget. The quality of the mission will be improved by removing images with too much noise (for example clouds). This prevents the occurrence of false positives for methane leaks.

There is a trade-off to be made considering whether or not this is a process that requires to take place on board of the satellite or not. Since this will inevitably increase the power budget. Still the choice was made to have this algorithm on board because of the following reasons:

- The quick alert signal could contain false positives if the noise due to the clouds skews with the data. On board cloud recognition could aid in removing this noise.
- One of the main bottlenecks when using a hyperspectral camera is the amount of data produced/downlinked. On board cloud recognition could help reduce this budget.

Cloud detection algorithms can be used to identify cloudy scenes. This allows the AI to get rid of those images thus saving on the telecommunication budget. There are different types of cloud detection algorithms [5]:

- Cloud/ no cloud
- Thin cloud/ thick cloud
- Ice/ snow cloud

Cloud/no cloud algorithms determine whether or not clouds are present in a taken image, thin cloud/ thick cloud detection is capable of determining the type of cloud present in an image, and ice/ snow cloud algorithms differentiate between ice, snow and clouds.

Seeing as the main refinery that this mission focused on is located in Rotterdam where it is cloudy about 60 % of the time [6] it is not preferred to filter out all levels of cloudiness and Rotterdam is rarely covered by snow. For this reason a thin cloud/thick cloud algorithm will be used.

The rest of the algorithm will be considered as a blackbox with the following assumptions attached to it:

- The algorithm will detect the level of cloudiness with high accuracy (around 90%)
- For no up to mild cloud conditions the algorithm will correct for the noise caused by the clouds
- For very up to fully cloudy conditions the algorithm will fully discard the data.

[2] https://ltb.itc.utwente.nl/page/498/concept/81765
[3] http://www.ciesin.org/docs/005-477/005-477.html
[4] http://www.ciesin.org/docs/005-477/005-477.html
[5] https://link.springer.com/article/10.1007/s40747-019-00128-0#Tab2
[6] https://weatherspark.com/y/51258/Average-Weather-in-Rotterdam-Netherlands-Year-Round

6.6. Classical Algorithm Processing

This section will go over the actual implementation of AI in this mission. As stated in Section 3.4 the satellite will provide a quick response signal with a small amount of info and will later on in the orbit send the full useful data obtained. First the quick response signal will be considered. The signal is expected to contain the following information:

- Location of the leak
- Type of gas that is leaking (CO_2 or CH_4)
- Amount of different leaks

For this the AI needs to identify various things:

- The presence of CO_2 or CH_4
- The amount of CO_2 or CH_4
- The location of the pixel containing the highest level of CO_2 or CH_4

The rest of this section will cover the points in the second list.

6.6.1. The presence of CO_2 or CH_4

As stated in **midterm report**, the unique electromagnetic fingerprint of CH_4 and CO_2 is present in only two windows in the spectrum. For methane, it's most prevalent in ranges of 1620-1720 nm or 2150-2500 nm. These are chosen specifically to prevent interference from H20 features. For CO_2 however, the fingerprint is most prevalent from 1900 - 2100 nm. So the final spectral ranges our camera will be looking at are 1900-2500 nm. Taken that the camera has a spectral resolution of 14.5 nm, this will entail 42 different spectral bands.

The refinery will have a baseline of a constant amount of CO_2 or CH_4 present in the images. Either due to the atmosphere or small leaks. In order to allow the AI to differentiate between these noise emissions versus actual leaks the AI will be trained with training data. This will be discussed in Section 6.9.

6.6.2. The amount of CO_2 or CH_4

Every pixel measured will obtain a certain possibility of there being methane present based on how much the measured spectrum matches that of methane and carbon dioxide. This is closely related to the amount of CH_4 or CO_2 present. The exact execution of this will be treated as a blackbox.

6.6.3. The location of the pixel containing the highest level of CO_2 or CH_4

Knowing the amount of CO_2 or CH_4 present in a pixel allows an AI to retrieve the pixels with the highest densities. This AI will be treated as a blackbox with the following assumptions:

- The AI will be able to recognize different leaks separately
- The AI will be able to combine the ADCS and Payload data in order to obtain the coordinates of the leak.

Some further research was conducted with regards to plume detection. However, since this method requires a LIDAR camera, it is added to the section of future recommendations.

6.7. Valuable Info Extraction

The swath width of the camera is larger than the expected width of an average refinery. Additionally, the camera is recording more spectral bands than what is required for the detection of methane and carbon dioxide. Both these aspects allow for a significant reduction of redundant data. The calculations in this section will be done with the scenario of best spatial resolution in mind. Since this will indicate the maximum amount of useful data obtained.

$$Data_{useful} = N_{bits} * \frac{W_{refinery}}{Swath} * \frac{N_{usefulbands}}{N_{totalbands}} \tag{6.1}$$

The values entered into Equation 6.1 are:

- $Swath$ = Swath width = 11.03 km
- $N_{totalbands}$ = Total spectral bands = 150

- $N_{usefulbands}$ = Useful spectral bands = 42
- N_{bits} = Amount of megabits in scan = 1296

This results in a final amount of data of 224.8 Mb

6.8. Storage, Compression and Downlink

After the data is processed it needs to be stored onboard the satellite awaiting the downlink of either the signal to the refinery or the raw data to the polar. Both the OBS and the camera itself have sufficient data storage available for this purpose.

Due to the downlink budget the data produced by the hyperspectral camera has to be compressed. However, lossy compressions are unsuitable for this mission, since accuracy is preverred in order to ensure that the data can be used for further analysis on the ground and that the data can potentially be used as training data for later missions. For this exact reason great advanced have been made for hyperspectral lossless compressions, reaching compression rates of 4 or greater (Yongjian et al., 2016). For this reason a compression ratio of 4:1 will be assumed resulting in a data value of 56.2 Mb. This will be made possible by the communications subsystem and more info can be found in Chapter 10.

6.9. Training Data

In order for the algorithms to be trained, training data is necessary. This is data that is similar to the expected outputs of the hyperspectral camera. 90% of this data will be used for the training of the algorithms and the other 10% will be used to test the algorithms.

This data can be obtained by either gathering data from similar past missions or creating artificial data.

Data from past missions

There are two past missions that offer a public database that can be used for the training data. These missions are: Sentinel 5p[7] and GHGSat[8]. The main issue with using the data from these missions is that their data has different variables than those of the SigmaSat concerning of spatial resolution and spectral resolution. So in order for this data to be useful it has to be changed accordingly. For the spectral resolution this will be no problem because the one from the Chameleon is lower. However, since our spatial resolution is about 5 times as high as those of the other missions, a lot of the pixels will have to be derived from lower quality samples. This will effect the quality of the training data.

Artificial data

Artificial data is the other possibility of obtaining training data. As the name implies it is artificially made, meaning that no previous measurements or missions are required. The downside of this is that it will not be as realistic as actual past data and it will be difficult to include the background noise of the refinery itself.

Being able to account for the background noise of the refinery is the main reason for choosing for the option of using data from previous missions. About 90% of this data will be used for the training of the algorithm and the other 10% will be used to test the algorithm.

6.10. Payload Processor

This chapter so far described what exactly is expected to happen to the obtained data. This section will add to this by diving into how this will actually happen.

The possibility of using a separate processor for the data processing will be researched. A trade-off was conducted to find the optimal processor for this use. The evaluated processors can be found in Table 9.1. Several other processord were considered. However, due to some of their specifications they were removed from the trade-off to make it more compact. These processors and the reason they were removed are stated in the following list:

- **CFC-500 TFLOP:** had a volume of 2 U. Which is too big for the cubesat
- **Google Coral:** was not designed for space

[7] https://sentinels.copernicus.eu/web/sentinel/missions/sentinel-5p/data-products
[8] https://www.ghgsat.com/en/

- **NVIDIA Nano:** was not designed for space

The specifications of the remaining processors can be found in Table 9.1. These values were then used for the final part of the trade-off.

	FLOPS/TOPS	**Power [W]**	**TRL**	**Volatile memory [GB]**	**Size**
Spacecloud iX5-100 EDU/EM [1]	4 TOPS	10-30	flown	2.5	0.5 U
Myriad 2 [2] [3]	80-150 GFLOPS	1	flown	4	9.5*8.0 [mm]
Myriad X [4] [5] [6]	4 TOPS	-	not to our knowing	4	8.8*8.0 [mm]
Leopard [7]	3 TOPS	7.5-40 [W]	flown	16	<1 [U]

Table 6.3: Specs of various payload processors

The following trade-off criteria and weights were constructed:

- FLOPS/TOPS - 4
- Power - 3
- TRL - 3
- Volume - 2
- Volatile memory - 1

FLOPS/TOPS determine the processing speed of the processor. This is of utmost important since this is a quick response mission and the hyperspectral camera produces a significant amount of data. That's why this criteria was given a weight of 4. Power and TRL both have a significant effect on the mission. The power budget is expected to be tight since the SigmaSat will be a relatively small cubesat. And TRL is important since the used technology is relatively new in space, thus a properly used and tested component is preferable. This is why both of these criteria got a weight of 3. Volume received a weight of 2. This is because it doesn't effect the design significantly as long as it fits. Making it more of a killer requirement. However, it's always nicer to have smaller components for simplicity, which is why the 2 was assigned. The volatile memory holds very little importance in the performance and design of the satellite, thus getting a weight of 1.

Combining the weights and specifications Table 6.4 was created.

[1] Spacecloud data sheet
[2] Myriad 2 data sheet
[3] Myriad 2 data sheet 2
[4] Myriad X data sheet
[5] Myriad X data sheet 2
[6] Myriad X data sheet 3
[7] Leopard data sheet

		FLOPS/ TOPS	Power	TRL	Volume	Volatile memory	Total
	Weights	4	3	3	2	1	
Reference Model							
Spacecloud iX5-100 EDU/EM	**Score**	5	2	5	3	2	
	Weighted	20	6	15	6	2	49
Myriad 2	**Score**	4	5	4	5	4	
	Weighted	16	15	12	10	4	57
Myriad X	**Score**	5	5	2	5	4	
	Weighted	20	15	6	10	4	55
Leopard	**Score**	4	2	5	1	5	
	Weighted	16	6	15	2	5	44

Table 6.4: Payload processor trade-off

A sensitivity analysis was conducted and the conclusion is that the winner of the trade-off switches between the Myriad 2 and Myriad X. The final decision was to go with the Myriad 2. This because it has already flown in space and because Ubotica offers a payload processing platform on which the Myriad 2 is integrated. This saves further developmental efforts.

6.11. Payload Processing Requirements

In this section the requirements that come with obtaining and handling the payload data will be determined and discussed. The variables considered are:

- Processing time
- Required power
- Amount of data to be downlinked

6.11.1. Processing time

The Myriot 2 can process a picture of 256x256 pixels with 3 bands per pixel in a timeframe of approximately 0.25 seconds. Again assuming a refinery of $7km^2$ and knowing the spatial resolution of 15.2 m the produces images of this mission will contain 461*461 pixels. Each pixel will contain 42 spectral bands. Using Equation 6.2 the following processing time can be derived: 6.3 seconds. However, this time is influenced by a lot of other factors. For example: the type of algorithm or the amount of algorithms. Since the images will be analyzed multiple times (cloud recognition, methane detection, CO2 detection, potential other algorithms) and since the other relevant factors are unknown this processing time will be multiplied by a safety factor of 30 to be sure to always stay within this range. Resulting in a final processing time of 189 seconds. Seeing as we have a timeframe of 15 minutes to transfer the rapid alert, this processing time is well within the requirements.

$$t_{processing} = 0.25 * \frac{N_{pixels}}{256} * \frac{N_{spectralbands}}{3} \tag{6.2}$$

6.11.2. Required power

The Chameleon Hyperspectral Imager requires 10 watts of power while recording data. Seeing that the camera will be actively obtaining data for 2.7 seconds, as determined in Section 6.3, this process will take 27 J. Besides this the camera will need some time for a start-up sequence and time to readout the images. The readout mode requires 5 watts and it is assumed that the start-up sequence requires the same amount. The following assumptions are made:

- Turning the camera on will require the same amount of power as the readout mode (= 5 W)
- The camera will be turned on 5 minutes before the recording of the data
- The readout mode will take a similar amount of time as the imaging itself (= 2.7 s)

These assumptions combined with Equation 6.3 bring a total energy consumption of 1729.5 J

$$E_{total} = W_{startup} \cdot t_{startup} + W_{imaging} \cdot t_{imaging} + W_{readout} \cdot t_{readout} + W_{processing} \cdot t_{processing} \tag{6.3}$$

6.12. Validation and Verification

In the payload subsystem there are three different sections that need validation and verification:

- The Chameleon Imager
- The algorithms
- The payload processor

The camera will be validated and verified by having a test model record data on earth. This data will then be checked to see if it is in the expected format and contains the expected values. The algorithms and payload processor will be validated and verified by using the test data. If the algorithms can successfully remove noise and identify leaks then they are deemed successful. For the payload processor the checks need to confirm that the expected power and processing time are realized.

6.13. Future Recommendations

The use of a plume detection algorithm could vastly improve the precision of the estimated location of the leak. For this algorithm however a LIDAR camera is required. This is something that could be researched further in order to potentially improve the mission.

6.14. Conclusion

This concludes the chapter about the payload and on board data processing. The use of AI on board combined with the payload processor allow for a quick response mission with smaller amounts of downlink data. Without the AI this would not have been possible. All the requirements stated in Table 6.1 have been met.

7 Astrodynamics

This section will discuss the determination of the final orbit, an estimations for a ΔV budget for the mission which is passed to the propulsion department and will discuss the end of life strategy.

7.1. Orbit Determination

After an evaluation done after the midterm, it was found that the previously determined orbit at an altitude of 525 km was infeasible. To satisfy the market analysis and specifications for the payload, it was necessary to reevaluate the orbit. As such, a new requirement was determined, namely that the orbit should be Earth-repeat. This way, the satellite can pass over the target every day and hence collect data continuously. Additionally, the satellite should be Sun-synchronous, as this keeps the lighting conditions constant for the targets, thus improving data collection. This lead to the conclusion that the satellite should be in an Earth-repeat Sun-synchronous (ERSS) orbit.

For this purpose, the methods outlined by (Noomen, n.d.) were used, which will be briefly explained below. For the sake of these calculations, only the J2 perturbation effects were considered. For an ideal scenario, the equatorial spacing Δ_{eq} would be kept as small as possible and using Equation 7.1, it is possible to determine the number of orbits j that would satisfy this condition.

$$j = \frac{2\pi R_e}{\Delta_{eq}} \tag{7.1}$$

Leading on, it was of significance that the orbit would repeat every day, hence the amount of days k, was set to 1. In turn, these values can be used in Equation 7.2 to determine the orbital period P that would satisfy these conditions. Both the Earth's rotational period P_E , and the Earth's period around the Sun P_{ES} were used to make sure that the period satisfies the requirement of being ERSS.

$$P = \frac{k}{j|\frac{1}{P_E} - \frac{1}{P_{ES}}|} \tag{7.2}$$

Having calculated the period, it was possible to determine the semi-major axis a of the orbit, as well as the inclination i that is required to satisfy the requirements. The eccentricity e, was considered to be 0, as the actual eccentricity is close to that value. Hence any terms including e were omitted from the equations. This is shown in Equation 7.3.

$$i = cos^{-1}\left(\frac{-2\pi T}{P_{ES} 3\pi J_2 \left(\frac{R_e}{a}\right)^2}\right) \tag{7.3}$$

Using this method, it was possible to generate a plot that would give possible solutions for ERSS orbits with a single day of repeat. Figure 7.1 below shows these orbits with their respective orbit altitude and inclination.

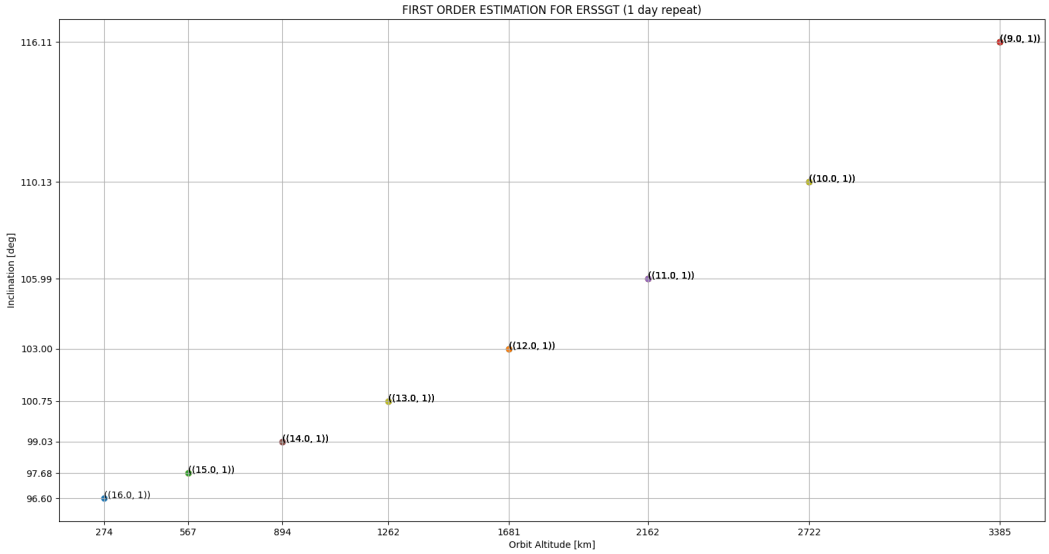

Figure 7.1: A plot of possible earth-repeat, sun-synchronous orbit solutions

From Figure 7.1 the only viable option for this mission was then found to be the orbit with 16 orbits a day flying at an altitude of 274 km. This stems from the fact that the resolution of the payload should be greater than GHGSat, which has a spatial resolution of 50 m. When flying at an altitude of 567 km, the resolution would be lower than previously anticipated. Hence the decision was made to place the satellite lower.

After this preliminary estimation, the General Mission Analysis Tool (GMAT) from NASA was used to refine the orbit. Since the calculations only considered the basic J2 value, there was going to be some discrepancies, which are usually in the magnitude of 2 km (Noomen, n.d.).

After some iterations, it was found that the best results were achieved when placing the satellite at a semi-major axis of 6656.1 km. The simulations indicated that there would only be a very minimal shift, namely 0.84° east-wards over the course of 2 years. This shift equates to only 90 km at the equator and over the course of the mission (Scripts, 2019), which was assessed to be within an acceptable limit. The shift does not interfere significantly with the observation quality of the payload, nor does it directly restrict communication with the ground station. GMAT is able to output a locator, which measures how often and long a satellite can be in contact with a given ground station. Further feasibility calculations were done in Chapter 10, which indicate that communication will always be possible. An image of the ground track is given in Figure 7.2.

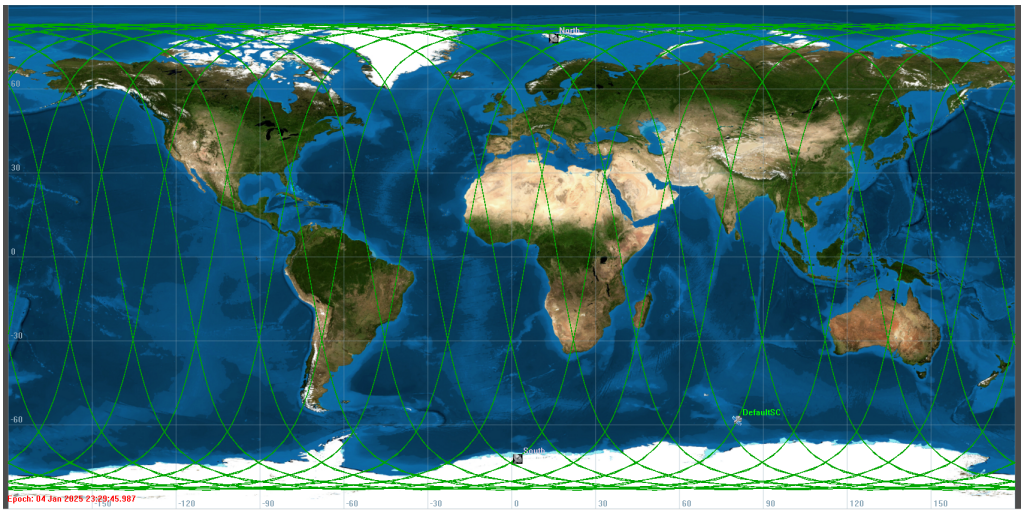

Figure 7.2: The ground track of the satellite

7.2. Optimization for Longitude of the ascending node

After having selected i and a, it was favorable to determine the longitude of the ascending node Ω. This parameter could be optimised such that the ground track of the orbit passes more closely to the target and the ground stations. This was done by running multiple GMAT simulations with different values for Ω. Using a python script, the longitude and latitude locations of the satellite were evaluated to determine which value would give make the ground track come closest to the target. Due to time constraints only 5 simulations were run, which gave that the best value for Ω was 5 °. Further optimisation could be done in the future.

7.3. Orbit Maintenance

Due to the newly determined orbit, it is also imperative to recalculate the ΔV budget for the mission. At the given altitude, the satellite is now flying in a Very Low Earth Orbit (VLEO). To ensure that the satellite can stay in orbit, the ΔV budget needs to be determined, so that the propulsion system can converge on a feasible design. For these calculations, the effect of aerodynamic drag was considered. To determine the necessary budget, the total impulse J was calculated using Equation 7.4.

$$J = F_D \cdot 86400 \cdot 365.25 \cdot T_m \tag{7.4}$$

Where F_D is the force of drag at the given orbit altitude and T_m is the mission life time in years, in this case 2. The drag area A was taken to be 0.04 m^2 (2 U) and the drag coefficient C_D was taken to be 2.2 (Oltrogge & Leveque, n.d.). The density ρ of the atmosphere at 6656.1 km was determined using the US Standard Atmosphere (Braeunig, 2014). Upon calculating J, a safety margin of 5 % was implemented as well. This equates to around 18 days extra in orbit and was taken to account for the system booting of the satellite before the mission commences. This results in a total impulse of 9652.76 Ns over the course of the mission.

$$\Delta V = \frac{J}{m} \tag{7.5}$$

Using Equation 7.5 a final ΔV budget was drafted. Using mass estimations from previous reports it was possible to calculate the budget. Mass estimates ranged from 15 to 20 kg, which yielded a final budget of 643.52 - 482.64 ms^{-1}.

7.4. End of Life Maneuver

As dictated by the requirements, the satellite shall have an end of life (EOL) maneuver, such that it does not result in space debris. The strategy for this will be the same as presented in (Canosa et al., 2021b). Namely, that the satellite will not need to make use of a propulsion system, but rather can de-orbit naturally. In (Canosa et al., 2021b), it was determined that when orbiting at an altitude of 550 km, the satellite would exceed it's 2 year mission life time. Since the orbit altitude has now been cut down, the decay rate will have to be recalculated.

Similar to the previous report's approach, GMAT was used to simulate the satellite in orbit. For this purpose, the Jacchia-Roberts atmosphere model (Jacchia & NASA, 1964) and fourth degree JGM-2 gravity model (Vetter, n.d.) were used. For the simulation, the satellite was first put in orbit and propagated using only the influence of the $J2$ perturbation. For this part of the mission it is assumed that the propulsion system will be able to maintain the orbit. Upon propagating for 730 days (2 year mission life time), the propagator switches to also considering atmospheric drag. This section was then propagated until the satellite reaches an altitude of 180 km, which was considered to be decayed (Panwar, 1999).

Upon the simulation finishing, GMAT produces a .txt file, which holds the mission's epoch, elapsed days, satellite latitude, satellite longitude, satellite orbital altitude. These values were then read into a python script to produce the graphs in Figure 7.3. The ballistic and mass parameters that were used can be found Table 7.1. For this case, the drag area is considered to be larger than for the total impulse calculations. It was assumed that upon EOL, the satellite would not be restricted to turning, such that the solar panels are perpendicular to the velocity vector. This would increase the drag area, and, for this case, is the most critical case, which is why it was simulated.

Parameter	Value
Dry Mass	15 kg
C_D	2.2
Drag Area	0.237 m^2

Table 7.1: Ballistic and mass values used for orbit simulation

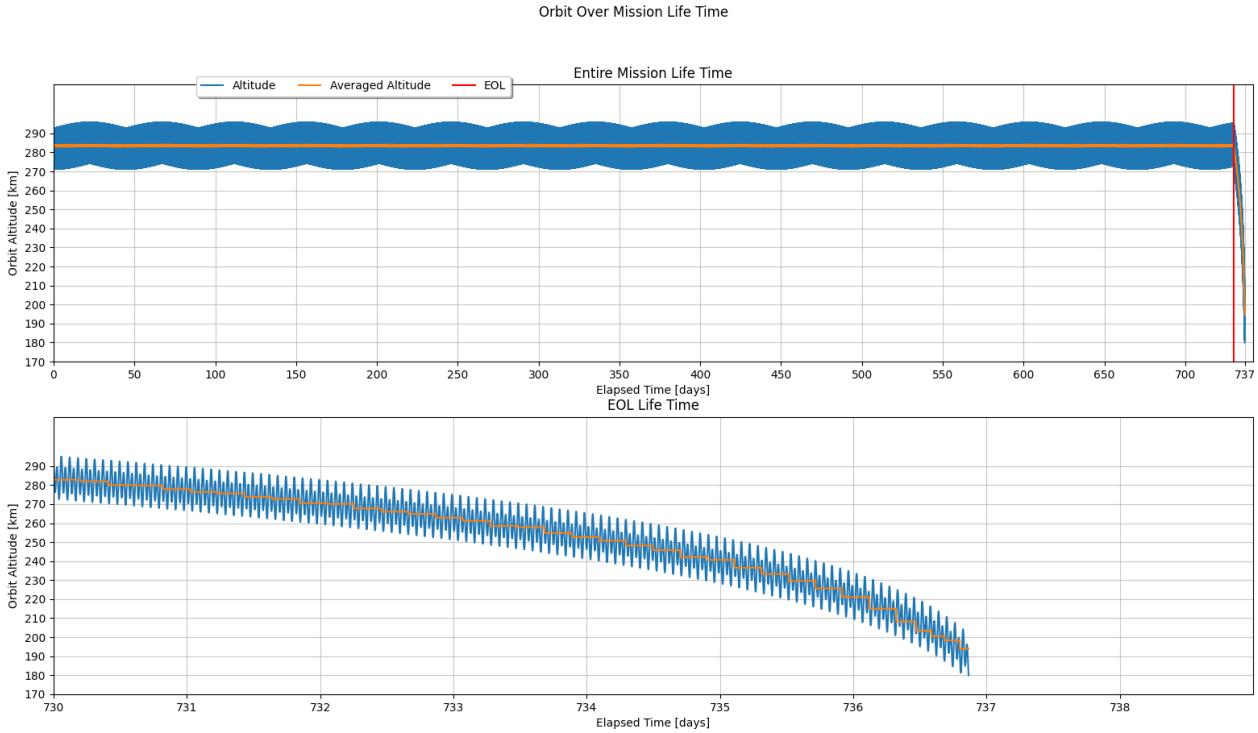

Figure 7.3: Overview of the Orbital Life Time

From the simulation, it can be seen that once the propulsion system shuts off, the satellite decays within less than 7 days. When re-entering the Earth's atmosphere, the satellite will not be large enough to survive re-entry and will burn up. In turn, this also means that the propulsion system will only need to focus on maintaining the orbit over the mission life time, and does not need to conserve propellant for an EOL maneuver.

In any case, if the mass of the satellite increase, the EOL maneuver will last longer than currently calculated. Also, an increase in mass would not impact the drag (and hence the propulsion system); only an increase in volume would constitute to changing the parameters being passed on to propulsion. At the time of designing and calculating the orbit, the volume would not increase anymore, which is very favorable.

8 Ground Segment

Besides determining the ground segment infrastructure, this section will analyse possible communications streams from ground station to customer, to ensure mission completeness. This chapter is based on the ground segment analysis performed in (Canosa et al., 2021b).

8.1. Communications Medium

Satellite communications can be done using either radiofrequencies or optical communications/laser communications. Optical communications use optical wavelengths of electromagnetic radiation for data transfer (Yost & Weston, 2021). Laser communications is a type of optical communications which beams data using a narrow beamwidth. Overall optical and laser communications are able to provide higher data rates, have a better signal to noise ratio, require a smaller antenna and don't need coordination of the International Telecommunication Union (ITU) (Curtis, 2020). However, there are some strong disadvantages related to the usage of optical communications. Optical communications are vulnerable to weather conditions such as rain, snow, fog and low clouds (Fischer et al., 2004), as they attenuate the emitted power by the free space laser transmitters. Additionally, to be able to make use of optical communications a higher pointing accuracy is needed. Combining these two factors and the fact that the sun acts as a noise source for the optical detectors drastically increases the mission complexity and risk. Radio frequencies are more commonly used on small satellite missions. As such, antennas and transmitters for radio frequencies are widely available at any CubeSat parts supplier. Data transmission using radio frequencies can be done at various frequencies, which are subdivided into bands. The most common frequency bands used by CubeSats are: VHF (30-300 MHz), UHF (300-1000 MHz), S-band (2-4 GHz) and X-band (8-12 GHz), where the higher frequencies allow for higher data rates (Yost & Weston, 2021).

While both of these communication options have flight heritage, radio frequency communications are the most commonly used and have the lowest developmental cost, lowest risk and greater ground infrastructure. This greater ground infrastructure allows for additional possibilities when it comes to ground operations. The combination of aforementioned advantages and the lower pointing accuracy requirements led to the choice of radio frequencies for satellite communications. It should be noted that if the demonstrator is successful and a constellation is build for increased revisit tima (and response time), laser communications are far superior for inter-satellite communications.

8.2. Ground Station Location

With the chosen sun-synchronous orbit, the satellite will pass over the poles on every orbit. This makes for an ideal spot for a ground station location as it would maximize the response time while minimized the amount of ground stations necessary. Other ground station locations, such as the, by the customer already available, TU Delft ground station were also considered. However, since the orbit crosses this ground station only once per day (revisit time of once a day), using only the TU Delft ground station would not be enough to satisfy the requirement of fast response. To be able to guarantee fast response without using polar ground stations, a whole array of ground stations would be necessary all over the world. In other words, the usage of the non-polar ground stations such as the TU Delft ground station, would either lead to an increase of necessary ground stations or a reduction of response time, and thus the idea of using non-polar ground stations was discarded.

8.3. Ground Segment Providers

With the increase of private satellites, the number of services available to private satellites increased. One of the most interesting services from a ground segment point of view is the concept of Ground Segment as a Service, or GSaaS in short. The "as a Service" concept originates from the IT industry where the term is used to indicate a "pay-as-you-go" service (pwc, 2020). In Ground Segment terms this means that you can pay another firm for the usage of a fraction (of the time) of their ground station. In other words, you can rent time at a firms ground station for your satellite. This enables satellite operators to transform their capital expendi-

tures into operating expenditures, ensuring a lower initial investment. Considering that the ground segment can reach up to one third of the total cost of the satellites lifecycle (pwc, 2020), being able to reduce those costs, or transform them into operational costs is considered very beneficial to the satellite operator. While the exact communication specifications for this mission are not yet determined, is it already quite clear that a service such as GSaaS would be very beneficial to the mission. Seeing as the customer does not have a ground station on one of the poles, not choosing to make use of a GSaaS service would mean having to build a ground station on the poles. This means a high capital expenditure (the antennas, plot of land and housing for the antennas would have to be build) and a high operating expenditure (the cost of labor involved in manning the ground station). While recent developments in artificial intelligence might be able to reduce the cost of the labor of a ground station (allowing ground stations to be manned fewer hours by fewer personell), these do not weigh up to the competitive rates offered by GSaaS providers. Choosing a GSaaS service also means being able to enjoy the varied offering in frequency band coverage, the global ground station network, autonomous scheduling capabilities and even consulting services (pwc, 2020). In other words, especially for a singular mission, without an existing ground station network, choosing a GSaaS service is highly beneficial from a cost point of view compared to building, staffing and maintaining a ground station.

There are four major players in the ground segment as a service market. These are: Infostellar, Leaf Space, AWS Ground Station, ATLAS Space Operations and KSAT. Additionally, there are smaller players such as Satnogs, which provide free VHF & UHF ground station solutions. All of these providers have been considered in the detailed design. While choosing a ground segment provider multiple criteria have been considered, these were: pricing, ground station performance and service quality, service extensiveness and location.

Before analysing any of these criteria it is important to ensure the ground segment providers have antennas in the correct bands. For this mission, UHF and S Band radio frequencies will be used (additional explanation in Section Chapter 10, all of the major providers do allow for communications on these frequencies. Satnogs however, does not. Satnogs is limited to UHF and VHF, rendering it inoperable as stand alone ground segment provider for this mission. Combining service providers (opting for Satnogs and one of the major players) would allow for the usage of Satnogs network, the logistical consequences would be too grave however for a CubeSat mission. Additionally, as the satellite passes the pole every orbit, the time advantage of using Satnogs would be limited.

Due to the importance of the location of the ground station, this was the criteria examined. The mission requires two ground stations, one on the North Pole and one on the South Pole. While Infostellar is a ground segment provider, it acts more as a ground station broker. It does not own any ground stations, but rather sells idle time of other ground stations. This allows them to have a very extensive network, but comes with the drawback of risks when it comes to contract guarantees. While Infostellar does have a very extensive network, they lack ground station coverage on the pole, rendering this ground segment provider unsuited to this mission. Unlike Infostellar, Leafspace does own it's own ground stations, however, similarly to Infostellar, due to the lack of pole stations, render it unfeasble for this mission. With among others, locations in Punta Arenas, Chile and Stockholm, Sweden, Amazon AWS Ground Stations is a good contender, but lacks the pole ground stations sought after. ATLAS Space Operations does have a ground station in Sodankyla, Finland, and is planning on opening a ground station in Antarctica, but can not beat KSAT in ground station location offering. KSAT is the only mayor ground segment provider with ground stations on both poles. Their North Pole ground station is located on Svalbard at 78 ° N, and their South Pole ground station is located in Trollsat, Antartica at 72 ° S. Their availability of pole ground stations renders KSAT the most desired ground segment provider for this mission.

As mentioned before there are also other criteria that should be considered such as pricing, ground station performance and service quality, service extensiveness. In this regard, KSAT does not offer autonomous scheduling but does provide consulting services. These criteria are however, not as relevant as the available locations, leading to the decision of picking KSAT as ground segment provider for this mission. It should also be noted that from a RAMS point of view, much of it is handled by the ground service provider, reducing SigmaSats responsibilities.

8.4. Ground Station Properties

Having picked KSAT as ground segment provider, their antenna characteristics had to be determined. From **Source**, the following characteristics were found.

Table 8.1: KSAT Svalbard SG1 S-band Antenna

Characteristic	Value
Aperature	SG1
Location	78 ° 13’ 51” N, 15 ° 23’ 22” E
Diameter	11.3m
Frequency	2025 - 2120 MHz
Effective Isotropic Radiated Power	63.5 dBW
Polarization	RHC or LHC
Antenna 3dB beamwidth	0.8 deg typical
Antenna Gain	44.6 dBi
Modulation Index	0-2.5 Radian

Table 8.2: KSAT TrollSat TR2 S-band Antenna

Characteristic	Value
Aperature	TR2
Location	-72 ° 00’ 08” S, 02 ° 31’ 27” E
Diamater	7.3m
Frequency	2025 - 2120 MHz
Effective Isotropic Radiated Power	51 dBW
Polarization	RHC or LHC
Antenna Beamwidth	1.32 deg
Antenna Gain	41.2 dBi
Modulation Index	0-2.5 Radians

8.5. Usage of AI within Ground Segment

Having shaped ground segment, it was time to investigate the possibilities for AI usage inside of the ground segment. However, due to the fact that the ground stations are rented using a GSaaS service a lot of the possible AI implementations are not feasible. AI applications such as scheduling, orbit propagation and AI mission control are not implementable if the ground station is rented. In fact, many GSaaS providers offer services like it already to customers (pwc, 2020). Additionally, according to Gabrielle Meoni (Research Fellow at the ESA Φ-lab), AI applications within the communications system that look at noise reduction for example are beyond the scope of this investigation and not something he would advise one to do. While it is a shame no feasible AI application for the ground segment can be found for this particular mission, it is not detrimental to this project. The focus of the project is to demonstrate AI on board of a satellite. Therefore implementing AI within the ground segment is not considered part of the mission objective. To the contrary, adding risk to the ground segment due to the implementation of AI within the ground station could lead to negative results for the overall mission. If the ground segment is not able to support the space mission due to the addition of AI, the satellite might not be able to demonstrate AI on board of a satellite, and thus the mission objective will not be met.

8.6. Data stream from Ground Station to customer

So far the data stream from payload, to ground station has been determined. However, the ground station is not the final user of this data. From the ground station the payload data (alert and emissions datacube) has to be further processed and communicated to a customer. From conversations with potential customers it was discovered that as of right now there are no direct communication streams between emission data users and emission data creators. Especially with regards to rapid response. Of course companies such as GHGSat have contract with interested parties and supply them with data. Similarly, Sentinell data is freely available through their online portal. However, all of these communication streams rely on the customer doing the analysis of the data. For a potential customer this is cumbersome. This method of data transfer requires customers to invest in manpower and expertise to analyse this data and then act on the results.

Additionally, due to the (lack of) accuracy of current available satellite data, evidence of a leak does not easily lead to the location of the leak. In locations such as the Permian Basin, Texas, USA, leaks are of daily

occurrence, however determining the creator of the leak is a big challenge. Oftentimes, when a customer find a leaks using methods available today, it takes quite some time to determine whether it was caused by a oil well (or refinery) belonging to them. In case it does, they are able to send someone to inspect it. However, when it's not they will send the information to whoever it belongs to (if they are able to). However, due to the big amount of small players, especially in the Permian Basin, it can be quite difficult to track down and communicate with the owner of the location of the leak.

To reduce the global emissions of greenhouse gasses due to leakages, this process needs to be streamlined and improved. Therefore, SigmaSat would like to propose a platform and database that combines all available data from the SigmaSat mission, including other freely-available data from other missions. This platform would them present the raw data downlinked from the satellite but also processed information including leak alerts with location information and leak size. Additionally, the database would include information on refinery and oil well ownership, to ensure customers do not get false alarms of leaks not pertaining to them. A proposed platform and database would greatly reduce the investments necessary by energy producers to detect leaks. It would also allow smaller players in this industry that do not have the capital to invest in leak detection equipment and personnel to investigate and fix their leakages. Especially the smaller energy producers are the ones with the highest leakage to production ratio. While the bigger companies try to capture all the gasses that are byproducts of oil retrieval, smaller companies do not as they do not sell these gasses. Therefore there is less focus on ensuring the gasses don't reach the environment and their percentage of leakages are higher.

Setting up such a platform and database is quite costly Due to the maintenance of it, it would not just require a high amount of capital expenditure but also a significant amount of operational expenditure. Therefore, a subscription based service would be ideal for the platform. customers would pay a monthly/year fee depending on their area and service required. To reduce costs even further, grants can be requested by the European Union under NextGenerationEU. Further investments from governmental institutions are not inconceivable. Especially if governments are granted free unlimited access in return for their (financial) support they might be very interested. Such platform will allow them to investigate their own emissions and identify any potential dangerous leaks. The mission could even be expanded further into a constellation of satellites, allowing for more targets, with as end goal a global emission leak monitoring system with quick alerts. The results of which could lead to even greater emission reducing measures and solutions.

8.7. Ground Segment Cost

Cost is and remains an important factor in any space mission. Due to the competitive nature of the ground segment provider sector, prices are not readily available to anyone. Through extensive research a few indications of the cost for renting antennas were found. Prices were found for Amazon AWS Ground Stations, and RBC Signals. These prices will be used to find an indication of the cost of renting at KSAT. According to (pwc, 2020), Amazon AWS Ground Stations, charges between $3 and $10 per minute for Narrowband. For wideband AWS charges between $10 and $22 per minute. The price varies depending on whether the coverage was reserved or requested on-demand. To calculate the final cost range for using AWS Ground Stations, a few assumptions need to be made based on information provided in Chapter 10. The first is the bandwidth in which the data will be up and downlinked. This is determined to be 0.3 Hz, and thus SigmaSat can use the cheaper narrowband services. For AWS's pricing model, the contact minutes are also necessary. It is assumed for the cost analysis that the satellite will contact the ground station for 3 minutes per pass. Per orbit, the satellite has two ground station passes, as discussed in Chapter 5, and 16 orbits per day. It is assumed that the satellite is able to perform many functions autonomously, and therefore the number of ground station contacts is limited to orbits that include a payload execution task. Therefore, seeing as we assumed three targets will be analysed, only three orbits per day will include ground station contact. In emergencies, the TU Delft ground stations UHF connection can be used for Telemetry down and uplink, reducing the dependency on the ground segment provider and reducing costs in emergencies. With the afore mentioned information the ground station renting costs are calculated for the lifetime of the mission. For AWS Ground Stations, the cost ranges from €13,025 to €43,417 (using a 0.87 dollar to euro conversion factor).

RBC Signals has a different pricing philosophy, and charges the customer per pass. According to (pwc, 2020), RBC Signals charges a customer using their Xpress service, from $ 19.95 per pass. Using the same assumptions as stated before it was found that for the full duration of the mission the cost would mount up to €28,872. This number falls within the range given by AWS Ground Stations, thus validating the cost. Additionally, the mean of the AWS Ground Station cost range is €28,221, which is extremely close to the value given by RBC Signals. It should be noted however that the range of costs for AWS ground stations is quite large. This is due to there still being many unknown variables, for example, any cancelled contact will usually still require the customer to pay the reserved minutes. AWS Ground Stations does make an exemption for

reserved contact that are cancelled 24h in advance. Furthermore, the bandwidth required for this mission is very small and therefore more lucrative deals could be arranged, leading to a reduction of cost. However, due to the great amount of unknown variables, a conservative estimation is made and the cost for renting ground stations for this mission is set to: from €13,025 to €43,417.

8.7.1. Ground Segment Conclusions

The main takeaways from the ground segment analysis are the communication medium, ground segment provider, ground stations locations, customer data streams and overall ground segment cost. Radiofrequencies were chosen as communications medium. A ground segment provider to allowing access to ground stations all over the earth at a fraction of the cost of building and manning a ground station. The chosen ground station provider is KSAT, using their ground stations in Troll and Svalbard. A fugitive emissions database and platform have been explored to overcome complications present in data streams today. Additionally, a possible revenue model has been discussed for the proposed database and platform. The overall costs of the ground segment provider will be in the range of €13,025 to €43,417. Through these decisions all ground segment requirements have been fullfilled.

9 Propulsion

Despite being put off during the midterm review, a new orbit reintroduced the necessity of a propulsion system. Hence, the following chapter will concern the means by which the propulsion system was selected. Based on new orbit requirements, a new trade-off and sensitivity analysis was conducted.

9.1. Orbit Requirements

In Chapter 7 it was given that the ΔV budget for the mission is 643.52 - 482.64 ms^{-1}. For the sake of this analysis, only the upper bound will be treated, as scaling down is easier than scaling up. Furthermore, a preliminary thrust T value and total impulse J have to be determined, as it is an integral parameter when choosing a propulsion system. Since the propulsion system's only task is to counteract the aerodynamic drag the satellite is experiencing, it is assumed that $T = F_D$. As F_D and J have already been determined in Chapter 7, the value for T is given to be 0.15 mN and J was found to be 9652.76 Ns.

Based on these values, it was concluded that the propulsion system would need to be an electric propulsion system. During the previous design phases, electric propulsion was neglected, as it did not bring along enough benefits at the previous altitude (Canosa et al., 2021a). Nonetheless, a chemical propulsion system would be too big and the repeated firings, which would be necessary to maintain the orbit, would possibly disrupt the payload. Nonetheless, the system that "won" the trade-off in the midterm, will also be used in the trade-off for comparison sake and to make sure that the new decision makes sense.

9.2. Propulsion System Trade-off

As aforementioned, new electric propulsion systems were considered, but also the previously selected propulsion system was considered for the new trade-off. The results can be found below in Table 9.1.

	T **[mN]**	I_{sp} **[s]**	J **[Ns]**	**Mass [kg]**	**Power [W]**	**Dimension [mm]**	**Volume [U]**
100 mN HPGP [1]	30 - 100	196 - 209	>9600	3.9	6.3 - 8	55 + system	$\approx$ 1.5 U
ENPULSION NANO [2]	0.01 - 0.35	2000 - 6000	>5000	0.9	8 - 40	100 x 100 x 82.5	$\approx$ 1 U
multiFEEP [3]	0.001 - 0.12	2600 - 8500	<13000	0.28	0.4 - 19	90 x 45 x 45	$\approx$ 1 U
NPT30-I2 [4]	0.3 - 1.1	<2400	<9500	1.7	35 - 65	93 x 93 x 155	$\approx$ 1.5 U
RIT μX [5]	0.05 - 0.5	300 - 3000	10000	0.44	<50	78 $\varnothing$x 76	0.4 U

Table 9.1: New trade-off table with electric propulsion systems

It is of significance to mention that J for the HPGP model was assumed to always be greater than the previously mentioned threshold, as the possible impulse depends on how much fuel is used. The weights for the trade-off can be found below in Table 9.2. This time, thrust and total impulse were chosen to be of the highest importance. This was derived from the fact that the propulsion system's main job is to provide orbit maintenance, and as such needs to be able to deliver the necessary thrust (and even a little bit more, in case

[1] URL https://satsearch.co/products/ecaps-100-m-n-hpgp-thruster [cited 29 Nov 2021]
[2] URL https://satsearch.co/products/enpulsion-enpulsion-nano [cited 10 Jan 2022]
[3] URL https://satsearch.co/products/morpheus-space-multi-feep [cited 10 Jan 2022]
[4] URL https://satsearch.co/products/thrustme-npt30-i2-1-5u-electric-propulsion-system [cited 10 Jan 2022]
[5] URL https://satsearch.co/products/airbus-defence-and-space-rit-u-x [cited 10 Jan 2022]

the propulsion system cannot fire for a short period of time), while also being able to provide this thrust over the course of the mission. Following these parameters, power was chosen to have the second-highest rating. As the power budget is very tight, it seems logical to try and restrict the system from consuming too much power.

Lastly, volume and I_{sp} were ranked the lowest. As the satellite does not have any restrictions on it's size the actual volume of the system does not matter too much. Nonetheless, it is beneficial to not select a system that would grossly increase the size of the satellite. The I_{sp} is relevant for knowing how efficient the engine thrusts and hence how much propellant mass m_p has to be used. Similar to volume, there is no direct restriction for the satellite, but it would be favorable to limit it.

Parameter	**Weight**
Thurst	5
I_{sp}	3
J	5
Power	4
Volume	3

Table 9.2: Associated weights for the new propulsion system trade-off

Similar to how it was done in (Canosa et al., 2021b), the weights were given a value from 1 (being the lowest) to 5 (being the highest), based on how relevant to the trade-off they were deemed. In the trade-off itself, each parameter received a score from 1 (worst) to 10 (best), which was then multiplied with the associated parameter weight. The results of the trade-off can be found in Table 9.3.

		Thrust	I_{sp}	J	**Power**	**Volume**	**Total**
	Weights	5	3	5	4	3	
Reference Model							
100 mN HPGP	**Score**	2	5	9	9	8	
	Weighted	10	15	45	36	24	130
ENPULSION NANO	**Score**	10	9	9	6	9	
	Weighted	50	27	45	24	27	173
MultiFEEP	**Score**	5	9	10	10	9	
	Weighted	25	27	50	40	27	169
NPT30-I2	**Score**	5	7	7	7	8	
	Weighted	25	21	35	28	24	133
RIT muX	**Score**	10	7	8	7	10	
	Weighted	50	21	40	28	30	169

Table 9.3: New propulsion system trade-off

To briefly elaborate on the given scores; the ENPULSION NANO and the RIT μX both ranked highest in thrust, as they were the only two that were able to provide thrust within the necessary range. The HPGP model's thrust was too high, whilst the other two models did not provide enough thrust (which was still considered to be more favorable as too high thrust would propel the satellite out of orbit). For I_{sp} the highest values were ranked highest. The main motivation behind this ranking was, that the higher the I_{sp} the more efficiently the propellant would be used, which is beneficial to the weight. A similar ranking was done for total impulse, as a higher J would guarantee completion of the mission.

The power ranking was done based on how much power would be consumed by the system. For this category, the MultiFEEP was significantly better than the other models due to its minimal consumption, but also the HPGP model was ranked highly. Nonetheless, it should be noted that for the HPGP model, the power

consumption was only for the thruster, not the feed system, which would also increase the power consumption. Lastly, the volume, the lowest weighted category, was simply based on how large the system would be. For this the RIT μX was the best, whilst the HPGP and NPT30-I2 model were ranked the lowest.

9.2.1. Sensitivity Analysis

From the initial trade-off, it can be seen that the ENPULSION NANO scored the highest. Nonetheless, it is valuable to conduct a sensitivity analysis in order to conclude that this system is also the best match. To conduct this analysis, 8 more trade-offs were made and put up for comparison. Thurst and J were both weighted lower (4), whilst all the other parameters were weighted one higher and one lower. This was done to account for possible misjudgement of the weighting in the earlier trade-off. All of the trade-off outcomes were listed next to each other and the normal case. From there, an average ranking number was determined. The trade-off tables were omitted, but the results and the final ranking can be seen in Table 9.4 below.

	Base Case	**I_{sp} Higher (4)**	**I_{sp} Lower (2)**	**Thrust Lower (4)**	**Power Higher (5)**	**Power Lower (3)**	**J Lower (4)**	**Volume Higher (4)**	**Volume Lower (2)**	**Rank**
100 mN HPGP	130	123	101	119	123	101	121	123	101	5.00
ENPULSION NANO	173	182	146	163	179	167	164	182	164	1.25
MultiFEEP	169	178	140	164	179	159	159	178	160	2.38
NPT30-I2	133	140	112	128	140	126	126	141	125	4.00
RIT muX	169	176	146	159	176	162	161	179	159	2.38

Table 9.4: Sensitivity analysis for the propulsion system trade-off

From the sensitivity analysis, it becomes evident that the winner is the ENPULSION NANO. Overall, this system ranks first most, and only ever draws on comparisons. This means that for further evaluation, this propulsion system will be considered. As final remark, it is worth mentioning that the HPGP propulsion system is greatly out-ranked by the other propulsion systems. This reemphasises the conclusion that the shift to an electric propulsion system is more favorable.

9.3. Propulsion System

Following the trade-off and sensitivity analysis the ENPULSION NANO was selected as propulsion system for the satellite. The propulsion system is an ion thruster that uses the concept of field-emission electric propulsion (FEEP), which is an electrostatic propulsion system. The advantage of these propulsion systems is that they have a relatively low power consumption compared to other electric propulsion systems. In addition to that, they do not produce a strong electromagnetic pulse during operations, which could damage the on-board computer (Bock et al., 2014).

Leading on, the ENPULSION NANO system has also been successfully verified in orbit in 2018 with 37 propulsion units launched by mid 2020 and over 80 units having launched by mid 2021 (Enpulsion, 2018) (Enpulsion, n.d.). Since this propulsion system has been developed in corporation with ESA under a 15 year contract, it is a mature technology that can provide 20 000 hours ($\approx$ 2.2 years) of thrust without degrading in performance (Enpulsion, n.d.). As propellant, used for the ionization, the ENPULSION NANO uses Indium. It is given that for this specific configuration, 220 $g \pm$ 5% (Enpulsion, n.d.). Further comments on the propellant with respect to the requirements are given in Section 9.3.2.

9.3.1. Design Point Selection

After having selected an appropriate propulsion system, it is essential to determine T and I_{sp} configuration such that a power budget can be estimated from it. This can be done using a performance graph which is shown in Figure 9.1. The diagram indicates which values of T, I_{sp} and J are possible and what the required power would be. The aforementioned constraints of T and J are indicated by red-dashed lines. Possible design points for the mission can be selected from the area enclosed by the blue rectangle.

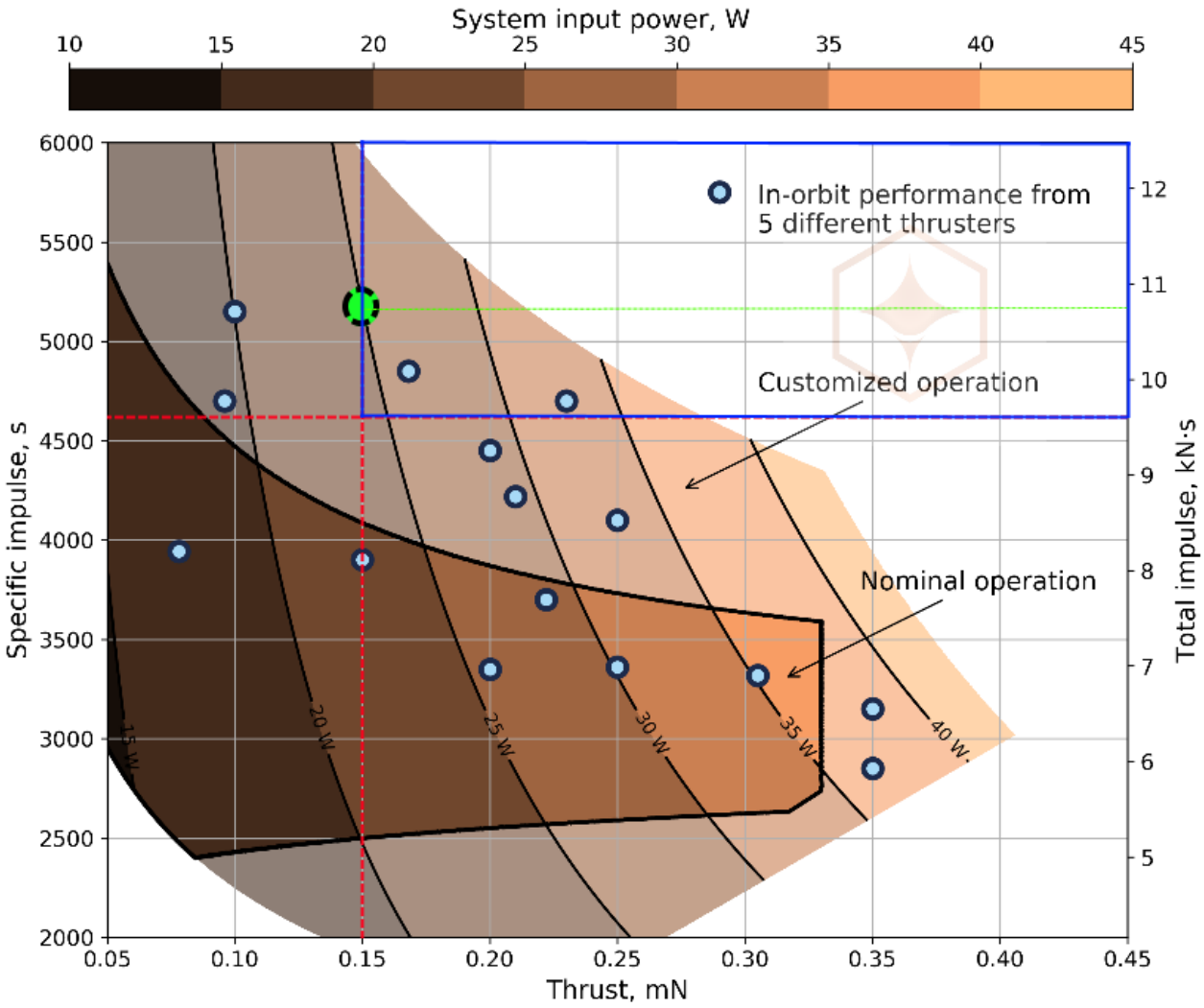

Figure 9.1: Mission configuration of the thruster based on the performance diagram (Enpulsion, 2018)

The design point that was chosen is indicated by the green dot on Figure 9.1. The point correlates to a thrust of 0.15 mN with a total impulse of approximately 10.75 kNs. This value is about 1.1 times the necessary J as stated above and thus the satellite will have a sufficient reserve. Furthermore, it is of interest to observe that the point lies on the 25 W power line.

The design point was chosen such that with the propulsion system can operate along the constant power line of 25 W. This way, the thrust can be varied upwards to up to 0.16 mN if needed, while still conserving the minimum J budget of 9.6 kNs. This can be used as an emergency solution to get back into orbit in case the satellite unexpectedly shuts off the thursters for a certain time. At the chosen design point, the thruster will be able to provide an I_{sp} of approximately 5170 s and if the thrust is scaled up, it can still provide a I_{sp} of approximately 4620 s. Lastly, in case the propulsion system is switched off for various reasons, it will only require 3.5 W for standby power mode.

9.3.2. Compliance to High-Level Mission Requirements

Finally, it is of interest to analyse the requirements for the propulsion system that were outlined in (Canosa et al., 2021a). A table summarising the achieved requirements is given below Table 9.5.

Identification	Requirement	Full Filled
AIS-TL-REQ-03	The operational lifetime shall span 2 years	✓
AIS-TL-REQ-04	The mission shall refrain from using radioactive materials	✓
AIS-TL-REQ-05	The satellite shall be comprised of commercial off-the-shelf components	✓
AIS-TL-REQ-16	The use of European components should be prioritized	✓
AIS-TL-REQ-23	The propulsion system shall use green propellant	
AIS-PROP-REQ-03	The propulsion system shall be able to maintain the spacecraft's orbit	✓
AIS-PROP-REQ-04	The propulsion system shall be able to provide the spacecraft with an end of life maneuver	✓

Table 9.5: Overview of requirements

As can be seen, the only requirement that is not directly full filled is AIS-TL-REQ-23. The use of green propellants was significantly inhibited due to the change in orbit, which subsequently required the switch to an electric propulsion system. The chosen propulsion system makes use of Iridium, which is not a green propellant. Despite this, there is an argument to be made that the chosen propulsion system is ”greener” than the LMP-103s that would have been used in the HPGP propulsion system. As Professor Cervone (assistant professor at TU Delft) mentioned, it is important to assess in which aspect the propulsion system is ”green”. Hence, a small comparison will be given below.

$$\frac{J}{g_0 I_{sp}} = m_p \tag{9.1}$$

Using Equation 9.1, where g_0 is the standard gravity, it is possible to estimate the necessary propellant mass for the propulsion system. Using upper bound for the HPGP from Table 9.1 and the chosen design point the equivalent propellant masses were calculated. The ENPULSION NANO will require 0.19 kg of Iridium while the HPGP system would require 4.71 kg of LMP-103s. The mass margin is significant and helps to demonstrate that for this specific mission, the use of green propellants is actually an issue. Apart from the fact that it would not be a COTS component, it would severely impact the mass and volume of the satellite. In addition to that, the use of a chemical propulsion would inhibit the payload quality. Thus, by choosing a less green propellant the propulsion system guarantees an overall more green solution.

10 Communications System

Having determined that the communications will be split into two separate systems, namely a UHF antenna and transceiver to transmit telemetry as well as alert notifications and an S-band communications system to transmit the images from the payload down to the ground station, this section will determine the final link budgets of the communications system.

10.1. Communications Approach

The approach to designing the communications system starts with defining the maximum bit error rate that is appropriate for space travel. The bit error rate (BER) is the probability that a bit being transmitted is received and decoded incorrectly. Assuming that a single bit error can corrupt an entire transmission, the BER will have to be low enough to assume that over a second of transmission, there will be no errors. Through using this value, modulation theory can be used to calculate an energy per bit ratio (EbN0) which will meet this value of the bit error rate for the selected modulation method. This value represents a base minimum value that must be met by the communications systems.

The next step is to start calculating the EbN0 of the system. The first step in doing this is finding the maximum bit rate that will be required by the system. As the granularity of transmitters and transceivers are not fine enough to exactly achieve this value, it will be rounded up to the nearest possible transmission rate. This data rate can then be calculated into a bandwidth through selecting a modulation method. Once this is done, the EbN0 equation can be used by inputting variables for the components selected, ground stations selected, and position of the satellite. This EbN0 can finally be compared to the theoretical minimum required (plus an additional 3dB safety factor). If successful, the communications system is complete.

10.2. Communication Flow

The communication flow describes the sequence of data, from both the satellite down to the ground station, and vice versa. This section is pulled from the functional flow diagram, but has been changed since the last iteration to add the new communication line between the payload and the s-band antenna.

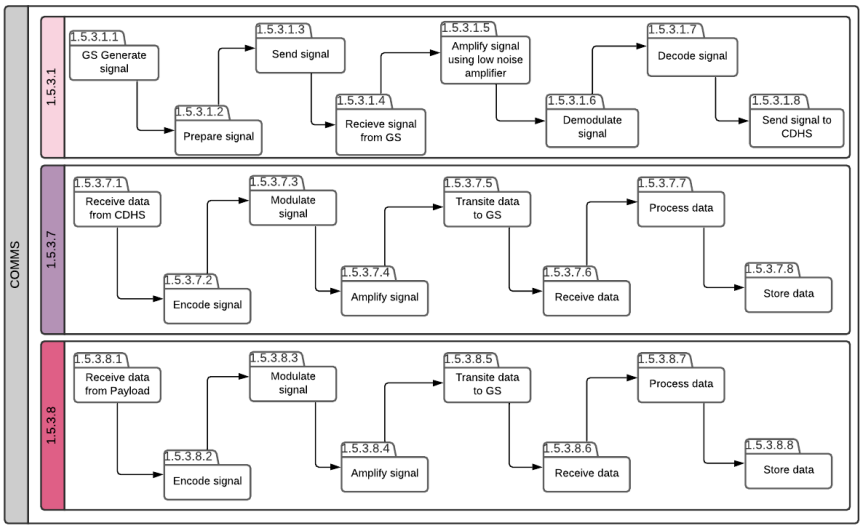

Figure 10.1: Communications Flow Diagram

10.3. Ground Station and Bandwidth

This section will talk about the link between the satellite communications systems and the ground stations. This includes calculating the distance between the two, as well as finding the minimum contact time between the two as well.

10.3.1. Ground Station Distance

To calculate the distance between the satellite and the ground station, several formulas can be used. To remove all orbital parameters such as the inclination, mean anomaly, etc, a calculation can be used to relate the elevation of the satellite with respect to the ground station, and its distance. This equation will therefore hold for all passes of the satellite, be it a pass just over the horizon or a direct overhead pass. A drawing to show the geometry of the satellite and the ground station can be seen below:

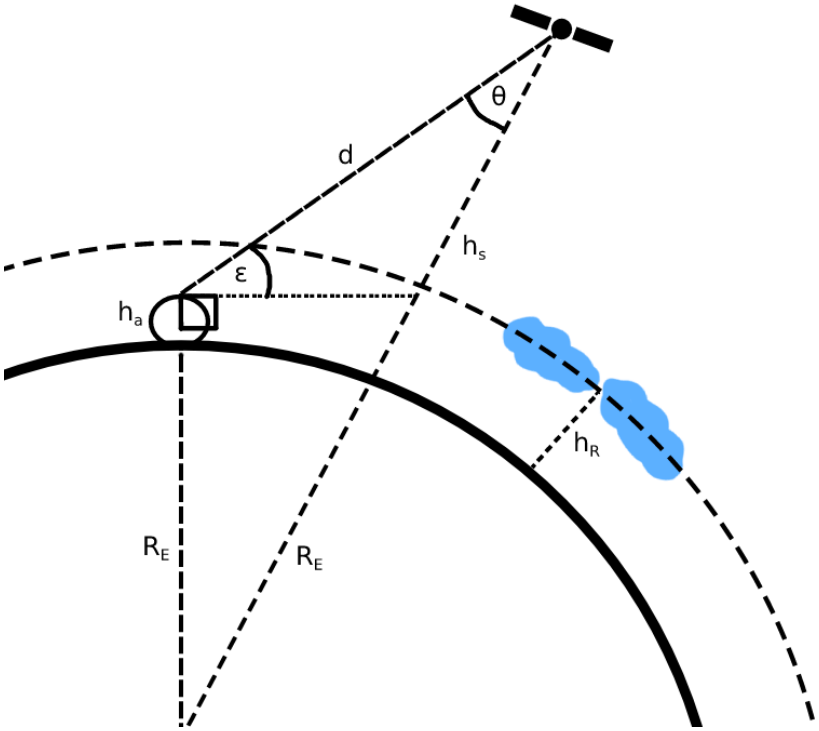

Figure 10.2: Distance between satellite and ground station as a function of elevation

The distance between the satellite and the ground station, otherwise known as satellite slant range, can be calculated using the following formula:

$$d = \sqrt{(B \cdot cos(\epsilon))^2 + r^2 - B^2} - B \cdot cos(\epsilon) \tag{10.1}$$

where ϵ is the elevation of the satellite, R_E is the radius of the Earth, h_a is the height of the ground station, h_s is height of the satellite, and h_R is the height of the rain clouds. Following this, $B = R_E + h_a$, and $r = h_s + R_E$. Later in this section, the height of the satellite will be replaced by the height of the rain clouds to calculate the distance the signal must travel through rain clouds to calculate the rain losses.

10.3.2. Ground Station Contact Time

The ground station contact time is important, as it allows for a calculation to be made for the required bit rate, which in turn allows the required bandwidth of the signal to be found. Through the same simulation run in GMAD as in Chapter 7, an output for the ground station contact time could be made. The input parameters for this were the ground station latitudes and longitudes, as found in Chapter 8, as well as the elevation of both ground stations. Next, the minimum elevation angle was input, which is dependant on the environment surrounding the ground station. After these values are input, GMAD can run a simulation and outputs every contact that the satellite makes with the ground stations and the contact times. The minimum value of the list of contact times is extracted, and then used as the most extreme case to calculate the data rate. This minimum contact time is found to be $143.4s$, which represents a very low elevation pass of the satellite. The payload

data to be transmitted is found from Chapter 6 ($56.2Mb$). In order to compensate for packet overhead, a 50% margin is added to the data, meaning the number of bits to transmit is now $84.3Mb$. Therefore the maximum data rate required for the payload data transmission is found to be $509.4kb/s$. Due to the granularity of the transmitter, this value cannot be exactly reached, therefore the data rate will be rounded up to $600kb/s$.

What can also be found is the average contact time that will be available during the mission. This is useful for the modes of operation, and the values for which are $180.2s$ for the North Station and $185.1s$ for the South Station.

10.4. Modulation methods

Signal modulation is the encoding of a digital signal by superimposing onto a high frequency carrier wave. There are several methods of doing this, such as amplitude modulation, frequency modulation, phase modulation, or a combination of all three. In general, the more complex modulation methods are able to transmit at much higher data rates, but require more specialised technology and high signal to noise ratios. The simple modulation methods are highly reliable and efficient, but are not as bandwidth efficient. Therefore, when selecting the modulation method, a trade-off between data rate and signal to noise ratio must be made. More information can be found in the later sections about the bandwidth spectral efficiencies and the selection of modulation methods.

Energy per Bit to Noise Power Spectral Density Ratio (Eb/No)

The EbN0 is an important parameter as it essentially describes how much noise there is allowed to be in a signal before it cannot be read reliably any longer. This value is preferred to be as low as possible, as it allows for less strict requirements for the communications system. This value is usually expressed in decibels.

Bit Error Rate

The bit error rate (BER) is the probability that when a modulated bit gets demodulated, the noise in the system causes a certain threshold to be crossed and the bit is decoded incorrectly. Therefore, this value is always preferred to be as low as possible. As a single bit error can render an entire transmission void, a value is calculated to ensure that for every second that a signal is sent, the number of bits that have an error is 0. This is known as allowable short term error performance, and the formula for calculating this can be seen below.

$$N_{bit_allow} = R_b \cdot P_{b_req} \tag{10.2}$$

Where N_{bit_allow} is the allowable number of bit errors, R_b is the bit rate, and P_{b_req} is the required BER. Substituting in the values of the bit rate of $9.6kb/s$ for the UHF system and $0.6Mb/s$ for the S-band system, the following table can be created.

Table 10.1: Number of bits in error during one second of transmission

Bit Rate	Required BER	Allowable Number of Bits in Error
9.6 kb/s	10^{-3}	10
	10^{-4}	1
	10^{-5}	0
1 Mb/s	10^{-3}	1000
	10^{-5}	10
	10^{-8}	0

Using this and knowing which modulation method will be used, the normalized signal/noise ratio can be calculated. An example of such a relation is for example, using the GMSK modulation (which will be used for the UHF communications system). This bit error probability for GMSK can be found using the following equation:

$$P_e = Q\left(\sqrt{\frac{2 \cdot \alpha \cdot E_b}{N_0}}\right) \tag{10.3}$$

Cappiello, 2019

where $Q(t)$ is found to be the Q-function, $\alpha = 0.68$ is the optimal value for transmissions using GMSK Cappiello, 2019. Plotting this value of the BER for a range of Eb/No, the data can then be interpolated to find a value of the normalised signal/noise ratio for a BER value of 10^-5. For GMSK, this value can be found to be $14.86dB$. A plot of several viable modulation methods can be found below:

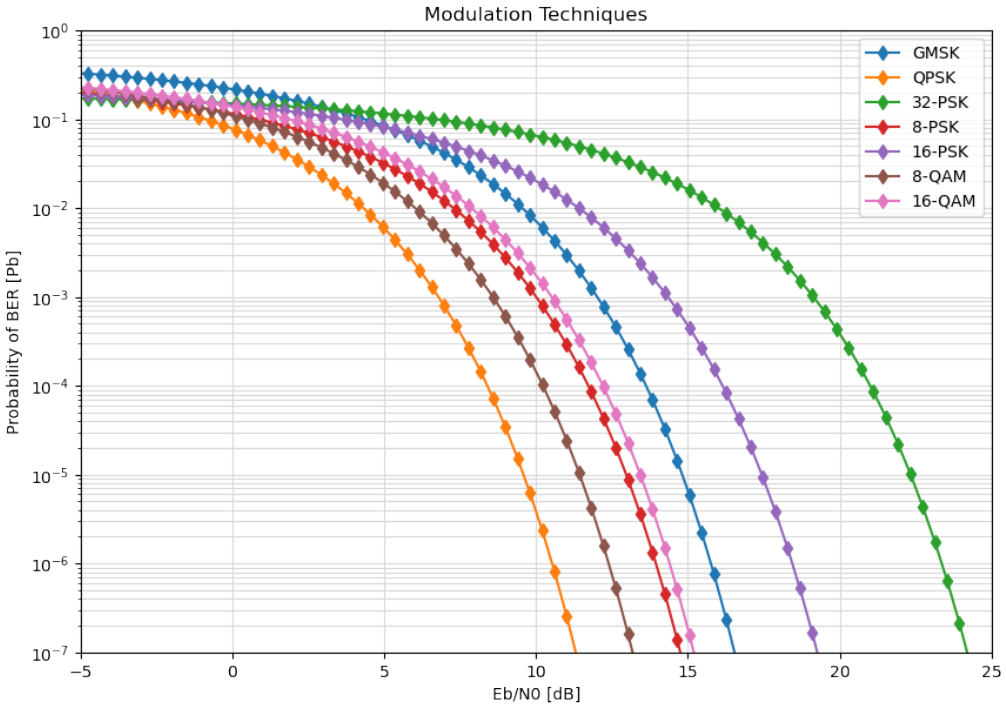

Figure 10.3: BER vs Eb/No for several Modulation methods

Bandwidth Spectral Efficiency

Through using the data rate calculated earlier, the bandwidth of the signal can be found. The maximum value of the bandwidth is equal to the bit-rate, but when considering the price of bandwidths, especially in the more congested channels, the more bandwidth required increases the cost of renting the frequency bands increases significantly. This is why modulation is used. Modulating a signal can reduce the required bandwidth of a signal. Each modulation method has a certain bandwidth spectral efficiency, which in essence describes how many bits can be send per Hz of bandwidth. The most simple modulation methods have a bandwidth spectral efficiency of 1, that is that only one bit can be sent per Hz of the signal, eg: binary phase shift keying (BPSK). The more advanced modulation methods can transmit up to 6 bits/s/Hz, however these methods are much more complex and require much higher EbN0 due to the sensitivity of the modulation. A table containing several modulation methods and their respective spectral efficiencies can be found below:

Table 10.2: Modulation Method Spectral Efficiencies

Modulation Method	Spectral Efficiency (bits/s/Hz)
FSK	1
BPSK	1
GMSK	1.35
QPSK	2
16-QAM	4
64-QAM	6

10.4.1. Selection of Modulation Methods

Due to the use of COTS transeivers and GSaaS, the available selection of modulation methods is somewhat limited. Both the transceiver and the GS must be able to communicate using the same modulation method. It has therefore been found that for the UHF COMMS system, a modulation method of GMSK has been selected, due to the highly reliable method, as well as a high spectral efficiency. For the payload COMMS system it has been selected to use QPSK. This allows for a 30% reduction of the bandwidth due to the spectral efficiency of 2. QPSK is also a relatively simple and reliable method and requires a low EbN0 to meet the BER probability of 10^{-8}.

10.5. Link Budget Calculations

The link budget is the most important parameter when describing a communications system. To relate the EbN0 of a system, a new parameter must be introduced. It is the carrier to noise (C/N) ratio. The C/N ratio is a ratio that describes how much energy from the noise there is in a signal, compared to the energy of the actual useful data in that signal. The carrier to noise ratio is distinct from the signal to noise ratio, as it defines the signal before it has been demodulated and decoded. The C/N ratio can be related to the EbN0 through the following equation:

$$\frac{C}{N} = \frac{E_b/T_b}{N_0 B} = \frac{E_b R}{N_0 B} \tag{10.4}$$

where R is the data rate and B is the bandwidth. Substituting this equation into the signal to noise ratio equation, a calculation can thus be made to calculate a communication systems EbN0. All values are converted to decibels to tidy up and factorise the different components of the equation:

$$[E_b N_0]_{dB} = [P_{EIRP}]_{dBW} - [L_{FS}]_{dB} - [L_{other}]_{dB} + \left[\frac{G_{AR}}{T_{sys}}\right]_{dB/K} - [k]_{dBW/Hz/K} - [B_n]_{dBHz} \tag{10.5}$$

Where:

- $[P_{EIRP}]_{dBW}$ = Effective Isotropic Radiating Power
- $[L_{FS}]_{dB}$ = Free Space Loss
- $[L_{other}]_{dB}$ = Further Losses
- $\left[\frac{G_{AR}}{T_{sys}}\right]_{dB/K}$ = Receiving Antenna Gain-to-Noise Temperature
- $[k]_{dBW/Hz/K}$ = Boltzmann Constant
- $[B_n]_{dBHz}$ = Bandwidth

The effective isotropic radiating power comes as a result of the type of transmitting antenna, receiving antenna gain-to-noise temperature is a constant that is given by the receiving antenna, and the bandwidth is a result of the data rate and modulation method used. The free space loss and other further losses are explained further below.

10.5.1. Losses

Loss is the decrease in power of a signal as it propagates through different mediums as they are exposed to outside interference's. The most significant loss is the free space loss, followed by the rain cloud losses. There is an infinite number of losses that can be considered in a transmission system, but most are marginal and can be neglected.

Free Space Losses

The free space loss is simply the decrease in power density of a signal due to the free-space propagation of the wave. This decrease follows the inverse square law, and can be written below:

$$[L_{FS}] = \left(\frac{4 \cdot \pi \cdot d}{\lambda}\right)^2 \tag{10.6}$$

or when written in decibel form:

$$[L_{FS}]_{dB} = 20 \cdot log_{10}\left(\frac{4 \cdot \pi \cdot d}{\lambda}\right) \tag{10.7}$$

where d is the distance from transmitting to receiving antenna, and λ is the wavelength.

Pointing Losses

Pointing losses of a communication system can be attributed to the misalignment of the transmitting and receiving antennas, which is known as antenna misalignment losses. Pointing losses also include the polarisation mismatch between the two antennas. Both the misalignment losses and the polarisation mismatch losses cannot be calculated, but are instead obtained from historical data (Roddy, 2011). For all calculations, each value was assumed to equal $0.3dB$, for a total of $0.6dB$ in losses.

Rain Cloud Losses

Rain attenuation is minimal at frequencies below 1GHz, but once higher frequencies are used, they can become quite significant. As an estimation, at 10GHz during a heavy downpour, the attenuation can reach up to $1dB/km$ [1]. A model for calculating the rain cloud losses have been provided by the International Telecommunication Union (ITU), more specifically P.837 and P.839. The specific attenuation is described as:

$$\gamma_R = k \cdot R^{\alpha} \tag{10.8}$$

("ITU-R P.838-3", 2013)

where γ_R is the specific attenuation measured in dB/km, and k and α are coefficients as a function of frequency. As the communication systems will be using circular polarisation, k and α can be calculated using the following two calculations:

$$k = (k_H + k_V + (k_H - k_V) \cdot cos^2(\theta) \cdot cos(2\tau))/2 \tag{10.9}$$

("ITU-R P.838-3", 2013)

$$\alpha = (k_H\alpha_h + k_V\alpha_V + (k_H\alpha_H - k_V\alpha_V) \cdot cos^2(\theta) \cdot cos(2\tau))/2k \tag{10.10}$$

("ITU-R P.838-3", 2013)

where the values k_H,k_V,α_H and α_V can be interpolated from given tables for a given transmission frequency. The elevation angle is again represented here as θ and for circular polarisation, τ is equal to $45°$ ("ITU-R P.838-3", 2013). Once the specific attenuation attenuation is known, the total attenuation can be calculated using the following formula:

$$[L_{rain}]_{dB} = \gamma_R \cdot h_R = \gamma_R \cdot (h_0 + 0.36km) \tag{10.11}$$

where h_R is the mean annual rain height alive mean sea level, and h_0 is the mean annual $0°$C isotherm height above mean sea level ("ITU-R P.839-4", 2019). The value for h_R is obtained through a data-set, in which certain coordinates can be provided to interpolate the data, of which are input as the latitude and longitude of the two ground stations. A plot of of this data set including the points of the two ground stations for reference can be found below.

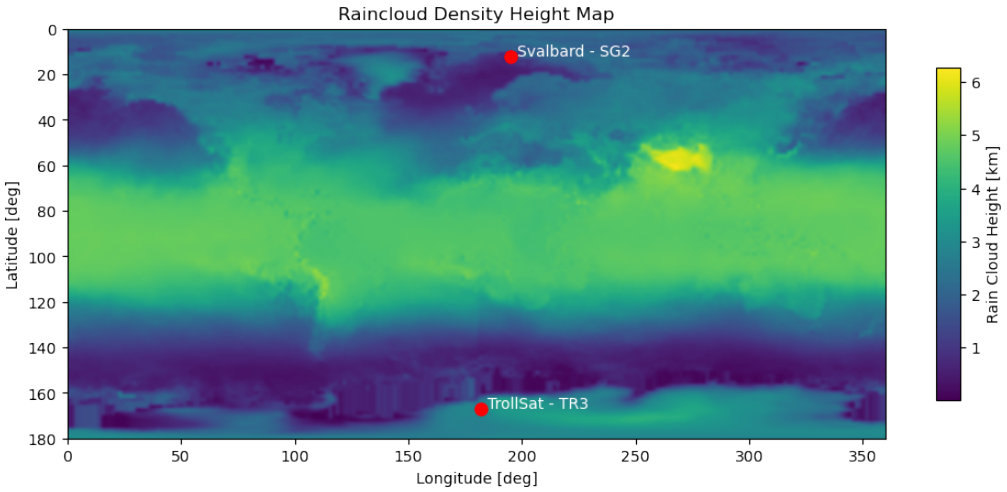

Figure 10.4: Rain cloud height

[1] URL https://www.everythingrf.com/community/what-is-the-impact-of-rain-on-rf-signal-propagation [cited 12 Jan 2022]

This height of the rain is of course only when considering a direct overhead transmission of the data. In reality, the worst case scenario includes a low elevation angle pass, and therefore the distance between the ground station and the height of the rain cloud between the ground station and satellite has to be calculated. This is simple enough, as Equation 10.1 can be used and instead of using the height of the satellite, h_R can be used instead. This value of the 'height' of the rain cloud can thus be used and input into Equation 10.8, which ultimately gives a final result for the rain losses.

10.5.2. Component Selection

When looking at Equation 10.5, the only unknown input now is the effective isotropic radiating power. This is fortunately a value that can be obtained from data-sheets from the selected off the shelf antenna. When looking at these values, a transmitter and an antenna will have different maximal output powers, therefore the lower of the two is used for all calculations as this is the limit of the combination of the particular two components.

S-Band Transmitter Selection

The selection of the S-Band transmitter was conducted by pulling a large list of existing components and then comparing to see which could be implemented into the system the most readily. The most important criteria was that the system could communicate to the CDHS system, as well as communicate with the payload data storage to be able to independently pull the data. Furthermore, the modulation method that the transmitter can implement must be able to be supported by the ground stations. Finally, the transmitter must also be able to meet the maximum data rate that would need to be reached to transmit the data. There were two possible transmitters to meet these criteria, and the selected one chosen was done so due to the power requirement being half (6.5W vs 15W). Furthermore, the maximum bit rate achievable of the higher power transmitter is ten times that of the required 0.6Mbit/s, therefore the design would be over engineered. Therefore, the final selected transmitter is the DP-CRF-5615 S-Band Transmitter, in combination with the CubeSat S-band patch antenna by ISIS.

The following table shows th

Combined S-Band Specifications

Table 10.3: S-band system specifications

Specification	Value	Unit
Transmitter		
Name	DP-CRF-5615 S-Band Transmitter	-
Frequency Range	2200 - 2500	MHz
Modulation	BPSK, QPSK, OQPSK	-
Peak Power	6.5	W
RF Output Power	27-30	dB
Interfaces	SPI for payload, I2C for command	-
Maximum Data Rate	2	MBps
Antenna		
Name	CubeSat S-Band Antenna ISIS	-
Frequency Range	2200 - 2290	MHz
Gain	6.5	dBi
RF Output Power	4	W

UHF Transceiver Selection

Similarly to the S-band transmitter, the UHF transceiver must be able to be implemented into the CDHS system and the ground station network. There was more flexibility in this design, as the UHF systems are highly reliant and tested, therefore the selection between different transceivers was done by finding the most efficient one (the one with the highest output radio frequency output power to input power ratio). This was found to be the NanoCom AX100 UHF transceiver, in combination with the ISIS deployable antenna system for 6U/12U CubeSats.

Combined UHF Specifications

Table 10.4: UHF system specifications

Specification	Value	Unit
Transmitter		
Name	NanoCom AX100	-
Frequency Range	430 - 440	MHz
Modulation	GFSK, GMSK	-
Peak Power	4.2	W
RF Output Power	24 - 30	dB
Interfaces	I2C, UART, CAN	-
Maximum Data Rate	38.4	kbps
Antenna		
Name	ISIS Deployable Antenna System for 6U/12U CubeSats	-
Frequency Range	430 - 440	MHz
Gain	0	dBi
RF Output Power	2	W

10.5.3. Performance Analysis

Now that all fixed values had been obtained, the only free variable when filling in Equation 10.5 is the elevation angle of the satellite. By inputting a range of values from $15°$ (the minimum elevation angle) and a maximum of $90°$, the performance of the communications can be conducted for all possible locations of the satellite with respect to the ground station.

Finally, for all calculations below, the worst case performance can be defined. This is the case for when the satellite is in communications with the Antarctic ground station, TrollSat TR3. This is because this ground station has lower gain and a higher temperature compared to the Svalbard SG2 ground station, as well as having higher rain cloud height. Next, the carrier frequency selected for the payload data downlink has been selected to be $2290MHz$, as this is the highest frequency band allocated for S-Band and involves the highest losses that can be encountered by the system.

COMMS Payload Downlink

Table 10.5: Link Budget S-Band, $e = 15°$

Payload Link Budget	Value	Unit
Contact Time	143.4	s
Frequency	2290	MHz
Maximum Bit Rate	0.6	Mb/s
Modulation Method	QPSK	-
Bandwidth	0.3	MHz
Free Space Loss	158.5	dB
Pointing Loss	0.6	dB
Polarisation Loss	0.3	dB
Rain Fade Loss	0.05	dB
Total Losses	159.5	dB
Gain Transmitter	6.5	dB
Gain Receiver	41.8	dB
Noise Temp Receiver	22.4	dB/k
Power Transmitted	0	dBW
Power Received	-111.2	dBW
Noise	-151.4	dB/k
Min EbN0	40.3	dB
Req EbN0	18.1	dB

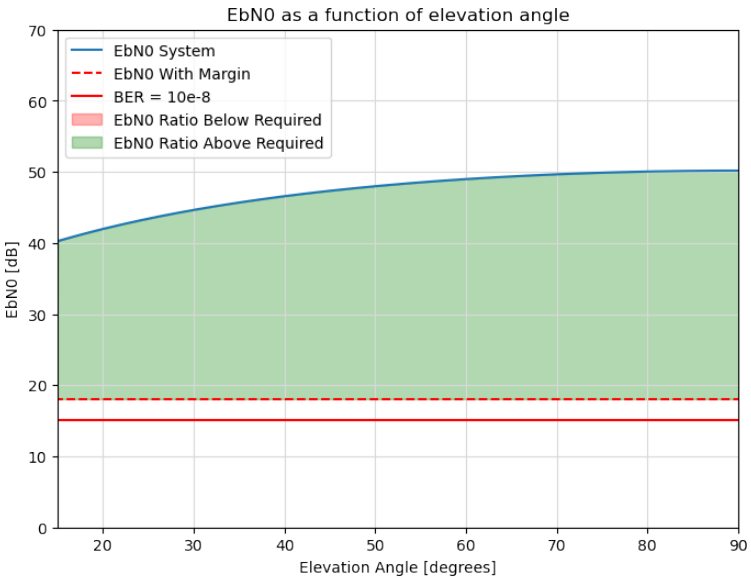

Table 10.6: S/N Ratio against Elevation Angle for COMMS Payload Downlink

UHF Telemetry Downlink

Table 10.7: Link Budget UHF Downlink, $e = 15°$

UHF Downlink Budget	Value	Unit
Contact Time	143.4	s
Frequency	436	MHz
Maximum Bit Rate	9600	b/s
Modulation Method	GMSK	-
Bandwidth	12960	Hz
Free Space Loss	144.1	dB
Pointing Loss	0.6	dB
Polarisation Loss	0.3	dB
Rain Fade Loss	0.01	dB
Total Losses	145.0	dB
Gain Transmitter	0	dB
Gain Receiver	41.8	dB
Noise Temp Receiver	22.4	dB/k
Power Transmitted	0.0	dBW
Power Received	-103.2	dBW
Noise	-165.1	dB/k
Min EbN0	61.9	dB
Req EbN0	16.6	dB

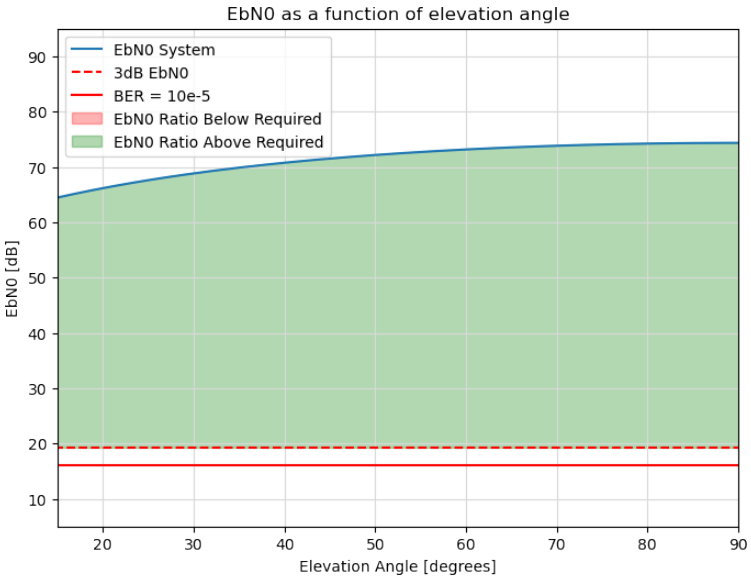

Table 10.8: S/N Ratio against Elevation Angle for UHF Telemetry Downlink

UHF Telemetry Uplink

Table 10.9: Link Budget UHF Uplink, $e = 15°$

UHF Uplink Budget	Value	Unit
Contact Time	143.4	s
Frequency	436	MHz
Maximum Bit Rate	9600	b/s
Modulation Method	GMSK	-
Bandwidth	12960	Hz
Free Space Loss	144.1	dB
Pointing Loss	0.6	dB
Polarisation Loss	0.3	dB
Rain Fade Loss	0.01	dB
Total Losses	145.0	dB
Gain Transmitter	15.5	dB
Gain Receiver	0	dB
Noise Temp Receiver	25.6	dB/k
Power Transmitted	10.0	dBW
Power Received	-119.5	dBW
Noise	-161.9	dB/k
Min EbN0	42.4	dB
Req EbN0	19.6	dB

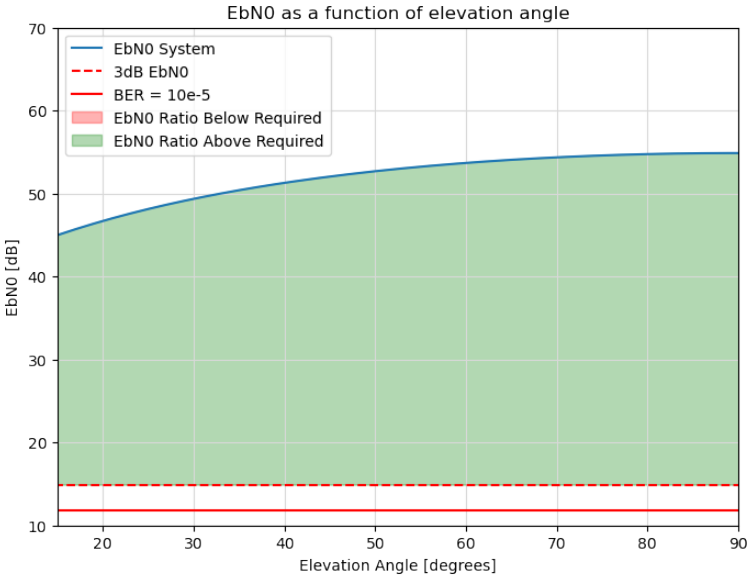

Table 10.10: S/N Ratio against Elevation Angle for UHF Telemetry Uplink

What can be seen from all three plots is that the signal is the weakest when the satellite is at its lowest elevation angle. This corresponds to the furthest away distance for the communications, as well as the furthest distance for the signal to pass through rain clouds. It is at this point that the calculated EbN0 must be above the EbN0 required (including the safety margin) required to reach a the respective BER seen in Section 10.4. As it can be seen, the communications system for both the UHF and S-Band antennas are able to meet this performance

specification, therefore for all passes and all elevations of the satellite over the entirety of the mission, the satellite is able to transmit the data down to the ground station when necessary.

10.6. COMMS Requirements

Now that the system had been fully designed, an analysis of the requirements set could be done, the results of which can be found in the table below. Several of the requirements have been changed and several more have been added since the inclusion of a communications system for the downlink of the payload data. Notably, requirements 8 to 14 have been removed and duplicated to independently include the UHF antenna requirements (req: 20-27) and the S-band antenna (req: 28-34).

Table 10.11: Communications Systems Requirements

Identification	Requirement	Requirement Met
AIS-COMMS-REQ-01	The COMMS shall be able to encode and decode GMSK and QPSK modulation.	✓
AIS-COMMS-REQ-02	The COMMS shall remain operational up to a total ionizing dose radiation level of 20 Krad.	✓
AIS-COMMS-REQ-03	The COMMS shall survive the launch environment.	N/D
AIS-COMMS-REQ-04	The COMMS shall be able to sustain temperatures between -20 and 70 degrees Celsius.	✓
AIS-COMMS-REQ-15	The COMMS shall not exceed a maximum mass of <tbd>g.	✓
AIS-COMMS-REQ-16	The COMMS shall take up a maximum of 1000 cm^3.	✓
AIS-COMMS-REQ-18	The COMMS system shall be able to process external signals to communicate with the CDHS.	✓
AIS-COMMS-REQ-19	The COMMS system shall be able to process signals from the CDHS to transmit to the Ground Control System.	✓
AIS-COMMS-REQ-20	The COMMS shall have a UHF antenna for telemetry up-link.	✓
AIS-COMMS-REQ-21	The COMMS shall have a UHF antenna for telemetry down-link.	✓
AIS-COMMS-REQ-22	The COMMS shall have a frequency of 436 MHz for telemetry up-link.	✓
AIS-COMMS-REQ-23	The COMMS shall have a frequency of 436 MHz for telemetry down-link.	✓
AIS-COMMS-REQ-24	The COMMS shall have a maximum telemetry up-link data rate of 9600 bit/s.	✓
AIS-COMMS-REQ-25	The COMMS shall have a maximum telemetry down-link data rate of 9600 bit/s.	✓
AIS-COMMS-REQ-26	The COMMS telemetry system shall transmit a maximum of 1 W during operational procedures.	✓
AIS-COMMS-REQ-27	The COMMS telemetry shall draw no more than 4.7W with 3.3V input voltage.	✓
AIS-COMMS-REQ-28	The COMMS shall have a S-band antenna for telemetry up-link.	✓
AIS-COMMS-REQ-29	The COMMS shall have a S-band antenna for telemetry down-link.	✓
AIS-COMMS-REQ-31	The COMMS shall have a frequency of 2210 MHz for payload data down-link.	✓
AIS-COMMS-REQ-32	The COMMS shall have a maximum payload data down-link data rate of 9600 bit/s.	✓
AIS-COMMS-REQ-33	The COMMS S-band system shall transmit a maximum of 1 W during operational procedures.	✓
AIS-COMMS-REQ-34	The COMMS S-band system shall draw no more than 6.5W with 3.3V input voltage.	✓

*Requirement AIS-COMMS-REQ-03 cannot be verified at this stage in the program, vibrational testing will be used to verify this test.

10.7. Recommendations

Hardware

One possible recommendation would be to find a payload transmitter that can reach a higher transmission rate. As it stands, the system can only transmit up to two images per pass. If another transmitter, for example the SWIFT-XTS, could be used, the data rate could be increased up to $10Mb/s$, which would allow for a transmission of up to 14 different images. However, this would increase the power consumption of the satellite, as more images would have to be processed and the power of the S-band transmitter would increase from $6.5W$ to $12W$. This would also increase the bandwidth required, which would increase the cost of the system to operate.

Furthermore, what could also be considered is the use of the S-band antenna to transmit the telemetry and command data. This would remove the need for the UHF system. The implications of this have already been explored in Chapter 8.

One final recommendation, in partner with the recommendations made in Section 13.7, is the possibility of flying in a higher orbit. This would substantially increase the time that a signal could be transmitted, increasing

the number of refineries that could be imaged. Due to the high overhead for the EbN0 vs required EbN0, the system could easily support more losses incurred by flying at a higher altitude. This would however have implications on the pointing accuracy of the satellite, but due to the use of a patch antenna ($3dB$ drop-off at $100°$) the pointing accuracy would not have to be significantly altered. The increased orbit could alternatively allow for the transmission of payload data in a lower frequency band, such as UHF, making the system much less complex and reliable.

Software

To improve the software, the estimates for the pointing losses could be simulated to meet the pointing accuracy of the ADCS system, rather than take a estimates. Additionally, an optimisation program could have been run to run an array of inputs so that the most optimal parameters (such as frequency, modulation method, bit rate, etc) for a variety of combinations of hardware could also have been created. Finally, a full simulation of the transmission could be created to see whether the EbN0 is high enough for error free transmission.

11 Command and Data Handling System

The Command and Data Handling System, CDHS for short, is essentially the brain and nervous system of the satellite. In this chapter first the selection of the OBC will be discussed in Section 11.1. More information about the Antelope OBC is given in Section 11.2. And a description of the different CDHS elements and their uses are given in Section 11.4. A part that can be seen as a shared venture between CDHS and Payload is the Payload processor, more about this subsystem can be found in Section 11.3. This will be linked to the implementation of the AI on the CDHS in Section 11.5. After a description of the subsystems, a more elaborate description of the data protocols that are to be used is given in Section 11.6, this section concludes with the electrical communication block diagram.

11.1. Selection of the OBC

For the selection of the OBC to be used on the SigmaSat, first a list of commercially off-the-shelf products has been gathered. After this, a more in depth research has been conducted to find individual subsystems that have either been designed with advanced data/ AI processing in mind or have shown the potential for AI to run on the system. These highlighted OBC's can be seen in Table 11.1.

Table 11.1: Table with commercially off-the-shelf On Board Computers. Data obtained from manufacturer technical data sheets.

Product	Manufacturer	Dim. (U)
IOBC	ISIS	0.124
Z7000-P3	Space Inventor	0.13
OBC-P3	Space Inventor	0.13
The Onboard Computer	Endurosat	0.15
Q8 processor	Xiphos Technologies	0.226
Q8S processor	Xiphos Technologies	0.122
Q8J processor	Xiphos Technologies	0.112
Sirius OBC LEON3FT	AAC Clyde Space	0.18
TRISKEL	Alén Space	0.126
The CubeSat On-Board Computer	IMT srl	0.1
The Antelope	KP Labs	0.15
ABACUS 2017	G.A.U.S.S. Srl	0.24
CP400.85	Hyperion	0.1
DSW CubeSat OBC	Dream Space World	0.18
NANOSATPRO	STM	0.19
SatBus 3C2	NanoAvionica	0.16
The KRYTEN-M3	AAC Clyde Space	0.06
e2160	Unibap	0.05
The Telos 10 series	Orbital Astronautics	0.07
The Telos 40 series	Orbital Astronautics	0.07
The Telos 60 series	Orbital Astronautics	0.1
GOS CubeSat OBS	GmbH	0.24
CFC-300	Innoflight	0.14
OBC	C3S Electronics Development	0.14
DP-OBC-0402	Data Patterns	0.15

The Q8 processor family from Xiphos Technologies, the Antelope from KP Labs and the e2160 from Unibap

were all found to fit this criterion and thus have been included in an in-depth analysis. This analysis has been performed with the help of professionals, and people with previous experience with the certain chips that are used on the selected on-board computers.

The Q8 family and the Antelope all make use of an UltraScale +, this system-on-a-chip(SoC) that has been developed by Xilinx consists of a Quad ARM Cortex-A53 CPU, a Dual ARM Cortex-R5 and an FPGA for custom function implementation. The Unibap e2160 houses a Microsemi SmartFusion2 FPGA based system, with as safety MCU an ARM Cortex M3 MCU. Through more elaborate research it was found that the UltraScale+ from Xilinx uses Vitis AI, development platform with a set of high-level libraries and API's that are specifically built as an efficient AI interface. Unibap, with the SmartFusion2 has a similar platform, however less supported when compared to Vitis AI. The Unibap also has an AMD SoC CPU and GPU, which would allow for good image processing, however from experience it was found that for running AI algorithms, this would not be the most power efficient. This is why it was suggested not to go for the Unibap e2160.

The Q8 family consists of the Q8, Q8S and the Q8J. All these OBC's make use of the UltraScale+ to run the AI and a Microsemi ProASIC3 as a controller system. The Q8 is the 'basic' model, the difference with the Q8S is that the Q8S has extra features for robustness in space and has for example a radiation tolerance of 30 KRAD. The Q8J extends the capabilities of the Q8 by incorporating additional support for high speed JESD204B interfaces, as well as access to external DDR4 memory.

For AI processing both the Q8 family and the Antelope make use of an UltraScale+ SoC. The biggest difference between the Antelope by KP Labs and the Q8 family is that the Antelope uses the RM57 Hercules microcontroller for the 'usual OBC tasks'; telemetry, tracking and commanding subsystems. For this, the Q8 family uses a Microsemi ProASIC3. Of the two, the Hercules was found to better fit our use-case because of it's versatility, processing power and efficiency, and the way that it is integrated in the board of the OBC. Additionally, the Antelope provides interface connections for SPI and options for SpaceWire, this is something the Q8 family does not have. The previously mentioned features, in combination with the additional services that KP Labs provides to integrate multiple mission elements, is the reason why the Antelope has been chosen for the OBC of the SigmaSat.

11.2. The Antelope by KP Labs

The Antelope is an on-board computer that has been specifically designed to fit the CubeSat standard. The main goal of the subsystem is to provide an intelligent detection of anomalies and deviations in telemetry data. The Antelope is able to do this due to the computing power of at least 160 Giga operations per second. More about the Antelope OBC's internal architecture can be read in Section 11.2.1. A more elaborate explanation about the FDIR and predictive maintenance of the Antelope can be found in Section 11.2.2.

11.2.1. Internal Architecture Antelope OBC

The Antelope on-board computer by KP Labs is a combination of a Telemetry, Tracking and Command (TT&C) module and Data Processing Unit (DPU). The specs of these two different modules can be found in Figure 11.1. In general, the OBC is able to control the satellite's basic task performance such as monitoring the health of the satellite's subsystems and supervising all the communications. The OBC is also capable of performing classic Fault Detection, Isolation and Recovery (FDIR), more about this will be explained in Section 11.2.2.

The main component of the TT&C part of the OBC is the RM57 Hercules micro-controller that houses a dual 300 MHz ARM Cortex-R5F. This part of the OBC also includes 4 types of memory; 12 MB of MRAM, ECC protected Program Flash, 256 kB of FRAM and up to 4 GB SLC flash-based filesystem storage with ECC. The Telemetry, Tracking & Command module is quite a versatile in the sense that seven different interfaces are compatible with the system, and there are even two additional custom interfaces upon request. The TT&C makes use of a PC-104 header as form-factor, this makes is more easy to connect other subsystems with this same form-factor. The TT&C module is responsible for telecommand processing, collecting telemetry from the other subsystems, and supervising the operation of the DPU.

The Data Processing Unit is equipped with a Zynq UltraScale+ MPSoc, this system-on-a-chip includes a Quad ARM Cortex-A53 CPU, a Dual Arm Cortex-R5 and a FPGA for custom function implementation. The DPU is a daughter board that is compatible with the TT&C and is connected on the same board. The DPU supports on-board data processing tasks and enables telecommunication and AI-based applications. Because of the UltraScale+, the over 160 Giga operations per seconds, the DPU can also be used for Earth observation objectives.

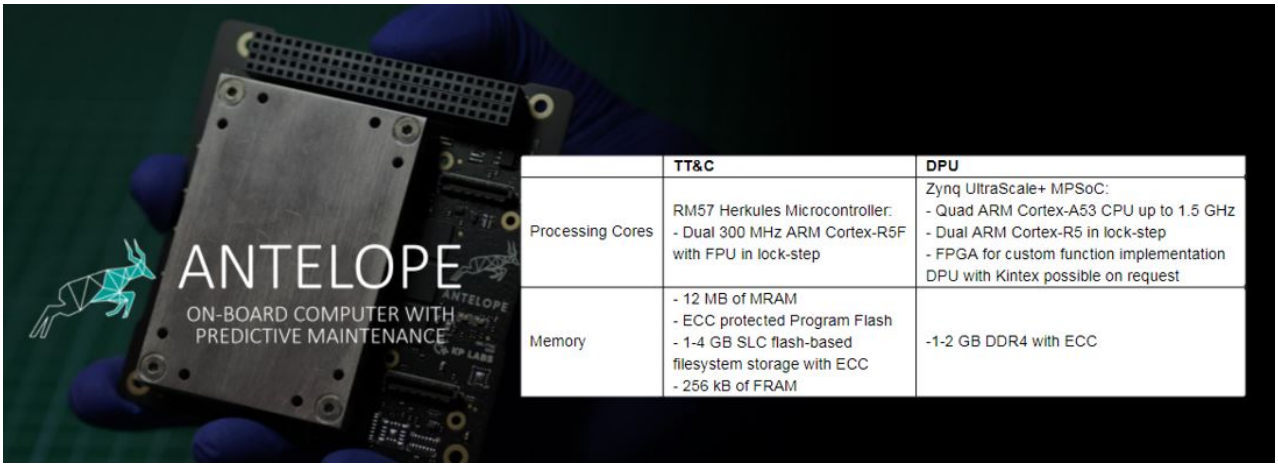

	TT&C	DPU
Processing Cores	RM57 Herkules Microcontroller: - Dual 300 MHz ARM Cortex-R5F with FPU in lock-step	Zynq UltraScale+ MPSoC: - Quad ARM Cortex-A53 CPU up to 1.5 GHz - Dual ARM Cortex-R5 in lock-step - FPGA for custom function implementation DPU with Kintex possible on request
Memory	- 12 MB of MRAM - ECC protected Program Flash - 1-4 GB SLC flash-based filesystem storage with ECC - 256 kB of FRAM	-1-2 GB DDR4 with ECC

Figure 11.1: Antelope TT&C and DPU specs

11.2.2. Maximising Spacecraft Safety

Due to the hardware architecture of the Antelope, the telemetry data can be processed in a fast fashion. If any anomalies are detected by the machine learning algorithm that are considered threatening to the security of the mission, the OBC will notify the operator, such that corrective action can be taken. Different types of irregularities can be found by the algorithms that run on the DPU of the Antelope; point, contextual and collective anomalies. A point anomaly is the case where an individual data instance can be considered abnormal with respect to the rest of the data. For a contextual anomaly the data points are considered irregular when viewed against meta-data that is associated with the respecting data-points. Collective anomalies are found when a collection of related data instances are found to be anomalies when compared with 'normal case scenario's'. In this last case, one data collection might not be seen as abnormal. However, in combination with other information, the combined occurrence can be seen as an anomaly. The combination of point, contextual and collective 'Smart Anomaly Detection' allows for the detection of situations that would otherwise have been impossible to detect by classic FDIR mechanisms.

The Antelope OBC also has predictive maintenance capabilities. Through the use of deep learning, recurrent neural networks are utilized to act as signal predictors. The predictive signal is then compared with previous and current telemetry to find any anomalies that are predicted to happen in the future. Since the predictive maintenance will also run on the OBC the OBC can react even more timely to changes that happen within the satellite ("Anomaly Detection", 2022).

11.3. Payload Processor

Why specifically the Myriad 2 was chosen for this process can be found in Section 6.10. In essence the Myriad 2 was chosen for its low power consumption and high frame rates. The processor is designed by Ubotica [1] and is already integrated on the CogniSat Platform which this mission will use as well. This platform is very versatile as it provides ten different interfaces and designed specifically for usage on a CubeSat, making it more easy to integrate with subsystem with the rest of the CDHS system. On top of that, Ubotica provides the CVAI Toolkit, Pre-trained OpenVINO models that have previously shown their potential to detect clouds, can be transferred and deployed directly on the CogniSat via the toolkit software. The CVAI Toolkit exposes the full feature set of the VPU to facilitate fast development and deployment of the AI algorithms to process data on the dedicated payload processor in a rapid and power efficient way. This has the possibility to greatly reduce development time and cost.

When the satellite is flying over an area of interest the OBC will task the Chameleon payload camera to take a hyperspectral image 'data cube'. This data cube is then sent to the OBC where pre-processing will happen. The way the OBC will do this is by cutting up the image into tiles. The pre-processed data is then sent to the Myriad on the CogniSat. The Myriad performs so-called 'inference', a process of running data points through a machine learning algorithm to get a certain output. When the AI is done with performing the analysis, the results will be sent back to the OBC. Here, the different parts first need to be put back together through a process called 'mosaicking'. When this is done the finalised data is acquired and the S-band Communication system can be prepared to send the data, and -if applicable- the alert down to earth.

[1] https://ubotica.com/

In the previous section, it was mentioned that the Antelope OBC consists of a TT&C and a DPU module. The UltraScale+ on the DPU has the potential to also house trained AI algorithms to detect for example methane leaks. However, by integrating both the Antelope and the AI accelerator that is the Myriad chip on the CogniSat, the satellite as a whole is elevated through design diversity. This creates the possibility to use both chips or either one for specific computations. In nominal operations, to save power, the Myriad could be used for inference and for more flexible network updating. The FPGA on the Antelope is re-programmable, this makes the mission more flexible, which is a great addition to a technology demonstrator mission. The extra services, software and benefits from KP Labs can potentially also be used for the CogniSat. Furthermore, having two chips capable of processing the payload data adds redundancy to the system and makes it possible to use the other chip as backup or to compare in-flight performances.

11.4. Additional CDHS Elements

The manufacturer of the Antelope, KP Labs also provides an integrated solution that takes care of multiple mission elements, including the hardware, software and AI algorithms. In the following subsection the different additional CDHS elements will first be discussed and explained. The combination is called 'Smart Mission Ecosystem', and will be used together with the payload processor to form an integrated entity. More about how all these separate parts will work together can be found in Section 11.4.4.

11.4.1. Oryx

Oryx is a modular software that is specifically made to manage the satellite as a whole. This brings the development costs down since it is not necessary to write all the code from scratch. Oryx makes it possible to use the existing building blocks of code, or to write small tailor-made blocks for the specific mission. This modular flight software tool has been developed for the control of small satellites and is fully compatible with the Antelope OBC. The tool uses a vast library of components, scheduling, testing, logging and communication amongst others. The Application Programming Interface, API, provides access to the selected sensors and peripherals. The Oryx is built out of three main elements, these are 'Development Tools', 'Software Development Kit', and the Oasis EGSE. The Development Tools are a set of automated tests and system simulators that enable extensive and comprehensive testing of the flight software. The Software Development Kit, or SDK for short is a set of libraries in C++ that have been written to incorporate essential on-board services for for example telemetry and telecommand. The Oasis EGSE, where EGSE stands for Electrical Ground Support Equipment, is an interface between simulators and the hardware of the flight model. More about Oasis will be explained in Section 11.4.3.

With the integration of Oryx, the system can make use of a plethora of different capabilities. First of all the satellite management with telemetry, tracking and command handling is one of the main building blocks of the flight software that will be run on the Antelope OBC. Oryx makes use of flexible task management that is proceeding from position, time and platform status. FDIR support is also included in the flight software, just as additional security layers for communication and telecommand channels. Through scripting language, in-flight issues are handled and OBC features can be extended after the launch. Another advantageous capability is the testability; the build-in algorithms, hardware and software in-the-loop tests will make for a more confident integration of the satellite.

11.4.2. The Herd

The Herd is a collection of AI-powered algorithms that has been specifically designed to facilitate the analysis of Earth Observation data analysis. The tool has been made to handle the entire processing pipeline and supports the Earth Observation processing chain as a whole; starting with data acquisition, data preparation, manipulation, classification, segmentation and compression to name a few. The Herd will be run on the DPU part of the Antelope OBC. This is where the full power of The Herd can be utilized through the high-dimensional data analysis that has been designed to be compatible with the Xilinx-based DPU, the ultraScale+ MPSoc. The Herd clusters data handling in three different key elements; data pre-processing, enhancement of spatial image resolution, and data analysis.

Data pre-processing uses algorithms to prepare the data through making use of for example band misalignment correction, optical distortion correction, sensor-level radiometric corrections and bad pixel masking. This step also adds georeference to the data, something that is specifically important for the mission of SigmaSat, as the importance of precise coordinates has been stressed by potential clients such as refineries.

The enhancement of spatial image resolution is done with the use of classical image processing, machine learning and deep learning algorithms. For the data analysis uses classical machine learning and deep learning in combination with rigorous validation pipelines. The use of feature extraction, dimensionality reduction,

classification and hyperspectral unmixing, has previously shown the potential for cloud detection. As a final product, the image analysis algorithms are able to accurately detect, segment and quantify objects of interest and perform temporal analysis. More about the underlying principles of data analysis can be read in **??**.

11.4.3. Oasis EGSE

The Oasis Electrical Ground Support Equipment, EGSE for short, serves as an interface between the flight hardware and a computer that would run system simulators. This is thus not part of the flight hardware itself, but rather acts as a tool for developing the satellite. Oasis makes it possible to integrate and validate performance of subsystems before launch. Through using Oasis from the initial stage of the development of the satellite, faster spacecraft integration and a better understanding of the inner-workings of the satellite are envisioned. Oasis is fully compatible with the Antelope OBC and is part of the 'Smart Mission Ecosystem'

11.4.4. Integration of Different CDHS Elements

The different elements the CDH system are the Antelope OBC, the CogniSat payload processor, The Herd algorithms, Oryx software and pre-launch the Oasis EGSE. The relations between these different parts can be seen in Figure 11.2. First the Hyperspectral camera takes the pictures, the data cube is then sent to the Antelope OBC. From here, two things can happen; either the (preprocessed) data is sent to the CogniSat dedicated payload processor where the algorithms on the Myriad will process the data and send the final product back to the OBC ready to be send down to earth. Another thing that could happen is that the data cube is processed on the OBC itself, for this the DPU would be used. In this case 'The Herd' AI algorithms would do the processing of the data on the DPU. There is technically also a third option where both the DPU an the CogniSat process the data to for example see differences in processing performance (after-all the mission is a technology demonstrator).

The DPU is also the physical part of the satellite where the algorithms for other implementations of AI on the CDHS will run. More about this can be read in Section 11.5.
The Oryx modular on-board software is the software that runs on the TT&C part of the Antelope OBC. Oryx helps here with the command of the satellite and performs preprocessing, data tracking and gathering of telemetry amongst others. From here the right information can be sent to the COMMS which in their turn transmit it back to Earth.
The Oasis electrical ground support equipment is only used pre-launch to ensure a better integration and testing of the satellite during development, so even though it is shown in Figure 11.2, it is not being used when the satellite is in orbit, also not as a ground system to communicate with.

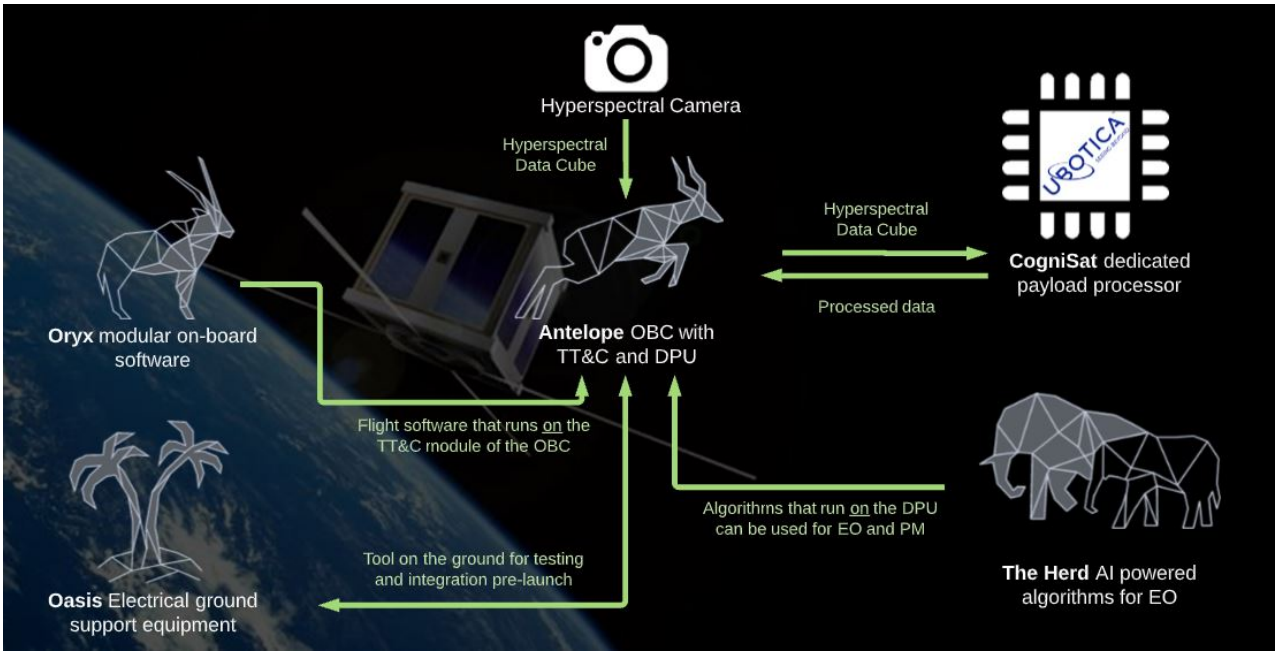

Figure 11.2: Connections between the different CDHS elements

11.5. Implementation of AI on the CDHS

From the different Potential use-cases for AI on the CDHS that were given in the Midterm report, a feasibility analysis was performed and six different applications were found to be interesting for the SigmaSat. These different implementations and their connections are given in Figure 11.3 and will be further explained in the subsections below. One of the requirements for the SigmaSat is that it should be able to operate autonomously for at least one day. The combination of different applications, whose algorithms will be run on the Antelope OBS, will work together to elevate the Mission Autonomy and thus lessen the need for ground interference.

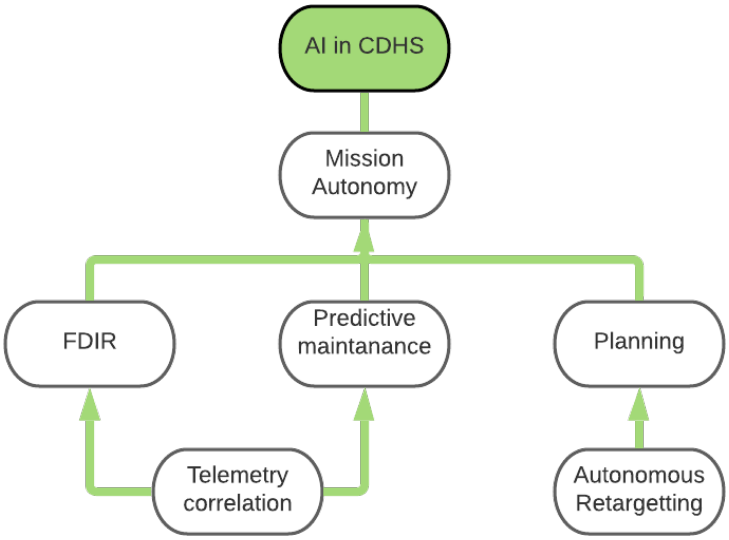

Figure 11.3: Different implementations of AI on the CDHS and their connections

11.5.1. Telemetry Correlation

Telemetry Correlation in the broadest sense means that the AI algorithm finds connections and interactions of the telemetry from different datapoints. From here, a model can be built to get a better insight into the innerworkings of the satellite. A connection could for example be found between which side of the satellite is in the sun and rising temperatures on that same side. But 'Telemetry correlation' could also entail when for example a filter is changed for the camera, then the ADCS logs an error because the movement of the entire satellite goes above a certain threshold. Telemetry correlation helps to understand a system on a deeper level. This can be used on board of the satellite for the autonomy for example, or even on the ground like the open-source project Polaris, that uses Machine Learning to correlate satellite telemetry and to let other people learn about interconnections within satellite systems. Before a satellite is able to perform efficient FDIR and Predictive Maintenance, it is important that such an adequate Telemetry Correlation model is built. This is the reason why in Figure 11.3, Telemetry Correlation is providing inputs for FDIR and Predictive Maintenance.

FDIR

Fault detection, isolation, and recovery (FDIR) could be combined with AI to do autonomous detection of anomalies in the satellite's performance and telemetry. When irregularities or faults have been found, the satellite will be able to react accordingly and do failure management without intersection of the ground station. A problem often found in using AI is that there is not enough data to train the algorithm, this will probably also pose a problem in this application. However it should be noted that the AI can first be trained exhaustively while being in orbit. This can also be interesting for constellations where first one satellite would be launched to acquire data about the inner-workings of the satellites and then make a model to be used for FDIR on all the other satellites.
FDIR is already implemented on the Antelope OBC, here the DPU uses point,contextual and collective anomaly detection. When a fault is detected and the type and location have been identified, FDIR mechanisms are trained to act accordingly apply fault mitigation.

11.5.2. Predictive Maintenance

Another application of AI that can be implemented on the Antelope is Predictive Maintenance. With the help of Telemetry Correlation, and to some extend FDIR, potential hazardous situations can be detected before they play out and timely measures can be taken. A possible application for Predictive Maintenance would be

if the satellite is able to sense that one of the reaction wheels is behaving in a less optimal way. The AI then is able to autonomously decide to use the other reaction wheels to compensate, before there is a total failure of a component. In a way the AI will be able to understand the health of the satellite and act accordingly.

11.5.3. Autonomous Retargetting

Autonomous re-targeting would be where a satellite senses something of interest during its initial orbit, and then is able to autonomously re-target this spot during sequential flyovers. for the SigmaSat this could be if there is a methane leak detected and the satellite is able to autonomously point the camera towards the field of interest when the satellite goes over the area again. This could also be for leaks that were found on the edge of refineries and that were previously not completely photographed. This could also be a good combination with constellations, where one satellite gives commands to other satellites to acquire data from the place of interest, instead of having to wait for the next time the one satellite passes over the area.

11.5.4. Planning

As previously discussed, planning is something that could be included in the autonomous operating of the satellite as a whole. Planning includes for example where the AI tries to achieve a goal from an initial state and finding autonomously smaller tasks and plan in this sequence of activities. Another example would be for the AI to allocate available resources and correlate this with known activities to produce optimized schedules, while using the available resources in an effective way. Autonomous re-targeting is seen as the Autonomously planning of taking pictures.

11.5.5. Mission Autonomy

The combination of FDIR, Predictive Maintenance and Planning that also include Telemetry Correlation and Autonomous Retargetting make for the SigmaSat to work autonomously with minimal ground interference. Through using the previously mentioned solutions, the satellite is able to find it's own best course of actions and deal with problems and faults accordingly. Through being aware of the innerworking of the satellite and planning it's own tasks with as goal to perform the mission effectively, the SigmaSat is truly designed to be 'The Smartest Satellite in the Class'.

11.6. Interface Architecture

After all the different subsystems have been chosen, a table with the respectful compatible electrical interfaces has been made, as can be seen in Table 11.2. It is beneficial that the subsystems that will be working with the payload data are all able to use SPI, these are the OBC(TT&C and DPU), the CogniSat payload processor, the Payload camera and the S-band COMMS. Most of the other systems are able to communicate via CAN. The subsystems that will need a dedicated different interface are the propulsion system, which makes use of RS422/RS485, the S-Band COMMS with I2C, and the GPS with UART. The observant reader could have seen that the S-Band COMMS have been named twice, this is because the data of the pictures for the CogniSat, the Chameleon and the S-Band COMMS will all be sent through SPI, but the telemetry and command data from and to the OBC will go through another line. More about this will be explained in Section 11.6.5. Additional details about the electrical interfaces can be found in the following subsections.

Table 11.2: Table with different components and their compatible electrical interfaces

Subsystem	**Specifics**	CAN	I2C	GPIO	LVDS	SPI	RS422	UART	GTY	GTH	SpaceWire
OBC	Antellope										
	TT&C	X	X	X	X	X	X	X			X
	DPU				X	X	X		X	X	X
Payload Processor	CogniSat	X	X	X		X		X			X
Payload Camera	Chameleon	X	X		X	X	X				
Propulsion System	Enpulsion Nano						X				
EPS	NanoAvionics EPS	X									
UHF COMMS	NanoCom AX100	X	X					X			
S-Band COMMS	DP-CRF-5615		X			X					
Solar Panels	NanoPower P110					X					
ADCS	iADCS400	X	X				X	X			
GPS	GNSS200							X			

11.6.1. CAN

CAN stands for Controller Area Network, to get a better understanding what CAN is you can see the on-board computer as the brain of the satellite and the CAN bus as the nervous system. This is because the CAN bus enables the communication between the different parts of the satellite. The CAN bus protocol was originally developed for the automotive industry, but since then it has been used in several smaller and bigger satellite missions ("CAN Bus Explained - A Simple Intro", 2022). The CAN bus allows for a signaling rate of 125 kbps to 1 Mbps while providing for 2048 different message identifiers (Bouwmeester, 2017). Communication happens between electronic nodes, also called ECU's (electronic control units). This type of bus is optimal for the communication between different microcontrollers and other processing units, like FPGA ("CAN Application Programming Interface", 2010). CAN is a so called 'multi-master' of 'peer to peer network', this means that that all the electronic nodes are connected in a web like structure and that the sender's message is able to take multiple different routes to get to the recipient. This makes the CAN bus more reliable since if one of the routes were to be damaged, the information is able to take another route. In a CAN bus each of the ECU's can both transmit and receive information. If multiple nodes were to send information simultaneously, the priority ID system will make sure that the higher priority tag's message will be relayed.

The physical communication of messages happens through the CAN bus wiring harness that consists of two wires; CAN low and CAN high. Since all the different nodes receive the information, they can decide for themselves to ignore or do something with the data.
The serial nature of the communication system helps to reduce the amount of area needed on the circuit boards. It also helps reduce the weight of the total system because there is no need for the additional wires a parallel interface would need to make use of. Since with CAN the cable connections can span a distance of up to forty meters, this will also be sufficient for an 8 U CubeSat.

There are different advantages that come with the using CAN as protocol for inner satellite communication, CAN is fully centralized, this means that there is only one connection needed to be able to talk to all the different ECU's instead of needing lines between every single node to all other nodes. Another big advantage of using CAN is that it is perceived as being robust, in the sense that it can handle electric disturbances and electromagnetic interference. The reliability of the signal transmission can even be further increased by making use of twisted pair connections as this reduces crosstalk or electromagnetic induction (Kyle, 2022). CAN is widely perceived as being relatively low cost and simple, since ECU's are able to communicate via a single CAN system instead of via direct complex analogue signal lines. This will help to reduce errors, cost, wiring and with that weight.

Communication over the CAN bus is done with the use of a so called 'Message Frame Architecture', in Figure 11.4 there is an example of what a standard CAN frames look like, with eight different message fields. First there is the 'Start of Frame', a so called 'Dominant zero', letting the other ECU's that the CAN node is going to start broadcasting information on the lines. This is followed by the standard identifier that serves to indicate the priority of the message. For the standard CAN frame, this part consists out of 11 bits. After that the 'Remote Transmission Request' field signals if the ECU is going to send or request data. Then the actual data will be sent, this can be as a response to a message request, because of a change within the system or an event. The sixth frame is the Cyclic Redundancy Check', this frame is included to confirm data integrity. After this the 'Acknowledgement slot' that consists of another 2 bits. The message frame concludes with the 'End of Frame' field.

Figure 11.4: The CAN data frame message fields

11.6.2. SPI

As previously mentioned, the Chameleon Payload, the CogniSat Payload Processor, the S-Band COMMS and the Antelope OBC will make use of SPI as interface. This protocol has been specifically chosen because

of the data transfer rate, as will be explained below. Another reason to use SPI for payload data transfer is the compatibility of all the subsystems that will play a role in handling the payload data. In addition, the solar panels will also make use of SPI.

SPI, or Serial Peripheral Interface, is a common interface for IC's(integrated circuits). SPI works with a master-slave system where in general the IC will be the slave and the master is often a microcontroller of FPGA. The master will always initiate a transaction and announce the sending or receiving of specific data. This is done by using four different signals, as can be seen in Figure 11.5. The SCLK or Serial Clock makes SPI a synchronous interface, in general interfaces that make use of a clock are perceived to be faster data interfaces. This is also one of the reasons why SPI has been chosen for the inter satellite sending of payload data. With a data rate of 16 to 32 MHz, this is quite a difference compared to CAN's 1 MHz. MOSI, or 'Master Out Slave In', is a data line that is able to send data from the master to the slave. This is exactly the other way around for MISO, Master In Slave Out. The last type of data line is Slave Select or Chip Select CS.

By using SPI there can be multiple slaves on the same line, they are all connected to the same SCLK MOSI and MISO line but have a different Slave Select that will tell the slave is the information is intended for that particular subsystem. This is different from for example I2C where you have to work with addresses and all the slaves are decoding the messages to see if it is intended for them. In Figure 11.5 an example of a singular-master-multiple-slave system is shown.

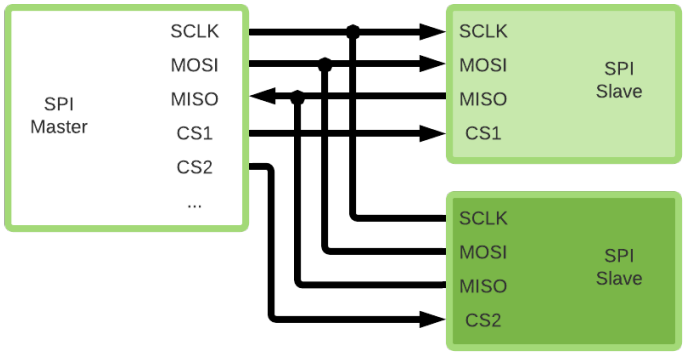

Figure 11.5: Serial Peripheral Interface with multiple slaves

One of the major advantages of using SPI is that this is a full-duplex interface, this means that you can send and receive information at the same time. Another previously discussed advantage is that the data rate is relatively high, faster than CAN, UART, I2C and RS485. However, to be able to use SPI there are at least 4 connections needed and with every additional slave there will be another connection/pin that needs to be added on the master. Overall SPI has been found to be an optimal solution for PL busses in the study performed by [Stefan van der Linden]. This is because SPI provides a relatively high data throughput while at the same time having a low power consumption. Combined with the aforementioned advantages and the compatibility of the subsystems is this why the SigmaSat will also make use of a SPI bus for the payload data transfer.

11.6.3. RS422/RS485

The propulsion system of the satellite, the Enpulsion Nano can make use of the command interface RS422 or RS485. The main difference between RS422 and RS485 is that RS422 is a point-to-point link while RS485 is able to tolerate multi-point connections. The physical difference is that the driver in a RS422 network is always on and for RS485 you can turn it on and off because there are multiple drivers that could command it. For both interfaces, the way you interpret the bits is completely custom. This includes the way that you do addressing, way the messages are shaped, the meaning of the bits. This could make development harder, but in the end the system can be designed to be optimized for the specific use-case. It is important to note that if multiple systems were to be integrated on an RS bus, they would need to share the same higher level data protocol, if they are not compatible in that sense they will only disturb each other.In general, when it comes to the physical architecture, RS485 is compatible with RS422 but its not the other way around. Since we only have one system on the SigmaSat that will make use of RS, the propulsion system, the choice was made for the point-to-point interface RS422.

11.6.4. UART

UART stands for Universal Asynchronous Reception and Transmission. Just like CAN and SPI is UART a serial communication protocol. This protocol makes use of two data lines, one to transmit information, TX, and one to receive information, RX. UART supports bi-directional and asynchronous data transmission. UART can be operated in different ways, it is quite versatile in the sense that it is able to communicate in simplex, half-duplex and full-duplex. Simplex is where data transmission only goes in one way, this is unlike half-duplex where data transmission goes in either direction but not simultaneously. Full-duplex is where data transmission can go in both directions simultaneously, this is also the case for SPI. As mentioned before, is UART an asynchronous serial transmission protocol, this means that the protocol does not make use of a clock, this is why UART adds a start and stop bit at the beginning and end of a message that is being transferred (Cook et al., 2020). The GPS receiver, the GNSS200 by Hyperion Technologies, uses a TTL UART interface with a baud rate of 9600 bps, the baud rate is the transmission speed. Advantages of using UART are that this is a relatively simple to operate and well documented protocol. The underlying system is also relatively simple as there is no clock needed, and a parity bit allows for error checking. Disadvantages are the relatively low transmission speed and the size of the data frame that is defined to only 9 bits (Yida, 2022). Another general disadvantage is that it is not possible to operate multiple master systems and slaves, however, since the GPS is the only subsystem within the SigmaSat, this is not seen as a problem.

11.6.5. Block Diagram

Through making use of Table 11.2 and with additional information about the different electrical interfaces, the final Block Diagram can be made. The Block Diagram in Figure 11.6 shows the connections of all the different subsystems to ensure proper communication, commanding, sending of telemetry and sending of other data. The OBC houses that TT&C and the DPU that both have their own connections. On the right hand side of the Block Diagram, the subsystems that are involved in handling the payload data are listed. Through the fast data interface SPI the data from the payload will either first be sent to the OBC TT&C or the DPU. If the data is to be processed by the algorithms from 'The Herd', the data will go directly to the DPU. Otherwise the data can also go to the TT&C from the OBC that will perform pre-processing of the data before sending it to the CogniSat payload processor. From the CogniSat the processed data will be send back to the OBC for mosaiicing, after which the final data goes through SPI to the S-Band COMMS sends the information to Earth. Each of the subsystems that use SPI are connected to the same bus, however they all have their own Chip Select wire.

For the telemetry and command data link, all compatible systems have been connected to the CAN bus. For the other systems, a different and separate data interface has been chosen; for the GPS this is TTL UART, for the propulsion system RS422, and for the S-Band COMMS I2C.

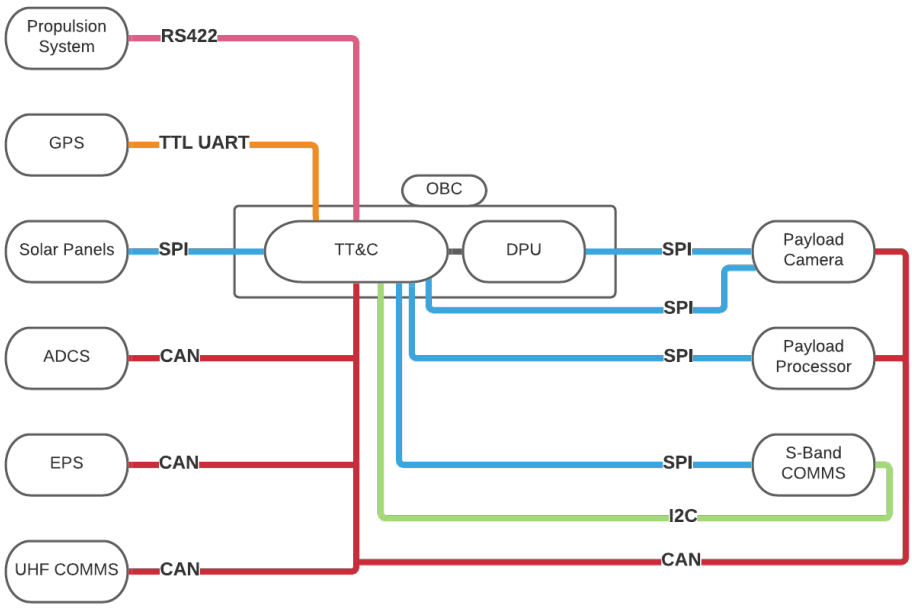

Figure 11.6: Block Diagram SigmaSat

11.7. Radiation Analysis

Before going into the radiation analysis performed for this mission, it is important to touch upon some general concepts related to radiation. This information has been compiled from (Baumann & Kruckmeyer, 2013) and (Nwankwo et al., 2020), resulting in a general overview with regards to radiation, split up in radiation environments, radiation effects in matter and radiation effects in electronics.

11.7.1. Radiation Environments

When using electronics in space one must be wary of radiation effects. The type and magnitude depend greatly on the radiation environment and the components used. Regarding the radiation environment there are three sources of radiation: Galactic cosmic rays (GCRs), Solar Radiation and Radiation belts.

Galactic cosmic rays are a nearly isotropic flux that is composed of 89 percent ionized hydrogen protons and 9 percent ionized helium alpha particles.

Solar radiation is a stream of lower-energy photons, plasma and magnetic flux, highly dependent on solar storms, solar flares and coronal mass ejections(CMEs). Magnetic storms result is the most harmful solar radiation. Radiation belts can be formed around any magnetic field containing body and contain energetic particles diverted and trapped into toroidal-shaped regions. As many other celestial bodies, Earth contains radiation belts. While they are not present at the poles, the equator has the highest altitude range for the belts. At the equator the radiation belts are present from 1,200 km to 60,000km where the inner belt ranges from 1,200-6,000km and the outer from 13,000 to 60,000km. Given our altitude it is important to focus on the inner belts that contain electrons with kinetic energies of roughly 1-5 MeV and protons with roughly 10 MeV. Additionally, the belts shield the spacecraft from GCRs. Due to asymmetries between the Earths rotational axes and its magnetic field, a radiation hotspot is formed called the South Atlantic Anomaly (SAA). The SigmaSat will also fly through the SAA.

As can be seen in Figure 11.7, in the current orbit of the satellite, SigmaSat will see a relative big amount of electrons compared with protons. Usually in LEO protons are to more prominent radiation source, however since the satellite is in a polar orbit, the satellite will see more electrons from the outer belts. This is because at the poles the magnetic field is weaker and the outer belts 'dip' towards the earth, something that can also be seen through the phenomena of the Northern Lights.

The previously discussed sources of radiation affect the microelectronic components within the satellite and can be characterized by the accumulation of ionizing and displacement damages dose (DDD), and high rate of single-event effects (SEEs). The main parameters that determine radiation exposure are: spacecraft orbit, mission duration, leven of shielding and number/magnitude of solar flares on CME's. Microelectronic reliability mainly depends on SEEs, where most failures are single-events upsets SEU's, such as bitflips.

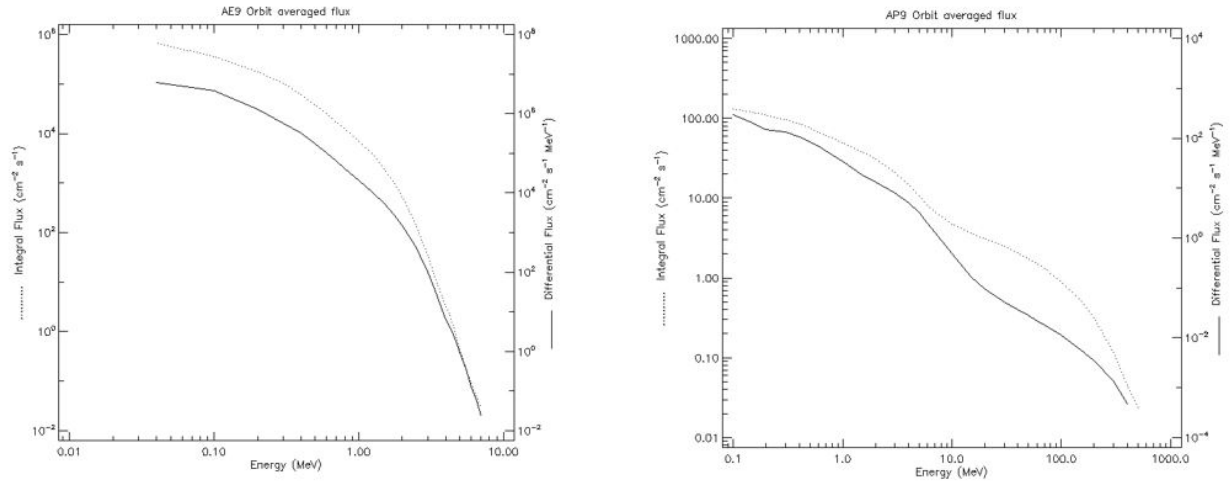

Figure 11.7: Trapped electrons(left) and protons(right) in the current SigmaSat orbit of 277.96 kilometers

11.7.2. Radiation Effects in Matter

To assess the effects of radiation to matter, particle properties have to be investigated. A particles wavelength is what defines a particles interaction with matter. Therefore, according to particle properties, as a particle's energy increases, so do its velocity and momentum. This also means that its wavelength gets smaller. Keeping

these properties in mind, more specific cases can be examined. Neutrinos for example, do not have a charge and are almost massless, allowing them to have very weak interactions with matter. Weak interactions with matter, result in less reliability concerns for microelectronics. Particles with greater interactions will lose more energy per travelled distance and thus travel less far in a matter, but doing more damage along this smaller distance. A denser material leads to more energy loss per traveled distance. These physical properties are important a most of the energy absorbed from radiation in microelectronics is converted in a charge. Within microelectronics, these charge productions can lead to parametric and functional failures, as microelectronic operation is based on charge modulation.

Every particle interacts with matter and loses energy in different ways. For protons the main worry is the photoelectric effect that describes the phenomenon of a photon using its energy to free an electron from valence band, leaving a positively charged vacancy. The probability of such an event happening depends on the energy of the photons and the binding energy of the electrons in the matter. In silicon for example, the photoelectric effect is the dominant interaction manner. It should be noted that in terrestrial and space environments, X-ray and gamma ray fluxes are not significant.

Moving on to electrons, it is important to realize they react with orbital electrons and nuclei in target matter via the coulomb force. A redirected electron is the result of this interaction. For space applications, the effects of electron penetration can be seen as significant, especially near radiation belts. Due to the electron's high energy in these belts (0.1 MeV – 10 MeV). Nucleons contain protons and neutrons, where the protons are main issue as most have sufficient energy to traverse shielding and packaging materials. Especially when occurring in high fluences, these protons can induce TID and displacement damage dose effects on top of SEE's. When considering ions, heavier ions should be treated with more caution due to their higher positive charge. Energetic ions are able to leave localized filamentary cylindrical distributions of highly ionized charge in their wake due to their high energy deposits. This explains why heavy ion elements dominate SEEs compared to other radiation types. Luckily however, heavy ions are rare in space and do not occur in high-enough fluences to induce ID and displacement damage to microelectronics.

11.7.3. Dose Effects

Total ionizing dose (TID) is defined as the energy absorbed by a unit mass of material when exposed to ionizing radiation. The unit quantifying the amount of overall exposure is radiation-absorbed dose (rad). A rad is a measure of the absorbed energy per unit mass of a specific material. The ISU unit for rad is grays (Gy), where 1 Gy = 100 krad. There are three ways in which radiation affects semiconductor devices leading to effects such as TID. These are: single-event effects (SEEs), dose effects and dose-rate effects. Dose effects can be subdivided into two categories, total ionizing dose (TID) and displacement damage (DD). TID is caused by the radiation-induced charge generation and trapping, which can limit a semiconductors reliability and functionality. Globally, TID is the generation, transport and trapping of holes in the insulation used as gate and isolation oxides in metal-oxide semiconductors (MOS) and bipolar devices at or near the silicon-oxide interface. When a high enough dose of radiation is absorbed, functional failures will occur due to isolation leakage in complementary MOS (CMOS) circuits. In bipolar transistors the base current will be increased due to the oxide charge, leading to a reduction in current and gain of the device. Displacement damage describes the NP/PD effects related to the accumulation of physical damage to crystal structures. An increase of NP/PD degrades electrical properties. Similarly to TID effects, DD can limit semiconductor reliability and functionality. DD is the results of accumulated physical damage within the semiconductors crystal structure due to radiation causing accumulated physical damage to semiconductors.

Through a simulation in SPENVIS the dose as a function of shielding thickness can be found. In Table 11.3 the different subsytems of the satellite can be found with their respective radiation tolerance. It can be seen that the lowest radiation tolerance is found to be 20 KRAD. When a line is draw in in Figure 11.8, the intersection with the total dose leads to a required aluminium absorber thickness of at least around 4 mm.

Table 11.3: Table with different subsystems and their respective radiation tolerances

Subsystem	**Specifics**	Radiation tolerance (TID)
OBC	Antellope	20 KRAD
Payload Processor	CogniSat	49 KRAD
Payload Camera	Chameleon	30 KRAD
Propulsion System	Enpulsion Nano	-
EPS	NanoAvionics EPS + External Battery Pack	20 KRAD
UHF COMMS	NanoCom AX100	-
S-Band COMMS	DP-CRF-5615	-
GPS	Hyperion integrated subsystem	36 KRAD
ADCS	iADCS400	45 KRAD

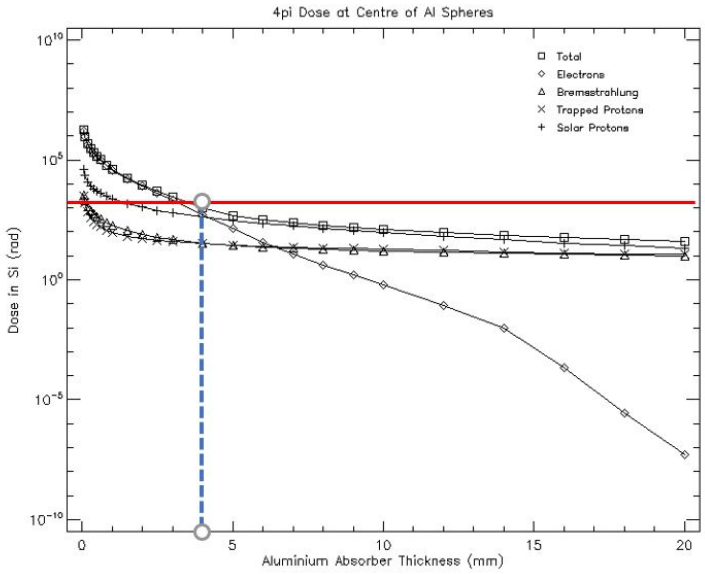

Figure 11.8: Total radiation dose with required aluminium absorber thickness

11.7.4. Single-Event Effects

Single-event effects can be categorized in destructive and nondestructive SEEs. Often referred to as soft errors, nondestructive SEEs cause an observable event or corruption in an output or data state, but do not damage or destroy the circuit component itself. When occurring in digital sequential or memory components, nondestructive SEEs can change the data state in the affected node, resulting in erroneous data within the system. A variety of different SEE types fall under nondestructive SEEs, such as single-event transients (SETs), single-event upsets (SEUs), single-event functional interrupts (SEFIs and single-event latchups (SELs). Often referred to as hard errors, destructive SEEs cause permanent damage to circuit components resulting in observable corruption in data outputs.

For all of the aforementioned single-event effects there is a archetype covering them all. Single-event transients (SET) will always occur when an energetic ion traverses an electronic device, leaving a high density of ionized excess electron hole pairs in its wake. Within microelectronics, the reverse-biased junction is the most charge-sensitive part, making it a great radiation detector. One of the reasons for why a reverse-biased junction is such a great radiation detector is because at the junction, large depletion regions form that are effective at separating electrons and holes before they can recombine, resulting in maximum charge collections at the junction. There are differences between SETs in digital and analog systems, where more advances higher speed technologies are more sensitive to SEUs caused by digital SETs (DSET), due to their occurrence probability and ability to propagate over multiple stages.

For memory in space, single-event upsets are a possible cause of erroneous data that needs to be taken into account. The process of creating SEU's is different for SRAM when compared to DRAM, but in the end the product can be seen as the same; namely bits of the data that is stored on the RAM has been changed. ECC's(error correcting code) is something that can be added onto the system to reduce the effect of SEU's.

Single-event latchups(SEL) can be potentially fatal for the electric systems used within the satellite. An SEL

is created when a low-impedance path develops suddenly between ground and power. If a latch-up happens the high-current state is upheld, the remedy is to remove the power from the device, however this does not always prove successful and thus SEL's are potential catastrophic mechanisms. The Antelope OBC uses the Hercules Microcontroller, this part has as one of the key components that it is latch-up immune.

11.7.5. Multi-Layered Shielding Simulation and Future Recommendations

For one of the most critical subsystems of the satellite, the OBC the Hercules chip has an LET(Linnear Energy Transfer) of 43 MeV. This, together with the environment in which the chip operates can be used to predict the amount of bitflips and other radiation effects that the chip will experience. The environment that has been mentioned in the previous sentence, is not only the orbit and radiation environment, but also the satellite itself and the different subsystems and for example solar panels that shield the chip. For this, the Geant4 tools in SPENVIS can be used. In Figure 11.9 an intersection of the satellite can be seen, on top there is the ADCS, then the OBC with the Hercules chip, the payload processor , the UHF transmitter, and finally the S-Band COMMS.

The final multi-layered shielding simulation has not been completed and is recommended to be performed with the previously mentioned information to decide whether or not additional radiation shielding is needed. A similar simulations will need to be performed for the other critical subsystems, plus a solar cell radiation damage simulation using EQFLUS and MC-SCREAM.

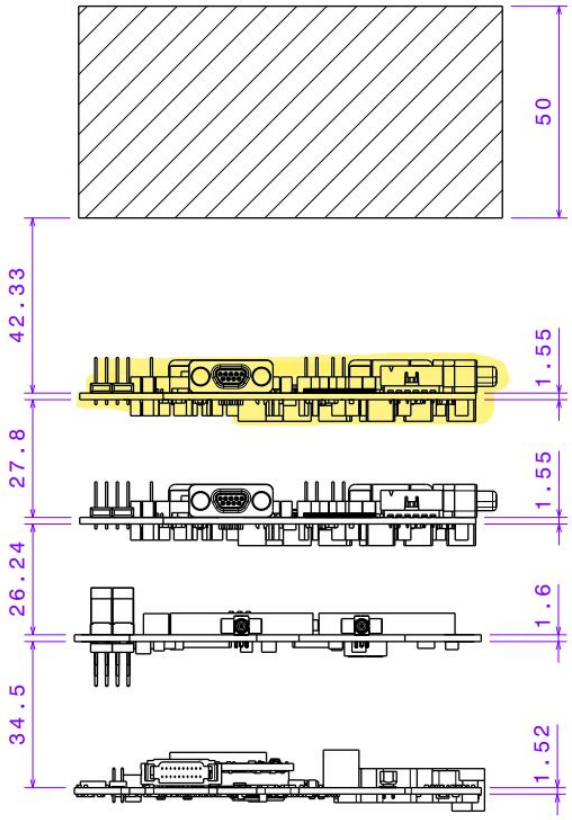

Figure 11.9: Cross-section of part of the SigmaSat with the OBC highlighted, without the solar panels

11.8. Requirements

In Table 11.4 the different requirements for the CDH system are listed, there requirements were set at the beginning of the project and have since then been kept as a guide through the entire design phase. At this stage of the project all the previously stated requirements have been met for CDHS.

Identification	Parent	Requirement
AIS-CDHS-REQ-01	AIS-TL-REQ-27	The CDHS shall have a processing unit that will handle all the operations of the satellite.
AIS-CDHS-REQ-02	AIS-TL-REQ-27	The CDHS shall be able to communicate with all the other SC subsystems.
AIS-CDHS-REQ-03	AIS-TL-REQ-27	The CDHS shall provide data interfaces to all other SC subsystems.
AIS-CDHS-REQ-04	AIS-TL-REQ-27	The CDHS shall provide monitoring of all other SC subsystems.
AIS-CDHS-REQ-05	AIS-TL-REQ-27	The CDHS design shall be latch-ups free.
AIS-CDHS-REQ-06	AIS-TL-REQ-27	The CDHS shall be capable to recover from single event upsets, single event effects.
AIS-CDHS-REQ-07	AIS-TL-REQ-28	The CDHS shall not exceed a mass of <500>grams.
AIS-CDHS-REQ-08	AIS-TL-REQ-29	The CDHS shall not exceed a volume of <1 U>cm^.
AIS-CDHS-REQ-09	AIS-TL-REQ-27	The CDHS shall provide a mass memory of at least <1>GB.
AIS-CDHS-REQ-10	AIS-TL-REQ-27	The CDHS shall provide <10>MB of volatile memory.
AIS-CDHS-REQ-11	AIS-TL-REQ-27	The CDHS shall have a watchdog to help mitigate runtime errors.
AIS-CDHS-REQ-12	AIS-TL-REQ-27	The CDHS shall have a Real Time Clock(RTC) with a back-up battery to maintain accurate time keeping.
AIS-CDHS-REQ-13	AIS-TL-REQ-27	The RTC shall have a frequency of <200>Hz.
AIS-CDHS-REQ-14	AIS-TL-REQ-27	The CDHS shall be able to communicate via COMMS with the ground station.
AIS-CDHS-REQ-15	AIS-TL-REQ-27	The CDHS shall be able to receive information via COMMS from the ground station.
AIS-CDHS-REQ-16	AIS-TL-REQ-27	The CDHS shall provide temperature monitoring of critical locations of the SC.
AIS-CDHS-REQ-17	AIS-TL-REQ-27	The CDHS shall perform housekeeping tasks such as logging system activity.
AIS-CDHS-REQ-18	AIS-TL-REQ-13	The CDHS shall draw no more than <10>watts.
AIS-CDHS-REQ-19	AIS-TL-REQ-21	The CDHS shall be able to sustain temperatures between <-20>and <40>degrees Celsius.
AIS-CDHS-REQ-20	AIS-TL-REQ-27	The CDHS shall support different operational modes.
AIS-CDHS-REQ-21	AIS-TL-REQ-12	The CDHS shall support a safe mode.
AIS-CDHS-REQ-22	AIS-TL-REQ-27	The CDHS shall be updatable by the ground station.
AIS-CDHS-REQ-23	AIS-TL-REQ-12	The CDHS shall produce and communicate diagnostic information to the ground station when non-nominal conditions occur.

Table 11.4: CDHS requirements

11.9. Conclusion

For the selection of the OBC, over 20 possible On Board Computers were compared and 5 potential candidates were selected based on applicability of AI algorithms on the subsystem. From here, a more in depth analyses has been performed with the help of experts. The Antelope by KP Labs was found to be the best choice, and together with the additional services provided by KP labs and the Payload Processor from Ubotica, a CDHS integrated setup has been created. These additional building blocks of the CDH system include Oryx modular on-board software, the Herd AI powered algorithms for EO and Oasis electrical ground support equipment.

The six different implementations for AI on the CDH system have been analysed and elaborated upon, these are; Telemetry Correlation, FDIR, Predictive Maintenance, Autonomous Retargetting, Planning and Mission Autonomy.

Through a more in-depth analysis of the compatible electrical interfaces a block diagram has been created that shows the connections between all subsystems of the satellite.

In the end, the requirements for CDHS that had been listed at the start of the project, have all been met.

12 Attitude Determination and Control

The design of an Attitude Determination and Control System (ADCS) capable of satisfying the operational requirements of the SigmaSat will be discussed in this chapter. Building on the foundation of the requirements and ADCS configuration presented in the previously delivered Midterm Report (Canosa et al., 2021b), Section 12.1 discusses the approach taken to integrate the components, the ensuing market search and trade-off, and summarize the final ADCS hardware configuration and its characteristics. The operational profile and control modes of the satellite will be discussed in Section 12.2, followed by a discussion of automated target acquisition in Section 12.3. The reliability, availability, maintainability and safety of the system is analyzed in Section 12.4.

The ADCS of SigmaSat, under the command of its OBC, provides for the pointing and recovery needs of the satellite, and enables it to independently identify, plan and execute all target acquisition manoeuvres.

12.1. Attitude Determination and Control Suit and Approach

A sensor suit was determined in the previously delivered Midterm Report (Canosa et al., 2021b) to satisfy a set of requirements which may be summarized as follows:

- The attitude and position of the spacecraft must be known at all times.
- The attitude control error must be such that the entirety of a large refinery remains in sight, of 1507 arc seconds at an altitude of 276 km.
- The spacecraft must be capable of conducting pointing manoeuvres as required by the imaging and communications systems.
- There must not be any single point of failure in the ADCS system.

Two possibilities exist to deliver an ADCS fit for SigmaSat's mission: separately identifying, purchasing and integrating components available in the market, or purchasing an integrated ADCS unit. While the first offers larger flexibility and room for optimization, it requires a large investment in market research, mechanical and electrical system integration and shielding, followed by similarly large qualification efforts, as the system would have to undergo extensive verification and validation procedures to demonstrate its fitness for flight. The investment required to achieve this is large, and may not be met within the constraints of this design phase. On the other hand, integrated ADCS units provide compact, verified and -in the case of those with flight heritage- validated architectures, refined by specialist companies in the field for ease of use and integration with the rest of the satellite. The choice to search for a integrated unit fit for the mission was thus made. If none could be found fit for the mission, the the component integration approach would be followed.

The leading reference for ADCS hardware in the Midterm Report was the NASA Small Spacecraft State of the Art Report (Yost and Weston, 2021). The reason for this was the wide scope of the report and its prestige. To choose specific components however, market availability must be considered. Thus, the search was conducted on two leading satellite component databases, SatCatalog[1] and SatSearch[2], and the CubeSat component marketplace CubeSatShop[3]. All components mentioned in this chapter are to be found in one of these three sources. All component characteristics in the following pages have been obtained their respective datasheets.

Missing Data:
At times, not all data was available for a given component. To proceed with the trade-offs, this data was estimated as follows. Two classes of criteria were identified: those on a increasing scale (where for example, a higher ionizing dose is best), and those on decreasing scales (ie: where a lower peak power consumption is best). Component performance on increasing scale parameters was estimated to be equal to 75% of the

[1] www.satcatalog.com
[2] www.satsearch.com
[3] www.cubesatshop.com

median across all components in the market. Component performance on decreasing scales was estimated to be equal to the median plus one standard deviation across all components in the market.

12.1.1. Integrated Unit Selection

A search in the ”Integrated ADCS” category of SatCatalog, SatSearch and CubeSatShop ensued. Of all listed components, all integrated units with 3-axis control capability were considered. To avoid ITAR and other import complications, all components manufactured by companies from the United States and China were eliminated from the selection process.

The results of this search, as well as the GPS module search that will be discussed later, including components manufactured in the United States and China, can be seen in the page below. The trade-off ensues.

Integrated ADCS Unit Market

		Manufacture	Heritage	m [g]	x [mm]	y [mm]	z [mm]	U [U]	GPS	Optical AD	Inertial AD	ADA_{sun} [arcsec]	ADA_{umbra} [arcsec]	PA_{sun} [arcsec]	PA_{umbra} [arcsec]	H_{max} [mNms]	M_{max} [mNm]	V [V]	I_{max} [A]	$\bar{P}$ [W]	P_{peak} [W]	Controller	T_{min} [C]	T_{max} [C]	LEO lifetime [years]	☢$_{tol}$ [krad]	Data int.	Price	Number
Tensor Tech	ADCS100	Taiwan	Yes	300	80.0	80.0	100.0	0.64	Yes	Yes	Yes	360	3600	720	3600	10.0	1.0	3.3	-	-	1	Yes	-20	60	3	-	I2C/UART	€ 50,000.00	1
Tensor Tech	ADCS400	Taiwan	Yes	1200				2.56	Yes	Yes	Yes	360	3600	720	3600	40.0	4.0	3.3	1.21		4	Yes	-20	60	3	-	I2C/UART	€ 200,000.00	1
Space Inventor	ADCS-R3	Denmark	-	600	94.0	91.0	37.5	0.32	No	No	Yes					15.0	2.0	7	-	-	-	Yes	-	-	-	-	CAN	€ 51,541.60	1
CubeSpace	3-Axis - Small	South Africa	Yes	530	96.0	96.0	57.0	0.53	No	Yes	Yes	720	-	-	-	1.8	0.2	-	-	-	-	Yes	-10	60	-	24	TC/TLM	€ 52,800.00	1
CubeSpace	3-Axis - Medium	South Africa	Yes	960	90.0	96.0	82.0	0.71	No	Yes	Yes	720	-	-	-	10.8	1.0	-	-	-	-	Yes	-10	60	-	24	TC/TLM	€ 52,800.00	1
CubeSpace	3-Axis - Large	South Africa	Yes	1150	90.0	96.0	32.0	0.68	No	Yes	Yes	720	-	-	-	30.6	2.3	-	-	-	-	Yes	-10	60	-	24	TC/TLM	€ 41,360.00	1
Space Micro	MIST	USA																											
CubeSat Pointing	Arcus ADCS	Belgium	-	715	-	-	-	-	No	Yes	Yes	144	144	396	396	4.0	0.5	3.3	0.42	0.3	1.4	Yes	-	-	3	-	I2C/CAN	-	1
D-Orbit	D-Sense	Italy	-	200	70.0	70.0	55.0	0.27	No	Yes	Yes	-	-	-	-	-	-	-	-	0.3	0.5	Yes	-30	70	-	-	CAN	-	1
Adcole Maryland Aerospace	MAI-25	USA																											
Adcole Maryland Aerospace	MAI-400	USA																											
Adcole Maryland Aerospace	MAI-500	USA																											
Blue Canyon Technologies	XACT-100	USA																											
Blue Canyon Technologies	XACT-50	USA																											
Blue Canyon Technologies	XACT-15	USA																											
Hyperion Technologies	iADCS400-50	Netherlands	-	1700	95.4	95.9	67.3	0.62	No	Yes	Yes	30	-	360	-	50.0	2.0	5	1.2	-	6	Yes	-20	40	-	45	I2C/CAN/RS422/RS485/UART	-	1
Hyperion Technologies	iADCS400-30	Netherlands	-	1300	95.4	95.9	67.3	0.62	No	Yes	Yes	30	-	360	-	30.0	2.0	5	1.2	-	6	Yes	-20	40	-	45	I2C/CAN/RS422/RS485/UART	-	1
Hyperion Technologies	iADCS400-15	Netherlands	-	1150	95.4	95.9	67.3	0.62	No	Yes	Yes	30	-	360	-	15.0	2.0	5	1.2	4	6	Yes	-20	40	-	45	I2C/CAN/RS422/RS485/UART	-	1
Hyperion Technologies	iADCS200-6.0	Netherlands	-	470	90.0	90.0	32.0	0.26	No	Yes	Yes	30	-	360	-	6.0	0.1	5	0.9	1.4	4.5	Yes	-20	85	-	45	I2C/RS422/RS485/UART	-	1
Hyperion Technologies	iADCS200-3.0	Netherlands	-	435	90.0	90.0	32.0	0.26	No	Yes	Yes	30	-	360	-	3.0	0.1	5	0.9	1.4	4.5	Yes	-20	85	-	45	I2C/RS422/RS485/UART	-	1
Hyperion Technologies	iADCS200-1.5	Netherlands	-	400	90.0	90.0	32.0	0.26	No	Yes	Yes	30	-	360	-	1.5	0.1	5	0.9	1.4	4.5	Yes	-20	85	-	45	I2C/RS422/RS485/UART	-	1

GPS Module Market

		Manufacture	Heritage	Protection	x [mm]	y [mm]	z [mm]	U [U]	m [g]	Antenna	e_X [m]	e_V [cm/s]	Channels	Rate [Hz]	V [V]	I_{max} [A]	$\bar{P}$ [W]	P_{peak} [W]	T_{min} [C]	T_{max} [C]	LEO lifetime [years]	\faRadiation$_{tol}$ [krad]	Data int.	Price	Number
NewSpace Systems	NGPS-01-422 GPSR	South Africa	Yes	Yes	155	76	34	0.401	500	No	10	25	12	1	24	-	-	1.5	-10	50	-	10	RS422/UART	-	2
NewSpace Systems	NGPS-03-422 GPSR	South Africa	Yes	Yes	96	91	18	0.157	130	No	10	25	12	1	5	-	-	1	-10	50	-	10	RS422/UART	-	2
Tamagawa Seiki	MEMS IMU/Gyro + GPS	Japan		No																					
Accord Software & Systems	ACC-GPS-NANO-DR	India	-	Yes	65	75	20	0.098	45	No	10	20	32	1	3.3	-	-	0.5	-10	50	-	-	RS232	-	2
Accord Software & Systems	ACC-GPS-NANO-ACTIVE	India		No																					
Pumpkin	GPSRM 1	USA																							
Meisei Electronic	Meisei GPSR	Japan	-	Yes	107	131	31	0.435	500	No	3	-	16	-	5	-	-	2.5	-20	60	-	Tolerant	EIA422	-	2
WARPSPACE	WARPSPACE GPSR	Japan		No																					
NEC Corporation	NGPSR	Japan		Yes	63	218	155	2.129																	
General Dynamics	Explorer	USA																							
General Dynamics	Explorer-D	USA																							
General Dynamics	Viceroy	USA																							
General Dynamics	Viceroy-D	USA																							
General Dynamics	Monarch	USA																							
General Dynamics	Monarch-M	USA																							
General Dynamics	Sentinel-M	USA																							
SkyTraq Technology	Venus838FLPx	Taiwan		No																					
Space Inventor	SpaceInventor GPS-2.5	Denmark		No																					
NovAtel	OEM4-G2L	Canada		No																					
NovAtel	OEM615	Canada		No																					
NovAtel	OEM617	Canada		No																					
NovAtel	OEM617D	Canada		No																					
NovAtel	OEM628	Canada		No																					
NovAtel	OEM638	Canada		No																					
NovAtel	OEM719	Canada		No																					
NovAtel	OEM7600	Canada		No																					
NovAtel	OEM7700	Canada		No																					
NovAtel	OEMSTAR	Canada		No																					
Spacemanic	SM-GNSS-MSP430-SKTRQ	Slovakia	Yes	Yes	67	42	5	0.014	25	No	2.5	-	-	-	3.3	0.1	-	0.33	-40	85	-	20	I2C/RS485/UART/CAN	-	2
DLR	Phoenix	Germany	-	Yes	70	47	15	0.049	20	No	10	10	12	1	-	-	-	0.85	-20	50	-	10	ASCII	-	2
ASTROFEIN	ARGO-L1 GNSSR	Germany		Yes	130	216.6	34.4	1.208																	
Surrey Satellite Technology	SGR-Ligo	UK	Yes	Yes	97	87	12	0.101	90	No	5	10	12	-	5	-	-	0.5	-20	50	-	5	UART/CAN/I2C	-	2
Surrey Satellite Technology	SGR-05P	UK		No																					
Surrey Satellite Technology	SGR-05U	UK		No																					
Syrlinks	G-SPHERE-S GNSSR	France	-	Yes	-	-	-	-	-	No	-	-	-	-	-	-	-	-	-	-	-	-	-	-	2
Sputnix	SX-NAV-03	Russia	-	Yes	70	50	20	0.070	70	Yes	30	6	-	-	6	-	-	2.5	-30	60	-	-	CAN	-	2
u-blox	MAX-M8W	Switzerland		No																					
u-blox	MAX-M8Q	Switzerland		No																					
u-blox	MAX-M8C	Switzerland		No																					
u-blox	MAX-M8Q-01A	Switzerland		No																					
GranStal Solutions	GSD800 GNSSR	China																							
GranStal Solutions	GS50 GNSSR	China																							
SkyFox Labs	piNAV-NG	Czech Republic		No																					
Hyperion Technologies	GNSS200	Netherlands	Yes	Yes	20	14.5	3.1	0.001	3	No	8	-	-	10	3.3	-	-	0.165	-40	85	-	36	UART	-	2
GomSpace	NanoSense GPS	Denmark	Yes	Yes	46	72	11	0.036	31	Yes	1.5	3	-	-	3.3	-	-	0.4	-	-	-	-	-	-	2

Legend

Red: components excluded due to import concerns. **Purple**: components excluded due to excessive volume. **Blue**: components excluded due to their requiring custom radiation protection, or embedding on a custom PCB.

↪ **Integrated Unit Selection**

Integrated unit selection was conducted in three steps, one for each of the tables below. Firstly, the performance of each candidate was assessed in 10 key trade-off criteria, as seen in Table 12.1. Notably, performance is measured on a linear scale, with 5 points awarded to best-in-class performance. When a given component largely overperforms others decimals are used to avoid displaying rankings of 0 points. Data interface protocols were ranked according to the preference of the OBC engineer, as follows: 5 for CAN, 4 for SpaceWire, 3 for RS485, and 2 for I^2C, with all other protocols scoring 0, meaning significant inconvenience.

To determine the weights for the trade-off criteria, four competing design priorities were identified: precision and reliability, volume and mass, power consumption and data interfaces, and cost. Trade-off criteria weights were set from these four design stand-points, resulting in the four sets of trade-off criteria weights seen in Table 12.2.

Lastly, the weighed performance of each candidate on each of the discussed design priorities was obtained. The results of the four trade-offs were then averaged to obtain a single, final ranking for each candidate. Table 12.3 shows the sensitivity of the ranking of each candidate to the weight changes seen in the table above it. The sensitivity analysis is thus informed by the different design priorities of the project, and integrated in the final ranking.

The Hyperion Technologies iADCS400-50 is the winner of the trade-off, with high attitude determination and control accuracies, momentum storage capability and ionizing dose, reasonable maximum torque and convenient data interface, notwithstanding its lack of flight heritage, large mass and volume and high power consumption.

Table 12.1: Performance of integrated unit models in the chosen trade-off criteria. From left to right-most column: heritage, mass, volume, attitude determination accuracy, attitude control accuracy, maximum momentum storage, maximum torque, peak power consumption, ionizing dose, and data interface protocol.

		Heritage	m	U	ADA_{sun}	PA_{sun}	H_{max}	M_{max}	P_{peak}	☢$_{tol}$	Data int.
Tensor Tech	ADCS100	5	3	2	0.42	3	1.00	1.25	2.50	3.90	2
Tensor Tech	ADCS400	5	1	1	0.42	3	4.00	5.00	0.63	3.90	2
CubeSpace	3-Axis - Small	5	2	2	0.21	4	0.18	0.29	0.38	2.67	0
CubeSpace	3-Axis - Medium	5	1	2	0.21	4	1.08	1.25	0.38	2.67	0
CubeSpace	3-Axis - Large	5	1	2	0.21	4	3.06	2.88	0.38	2.67	0
CubeSat Pointing	Arcus ADCS	0	1	3	1.04	5	0.40	0.63	1.79	3.90	5
D-Orbit	D-Sense	0	5	5	0.40	4	0.78	0.94	5.00	3.90	5
Hyperion Technologies	iADCS400-50	0	1	2	5.00	5	5.00	2.50	0.42	5.00	5
Hyperion Technologies	iADCS400-30	0	1	2	5.00	5	3.00	2.50	0.42	5.00	5
Hyperion Technologies	iADCS400-15	0	1	2	5.00	5	1.50	2.50	0.42	5.00	5
Hyperion Technologies	iADCS200-6.0	0	2	5	5.00	5	0.60	0.13	0.56	5.00	3
Hyperion Technologies	iADCS200-3.0	0	2	5	5.00	5	0.30	0.13	0.56	5.00	3
Hyperion Technologies	iADCS200-1.5	0	3	5	5.00	5	0.15	0.13	0.56	5.00	3

Table 12.2: Integrated unit trade-off criteria weights.

	Heritage	m	U	ADA_{sun}	PA_{sun}	H_{max}	M_{max}	P_{peak}	☢$_{tol}$	Data int.
Precision, Reliability	5	1	1	5	5	3	5	1	5	1
Volume, Mass	3	5	5	3	3	3	3	1	3	1
Power, Interface	3	2	2	3	3	4	5	5	3	5
Cost	5	4	5	3	3	4	4	5	5	1

Table 12.3: Integrated unit trade-off and sensitivity analysis.

	Precision, Reliability	Volume, Mass	Power, Interface	Cost	
ADCS100	0.49	0.49	0.45	0.51	**0.49**
ADCS400	0.63	0.48	0.53	0.51	**0.54**
3-Axis - Small	0.40	0.39	0.27	0.38	**0.36**
3-Axis - Medium	0.44	0.37	0.30	0.38	**0.37**
3-Axis - Large	0.52	0.44	0.39	0.45	**0.45**
Arcus ADCS	0.39	0.40	0.43	0.38	**0.40**
D-Sense	0.41	0.58	0.58	0.58	**0.54**
iADCS400-50	0.69	0.58	0.63	0.54	**0.61**
iADCS400-30	0.65	0.54	0.58	0.50	**0.57**
iADCS400-15	0.63	0.52	0.55	0.47	**0.54**
iADCS200-6.0	0.55	0.58	0.46	0.50	**0.52**
iADCS200-3.0	0.55	0.58	0.45	0.50	**0.52**
iADCS200-1.5	0.54	0.58	0.45	0.50	**0.52**

12.1.2. Position Determination: GPS Hardware Selection

The iADCS400-50 does not contain an integrated GPS receiver and antenna. As the spacecraft must be able to measure its position, this meant that a GPS receiver and antenna needed to be found to best suit the needs of the mission.

A trade-off was conducted in the same fashion as previously discussed, where the performance of all candidates was first assessed, as seen in Table 12.4, the weights of the trade-off criteria were set according to four competing design priorities, the results in Table 12.5, and the candidates traded-off based on their weighted performance. The GPS receiver trade-off resulted in the win of the Hyperion Technologies GNSS200 receiver, as seen in Table 12.6, thanks its low mass, volume and peak power consumption, high measurement rate and ionizing dose and its flight heritage, however at the cost of a relatively high positioning error of 8 meters and an untested (*TBD* in the Hyperion Technologies datasheet) velocity measurement error.

GPS antenna selection ensued. Two candidate antennas were identified: the NewSpace Systems NANT-PTCL1 and the ISIS-GAPA-DSH-0001. The Communications engineer was responsible for the choice, selecting the active ISIS-GAPA-DSH-0001 for its low power consumption and high environmental resilience.

Table 12.4: Performance of integrated unit models in the chosen trade-off criteria. From left to right-most column: heritage, mass, volume, position measurement error, velocity measurement error, update rate, whether an antenna is included with the receiver, peak power consumption, ionizing dose, data interface protocol

		Heritage	m	U	e_X	e_V	Rate	Antenna	P_{peak}	☢$_{tol}$	Data int.
NewSpace Systems	NGPS-01-422 GPSR	5	0.03	0.01	1	1	0.50	0	1	1.39	0
NewSpace Systems	NGPS-03-422 GPSR	5	0.12	0.03	1	1	0.50	0	1	1.39	0
Accord Software & Systems	ACC-GPS-NANO-DR	0	0.33	0.05	1	1	0.50	0	2	1.04	0
Meisei Electronic	Meisei GPSR	0	0.03	0.01	3	1	0.38	0	0	1.04	0
Spacemanic	SM-GNSS-MSP430-SKTRQ	5	0.60	0.32	3	1	0.38	0	3	2.78	5
DLR	Phoenix	0	0.75	0.09	1	2	0.50	0	1	1.39	0
Surrey Satellite Technology	SGR-Ligo	5	0.17	0.04	2	2	0.38	0	2	0.69	5
Sputnix	SX-NAV-03	0	0.21	0.06	0	3	0.38	5	0	1.04	5
Hyperion Technologies	GNSS200	5	5.00	5.00	1	1	5.00	0	5	5.00	0
GomSpace	NanoSense GPS	5	0.48	0.12	5	5	0.38	5	2	1.04	0

Table 12.5: Integrated unit trade-off criteria weights.

	Heritage	m	U	e_X	e_V	Rate	Antenna	P_{peak}	☢$_{tol}$	Data int.
Precision, Reliability	5	1	1	5	5	5	2	1	5	1
Volume, Mass	3	5	5	3	3	1	1	1	3	1
Power, Interface	3	2	2	3	3	4	5	5	3	5
Cost	5	4	5	3	3	1	4	4	5	1

Table 12.6: Integrated unit trade-off and sensitivity analysis.

	Precision, Reliability	Volume, Mass	Power, Interface	Cost	
NGPS-01-422 GPSR	0.27	0.19	0.16	0.22	**0.21**
NGPS-03-422 GPSR	0.27	0.19	0.17	0.23	**0.22**
ACC-GPS-NANO-DR	0.11	0.09	0.11	0.10	**0.10**
Meisei GPSR	0.15	0.11	0.09	0.10	**0.11**
SM-GNSS-MSP430-SKTRQ	0.44	0.36	0.43	0.40	**0.41**
Phoenix	0.15	0.13	0.11	0.12	**0.13**
SGR-Ligo	0.34	0.26	0.35	0.29	**0.31**
SX-NAV-03	0.24	0.18	0.37	0.24	**0.26**
GNSS200	0.64	0.73	0.57	0.71	**0.66**
NanoSense GPS	0.61	0.45	0.49	0.52	**0.52**

12.1.3. ADCS Hardware: Summary and Integration

Table 12.7: ADCS hardware summary. The price of the integrated unit and GPS receiver could not be obtained from the manufacturer. Instead, an upper bound based on the price of similar systems is presented below.

	Manufacturer	Heritage	m	x	y	z	U	V	I_{max}	P_{peak}	T_{min}	T_{max}	☢$_{tol}$	Data int.	Price	Number
			[g]	[mm]	[mm]	[mm]	[U]	[V]	[A]	[W]	[C]	[C]	[krad]			
IU	Hyperion T.	-	1700	95.4	95.9	67.3	0.6157	5	1.2	6.000	-20	40	45	CAN	€ 150,000.00	1
GPSR	Hyperion T.	Yes	20	14.5	3.1	3.0	0.0009	3.3	0.05	0.165	-40	85	36	UART	€ 10,000.00	2
GPSA	ISISPACE	IPC-A-610	16	70	70	15	0.0784	3.5	0.01	0.035	-30	70	-	MMCX	€ 1,850.00	2
			1772				**0.7743**			**6.4**	**-20**	**40**	**36**	**CAN, UART**	**€ 173,700.00**	

ADA_{sun}	ADA_{umbra}	PA_{sun}	PA_{umbra}	H_{max}	M_{max}
[arcsec]	[arcsec]	[arcsec]	[arcsec]	[mNms]	[mNm]
30	-	360	-	50	2

e_X	e_V	TTFF	Rate
[m]	[cm/s]	[s]	[Hz]
8	-	90	10

G_{peak}	Freq range	Bandwidth	Signal gain
[dBi]	[MHz]	[MHz]	[dBi]
5.2	1572-1578	6	34.5

The characteristics of the Attitude Determination and Control System can be seen summarized in Table 12.7 below. There are two assembly possibilities for the GPS receiver: as a stand-alone component somewhere in the structure, or integrated in the iADCS400-50 ADCS unit. As Hyperion Technologies advertises integration possibilities for OBCs and payload processors in the iADCS400-50, such an arrangement may be possible for the smaller GNSS200 GPS receiver (*iADCS-400*, 2019). The benefit would be to offload assembly and integration testing to a company with advanced assembly and testing facilities and experience, increasing the reliability of the system, and reducing design, assembly and testing workload, and thus cost. After discussion with Hyperion Technologies representatives, the integration of the GPS receiver and antenna in the iADCS400-50 was positively assessed.

The iADCS-400 has an integrated attitude determination and control processor. This unit is responsible for state estimation and actuator control. It receives all sensor inputs and performs sensor fusion to deliver a single attitude estimation with an accuracy of 30 arcseconds in sunlight. Actuator control is offloaded to the integrated unit as well, eliminating the need for controller design and verification and reducing OBC workload.

12.2. Control Profile and Operational Modes

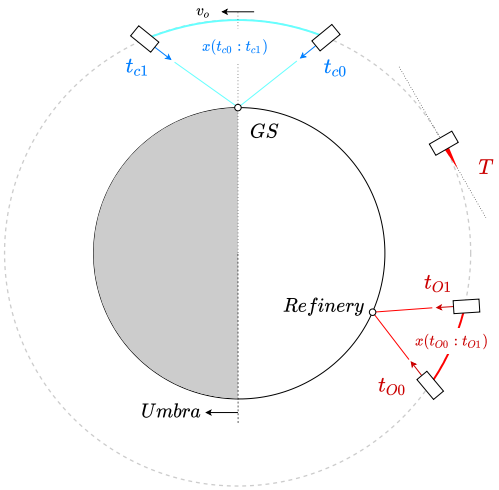

Figure 12.1: Control profile in a standard orbit with a single ground target visible.

Figure 12.1 above shows the main features of an observation orbit. Notably, as propulsion is provided by a constantly firing electric thruster, the thrust vector must be aligned with the velocity vector of the satellite at all times, with the exception of the ground station contact and observation phases. This means that in any given observation orbit, the satellite must be capable of pointing towards the ground station or target on the ground, and keep a nadir pointing at all other times.

The iADCS-400 controller has five default operational modes: nadir pointing, target pointing, slewing, intentional spinning and de-tumbling. The nadir pointing requirement is directly met by its control system. Target acquisition is met by conducting an initial target pointing manoeuvre and then slewing at a constant angular rate. A previous task must be accomplished before planning such a manoeuvre however: the satellite must be aware of which targets it may observe in a given orbit.

12.3. Target Acquisition

As per the previous astrodynamics discussion, SigmaSat will be in contact with a polar ground station once every orbit. Furthermore, its orbit is tuned so as to fly over the target Shell Moerdijk complex at least once every 24 hours. Radio communication with the ground station may only be achieved when the elevation of the satellite over the horizon as seen by the ground station is above a certain threshold. Successful observation of a ground target however depends on the achievable ground resolution by the payload.

SigmaSat must be capable of independently identifying all targets which may be acquired in an orbit, and its initial and final state for each target acquisition manoeuvre. As a consequence of this, it must also be capable of determining the ground resolution achieved by its payload as a function of its attitude and position with respect to the Earth. Knowledge of these initial and final acquisition states is enough for the iADCS400-50 attitude control system to ensure SigmaSat acquires any given target.

The solution to the target acquisition problem will be discussed in this section. The result can be seen in Figure 12.2 below, where the algorithm has successfully identified the initial and final acquisition states of SigmaSat for the Svalbard ground station, in blue, and the Shell Moerdijk complex, in red. With one execution per orbit SigmaSat can independently identify, plan and execute the acquisition manoeuvres of all targets in its target database.

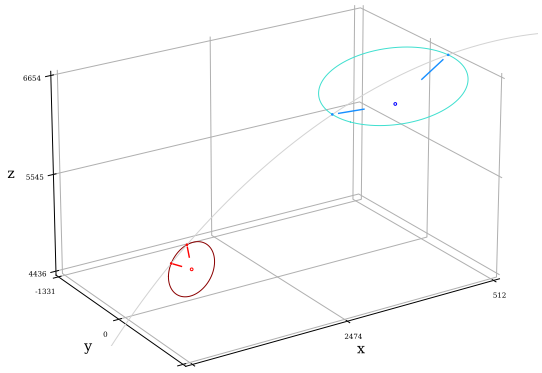

(a) Detail view. In dark red and light blue, the acquisition ranges of the ground facility and ground station.

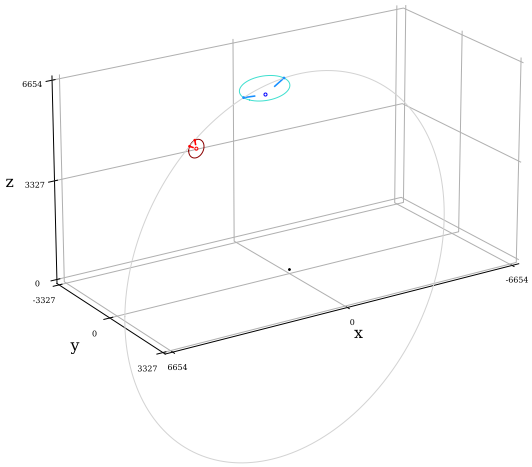

(b) Orbit view.

Figure 12.2: Acquisition of the Svalbard ground station, in blue, and the Shell Moerdijk complex, in red. A non-nominal orbit with an inclination of $87°$ and an ascension node longitude of $4°$ is displayed. This is done to highlight the capacity of the algorithm to identify and plan multiple target acquisition manoeuvres per orbit. With nominal astrodynamics observation and ground station contact happen at different orbits within the same 24 hour period.

12.3.1. Optical Targets

SigmaSat may change its attitude to better acquire a given target. This flexibility comes with the complexity of identifying whether a target is within observation range. Two observations must be noted before continuing: the Earth is approximately spherical, and this will have an effect on the geometry involved, and second, as the satellite tilts, we can expect its eye to ”see” wider distances, albeit covering such wider distances with the same amount of bands.

Identifying if an optical target, a set distance away from our imager, is within observation range is equivalent to finding whether the (*average*) ground resolution delivered by the imager of it is above a threshold considered acceptable. The solution can then be inverted to find the maximum distance from which the on-board imager is capable of delivering a ground resolution above a chosen threshold.

The ground resolution achieved by the imager is equal to its swath width over the number of bands in the sensor. The satellite has three angular degrees of freedom. For the imager, this means the capacity to roll about the pointing axis, yaw and pitch. SigmaSat’s imager is a multispectral push-broom camera, which works by capturing successive single-band-height images. Its swath can be thus seen as a horizontal scan beaming from the satellite. Camera yaw α will be defined as the rotation parallel to this horizontal scan, about the velocity vector of the satellite, and pitch that perpendicular to the scan. Figure 12.3 shows the yawing plane.

The ground resolution loss due to pitching will be assumed to be equal to that of yawing for the sake of simplicity. The swath width increase due to pitching is significantly lesser to that caused by yawing: the assumption that they are equal will cause the satellite to underestimate the distance from which a target may be observed, reducing the time in flight in which the thrust vector is diverted, and by increasing the thrust time, reducing the peak thrust and thus the peak power consumption of the satellite. An exact solution may be found by extending the analysis that follows to the three dimensional case.

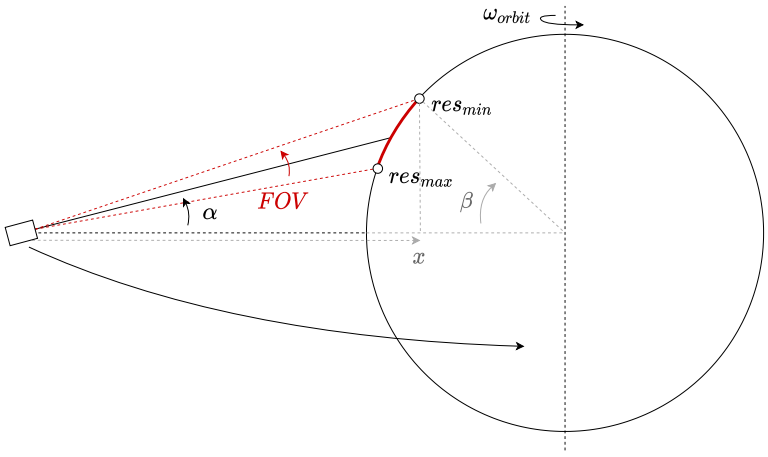

Figure 12.3: Diagram showing important elements for the swath width (and in consequence, ground resolution) calculation, in the yawing plane of the camera.

As per Figure 12.3 above, angle β may be found by solving the system of equations in Equation 12.1. The swath spanned by a ray with positive yaw α can then be calculate with Equation 12.2. The swath width of a camera pointed with a yaw α and a given Field Of View (FOV) follows in Equation 12.3. The distance spanned by each band in the sensor is not constant throughout the entire image, as can be seen in Figure 12.3. Considering the FOV of the camera is split into 1080 segments, the number of bands in the sensor, and substituting this $d\alpha$ for the FOV in Equation 12.3, the ground covered by a band of the sensor at any yaw angle α can be obtained. The resulting equation can then be formulated as a minimization problem with α as the minimization variable to find the maximum yaw of a ray shot from the satellite, such as to achieve a given ground resolution. GHGSat, the main competitor of SigmaSat, is advertised to achieve a ground resolution of 50 metersJervis et al., 2021. At an orbital altitude of 276 km, a ray from SigmaSat achieves this accuracy with a yaw of $25°$: this point is labeled res_{min} in Figure 12.3. This maximum yaw is that of the furthest point of the FOV of the camera. The yaw of the satellite is equal to this maximum yaw minus half the FOV, or $23.85°$.

Considering the fact that the satellite's altitude, at least during a single given orbit, can be approximated as constant, the calculated maximum yaw, again, such as to achieve a worst ground resolution at least equal to the advertised ground resolution of GHGSat, can be turned into a maximum observation distance using simple geometry. Thus, at an altitude of 276 km SigmaSat can capture targets up to 303 km away from itself, or 122 km away from its ground track.

$$\begin{cases} x \cdot tan(\alpha) = R_e \cdot sin(\beta) \\ x = h + R_e \cdot (1 - cos(\beta)) \end{cases} \tag{12.1}$$

$$s_{ray} = \beta \cdot R_e \tag{12.2}$$

$$s_{cam} = \left(\beta(\alpha + \frac{FOV}{2}\right) - \beta\left(\alpha - \frac{FOV}{2})\right) \cdot R_e \tag{12.3}$$

In summary, assuming that pitch and yaw equally affect ground resolution, and targeting a minimum ground resolution equal to that of GHGSat, the maximum distance from which an target may be captured by the on-board imager can be obtained as a function of the altitude of SigmaSat's orbit and the capabilities of its imager.

Finding the initial and final target acquisition states X_{obs} thus becomes problem of analytical geometry: that of finding the intersection of an Earth-centered sphere with radius equal to the orbital radius, the ecliptic plane, and a second sphere centered at the chosen target, with radius equal to the maximum distance from which it may be observed, formalized below in Equation 12.4, where I denotes the Earth intertial reference frame, $TGRF$ denotes the rotated and translated reference frame with origin at the ground target, and R_{obs} is the maximum observation distance just discussed.

An analytical solution may be found in different ways. In this case, the choice was made to find the intersection of the "observation sphere" and the ecliptic, obtaining a circumference in the ecliptic, and then solving the intersection of that with the circumference defined by the orbital radius. Knowing these initial and final

observation locations in the orbit and the coordinates of the ground target, the initial and final observation attitudes can be straightforwardly obtained.

The result can be seen highlighted in red in Figure 12.2, which displays the Shell Moerdijk complex, the intersection of its ”observation sphere” and the ecliptic, and the initial and final observation states, traveling from south to north.

$$\begin{aligned} X_{obs} = \{x, y, z : \ & |\vec{X_{obs}}|_I = R_{orb}; \\ & \vec{X_{obs}} \cdot \vec{n_{Ecl}} = 0; \\ & |\vec{X_{obs}}|_{TGRF}| = R_{obs}\} \end{aligned} \tag{12.4}$$

12.3.2. Communication Targets

The geometric condition for radio communication with a ground station is given: the satellite must be above a certain altitude over the horizon seen by the ground station. Finding the initial and final communication states of the satellite becomes is thus equivalent to finding the intersection between the cone defined by the altitude requirement above the horizon, with origin at the ground station, the sphere centered at the origin of the inertial reference frame of the Earth, defined by the orbital radius, and the ecliptic, formalized using spherical coordinates in Equation 12.5 below, where λ and δ represent longitude and latitude, z_{ERF} denotes the z component of X_{comm} in the rotated ecliptic reference frame, and $TGRF$ again denotes the rotated and translated reference frame with origin at the ground target.

The strategy to find a solution in this case was to find the intersection between the orbital sphere and the ”communication cone”. The intersections of the resulting circumference and the ecliptic were found numerically.

The result can be seen highlighted in blue in Figure 12.2, which displays the Svalbard ground station, the intersection of the orbital sphere and the ”communication cone”, and the initial and final communication states, traveling from south to north.

$$\begin{aligned} X_{comm} = \{\rho, \lambda, \delta : \quad & \rho = R_{orb}; \\ & \rho = \left(\frac{R_{tg}}{tan(\delta_{TGRF}) - tan(\alpha)} \right) \cdot \sqrt{1 + tan^2(\delta_{TGRF})}; \\ & z_{ERF} = 0\} \end{aligned} \tag{12.5}$$

12.3.3. Accounting for the rotation of the Earth

The methods previously discussed take as inputs the spherical coordinates of ground targets and the orbital parameters of SigmaSat. With an estimated 17 orbits in a 24 hour period, the rotation of the Earth cannot be neglected. The approach to solve the intersection problem as accurately as possible is the following: the point of closest approach of the satellite to the ground target is found, and the geometry problem is solved considering a stationary target located at the closest approach point.

While obviously delivering accurate results at the closest approach point, this method loses accuracy as one moves north or south of the closest approach point. This inaccuracy is considered reasonable however on the grounds that

- The method is compatible with the previously discussed geometric methods.
- The error is distributed evenly about the point of closest approach.
- And related to the previous, the acquisition ranges of ground targets, especially optical targets, which have the shortest acquisition windows and thus require the most accurate planning, are low. Thus, the latitudinal distance from the closest approach point to the farthest acquisition points from it can be expected to be low, and so will be the error.

As the position of both the satellite and ground target in the Earth inertial reference frame are known functions of time, the magnitude of their difference can be written as a function of time and minimized using a bounded minimization algorithm, where the input time may not exceed the time to complete an entire orbit. The SciPy (Virtanen et al., 2020) implementation of the Broyden–Fletcher–Goldfarb–Shanno algorithm (Fletcher, 1987) was used to find the time of closest approach.

The execution of this routine previous to the target acquisition routines previously discussed allows SigmaSat to identify and plan target acquisition manoeuvres accounting for the rotation of the Earth beneath it with reasonable accuracy.

12.4. Reliability, Availability, Maintainability and Safety Analysis

The safety of the Attitude Determination and Control System is fundamental, as its failure will cripple the mission. System qualification and reliability testing is largely offloaded to Hyperion Technologies as the manufacturer of most components in the system, its integrator, and provider of the flight software. The lead time for the hardware of the iADCS400 is noted to be between 6 to 9 months[4]. Taking into account the extra time required by the integration of the GPS receiver and antenna, the lead time is expected to be between 9 and 12 months. Maintainability may only be addressed preemptively, by positioning the ADCS in the satellite so that the ionizing dose received will be lower than its maximum ionizing dose by the end of the mission.

12.5. Conclusion

Thus ends the discussion of the Attitude Determination and Control System of SigmaSat. After determining a sensor and actuator suit, the approach was taken to search first for integrated ADCS units, and only if one could not be found to suit the needs of the satellite, purchase and integrate separate components. A search of the CubeSat integrated ADCS unit market followed. 12 units were trade-off on the grounds of four overarching criteria: precision and reliability, volume and mass, power and data interface, and cost. After conducting a due sensitivity analysis, the Hyperion Technologies iADCS400-50 was chosen, with attitude determination and control accuracies of 30 and 360 arcseconds respectively and high specific maximum torque and momentum storage capacity. Its lack of an integrated ADCS receiver prompted a similar search and trade-off, resulting in the choice for the Hyperion Technologies GNSS200 GPS receiver and the ISISPACE ISIS-GAPA-DSH-0001 antenna. Integration of the GPS receiver and antenna into the iADCS400-50 was discussed with Hyperion Technologies representatives and positively assessed.

The choice for an integrated ADCS unit, and for the integration of the GPS receiver and antenna in it offloads significant design, integration and testing effort to a company with extensive expertise and facilities, increasing the reliability of the final assembly and reducing engineering and logistics costs for the mission.

A target acquisition algorithm was discussed afterwards. Thanks to the on-board controller of the iADCS400-50 and the target acquisition algorithm, SigmaSat is capable of independently identifying, planning and executing all possible target acquisition manoeuvres, in each and every orbit, enabling it to fulfill its Earth observation mission.

[4] www.catalog.orbitaltransports.com

13 Electrical Power System

This section will talk about the approach that has been taken to design the EPS system. The outputs of this section will be an electrical block diagram and an EPS system design that includes battery size and solar panel area.

13.1. Electrical Power System Approach

The approach to designing the EPS system starts with defining the worst case scenario, which by doing so ensures that the satellite will be able to perform optimally for each orbit of the mission. The worst case is defined as the busiest orbit, by which the most power intensive subsystems are being used and for the most time. In order to ensure that the design is not over-designed, instead of running the EPS system at full power over an entire orbit, the times that each subsystem is turned on and for how long is simulated. By doing this, the power levels of each component over the duration of the orbit can be added up, which will give the total power flow coming out of the storage system on board. When this power graph is integrated with respect to time, the energy consumed by the satellite can then be calculated. This value is directly related to the sizing of the battery, where there must be a certain number of Watt-hours that must be stored during the eclipse. The power required during the sunlit period of the orbit is then easily calculated as well. This then lets the sizing of the solar panels to take place, as they must generate enough power to power the satellite as well as charge the batteries, so that after one orbit the battery level is equal to that when it started.

The final step is to find an EPS system that not only can support the battery size, input and output powers, but one that can integrate all the subsystems on board successfully by powering them according to their own requirements. Once all these factors have been met, then the EPS system is successfully designed and is a feasible design.

13.2. Power Distribution System

In order to meet the strict power requirements set by other subsystems, a highly demanding EPS system would have to be found. Fortunately, such a component exists, which is the NanoAvionics Electrical Power System-2S7P. This EPS system is configurable to come with an external battery that is capable of storing up to 161 Wh to reach a total of 175 Wh of energy. This system also has a range of output powers, ranging from 25 to 175W. This is important, as the presence of the propulsion system alongside the artificial intelligence processing, means that the satellite will inherently require a large output power. The most important parameters of this selected EPS system can be found in the table below:

Table 13.1: NanoAvionics EPS 2S7P Specifications

Features	Value	Unit
Outputs		
MPPT Efficiency	96	%
Power Storage	175	Wh
Regulated Output Rails	3.3, 5	V
2 Configurable Output Rails	3 - 18	V
Unregulated Power Rail	6 - 8.4	V
3.3V Output Converter Power	20	W
5V Output Converter Power	20	W
Inputs		
Number of Solar Panel Inputs	8	-
Solar Panel Voltage Range	2.6 - 18	V
Maximum Charging Power	70	W

Some additional features of this EPS system include the presence of the watchdog, which logs all important

parameters (such as input and output currents), overcharging of the batteries, and the ability to power the satellite solely through the solar panels should the batteries fail. The watchdog log can be sent to the OBC for analysis and then can further be transmitted through the UHF COMMS system if necessary for ground staff to analyse the data independently.

Finally, the two configurable output rails have been configured to 12V and 5V. The 12V rail is for the propulsion system, as it has a high power requirement and other subsystems cannot be connected to the same rail, otherwise the power would go over the allowed limit. The second configurable rail has been set to 5V. This has been done because the power required to run the ADCS components, the payload camera, and the OBC at the same time is too high. By configuring the second rail to 5V, the ADCS can be separated from this line and run independently.

13.2.1. Electrical Block Diagram

The electrical block diagram has been created based off of the specifications of the other components. It must be noted that not all components are turned on at the same time, therefore the maximum output rail power of 20W is never exceeded on any of the rails. The solar panels can be seen here, split into 2. These are the two deployable solar panels mounted on the side of the spacecraft. These solar panels are connected directly to the BCR (Battery charge regulator), which is already integrated into the EPS. The BCR is important as it contains the circuity and logic to protect the rechargeable battery against overcharging, as well as over and under current. The EPS system then uses several power conditioning modules (PCM), which can be separated into three distinct tasks. The first task of the PCM is to regulate and protect not only the components being supplied the power, but also any back-current that may come back and damage the EPS system as a whole. The next task of the PCM is the monitoring and control of the power rails, and the final task is distribution and fault protection.

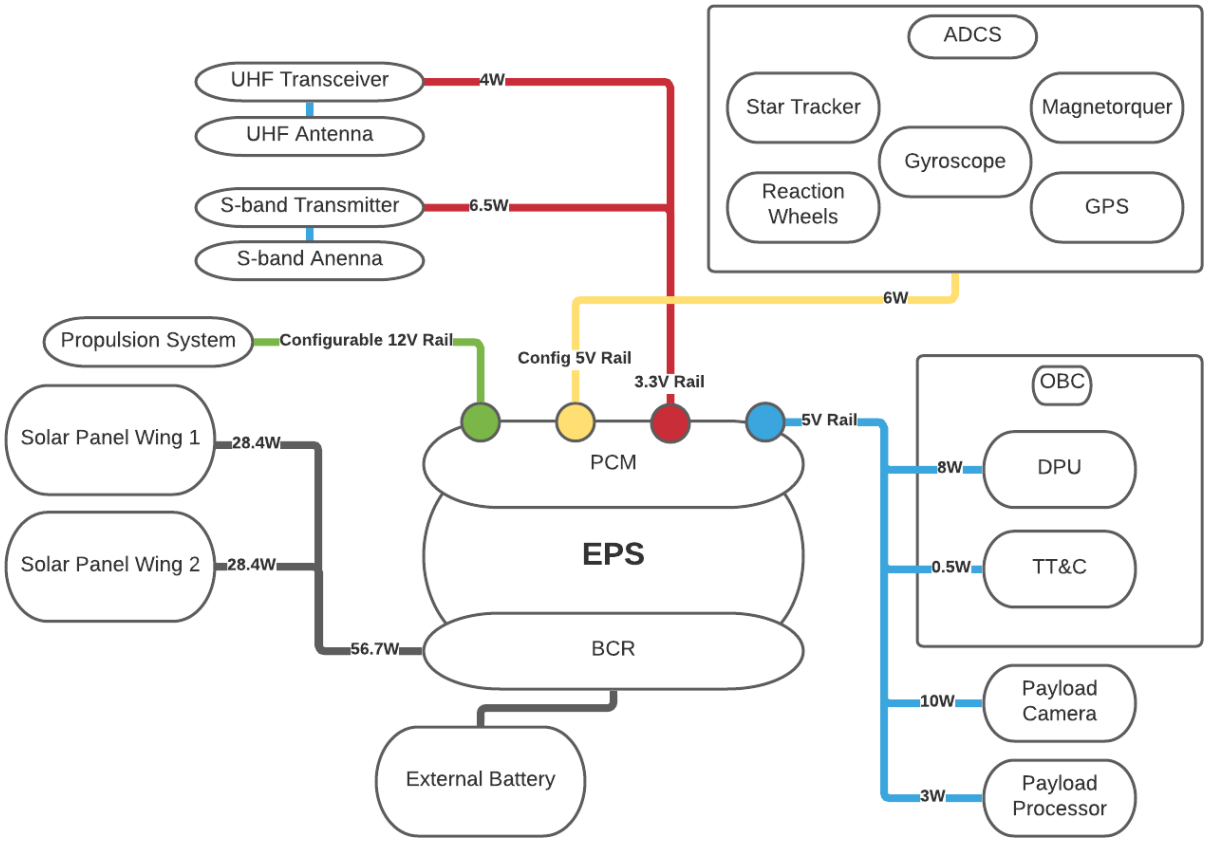

Figure 13.1: Electrical Block Diagram

13.2.2. Wires and Cables

The wires used for powering the subsystems will be ESCC 3901-002-P SERIES wires. This is due to their radiation resistance and light weight capabilities. A radiation resistant cable will be able to protect against over-

current, and the shielding will protect the cabling for EMC testing and interference with the communications system. A table of the wires and their specifications can be found below:

Table 13.2: ESCC 3901-002-P Series Light Weight Radiation Resistant Shielded Cables

Draka Part Number	AWG	Number of Cores	Maximum Resistance (ohm/km)	Maximum Weight (g/m)	Current Rating (A)
F A3901-2-P-3-28HG	28	3	254	7,9	1,5
F A3901-2-P-3-26HG	26	3	155	10.6	2,5
F A3901-2-P-3-24HG	24	3	110	13.3	3,5
F A3901-2-P-3-22HG	22	3	53,5	19.2	5
F A3901-2-P-3-20HG	20	3	33,8	28.4	7,5
F A3901-2-P-3-18HG	18	3	21,6	42.0	10

Table 13.3: Required Power Line Cabling for EPS

Subsystem	Name	Maximum Power	Voltage	Current	Wire required
OBC	Antellope	8,5	5	1,7	F A3901-2-P-3-26HG
Payload Processor	CogniSat	3	5	0,60	F A3901-2-P-3-28HG
Payload Camera	Chameleon	10	5	2,0	F A3901-2-P-3-26HG
Propulsion System	Enpulsion Nano	25	12	2,1	F A3901-2-P-3-26HG
EPS Distribution	NanoAvionics EPS 2S7P	0,15	3,3	0,05	F A3901-2-P-3-28HG
EPS Battery	NanoAvionics EPS 2S7P	38,8	3,3	11,76	2 x F A3901-2-P-3-20HG
UHF COMMS	NanoCom AX100	4	3,3	1,2	F A3901-2-P-3-28HG
S-Band COMMS	DP-CRF-5615	6,5	3,3	2,0	F A3901-2-P-3-26HG
Solar Panels	NanoPower P110	28,4	9,4	3,0	F A3901-2-P-3-24HG
ADCS	iADCS400	6	5	1,2	F A3901-2-P-3-28HG

13.3. Modes of Operations

To be able to calculate the energy required by the satellite, the times that each subsystem is switched on must be known. To get this value, the 'busiest' orbit must be explored. A diagram of the busiest orbit can be found below, but it includes a UHF transmission at the start of the orbit. The satellite then flies over one of the selected refineries, and takes a picture. This picture is then read from the payload into the AI image processor, which then processes the image. Once the image has been processed, the satellite then transmits this data down during the next ground station pass, as well as transmitting TT&C data. The satellite then completes the rest of the orbit with only essential functions running, such as the ADCS, the propulsion, and the watchdogs on the OBC and the EPS systems. The different phases and what components are on for each phase can be seen below. The timings for the communications systems come from the simulations run in Chapter 7 and explained in Chapter 10, where $123s$ is equal to the longest communications connection time between the ground station and the satellite.

Table 13.4: Busiest Orbit Component Activity

Task	Total Time On Sunlit [s]	Total Time On Eclipse [s]
Payload Warmup + Imaging	300	0
Payload Image Reading	2.7	0
Payload Image Processing	187	0
Communications S-Band	0	213
Communications UHF	213	0
ADCS	3201	2203
OBC	3201	2203
EPS	3201	2203
Propulsion	3201	2203

13.4. Eclipse Function

Due to the fact that the satellite is in a sun synchronous orbit, the "solar lighting remains about the same every cycle" (Ehren, 2019). This is beneficial for the design of the satellite as by using just one single degree of

freedom for the rotation of the solar panels, an optimum energy production can be achieved for every orbit. This is explained further in Section 13.5.1. Furthermore, due to the sun synchronous orbit and hence high inclination, the first order eclipse calculation is suitable for all further calculations of the power requirements. One consideration that has been made is the existence of the penumbra and umbra of the Earths shadow. As can be seen in Figure 13.2, due to the size difference between the Earth and the Sun, light rays from the sun may be able to be seen on the side of the Earth where if the sun rays were exactly perpendicular, a shadow would be. This region is known as the penumbra, while the umbra is the actual total shadow of the Earth from the Suns rays.

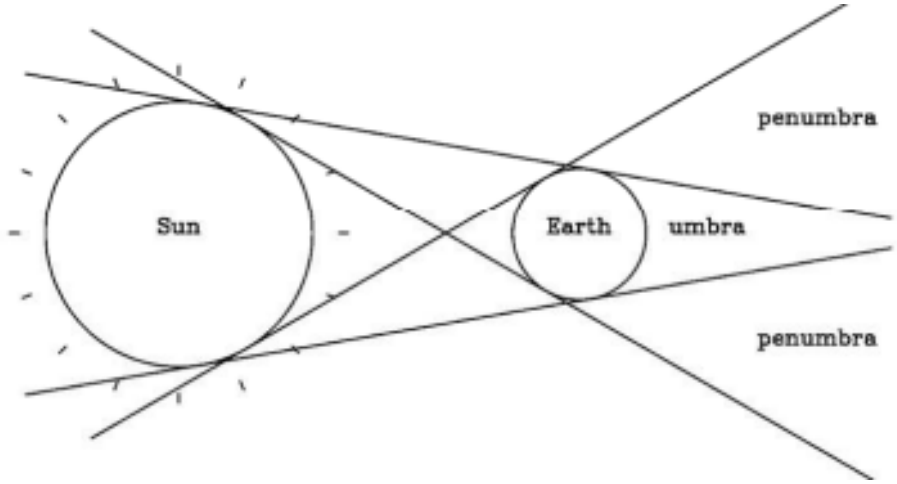

Figure 13.2: Exaggerated Diagram of Numbra and Penumbra of Earth Shadow

Due to this effect, the eclipse time will decrease by a maximum of 8s in LEO (Noomen, 2022). This was however not included in the calculations as by omitting it then the design of the solar panels becomes a marginal overestimate, which is desirable in terms of redundancy and reliability. The formula to calculate the eclipse fraction can be found below:

$$(f_E)_{max} = \frac{1}{\pi} cos^{-1}\left[\frac{\sqrt{h^2 + 2Rh}}{(R+h)}\right] \tag{13.1}$$

where R is the Earth's radius, h is the height of the satellite. This can then be multiplied by the period P of the orbit, to obtain the time spent in the eclipse. At an orbital height of $277.96km$, the period is equivalent to $5404s$, and the eclipse function is equal to 0.408. This results in an eclipse time of $2203s$. The battery must therefore be able to store enough energy to provide power during this time, and the solar panel must be able to charge the battery to full as well as power the satellite during the sunlit period of the orbit.

13.5. Power Simulation

In order to calculate accurate values for the battery storage's and solar panel sizes, a simulation of the busiest orbit could be carried out. To simulate the EPS system, the orbit is analysed from 0s to 5404s. Each component can then be made into an object with values for their power, standby, and when they turn on and off during the orbit. There are 4 different classes for the objects:

1. Active Component: A component that consumes power in order to function
2. Power Storage: A component that is able to store energy
3. Power Generation: A component that is able to generate energy

A program is then run to simulate when each component is turned on, if the satellite is charging whilst in the sun, or discharging while in the eclipse. The power (in W) is then interpolated to find the area under the power graph, which will give the energy used and generated in a certain time period (in Wh). This in turn can be used to calculate the maximum size of the solar panels, as well as the batteries.

13.5.1. Power Generation

Due to the sun synchronous orbit and the single degree of freedom solar panels, the moment the satellite is out of the eclipse of the Earth, it can begin to generate maximum power. If the satellite were not to have this feature, and instead relied on stationary solar panels, then this would double the size and power of the panels.

At the beginning of life, the solar panels have a generation of $2.27W$, but due to the radiation and general degradation of the solar panels, this will decrease over the duration of the mission. To calculate the efficiency of the solar panels at the EOL versus the BOL, the following equation can be used:

$$\eta_{EOL} = \eta_{BOL}(1 - YD)^{YM} \tag{13.2}$$

By using a value of $YD = 3.75\%$ for the degradation of gallium arsenide solar cells, a satellite life of $YM = 2$ years, and a beginning worst case efficiency of $\eta_{BOL} = 0.28$, we find that the end of life efficiency is 25.9%, therefore the power generated per panel at the end of life is equal to $2.10W$.

To obtain a size of the solar panels, the simulation is run and the power requirements of the solar panels is outputted. By calculating the energy required in the sunlit period as well as the eclipse, a simple calculation can be made to obtain the power input required by the solar panels. This value comes out to equate to $56.7W$. This is under the $70W$ requirement of the EPS system, therefore this value is possible. To reach this power, a total of 27 solar cells are required. Each panel unit is 1U in area, therefore with a side profile of 4U, each extendable panel is a total of 4 units. To calculate how many extendable panels are required, a simple division and rounding up to the nearest even number can be conducted. $27/4 = 6.75 = 8$, so therefore there must be a total of 8 panels; which is 4 panels (16 panel units) on each side of the satellite. As each side has 16 units, to connect them in series this would equate to a value of $4.82V \cdot 30 = 77.12V$ which is above the maximum EPS solar panel voltage input of $18V$ found in Table 13.1. Therefore, the cells will be wired by 2 units in series, with 8 of these in parallel, which equates to an input voltage of $4.82V \cdot 2 = 9.64V$. Because there are 32 cells instead of 27, there is some redundancy in the system should some of the cells fail. To counter over-wattage, a feedback system between the EPS and the rotating solar panels would allow the cells to be angled away from the sun. At the end of life however, at 32 cells running at $2.1W$, the maximum input is equal to $67.2W$ which is below the maximum required. In fact, this would occur roughly one year into the operations of the satellite.

The maximum lifetime of the solar panel system before the degradation of the cells would mean that the power being generated is below the required can also be calculated. Using Equation 13.2 and the same inputs for the yearly degradation (3.75%), what can be found is that after 6.48 years, the solar panels will reach a point where the power generation is too low to support full operations.

Now that the solar panels have been designed and sized, a power generation component can be added to the simulation, and the final energy flow can be calculated.

13.5.2. Power Storage

To calculate the power storage required, the simulation is able to output and calculate the enrgy flow, to and from the battery. By finding the maximum energy flow out of the battery, a calculation using the depth of discharge of the battery can be made to find the maximum charge that the battery will experience. As the Nano Avionics©EPS uses Li-Po batteries, there is a minimum requirement for the depth of discharge which is 30%. This equates to a battery storage requirement of 88.6Wh, which is well within the limits stated in Table 13.1. The calculations for the power dissipation of the batteries so that thermal calculations could be made are as follows. Firstly, the internal resistance (R_{int}) and nominal voltage (V_{nom}) of the batteries must be known. These are given in the data sheet of the EPS, and are $7.4V$ and $24m\omega$ respectively. Using these values, as well as the total power (P_{out}) coming out of the batteries ($38.8W$), Ohms law can be used to calculate the voltage drop across the batteries can be calculated as follows:

$$V_{drop} = I \cdot R_{int} = \frac{P_{out}}{V_{bat_{nom}}} \cdot R_{int} \tag{13.3}$$

which equates to a voltage drop of $0.126V$. Once again Ohms law can be used to calculate the power dissipation of the batteries:

$$P_{diss} = \frac{V_{drop}^2}{R_{int}} \tag{13.4}$$

to give a value of $0.80W$. This means that while operational, roughly 2% of the power of the satellite while in use is being dissipated as heat, directly from the batteries.

Due to the high input power required by the solar panels, the batteries have to be slightly over designed. As mentioned earlier, the required maximum storage is $88.6Wh$, whilst the maximum available storage is actually $161Wh$. This means that the batteries are only experiencing a depth of discharge of 15%. This can be beneficial for the design of the satellite however, due to the high number of cycles and the cold temperatures of the batteries. The more frequent a battery is cycled the faster the battery will degrade. A plot of the degradation of Li-ion batteries can be found below (Cook et al., 2021), simulating the LEO conditions.

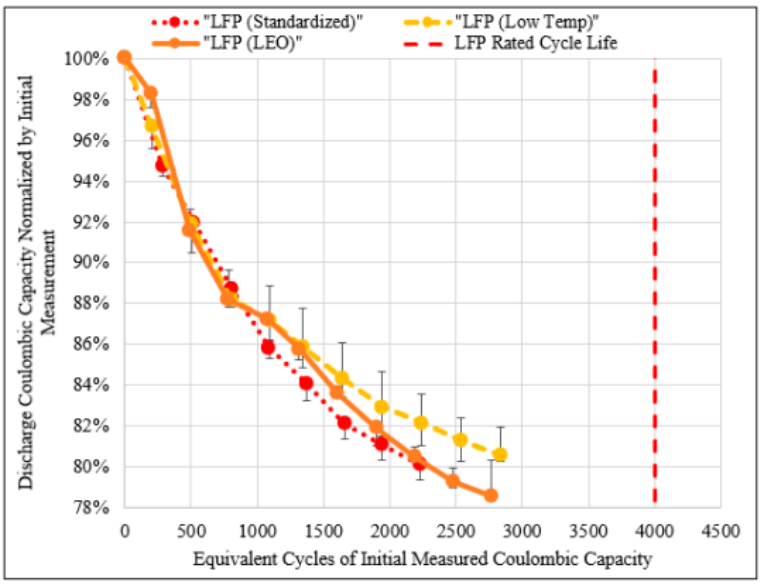

Figure 13.3: Normalized discharge energy capacity degradation

This graph can then be extrapolated to estimate a value for the capacity at the end of the mission. At 15 orbits a day for two years, after 10950 orbits it can be estimated that the capacity of the batteries will have dropped to 70.6%. As the system only requires 55% of the capacity to function, the batteries will be able to store and provide power for the entirety of the mission.

13.6. EPS Summary

Finally, now that the energy flow in and out of the battery is known, some plots can be made to visualise the power requirements, as well as when the battery is charging and discharging. Figure 13.4 shows the input wattage from the solar panels, the output wattage of the battery, and the total power flow of the battery. The green shaded region represents spare energy that is being stored into the battery, while the red shaded region represents the battery being discharged. Figure 13.5 represents the charge level of the battery over the orbit. For a successful system, the end charge level must be equal to or slightly higher than the start charge level.

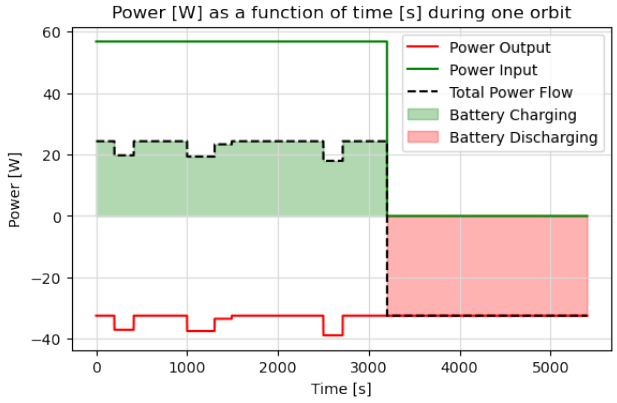

Figure 13.4: Charge and discharge battery diagram

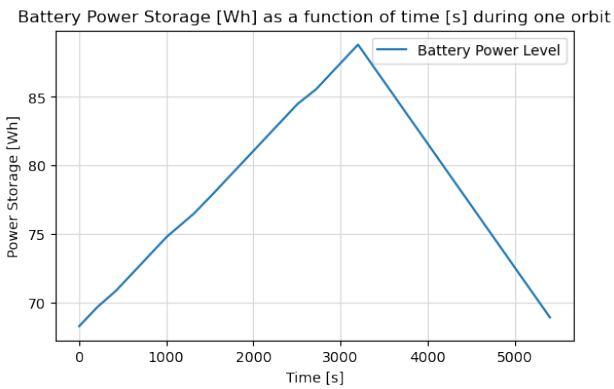

Figure 13.5: Battery power level over one orbit

A list of important parameters of the EPS system can be found below:

Table 13.5: Final EPS Design

EPS Parameter	Value	Unit
Power Distribution Board		
Maximum Allowed Input Voltage	18	V
Maximum Allowed Input Power	70	W
Maximum Allowed Output Power	175	W
Maximum Allowed Power Storage	161	Wh
Power Generation		
Number of Panels	32	-
Maximum Input Voltage	9.64	V
Maximum Power Generated	56.7	W
Power Storage		
Battery Maximum Charge Required	88.6	Wh
Minimum Battery Charge	68.2	Wh
Maximum Power Output	38.8	W

What is important to note is that:

- The input voltage is lower than the maximum allowed input voltage. **(9.64V < 18V)**
- The input power is lower than the maximum allowed input power. **(68.1W < 70W)**
- The battery charge required is lower than the maximum available storage. **(86.0Wh < 161Wh)**
- The output power is lower than the maximum allowed power output. **(49.5W < 175W)**
- The solar panels produce more energy than required. This in combination with containing a battery that is larger than required, means that the EPS can store extra energy for cases where optimal energy production is not required, or for unforeseen circumstances where more energy must be used during the eclipse than previously thought.

Because all these limits were met, the EPS is a working and fully functioning system and meets all requirements of the EPS system chosen. A list of all the EPS requirements can be seen below.

Table 13.6: Electrical Power System Requirements

Identification	Requirement	Requirement Met
AIS-EPS-REQ-01	The EPS shall regulate power from the energy source.	✓
AIS-EPS-REQ-02	The EPS shall regulate the charging of the power storage system.	✓
AIS-EPS-REQ-03	The EPS shall regulate the discharging of the power storage system.	✓
AIS-EPS-REQ-04	The EPS shall monitor the total voltage of the bus.	✓
AIS-EPS-REQ-05	The EPS shall monitor the individual power consumption of each system.	✓
AIS-EPS-REQ-06	The EPS shall regulate power to individual systems on the bus.	✓
AIS-EPS-REQ-07	The CDHS shall draw no more than 0.15 watts.	✓
AIS-EPS-REQ-08	The EPS shall have a state of charge.	✓
AIS-EPS-REQ-09	The EPS shall have a state of health.	✓
AIS-EPS-REQ-10	The EPS shall be able to receive commands from the OBC.	✓
AIS-EPS-REQ-11	The EPS shall be able to send data to the OBC.	✓
AIS-EPS-REQ-12	The EPS shall have an energy capacity of 91.2 Wh.	✓
AIS-EPS-REQ-14	The EPS shall remail operational between -20 and 60 degrees Celsius.	✓
AIS-EPS-REQ-16	The EPS shall survive the launch environment.	N/D
AIS-EPS-REQ-17	The EPS shall remain operational up to a total ionizing dose radiation level of 20 Krad.	✓
AIS-EPS-REQ-18	The EPS shall be protected against ESD.	✓
AIS-EPS-REQ-20	The EPS shall not exceed a maximum mass of <tbd>g.	✓
AIS-EPS-REQ-21	The EPS shall take up a maximum of <tbd>cm^3.	✓
AIS-EPS-REQ-22	The EPS shall provide a peak electrical wattage of 25 W on one single rail.	✓
AIS-EPS-REQ-23	The EPS shall provide a peak total electrical wattage of 38.8 W.	✓

*Requirement AIS-COMMS-REQ-03 cannot be verified at this stage in the program, vibrational testing will be used to verify this test.

13.7. Recommendations

One recommendation for the EPS system is the layout of the solar panel system. Instead of having four units of four cells (4x4) for each panel (16 cells on each side, 32 total), what could be an option is to have three units of four cells (3x4) (12 cells on each side, 24 total), including four cells that are body mounted but not always facing the sun. This would be a total of 28 cells, which is above the required 27 cells. This would greatly reduce the drag and area of the solar panels, which could reduce the propulsion system requirements and make the satellite much more compact and efficient.

Furthermore, another recommendation would be to fly at a higher altitude. The result of which would be a decrease the solar panel size and an increase on the size of the battery, as the satellite would be spending more time in the eclipse. As the battery is only being used at half capacity, this is certainly possible and it would increase the efficiency of the system as there would be no 'wasted' power storage capabilities. An example simulation was run at an altitude of $550km$, which reduced the number of solar panels required from 27 down to 24, which would result in the system described above (3x4) without the need for the body mounted solar panels. This would also increase the battery requirements from $88.6Wh$ of storage to $122.0Wh$. In fact, the highest orbit that the EPS can still function at is at $1400km$ before requiring a larger battery (not considering the changes in modes of operation). At this altitude, only 22 solar panels would be required. A plot of the battery size and number of solar panels versus orbital altitude can be found in Figure 13.6. As can be seen in this graph, by flying at the current altitude of $277.96km$, the design is at an extreme end for the solar panel size and battery capacity required. Finally, by flying at a higher orbit, the number of cycles on the batteries would decrease, increasing their lifetime and slowing the degradation of their capacity.

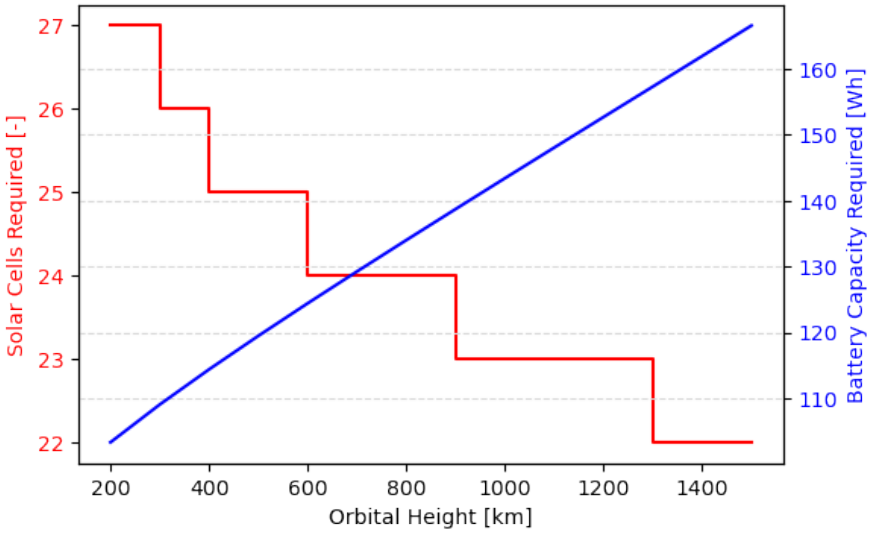

Figure 13.6: Battery size and number of solar panels for different orbits

14 Structures

This chapter will discuss the design process of the structure of the satellite. First the possible off-the-shelf solutions and primary structure of the structure will be discussed in Section 14.1 and Section 14.2. Then secondary structure will be discussed in Section 14.3. The deployment, attachment en structure of the solar panels will be discussed in Section 14.5. Using the obtained information an optimal internal layout was designed and rendered in Section 14.6. The chapter is ended with a list of requirement, RAMS analysis, conclusion, and recommendations.

14.1. Off the Shelf Solutions

From initial volume estimations it is known determined that the size of the satellite must be between 6U and 8U, some off-the-shelf solutions were found for these forms. The 6U solution is seen below in Figure 14.1 and the 8U solution in Figure 14.2.

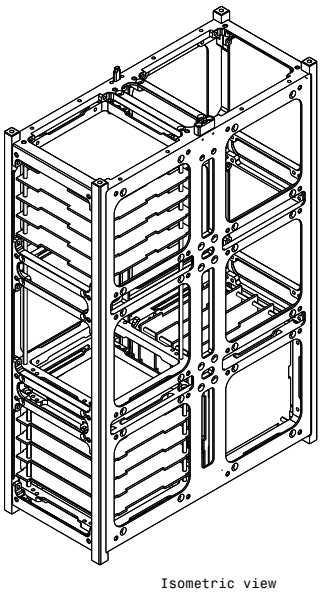

Figure 14.1: Off-the-shelf solution 6U [1]

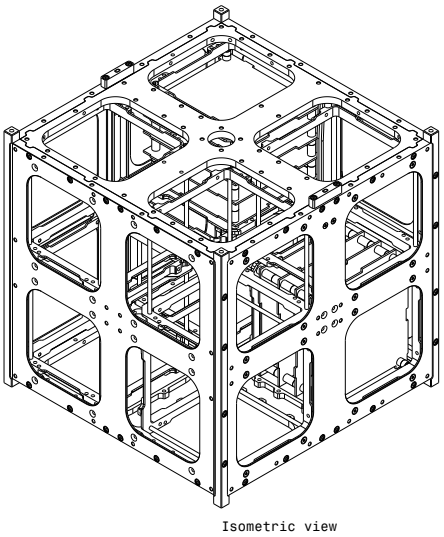

Figure 14.2: Off-the-shelf solution 8U [2]

In a regular CubeSat it makes sense to take an off-the-shelf solution but due to several factors this was not ideal for the mission. To start off with the payload of the satellite is spanning its whole length and a lens that would not fit in the CubeSat's holes as well as needing large solar wings to provide the power required for the satellite. This power requirement comes from the following top level requirement **AIS-TL-REQ-11** that states that the spacecraft shall have a propulsion system. Due to the unconventional loads that the large solar panels would force on the structure and the fitting of tilt motors for the solar panels a more tailored design was needed. Another reason for which a new structure was designed was to integrate the solar wings into

the structure of the spacecraft to save space and weight.

14.2. Summary

In Canosa et al., 2021b the primary structure had been sized for a 6U CubeSat with mass values derived from statistics. Then a set of conservative assumptions were used to find the loads on the primary structure.

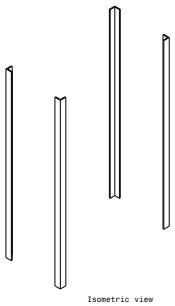

Figure 14.3: Primary Structure 6U

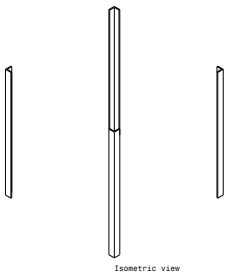

Figure 14.4: Primary Structure 8U

From these assumptions a simplified model for the loads on the primary structure was made and used to create a script. The script uses the requirements in Table 14.2 to create the primary structure so the output of the script is a element able to meet all the load requirements. Then the other elements would transfer loads to the primary structure and to itself. This script uses a set of simplified models for both the dynamic and static loads which then results in the flange lengths of the corner L-beams. The result of the scripts can be seen above, Figure 14.3 shows the one for a 6U CubeSat and Figure 14.4 shows that of a 8U one.

14.3. Secondary Structure

The primary structure is joined together through the secondary structure and the bolts that hold them together. Therefore the skin and mounting points need to be designed. Firstly the skin of the spacecraft is sized to transfer loads between member of the primary structure, then the bolts that integrate the skin onto the primary structure where designed.

14.3.1. Skin

The primary structure to this satellite has been defined, but in order for this structure to perform its required function it must displace cohesively and distribute the load between all the four members. In order for this to happen a so called ”skin” is going to act as the load path between the primary structure, as well as some caps on either side of the L-beams. The cap on the lower side will also have to transfer the load from the mounting points on the LV to the primary structure. In Figure 14.5 the influence of the skin can be seen in the compression and tension stresses of the primary structure, since in the no skin concept the beams move separately they bend around their own respective neutral lines and are loaded in both compression and tension whereas the skin concept makes the top beam load in tension and the bottom beam load in compression.

[1] ISISPACE site 6U cubesat structure. Visited on the 10-01-2022.
[2] ISISPACE site 8U cubesat structure. Visited on the 10-01-2022.
[3] Intechopen paper on radiation in space. Visited on the 17-01-2022.

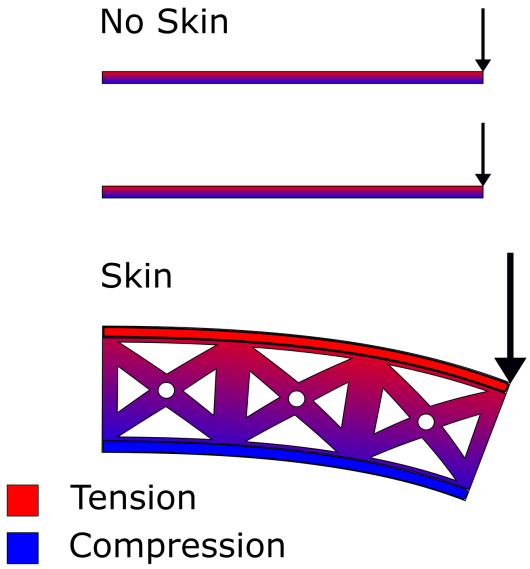

Figure 14.5: Influence of skin on the load transfer

The skin has cut-outs to increase the effectiveness of the material used, so areas that do not get loaded under high stress are removed leaving the shape shown below in Figure 14.6. This process of topology optimization was not done in this project and is out of the scope of the current phase of the project so a approximate shape from past missions was used.

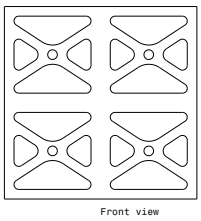

Figure 14.6: CubeSat Skin

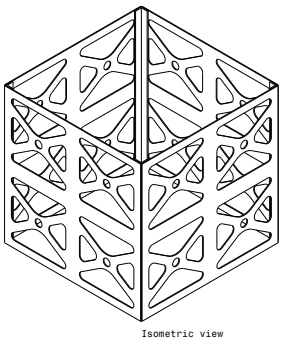

Figure 14.7: Structure of the CubeSat

The skin elements are then placed on the sides of the primary structure forming a load path between all members this is shown in Figure 14.7. As for the connections between the skins and the primary structure, that will be done using bolts made out of AL7076-T61, the same material as the structure due to its high yield strength and low density.

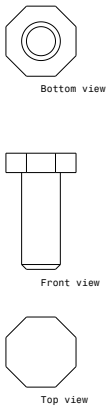

Figure 14.8: Bolt

First moment of area equation: $Q = \bar{y}' A'$

Shear stress equation: $\tau = \frac{VQ}{It}$

Shear flow equation: $q = \frac{VQ}{I}$

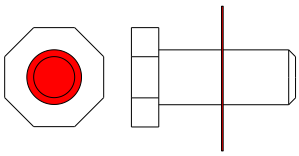

Figure 14.9: Bolt Failure Point

Assumptions for the design of the attachments.

- No internal moment is transferred to the bolt.
- The bolt will not pull-out.
- The critical mode of failure is shear-out.

The critical part of the bolt to stop the skins from detaching from the primary structure is the body of the bolt shown in red in Figure 14.9. In order to size these bolts the equations shown above are used going from first moment of area, to shear stress and then to shear flow which can be used to find the required spacing between the bolts for every bolt. Which will be done in the next phase of design.

14.3.2. Mounting Points

The components in the satellite must be fastened to the primary structure in order for the system to withstand the launch environment and at the same time be removable. In order to fulfill these requirements bolts and nuts will be used. So the mounting points for the SC shall be able to connect to the component with a bolt specified by the hole diameter of such component.

14.4. LV Mounting

The launch loads experienced by the SC come from the dynamics of the launch vehicle and therefore the load path must go from the LV to the SC's primary structure. This is done using a structural cap on the L-beams this cap is both part of the primary structure and the secondary structure as it transfers loads from the launch vehicle to the primary structure and also holds the primary structure together.

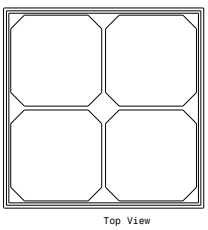

Figure 14.10: CubeSat end caps

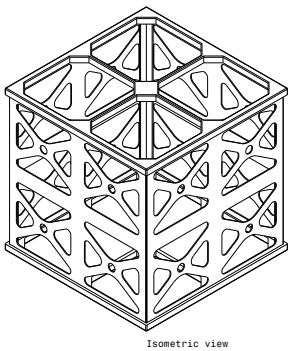

Figure 14.11: Structure of the CubeSat with end caps

The end caps are part of the load path from the LV to the spacecraft as well as holding the other structural components to each other. When designing the end caps there are some important things to consider:

- The structure must transfer the loads to the primary structure.
- The structure must have connections between the members of the primary structure.
- The structure must be symmetrical in the two planes perpendicular to the nadir.

From those the geometry shown in Figure 14.10 is found to be a fitting solution. These end-caps are then placed on the top and bottom of the structure with the bottom cap fastening into the LV.

14.5. Solar Panel Wings

From preliminary calculations of the EPS system and the surface area of the SC done in (Canosa et al., 2021b) it has become clear that body mounted panels will not meet the power requirement. From this it was calculated that some type of deploying solar panel is needed. A simple two wing design with one axis rotation system to find the sun was the concept that was chosen. Due to the fact that the solar panel area needed is 0.32 m^2 the wings would be too weak to withstand launch so a folding system was created so that the panels would be rigidly held in the launch vehicle and not take up too much space. This is shown below in Figure 14.12 with a series of steps to show how it deploys.

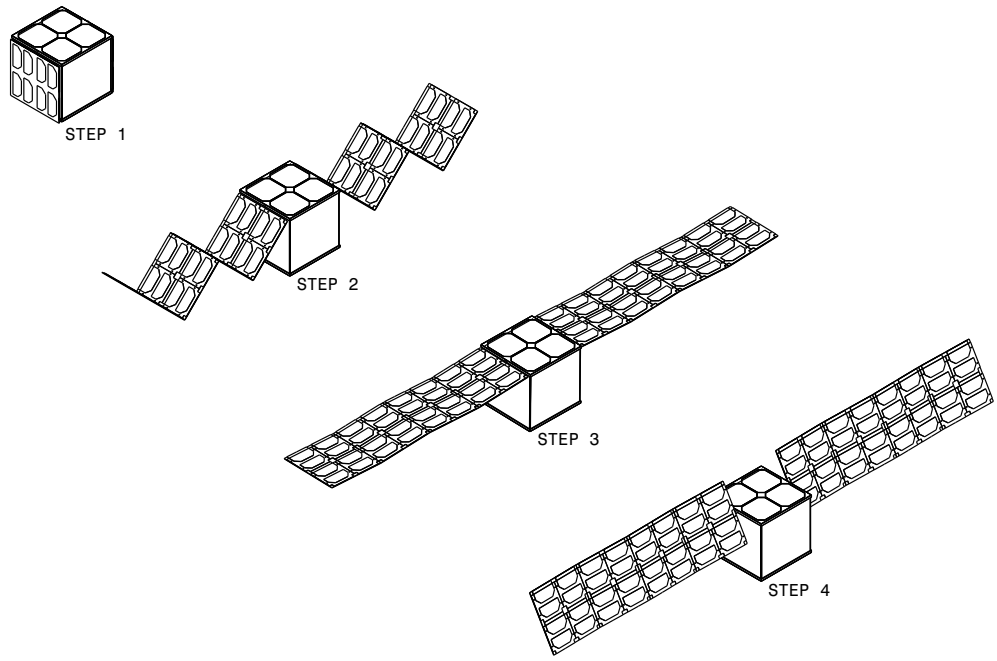

Figure 14.12: Solar panel wings deployment

14.5.1. Deployment

The deployment of the solar panel will be done using a torsional spring in a hinge that shall move the solar panel into place and then hold it there using retained elastic potential energy. The angle and speed at which it deploys will be tuned using the stiffness and pretension of the spring. This deployment is seen in Figure 14.12 where STEP 1-3 is the deployment and STEP 4 is the small electrical motors in the wing base tilting the wings to find the sun.

14.5.2. Structure

The structure of the solar wings are segments of 4 solar panel components placed together to a aluminium backing plate of 1 mm thickness these segments are then connected with hinges that have the previously stated torsional springs to deploy.

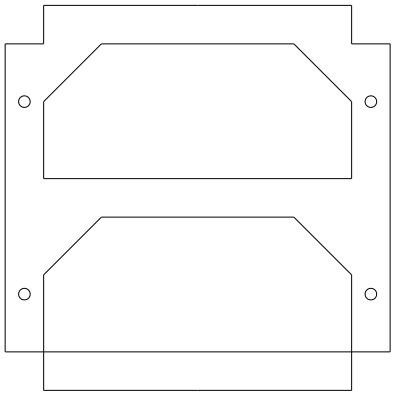

Figure 14.13: Solar panel component

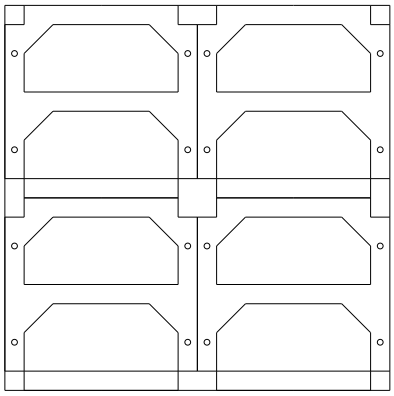

Figure 14.14: Solar panel segment

In Figure 14.13 the solar panel component is shown which is then placed in the segment in Figure 14.14 where they are conjoined using an aluminium backing plate as to add rigidity.

14.6. CAD

Computer aided design for this satellite was done using CATIA V5 which was used to make a 3d model of the packaging of the satellite, in order to get a visual representation of how all the components fit in the 8U form. The software was also used to find the volume of parts of known density such as structural components to perform a calculation on the mass of the components.

14.6.1. Packaging

For the purposes of reducing our reducing the MMOI and fitting the every subsystem in the bus an 8U cube-sat shape was chosen for the bus. The cube would locate all the components as close as possible to the geometric center therefore reducing the MMOI of the spacecraft. When placing the components throughout the spacecraft it was important to consider the following factors:

- The CDHS is sensitive to radiation and therefore must be placed in the inner most parts of the satellite, so that other less sensitive components can shield it from radiation.
- The Payload's scope must be facing towards the Earth.
- All the boards should be placed together in a stack.
- The propulsion's thruster should be facing the direction opposite the direction of travel.
- The ADCS component's star tracker must not be obstructed and must be facing away from the Earth and the Sun.
- The batteries must be as far as possible from temperature sensitive components or other components that produce a lot of heat.

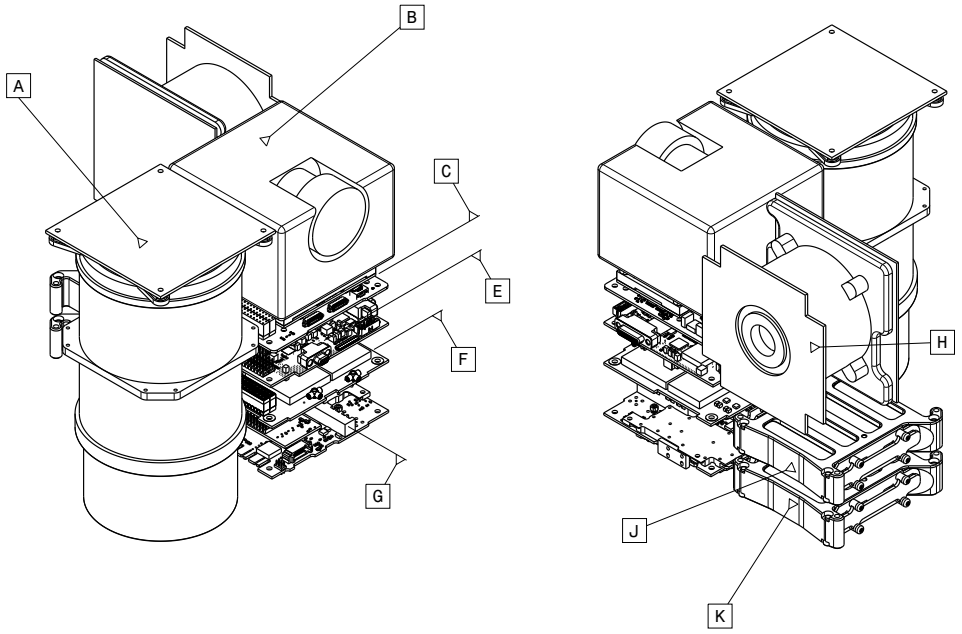

Figure 14.15: Packaging of components

The components corresponding to each letter label is shown in Table 14.1 and it is clear that this packaging scheme can pass every requirement stated above. In addition there is a 2U column to spare which in the future might open up possibilities to go back to a 6U CubeSat.

14.6.2. Components

The components in the satellite are listed below along with the mass in order to find the mass budget in Table 14.1. Departments were asked for the components and once a component was selected the packaging of that component had been estimated to check that it can properly fit in the spacecraft and will compatible with the other components.

Table 14.1: Mass budget

Component Name	Mass (kg)
Structure	22.2
Solar Panel Structure	1.3
Propulsion (H)	0.7 dry 0.9 wet
Payload (A)	1.6
Comms Board S-Band (G)	0.3
Comms Board UHF (F)	0.1
Cogni Sat Board (D)	0.3
Antelope OBC (C)	0.3
Silicone panels	1.0
Solar Panels	0.8
Batteries (J, K)	0.8
ADCS (B)	1.7
Total	31.2

The structure mass is 22.2 kg which in its own weighs more than the previous estimate for the satellite mass. This is because the satellite structure is not at all optimized, this will be done in the future.

14.7. Subsystem Protection

Since the satellite is orbiting in LEO the protection of the subsystems from radiation and EMF become critical to the mission. Therefore there will be a layer of protection for the subsystems in this calculation the bus will be protected as a whole rather than individual subsystems.

14.7.1. EMF Protection

High energy electro-magnetic waves have the ability to knock electrons out of the outer shells of atoms, therefore ionising them as well as emitting an electron with it too having potentially harmful effects. This effect combined with satellite self shadowing causes trapped charge differentials that can build up to have a potentially harmful effect.

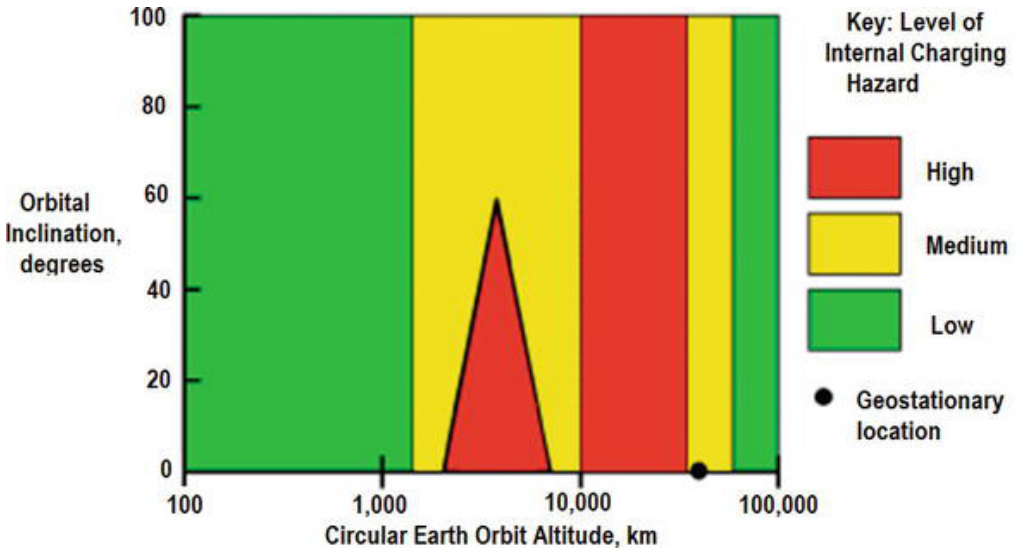

Figure 14.16: Charging hazard [3]

From Figure 14.16 it is found that differential charging of the satellite is of little concerned at LEO and therefore can be ignored. As for the secondary affects of high energy waves, that being the splitting of atoms and high energy particles made in the process, that will be addressed below in radiation protection.

14.7.2. Radiation Tolerance

The satellite must operate in low earth orbit polar orbit for a duration of 2 years, therefore the spacecraft will be crossing the Van Allen Belts as they converge in the poles. Since high energy particles get trapped in these belts crossing them may cause a potential threat to components in the satellite. The South Atlantic Anomaly is also a potential threat as it means there is a higher amount of high energy particles at a lower altitude. A further analysis of the total ionising dose experienced by the subsystems will be done in the next steps of design.

14.8. Requirements

The objective of any design is to fit the requirements and the requirements that were set for structures are listed below in Table 14.2. The check marks mean that the requirement is fully met and the circles mean that the requirement will be met in the future but needs further development in the next design phase.

Table 14.2: Structure Requirements

Identification	Requirement	Requirement Met
AIS-STRUC-REQ-01	The satellite structure shall withstand all the expected structural loads generated on a launch.	✓
AIS-STRUC-REQ-02	The satellite structure shall withstand all the expected vibration loads generated by prospective launch vehicles.	✓
AIS-STRUC-REQ-03	The satellite structure shall have a longitudinal natural frequency of greater than 90 Hz.	✓
AIS-STRUC-REQ-04	The satellite structure shall have a lateral natural frequency of greater than 35 Hz.	✓
AIS-STRUC-REQ-05	The satellite structure dimensions shall adhere to the CubeSat design standard.	✓
AIS-STRUC-REQ-06	The structure rails shall have a minimum width of <tbd> mm.	●
AIS-STRUC-REQ-07	The structure rails will have a surface roughness less than <tbd> µm.	●
AIS-STRUC-REQ-08	The edges of the rails will be rounded to a radius of at least 3 mm.	✓
AIS-STRUC-REQ-09	The satellite center of gravity shall be located within <tbd> mm from its geometric center in the X and Y direction.	●
AIS-STRUC-REQ-10	The satellite center of gravity shall be located within <tbd> mm from its geometric center in the Z direction.	●

14.9. Reliability, Availability, Maintainability and Safety Analysis

The reliability of the structure is very high since the mission outline did not set a cost cap on the LV cost, this means that mass is no longer as important as it would be on other missions, so a safety factor of 3 is used. Although the exact reliability is not quantifiable at this point in time it is clear that it is more than sufficient. The potential influence of the structure breaking during launch would be catastrophic to the mission and the mission would end there, but if it were to fail in orbit the consequences are very hard to predict.

The availability of the parts for the structure is very high as standard OTS parts were used for all of it except for the end caps which are machined to the correct geometry. As for the maintenance of the structure, there is not much that needs to be done apart from keeping the components in the correct temperature and in clean dry conditions until launch, after which maintenance becomes impossible.

14.10. Conclusion

The structure of a CubeSat is a fundamental part of the spacecraft and requires extensive amount of time to design fully but the fact is that a conventional OTS soloution would not be possible considering the fundamentally different design of the satellite. One of the aspects that makes this satellite so different to others in its class is the abnormally high power requirement. This mainly comes from the top level requirement **AIS-TL-REQ-11**. From the final CAD of the spacecraft it was found that the is a 2U column in the structure that is empty, although this is not necessarily a drawback it does mean that the spacecraft could be changed into a 6U satellite or more components could be added to improve the mission.

14.11. Recommendations

The structure for the cubesat is a very complex and critical part of the spacecraft and it is essential that this does not fail. Therefore a set of recommendations are explained to guide the next steps of the design process. The current design is a suitable structure but lacks the optimization and detail of a finalized version. From the current design iteration there is a excess in free unused space in the satellite so the next iteration could be a 6U CubeSat.

14.11.1. Integration

As this project is carried forward there will need to be more focus in the integration of the subsystems to the structure, the mounting points of the subsystems need to be designed as well as the holes in the structure needed for the components. Furthermore a plan for the wiring of the satellite needs to be devised to check that those wires actually fit where they need to go. Additionally the packaging of the satellite must also take into account the electro-magnetic compatibility of the components and make sure that they do not interact in harmful ways.

14.11.2. Finite Element Analysis

Finite element analysis is a vital tool in structural engineering, but at this phase of design the drawbacks of using FEA out weight the benefits that could be gotten from it. FEM would take a lot of working hours from the whole team to make an accurate model of all the subsystems in the SC and the structure. This would be very useful to reduce the weight of the satellite and spot possible points of concern but since the mission

profile states that launcher costs are not constrained the mass reduction aspect is no longer that important. This means higher safety factors can be used to avoid the failure of the structure.

14.11.3. Topology Optimization

Topology optimization and FEA are closely linked since TO can not be done without a good FEA model therefore the same reasons for not doing FEA apply to topology optimization. In the next steps of design all the individual parts in the structure will be analysed for their loads and those loads will then be used in a numerical topology optimization algorithm such that only just enough material is used in the structure and the position of that said material is in the best place.

14.11.4. Coating & Material Finishes

Coating and material finishes such as heat treating have minimal effects to the structural properties and is too in depth for the current phase of design and therefore it is considered and recommended to look into further in the future. This will also be considered for the thermal affects on the spacecraft as material finishes will change the emissivity and absorptivity of the structure.

15 Thermal Control

The following chapter will describe the design of the Thermal Control System. Firstly, the functional analysis and the subsystem requirements will be defined with which the basis for the upcoming analysis is set. This is followed by the recalling the 2 main system design options. Then the methodology behind the thermal analysis is explained, starting with the single-node thermal model. Consecutively, the specifications for the analysis with ESATAN are brought forward. Most importantly, the resulting data will be discussed followed by the surface material trade-off for the subsystems. Then the RAMS Analysis on the design is performed. The chapter concludes with the description of recommendation and future prospects. This chapter is based on the prerequisite work presented in the Baseline Report (Canosa et al., 2021a) and Midterm Report Canosa et al., 2021a)

15.1. Functional Analysis and Subsystem Requirements

The thermal control system regulates the temperature of the satellite. The CubeSat is prone to a variaty of temperature sources such as heat from solar radiation, planetary infrared radiation, albedo radiation and internal heat created by the satellite itself. Additionally to the heat retention and emission, the satellite subsystems must remain within their thermal design constraints as well as temperature gradients to protect its efficiency and lifetime. Therefore, the thermal control system must manage the temperature in favor of the different component requirements in order to ensure the success of the mission (NASA, 2021).
Table 15.1 summarizes the subsystem requirements to be accounted for during the thermal analysis as well as the definition of the design range, being a minimum temperature of 10 ° and maximum of 30 °. This range is defined by the minimum possible range among all subsystems characterized by the payload.

Table 15.1: Temperature Requirements of Subsystems

Component	T_{min} [deg]	T_{max} [deg]
ADCS	-50	100
EPS	-20	60
Hyperspectral Camera	10	30
Solar Panels	-200	130
Antenna	-120	120
General Electronics	-20	70
Design Range	**10**	**30**

15.2. Design System Options

The thermal control system can follow two design principles: active or passive systems.

15.2.1. Active Thermal Control

An active control system directly regulates the temperature through a power regulated system. This provides an advantage in case of strict temperature requirements and/or extreme conditions. Depending on the available power, mass and volume budget, an active system can be implemented although it not common in small CubeSats due to the respective restriction. Nevertheless, smaller heaters can be applied for the electrical power unit in eclipses. Next to that, cryocoolers are also a viable option for CubeSats due to their little power consumption in comparison with other active thermal control systems with a current tendency in an even more compact design. In accordance to that, fluid loops specifically, mechanically pumped loops, would require high power consumption and mass hence are not advisable for smaller satellites. Lastly, an active thermal architecture, despite being comprised amongst others of a micro mechanically pumped fluid loop, is considered to be an advanced active control system. Despite all power input required for active thermal management systems, they often include elements of passive systems for insulation. (NASA, n.d., NASA, 2021)

Throughout the preliminary and current design phase of the project, the strict and limiting constraint on the power budget inhibits the usage of an active thermal control system within the given time frame. Nevertheless, this decision should be reevaluated at a later stage of this project, in case iterations on the constraining power budget are executed. It should be noted that including an active system will add another possible point of electrical or mechanical failure. Especially in case of radiators with fluid pumps, can have a short functionality period or maintainable (J. Meseguer, 2012)

15.2.2. Passive Thermal Control

Passive control does not require power input but relies on the physical phenomena of radiation and conduction. Therefore all options are a viable option to be included in a CubeSat except thermal louvers, thermal storage units and deployable radiators. The main reasons are their extensive volume requirement within the limited satellite structure and for deployable radiators, the limited surface area (Sheldahl, 2020, NASA, 2021).
With this in mind, the main aim of the passive thermal control system is to control the system through the absorbed and emitted energy. It allows the spacecraft to be either isolated from the surrounding environment or to radiate concentrated heat load within the bus.
The upcoming single-node thermal model will provide a design option for the outer satellite panel surfaces. The multi-node thermal model will then provide a more detailed analysis on the option. Thereafter, a trade-off on different surface materials for the thermal control within the satellite will be executed.

15.3. Methodology for the Thermal Analysis

The following chapter will describe the assumptions made throughout the design process, the reiteration of the single node method as it serves as a basis for the elaborated analysis, and the general functionality behind the used thermal analysis software 'ESATAN'.

15.3.1. Design Assumptions

The following section will summarize all assumptions made throughout the thermal analysis. Each assumption will include a label and rationale. For assumptions whose rationale is solemnly simplicity, the reason will not be included

AI-TC-ASSU-01: All faces of the satellite are constituted of the same material.
AI-TC-ASSU-02: The deployable solar panels will not be included.
AI-TC-ASSU-03: The only source of internal power dissipation is the battery.
AI-TC-ASSU-04: The Earth's radiation intensity remains constant at 237 W/m^2K^4 .
AI-TC-ASSU-05: The Multi Node Thermal Model using ESATAN will be performed using a lumped parameter method.
Rationale: By applying said mathematical model formulation, each node becomes isothermal, thus the temperature difference within the node is negligible.

AI-TC-ASSU-06: All subsystems in the model are comprised of one material - Silicon from the printed circuit board - except the propulsion system, which is set to be composed from Aluminium 7076 T61.
Rationale: As most subsystems are constituent from printed circuit boards, such as the Transceiver or the CDH System, for the sake of simplicity in this analysis, the assumption was followed.

AI-TC-ASSU-07: The cutouts in the actual OTS structure will be neglected, but the actual skin thickness of 1 [mm] will be used.
Rationale: At the current design stage of the project, the cutouts' effect is not analysed. By applying a top surface of gallium arsenide (GaAs) solar panels or epoxy black paint, generally, the effect of aluminium is insignificant from an optical properties perspective by comparing the emissivity of 0.8 and 0.85 of GaAs solar panels and epoxy black paint to aluminium's value of 0.03 (Sheldahl, 2020). Therefore, the effect of the cutouts can be assumed to be negligible.

AI-TC-ASSU-08: The epoxy black paint and the GaAs solar cells are assumed to have the same thickness.
AI-TC-ASSU-09: All dissipated power is converted into a radiative heat load.
AI-TC-ASSU-10: All systems, except the payload, are turned on throughout the orbit.
Rationale: Intuitively, this is not the case as per Chapter 5 but due to time constraints, this detail cannot be guaranteed at this stage of the design.

15.3.2. Single Node Thermal Model

For the more detailed design, the orbital parameters have been reestablished. Therefore, the single node method as outlined in ((Wertz et al., 2011)) conducted in the preliminary design has to be corrected accordingly. With a new orbit height of 285.1 km and an updated geometry of an 8U CubeSat, all parameters change and will result in new balance temperatures for a hot and cold case. The adapted values for either case is summarized in Table 15.2 and Table 15.3. It should be noted that only for this model the assumptions AI-TC-ASSU-01 and AI-TC-ASSU-02 are valid.

Table 15.2: Most important values: general and for the cold case

Constant	σ $[W/m^2K^4]$	$\dot{Q}_{int}$ [W]	J_p $[W/m^2]$	A_{IR} $[m^2]$	A_{alb} $[m^2]$	A_{total} $[m^2]$	$J_{s_{cold}}$ $[W/m^2]$	$A_{sun_{cold}}$ $[m^2]$	$J_{a_{cold}}$ $[W/m^2]$
Value	$5.67 \cdot 10^{-8}$	5.334	217.2	0.04	0.04	0.24	1314	0.04	553.14

Table 15.3: Most important values: for the hot case

Constant	$J_{s_{hot}}$ $[W/m^2]$	$A_{sun_{hot}}$ $[m^2]$	$J_{a_{hot}}$ $[W/m^2]$
Value	1419	0.051	234.14

An analysis on different surface materials was performed, yet the most promising options are found in Table 15.4. It becomes evident that comparing the limits for Gallium Arsenide Solar Panels and Epoxy Black Paint to the set design limit of a minimum temperature of 10 ° and a maximum of 30 °, the analysis so far meets the requirements. The next step is to perform a more detailed analysis using the thermal control software design tool ESATAN.

Table 15.4: Temperature limits for different surface materials

	GaAs Solar Panels			**Black Paint (Epoxy)**		
	α	ε	α/ε	α	ε	α/ε
	0.88	0.8	1.1	0.95	0.85	1.12
T_{min} [deg]	17.90			18.73		
T_{max} [deg]	23.06			23.93		

15.3.3. ESATAN

ESA developed a thermal-radiative software tool for spacecraft thermal control design, ESATAN, which has been widely used in the industry for over 25 years. The tool allows to perform analysis on radiative and conductive heat transfer for space over a selected orbit. The biggest advantage of using ESATAN and the reason to be applied in this project is firstly, the reliance and application of the software in the space industry and secondly, the reliable prediction of radiative exchange of the model due to its high number of radiative couplings (Ltd., 2017).
Radiation is the biggest environmental factor to be considered in a thermal analysis. In the case of SigmaSat, with an orbital height of 277.96 km, the infrared radiation and albedo effect from Earth have the highest impact.

Mathematical Background

ESATAN offers a mathematical model formulation using either a lumped parameter or a finite element approach. As indicated in Section 15.3, the analysis for this design stage was done using the lumped parameter method. Similarly to the finite element formulation, the geometric model is divided using a grid with each part, node, representing a point to which the physical properties are lumped onto; this type of analysis in the context of thermal control is commonly denoted as a 'Multi-node Thermal Model' and thus, the extension of the single node thermal model executed earlier (Wertz et al., 2011).
The main difference to a finite element 'node' is the assumption of the lumped node being isothermal. After the meshing of the geometry, the connections between the thermal nodes represent radiative and conductive couplings with other parts of the model. This creates a nodal system similar to the finite element formulation, hence the set of equations used in either mathematical formulation are almost identical. The system of equations is then managed using a set of matrices followed by an approximate linearization and iterations (Ltd., 2017).
Throughout this thermal analysis, the radiation is considered to have the highest impact. The most important

aspects to consider in the radiative heat exchange between 2 surfaces are the surface temperatures, surface properties and the radiative view factors (Wertz et al., 2011). The amount of radiation dissipated via surface *i* and absorbed by surface *j* can be described with the following equation:

$$Q_{r_{ij}} = A_i F_{ij} \varepsilon_{ij} \sigma (T_i^4 - T_j^4) \tag{15.1}$$

with F_{ij} denoting the view factor of surface *j* with respect to surface *i*, and ε_{ij} defining the effective emittance, a property describing the relationship between two surfaces based on their optical properties and reflections, either with respect to each other or distinct neighbouring surfaces. This relationship is defined by Equation 15.2 (Wertz et al., 2011).

$$\varepsilon_{ij} = \frac{\varepsilon_i \varepsilon_j}{\varepsilon_i + \varepsilon_j - \varepsilon_i \varepsilon_j} \tag{15.2}$$

With this in mind, the next step is to perform an instantaneous heat balance of the *i*th node for a thermal model consisting of *n* nodes by following the thermodynamic principle of equilibrium (Wertz et al., 2011).

$$Q_{env,i} + Q_i = Q_{out,i} \tag{15.3}$$

Q_i denotes the internal heat dissipation of node *i*. $Q_{out,i}$ defines the dissipating heat from node *i* which includes the radiative heat exchange of diffusing surfaces, the conductive heat exchange and the total infrared dissipation of node *i*, with the former two denoting a relationship between node *i* and *j*. It should be noted that the occuring conduction occurs as the nodes are, for instance, located on the same satellite panel with its surface having the same material and thus conducting heat (Wertz et al., 2011).

$$\begin{aligned} Q_{out,i} &= \sigma T_i^4 \varepsilon_i A_{eff,i} + Q_{cond,ij} + \sigma \sum_{j=1}^{n} A_i F_{ij} \varepsilon_{ij} \sigma (T_i^4 - T_j^4) \\ Q_{cond,ij} &= \sum_{j=1}^{n} h_{ij} (T_i - T_j) \end{aligned} \tag{15.4}$$

$Q_{env,i}$ describes the radiative influence of the space environment accounting for the solar, albedo and infrared planetary radiation (Wertz et al., 2011).

$$Q_{env,i} = \alpha_i (A_{sun,i} J_s + A_{alb,i} J_a) + A_{IR,i} J_p \varepsilon_i \tag{15.5}$$

These equations are then linearized by ESATAN with respect to time and solved accordingly. The solution control, i.e. the numerical analysis method, is determined in the definition of the thermal cases and thus, will be explained in Section 15.4.3.

15.4. Analysis Outline

The following section will describe the set-up of the model and the decision made throughout the process and related assumptions are mentioned passim. Unfortunately, due to licensing issues, the original analysis including the power dissipation and the subsystems was unable to be performed. This meant for the analysis to be constrained by evaluating the solutions of the side panels and solar panels, solemnly. Nevertheless, the following section will still explain the set-up of the model for the intended analyses.

15.4.1. Geometric Model Definition

The first step in defining geometry is to set the bulk material and the optical sets that will be used. Intuitively, the geometry model in ESATAN will be the simplification of the actual geometry, starting with the structure as per Chapter 11.

Bulk Material and Optical Sets

Generally, 3 bulk materials were used in this thermal model: Aluminium 7076 T61, Silicon and 'Foil'. The aluminium results from the chosen material based on the structure. The silicon will be used to model the PCB material and the 'Foil' is a dummy bulk material which was used to apply the optical properties. This is needed as all panels, including the solar panels are modelled with the shell geometry type. The dummy material then assigns the given optical set a thickness. This dummy value as shown in Table 15.5 has 0 density, 0 specific heat but a value of 0.01 $[W/mK]$ due to a computational constraint from the software.

Table 15.5: Values of the bulk material properties used in ESATAN

Bulk Material	**Density** $[kg/m^3]$	**Specific Heat** [J/kg K]	**Conductivity** [W/m K]
AL7076 T61	2840	880	160
Silicon	2330	703	163.3
Foil	0	0	0.01

For the model, there are several optical sets defined: GaAs solar cells, epoxy black paint, multi-layer insulation (MLI), the emittance of the battery and of the uncoated PCB.
The emissivity and the absorptivity of the solar cells and the epoxy black paint remain the same as given in the single node thermal model Table 15.4 (Wertz et al., 2011). The MLI values are based on the a major manufacturer in the market, Sheldahl (Sheldahl, 2020). The emissivity from the battery and the uncoated PCB are used from the experimental research paper on the optical properties of nanosatellite hardware (M.M. Finckenor, 2014).

Table 15.6: Values of the optical properties used in ESATAN

Optical Set	**Absorptance** α	**Emissivity** ε
GaAs Solar Cells	0.88	0.8
Epoxy Black Paint	0.95	0.85
MLI	0.14	0.035
Battery	0	0.85
Uncoated PCB	0.74	0.88

After having defined the materials and optical properties, the actual geometry it set up. Throughout the process, AI-TC-ASSU-07 which defines the side panels of the satellite with an inner aluminium surface with 1 mm thickness. The outer surface is, for both the epoxy black paint and the GaAs solar cells, modelled with a 'Foil' thickness of 120 [nm] (Hutchins, 2021) while including AI-TC-ASSU-08. The solar panels are similarly modelled but with double the thickness, 240 [nm].

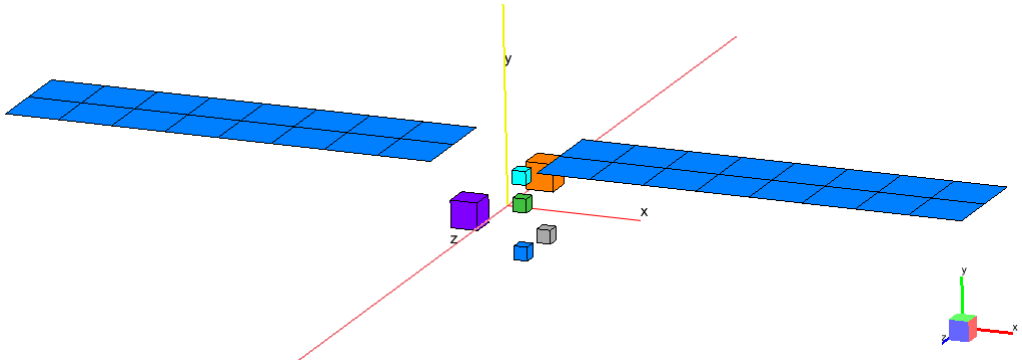

Figure 15.1: Geometry of the Model with the side panels hidden

.

The subsystems were thought to be originally modelled using a non-geometric thermal node as it enables to assign a source of, in this case, power dissipation. However, this requires to define all radiative couplings which, at the stage of the project, cannot be done due to the lack of a detailed satellite layout as well as the harness. Therefore, the subsystems were modelled as smaller solid blocks as seen in Figure 15.1, with the ADCS, CDHS, EPS and Comms of same size, and the payload and propulsion in the same dimensions. Regarding assigning the bulk material, assumption AI-TC-ASSU-06 was made, hence all subsystems are comprised of Silicon except the propulsion system which was assigned aluminium to.
Additionally, the optical sets were assigned to each surface. Firstly, the solar panels include the GaAs solar cells optical property. The panel sides are assigned either the GaAs solar cells properties or the epoxy black paint as they define either design option which will be traded off against. Furthermore, the EPS is assigned

the 'battery' property while the ADCS, Comms and payload the uncoated PCB and the propulsion the MLI. Once all components and panels were determined, the assembly was made. An assembly is to be defined not only by choosing the rotation axis and pointing vector, [0.0, 0.0, 1.0] and [0.0, 1.0, 0.0], respectively, but by defining the moving component with respect to the sun. For this analysis, the solar panels were decided to move, always perpendicular with the incoming sun vector, with respect to the fixed geometry, here the rest of the satellite.
With the main geometry defined, the conductive interfaces had to be specified as 'fused', 'contact', 'not connected' or 'not processed'. The only fused interfaces that were assumed to be present was between the top panel and the two solar panels, i.e. the geometries form one continuous surface, in the design option for which all side panels are covered in GaAs solar cells. All other side panels were assumed to have only a contact interface, meaning the surfaces are linked by a physical interface with each other. In the case of all side panels covered in epoxy black paint, all conductive interfaces are 'contact' interfaces.

15.4.2. Radiative Cases

The radiative cases serve as the basis for the upcoming thermal cases. The radiative cases entertained in this analysis are for both the hot and the cold case. The main difference with respect to the input parameters is the albedo effect and the solar declination angle ESA, 2008

Table 15.7: Radiative Cases

Variable	Cold Case	Hot Case
Orbit Height [m]	277,960	277,960
Eccentricity [-]	0	0
Inclination [°]	96.6	96.6
Solar Declination [°]	-23.45	23.45
Albedo [-]	0.306	0.35

15.4.3. Thermal Cases

With the radiative cases defined, the thermal cases can be determined. The most important step is the definition of the solution control logic. Separately, boundary conditions can be determined and applied.

Solution Control

The solution model used is a combination of first utilizing a steady state solution with the matrix factorization method and then a transient model whereas it is possible to decide upon the Crank-Nicolson, Forward Differencing and Forward-Backward Euler. Independently from the exact method, the solution is defined over the period of the orbit, i.e. 5,401.745 [s] where a total of 10 solution are given over the course of the orbit.
For this analysis, the Crank-Nicolson approach was chosen as it is implicit in time and is numerically unconditionally stable, convergent and consistent (Thomas, 1998). The Crank-Nicolson method can be described as a combination of both the forward and the backward Euler method. However, the Crank-Nicolson is not an average of both as the backward Euler is implicitly dependent on the solution. Although, numerical oscillations may occur at large time steps due to the forward Euler term in the definition, the backward Euler method is the more favorable instead. But the verification of this method and evaluation of either numerical solution can only be executed using a sensitivity analysis on the outcome of ESATAN. Due to time constraint, this cannot be performed but the rationale on a possible set-up of such a sensitivity analysis will be demonstrated in Chapter 13.

Boundary Conditions

The power dissipation of all subsystems in this thermal model was made available by modelling each subsystem as a box which would coincide with the packaging boxes in the CATIA model. From the incoming power as well as the efficiency the total power dissipation was obtained for each subsystem. It was assumed, following AI-TC-ASSU-09, that all power dissipation would fully convert into heat. ESATAN provides the option to define a heat load over a unit area with the values given in Table 15.8. This was used to then include all power dissipation from all components in the model analysis.

Table 15.8: Heat Load / Unit Area for the definition of boundary conditions

Component	**Power Dissipation** [W]	**Surface Area** [m^2]	**Heat Load per Unit Area** [W/m^2]
ADCS	0.32	0.00375	85.33
CDHS	0.03	0.00375	6.67
Payload	0.5	0.015	33.33
EPS	1.1	0.00375	293.33
Comms	1.95	0.00375	520
Propulsion	5	0.015	333.33

15.5. Post-Processed Data

Due to the tight power budget and inability of the EPS to manage the additional power input of possible solar panels on the side panels of the satellite, the following data stems from the analysis on the side panels covered in epoxy black paint.

Table 15.9: Minimum and Maximum Temperature of all (Solar) Panels for the Cold and Hot Case

	Cold Case			**Hot Case**		
	T_{min}	T_{max}	T_{ave}	T_{min}	T_{max}	T_{ave}
MX_Panel	-41.25	-24.47	-32.86	-41.61	-17.85	-29.73
MY_Panel	-38.18	12.47	-12.86	-38.23	19.64	-9.30
MZ_Panel	-38.88	12.31	-13.29	-38.94	19.55	-9.70
PX_Panel	-39.16	61.81	11.33	-39.37	57.29	8.96
PY_Panel	-38.75	12.57	-13.09	-38.81	20.02	-9.40
PZ_Panel	-39.04	20.02	-9.51	-38.97	11.53	-13.72
Solar Panel 1	-77.72	86.82	4.55	-77.83	89.28	5.73
Solar Panel 2	-80.84	84.04	1.60	-80.90	86.35	2.73

Table 15.9 states the minimum and maximum temperatures of each (solar) panel in the hot and cold case. Referring to Table 15.1, the solar panel requirements are met. Although the average temperatures of all panels being -11.71 [° C] and -10.48 [° C] for the cold and hot case respectively, are not located within the design range of 10-30 degrees, it should be noted that the these are the temperatures experienced of the panel itself rather than inside the satellite. Furthermore, the biggest missing link is the addition of internal power dissipation.

When examining Figure 15.2 and Figure 15.3, it becomes visible that during the eclipse all panel temperatures to an average of approximately -40 [° C] for either case. When incorporating the power dissipation of the EPS which during eclipse will raise the temperature by approximately 76 [° C], by assuming the eclipse to be approximately 1/3 of the orbit and using Table 15.10. Meaning the average will be raised to approximately 36 [° C]. Including the emissivity of the MLI, in which the EPS will be covered. Intuitively, another iteration will take place at the continuation of the design phase.

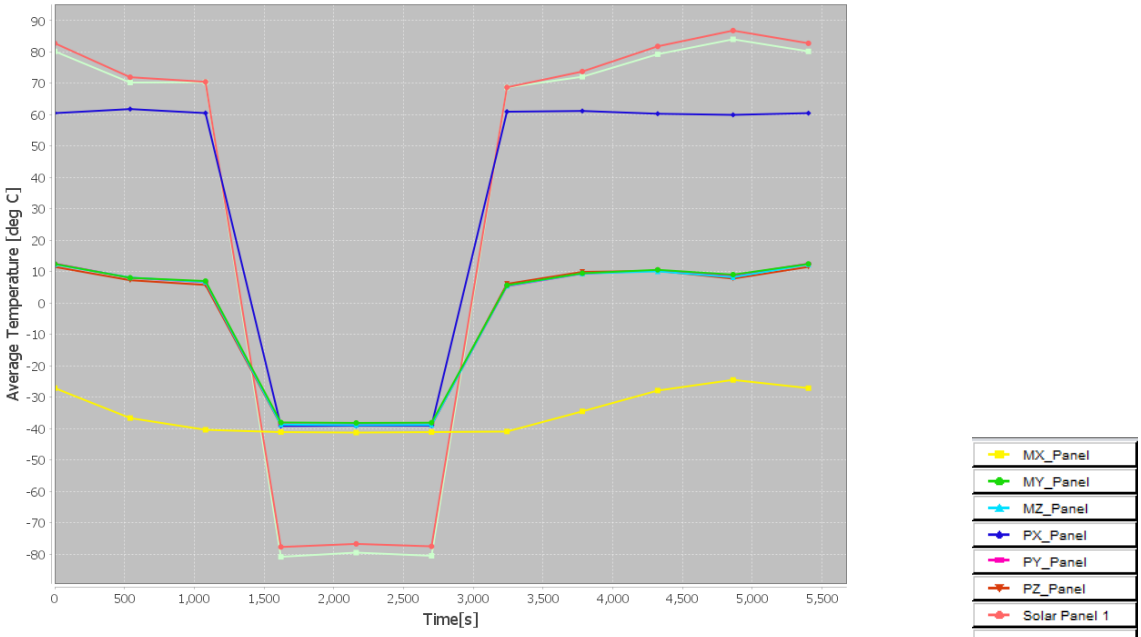

Figure 15.2: Average Temperature of all Panels in the Cold Case

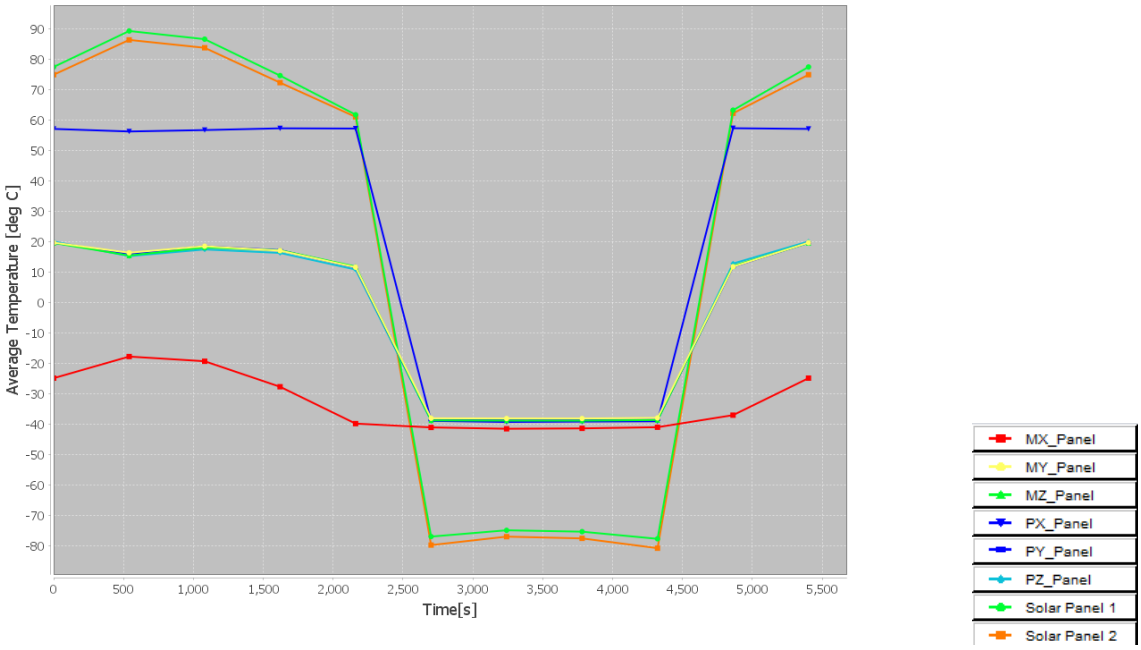

Figure 15.3: Average Temperature of all Panels in the Hot Case

15.6. Surface Material Trade-off

With the outer material of the CubeSat decided to be epoxy black paint, the material for possible component insulation must be determined. Table 15.10 outlines, based on elementary energy principles, the temperatures that each component emits based on assumption AI-TC-ASSU-10. For sake of completion, the payload was decided to be included as a reference.

Component	**Energy** [J]	**Volume** [m^3]	**Mass** [kg]	**Temperature** [° C]
CDHS	135.04	1.56E-05	0.04	5.28
ADCS	1728.56	1.56E-05	0.04	67.54
(Payload)	(2700.88)	(1.25E-04)	(0.29)	(13.19)
EPS	5941.93	1.56E-05	0.04	232.16
Comms	10533.41	1.56E-05	0.04	411.56
Propulsion	27008.75	1.25E-04	0.36	86.46

Table 15.10: Subsystem Temperature throughout the orbit. Volume and Mass are based on the ESATAN model

It becomes evident that the most critical subsystem is the communications system and the EPS on a large scale but with respect to the thermal design range, also the ADCS and the propulsion system pose a thermal threat. Overall, it can be said that the main issue is overheating, meaning for a passive system, the materials in question are insulators.
The different options in this trade-off will be evaluated with respect to the following criteria: emissivity, weight, thickness and sustainability. Each option was scored on a scale of 1-3, with 3 denoting 'the best' and 1 'the worst'. The weights are assigned similarly on a scale of 1-5 with 5 denoting the highest and 1 the lest importance. The most important criteria is the emissivity as it embodies the purpose to use MLI. Thickness would be of interest due to the confined space inside the CubeSat, especially without the harness being taken into account for this design phase. The project is not imposed to a strict mass budget to which the density was given a lower weight. Sustainability was not given the lowest possible weight as the sustainability does not only refer to the environment but also the ease of handling. However, the different options were contrasted with respect to the hazardous materials used.

Table 15.11: Multi-Layer Insulation Trade-off

		Effective Emissivity ε	**Density** [g/m^2]	**Thickness** [μ m]	**Sustainability**	**Total**
	Weight	5	2	3	2	
RUAG	Score	3	3	1	3	
Clean MLI	Weighted	15	6	3	6	30
Sheldahl 2xAl	Score	1	1	2	1	
Polyimide AOC	Weighted	5	2	6	2	15
Sheldahl 2xAl	Score	2	2	3	1	
PET	Weighted	10	4	9	2	25
Sheldahl 2xGold	Score	2	1	2	2	
Polyimide	Weighted	10	2	6	4	22

After performing a sensitivity analysis on the trade-off by changing the weights of each criteria, the outcome of the ranking remains: the chosen MLI is the first option by the swiss company RUAG. The effective emissivity of the clean MLI is 0.003 with a density of 140 [g/m^2] and a thickness of 30 [μ m] (RUAG, 2020).

15.7. Reliability, Availability, Maintainability and Safety Analysis

As passive thermal control is used in this project, the thermal control reliability and availability is very high due to its simplicity. This also holds for the maintainability due to the small size of the CubeSat and the short mission duration.
One complication that is possible to arise, more during the integration process of the satellite which in this case will be included in the task of maintainability' as no maintenance is taking place, per se, is the wrapping of MLI around objects. Ways to overcome this is by simple overlaps and Velcro or interleaved lapping. Fortunately, no mechanical loads are applied on the foil for these joints to create a point of failure (Miyakita and H., 2015). Lastly, passive thermal systems are very safe to use and do not pose a risk on the surrounding environment.

15.8. Recommendations & Future Prospects

The biggest dependency to finalize the detailed the design of the thermal system is on the power budget and the specifications of the chosen subsystems. Both impact the design on the temperature sensors as these must be researched, traded-off and chosen.

Nevertheless, the first task would be to reiterate the thermal analysis with the inclusion of the chosen MLI optical properties from RUAG. Afterwards, a thermal case could be set up with 'Chained Radiative Cases', allowing the user to define several boundary conditions dependent on radiative cases during one analysis run. This is particularly interesting as different subsystems are active throughout different sections of the orbit. In practice, this could be implemented by defining several radiative cases the same (with the same orbital parameters) and chained according to the modes of operation that are of interest. Such modes would be the payload, sun-tracking/charging, housekeeping and communications operations within the nominal mode. Aside from this, another possibility would be to entertain the option of heat sinks or other thermal control systems again. Intuitively, this is heavily dependent on the previously proposed thermal case.

16 Verification and Validation

16.1. Astrodynamics

Since most of the astrodynamics was done using GMAT, it is important to explain steps that were taken to verify the software. Despite NASA stating that the software had been verified and validated, and has also been used to evaluate missions (Hughes et al., n.d.), it is beneficial to evaluate the software by itself for the purpose of this project. Only the steps taken to verify GMAT are going to be explained in detail and screenshots from the simulation outputs are given. A short explanation of how validation could be done will be given as well, but due to time constraints, this part was not completed.

16.1.1. Gravity Model

To determine how the gravity model affects the simulation, comparative simulations were run. In the propagator settings it is possible to change the gravity model and select a degree and order. A total of 4 simulations were run with the same satellite and orbit parameters, while altering the degree of the simulation. The JGM-2 model was used was changed from one to four degrees, while keeping the order constant (one). The simulations were each run for 100 days.

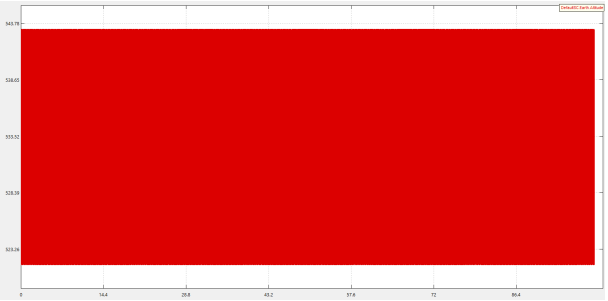

Figure 16.1: JGM-2 Degree 1 Order 1

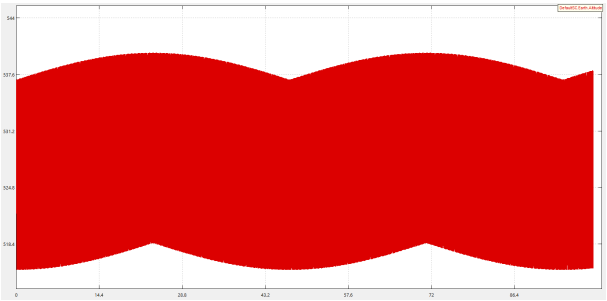

Figure 16.2: JGM-2 Degree 2 Order 1

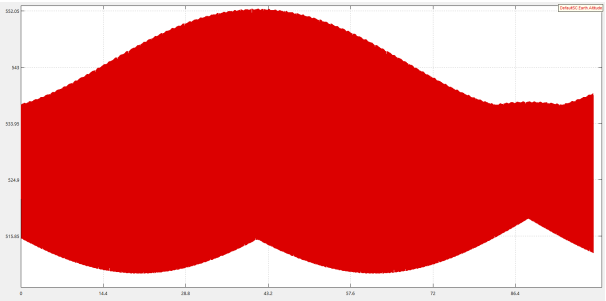

Figure 16.3: JGM-2 Degree 3 Order 1

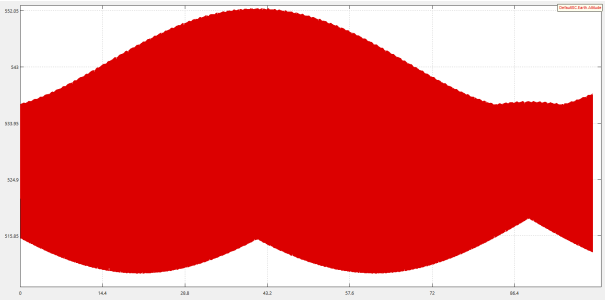

Figure 16.4: JGM-2 Degree 4 Order 1

From Figure 16.1 to Figure 16.4 it can be seen that the degree of gravity model does significantly affect the outcome. At first degree, the model does not include perturbation effects and starting from third degree the model also starts including more harmonics. This emphasizes that the outcome of the simulation greatly depends on the degree (and order) of the gravity model, at least until the fourth degree, after which the change is negligible.

16.1.2. Atmosphere

Another important factor to verify in the program is the use of the atmospheric model. To verify that the atmosphere model is indeed working, two simulations were run with the same orbital and satellite parameters;

one simulation had the atmosphere model turned off and the second simulation had the atmosphere model turned on. It was expected that the simulation without an atmosphere would simply propagate the satellite around earth, whilst the simulation with the atmosphere would cause the satellite to drop in altitude due to drag.

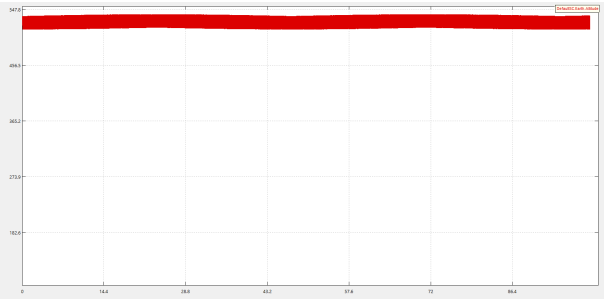

Figure 16.5: Simulation with no atmosphere model

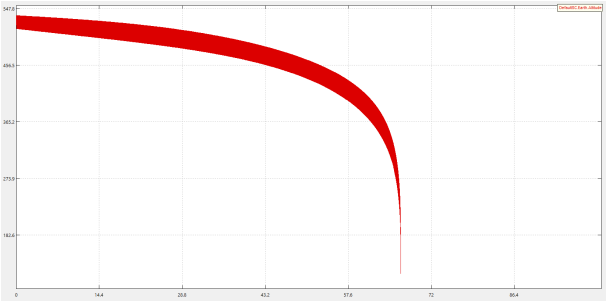

Figure 16.6: Simulation with atmosphere model

In Figure 16.5 to Figure 16.6 it can be seen that turning on the atmosphere model has a significant impact. Instead of propagating in orbit and only being moved by the perturbations, the satellite is decelerated and a visible change in altitude can be seen within the first few days. The decay is only gets worse with time, as the satellite drops further, becomes slower and is also decelerated even more due to an increase in density. This is also comparable to how decay was modeled by (Oltrogge & Leveque, n.d.) and (Panwar, 1999).

16.1.3. Mass of Satellite

Upon having verified that the orbital calculations work, it was necessary to verify that the parameters of the satellite produce the necessary outcomes. At first, the impact of size of the satellite was checked. A satellite of the same size, but with greater mass has a larger ballistic coefficient. In turn, this means that the impact of drag is less severe, as the satellite has a greater force moving it, and it can stay in orbit longer. Two satellites were simulated, one with a mass of 100 kg and another with a mass of 200 kg. Wertz et al., 2011

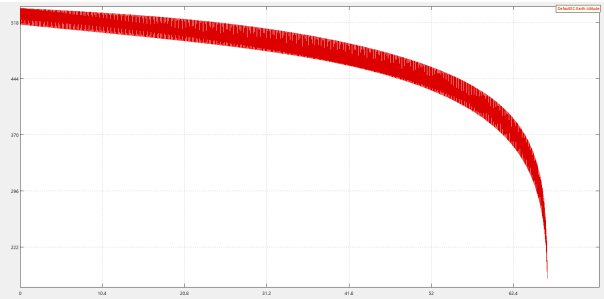

Figure 16.7: Satellite with a mass of 100 kg

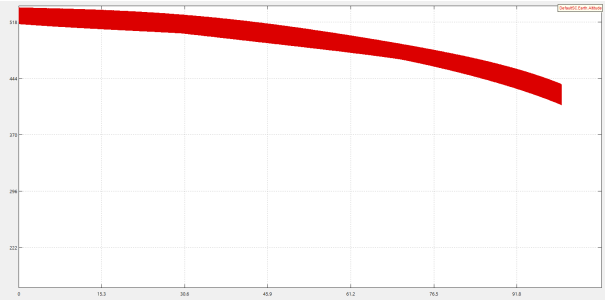

Figure 16.8: Satellite with a mass of 200 kg

The program works as intended, as the satellite with the greater mass takes longer to decay than the lighter one (as can be seen in Figure 16.7 to Figure 16.8). This indicates that the atmospheric and gravitational model both work together as intended and can produce the expected results.

16.1.4. Area of Satellite

As a last verification test, the effect of the satellite's drag area (area) was assessed. Similar to the explanation in the previous test, the area affects the ballistic coefficient (and the experienced drag). Therefore, the higher the area, the faster the satellite should decay. Hence, the same orbit parameters were used, and the area of the satellite was changed to compare results.

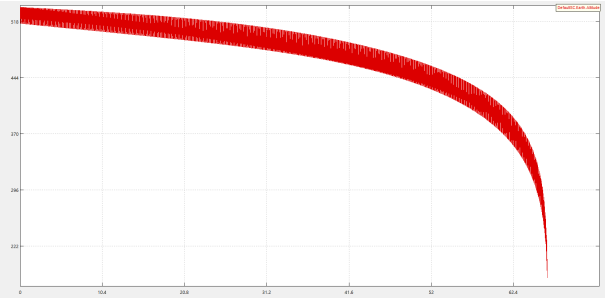

Figure 16.9: Satellite with a drag area of 15 m^2

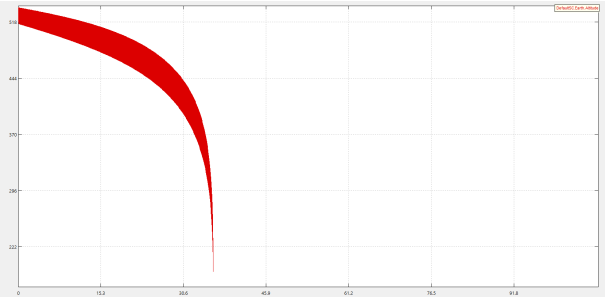

Figure 16.10: Satellite with a drag area of 30 m^2

Figure 16.9 to Figure 16.10 show that doubling the area has an effect on how quickly the satellite decays. The satellite with the larger surface area decays faster, since the drag it experiences is greater.

16.1.5. Validation

In an ideal case, the validation of the obtained results would either happen with a previously validated software or directly with data from orbit that can be used to validate. If we assume that GMAT is not validated, then the best idea would be to use in-orbit data for validation of the program. It would be possible to set up new simulations with the given satellite parameters, and cross-check if positions and velocities would coincide.

Nonetheless, due to the time constraint imposed by the DSE, it is not possible to fully validate GMAT by one person alone. Furthermore, the cost to obtain proper satellite data can be very pricey, and as such would also exceed the budget of the team currently, it is accounted for in the cost breakdown though.

16.2. Radiation Analysis

The in depth radiation analysis was done using SPENVIS a industry standard tool for radiation environment analysis of a spacecraft. The verification of this software can be done using reference radiation intensity values from research papers as well as proton to electron ratios that would be found from SPENVIS compared to that of certain regions in the Van Allen belts.

The validation of SPENVIS can be done by doing a test using the another OBC and placing it a artificially created radiation environment using proton and electron beams and shielding the OBC as it would be in the spacecraft then shooting the high energy particles and testing whether the bit-flip rate is similar to that found using SPENVIS. Then to test the other part of the program, that being the kRads experienced by the satellite can be validated using past missions in LEO.

16.3. Structures

For structural analysis the cross-verification of geometric formulas for areas, moments of inertia and volumes from scripts developed for design and the current 3D CAD software that is industry standard CATIA which is both verified and validated over and over again will be done using the numerical property checking functions built in the software. These will then be compared with the values from the scripts developed in-house with a tolerance of 10^{-8} to account for rounding errors. This will be done along with the standard code verification tests mentioned below.

For the validation of the structure a series of tests will be done, firstly a series of material tests will be done on the parts that are ordered for the satellite. Since the cost of the parts are very low compared to the satellite budget sets of spare parts will be ordered to run destructive tests on to test parameters that were used during the design phase, such as E-modulus, density, yield strength and G-modulus. Then a series of non-destructive tests will be run on the components that are to be used in the spacecraft, these include x-ray, eddy current, ultra sound and dye tests as well as the obvious visual inspection.

16.4. Communications Analysis

In order to verify and validate the code, the main method that was used was to use example data and results and compare them to the outputs given in the code. For example, link budgets given in literature were inputted and then the signal to noise ratio outputted was compared to the calculated result in the books. Furthermore, checks were implemented in the code to ensure that the results were realistic and achievable. Bug fixing and analysis was also constantly taking place to ensure that that everything was being calculated correctly.

Finally, the code was reviewed by an expert and the inputs and outputs were checked to see if the values were reasonable, and hand calculations were made to verify these findings.

16.5. EPS Analysis

To verify and validate the code, several methods were implemented. Firstly, before moving on to more complex models with a lot of interacting components, simple designs were done and then checked against calculations made by hand to see if they fit. The time-steps used to integrate and calculate the energy were also changed to see if the value was converging to a final result and to see if the system was stable. There were also checks implemented in the code to verify whether the inputs were realistic (such as not having negative voltage inputs) and also to see if the outputs were realistic as well. Checks were also implemented in the code to aid in the debugging of the program.

16.6. Thermal Control

The advantage of using ESATAN, is the software's option to provide verification and validation of the chosen parameters such as the definition of the conductive interfaces. Furthermore, the tool offers intermediate results as for the radiation analysis which can also be verified in a visualization module.
In the executed analysis, the results were verified using the single-node thermal model whereas the differences were contrasted. Additionally, smaller back-on-the-envelope calculation based on elementary thermodynamics or electronic engineering were performed to verify specific input values. But it should be noted that the thermal analysis was executed on a very extensive tool. If more time was provided, the next step would have been to establish an analysis tool using either Matlab or Python to examine the sensitivity of the outcome by altering certain inputs. This would not only enable the verification of the values on a physics basis but also on a numerical basis. One can evaluate possible oscillations due to the use of the Crank-Nicolson method by altering the time steps and the related error.
The add-on software to ESATAN, Therm-NV, enables the engineer to validate intermediate values as the overall system validation is only possible through testing. A major component to be tested after being chosen is the thermal sensors. With the surface materials being procured OTS, the biggest thermal test, also serving as validation of the model, is the thermal-vacuum test simulating the space environment. This commonly occurs towards the end of the satellite testing phase.

16.7. Code Verification

Code Verification for the tools used to design the satellite is done by compiling the code and using the IDE's debugger to find syntax errors and then when it runs properly the code must pass a series of unit tests.

16.8. Full Satellite Verification

Requirements can be verified in four fundamental ways: Inspection, Demonstration, Test, and Analysis.

Inspection involves the nondestructive examination of the system. This is usually done using one of the senses of the human body, such as visual, audio, smell, touch, or taste. It is not common for engineers to taste a satellite to verify requirements, therefore the inspection usually involves visual, audio, smell, and touch inspections. This could for example involve taking physical measurements of the satellite, or listening to make sure that there are no loose components that could be making noise when moved.

Demonstration involves the manipulation of a product as it has been intended to be used. It is very similar to testing, however when running demonstration tests no special test equipment is used, and no data of the test is collected. In the sense of a CubeSat, this could for example be deploying the solar panels and visually inspecting the results to see if they have deployed correctly.

Testing involves inputting a predefined sequence of inputs and environments, and verifying whether the outputs are as predicted. This testing usually involves specialised equipment and measuring devices to ensure that there is data that is being collected which can be analysed at a further date. For example, vibrational testing is verifies whether or not a CubeSat can withstand the vibrational loads caused by a launch vehicle.

Finally, there is analysis. Analysis involves the use of models and calculations to make predictions about the performance of a system This is usually done when the physical test is not feasible, or when the limits of a design want to be verified without the cost of building, testing, and breaking a system. One of the most common analysis that are done on satellites is radiation, where the cost and preparations of conducting a radiation test are not worth the effort compared to the accuracy and simplicity of running a radiation analysis. Additionally, the cost of a system is performed by analysis as this is the only method of verification for this.

16.8.1. Inspection

Before a satellite can be handed to a launch partner, several inspections must be made about the satellite. These include the dimensions of the satellite along all axes, the mass of the satellite, and the moment of inertia of the satellite. These inspections are usually listed as 'tests' in the testing regime, however they do fall under inspection.

Further inspections that can be made are the placements and polarities of cables. This is especially important as reversing the power cables can destroy entire assemblies and electronics. Additionally, for the ground segment, an inspection of the software that the end user will see is also done to ensure that all buttons and data are visible, and that all the fields required for functioning are present as well.

16.8.2. Demonstration

As mentioned earlier, demonstrations are tests without data or specialised equipment. The deployment and testing of all mechanical interfaces is counted as demonstration, given that there is no special environment that they are being tested in. This could be for example, the deployment of the solar panels, or the deployment of the UHF antennas.

For the ground station software, inputs can now be made and the software can be interacted with. The demonstration is successful if all the data that is needed by the customer can be accessed.

16.8.3. Testing

In order to verify the requirements that are dependant on the launch environment, the satellite will have to go through a testing regime. There are different methods of doing this. The first includes creating three different models for: developmental testing, the qualification testing, and finally the flight model. Another method involves creating a protoflight model, which is tested to lower levels than qualification testing, yet higher levels than flight level testing. The method chosen for this project is to go with a protoflight model. This is due to the fact that the satellite is being designed and built using commercial-off-the-shelf hardware. Typically, when designing, components are selected with high TRL levels, such that the development and qualification of the hardware has already been completed. This drastically reduces the cost and time of production, as only one model has to be built and tested. All test methodologies and levels will be following the recommendations by the testing standard set by the European Cooperation for Space Standardization (Secretariat, 2019). Most of the information in this section can be found in this standard, where sections of it has been copied here for completeness. Protoflight testing can be separated into five groups:

- General: These tests include the functional and performance tests and the life tests.
- Mechanical: These tests include the physical aspects of the tests, such as the vibrations and accelerations that the satellite will experience during launch.
- Structural Integrity Tests: These tests are aimed towards testing pressure vessels, such as fuel storage systems.
- Thermal: These tests involve simulating the space environment, both in terms of pressure and temperature
- Electrical: These tests aim to test the satellites communication system, but also the compatibility of the electronics on board

The sequence of testing will follow the sequence as specified by the ECSS standard. The standard appears to follow the 'test-as-you-fly' sequence, which is to test in order of the environments that would be experienced by the satellite during it's lifetime. An example of such a test sequence can be found below:

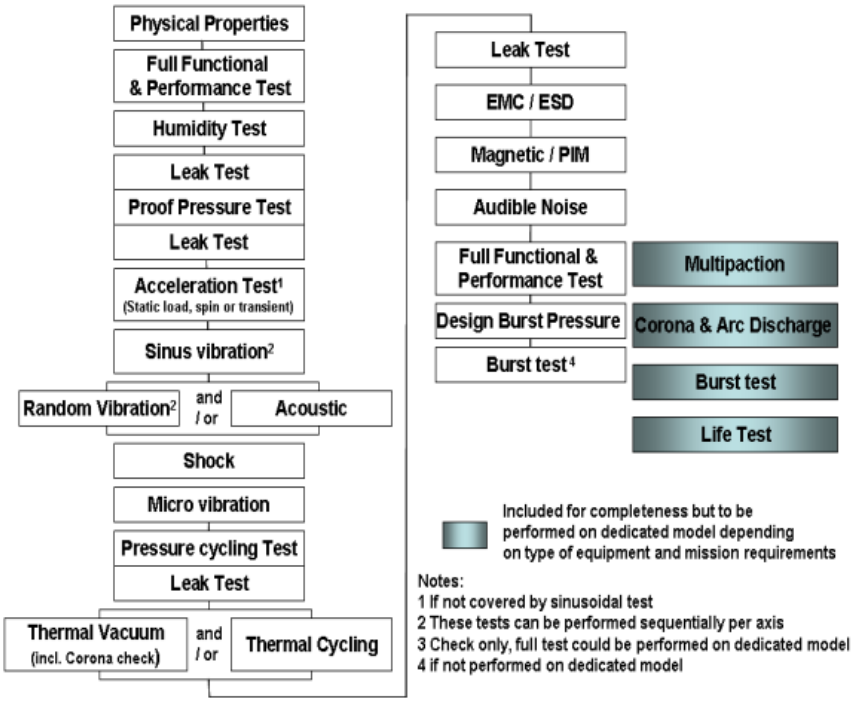

Figure 16.11: Test Sequence

It should be noted that the shock testing will be done on the qualification model, if need be. Furthermore, the exact tests to be competed depend on the requirements set by the launch provider. For instance, the shock test is often not necessary for CubeSats, hence an analysis is sufficient.

After the protoflight model testing has been completed, as test review will be conducted tot study the results of the testing and verify the requirements. The satellite can finally go on to the pre-launch testing, which confirms all elements re needed for the launch and that their parameters are within the specified limits.

16.8.4. Analysis

There are several analysis that can be run during the design of the satellite. Commonly, simulations are run for each test that is run, so that the outcomes can be compared and the model as well as the test can be verified. This is particularly useful in the case that the design of the satellite must change. Instead of running a full test again, once a model is verified, the updated design can be run in the simulated test and the results of which can be used to verify the design.

Not all tests can be simulated and physically run on the entire system however. For example, radiation testing is not usually done on an entire system, but rather critical components are identified and independently tested. For example, an analysis could be done on the OBC and all the chips and components on the board. The components will have to be checked to see if they have been radiation hardened or have flight heritage. Critical components that have neither could then be directly irradiated and tested to ensure that they will function throughout the entirety of the mission.

17 Sustainability

Sustainability has played an important role over the entire duration of this project. It was a priority during the technical design of the mission, and had an effect in, amongst others, identifying an End-of-Life strategy, using green propellant for the propulsion system, and using sustainable manufacturing and integration of the satellite. Next to these technical applications, other sustainable factors have also been taken into account. Examples of these other factors include having a sustainable mission, looking at sustainability for the ground station and operations, launch vehicle, transparency, and complying with standards and regulations. The goal is to create a complete picture of the sustainability for the entire duration of the life cycle of the satellite and the project. For this, research has been done to current implementations of sustainability encouraging regulations, standards and services. Taking the best from all these individual practices the Elaborate Life-cycle Space Sustainability Indicator was developed. The Elaborate Life-cycle Space Sustainability Indicator, ELSSI for short, aims to identify the different factors that play a role in sustainable development and operations of space systems. The ELSSI has been invented to provide an innovative way of addressing the sustainability challenge by encouraging responsible behaviour. The Classification can be applied for different types of missions and uses relative weights to bring different aspects of the project into perspective. During this project ELSSI was implemented to get a complete overview of sustainability for the entire duration of the project and life cycle of the satellite. This chapter is based on the sustainability analysis performed in (Canosa et al., 2021a) and (Canosa et al., 2021b).

17.1. What is space sustainability and why is it important?

”Ensuring that all humanity can continue to use outer space for peaceful purposes and socioeconomic benefit now and in the long term”, the first sentence in the ’Space Sustainability a Practical Guide’ from the Secure World Foundation(“Space Sustainability A Practical Guide”, n.d.), and a statement that perfectly encapsulates the need for a sustainable mindset while working on space systems. Sustainability refers to the ability to ’sustain’ or maintain something over time. This includes a profusion of factors that all play a role over the entire duration of a project, from idea, to design, integration and application, and finally the end of the project. All these factors, or indicators, have an effect on limited physical, natural and social resources. To make sure that future generations will also have the opportunity to make use of- and to explore space, it is important to put measures into place that focus on sustainability and on maintaining the health and safely of the space environment.

17.2. Elaborate Life Cycle Space Sustainability Indicator

There are many ways to evaluate the level of sustainability of a mission/project. However, many of them are qualitative, rather than quantitative. The main quantitative measures of sustainability are: carbon footprint, water usage, energy usage, land usage and emissions. However, these are not enough to create a full picture of the level of sustainability of a mission.

To be able to quantify the ”level of sustainability” of a entire mission/project one can make use of the Elaborate Life Cycle Space Sustainability Indicator (ELSSI) (Regnery & Manieri, 2021). While there are more indicators available to evaluate the level of sustainability of a system, most of them are either specific to a certain part of the mission (manufacturing or energy usage for example), and are not specific to space missions. The ELSSI indicator is specifically tailored to space missions and analyses every aspect of it. Considering the fact that members within the team were involved in the creation and development of the indicator adds to the confidence that ELSSI is the right tool for analysing sustainability within this project. The ELSSI is a key performance indicator that analyses different aspects within the space mission, using a variety of indicators. The indicators that the ELSSI analyses are divided up into 9 categories. These are:

- Sustainable System
- Transparency
- Overcrowding

- Sustainable Mission
- Ground Operations
- Manufacturing
- Standards & Regulations
- Launch

Within each of these categories there are a range of indicators that are scored on a scale of 1-5 (5 being most sustainable). Each indicator has a certain specified weight (or importance) within the category. These scores and their weights are combined to create a categorical score. Similar to how the indicators are weighed the categories are weighted as well, creating a universal ELSSI grade, on a scale of 1-5. The individual categories and indicators are explained below.

17.2.1. Sustainable System

The indicator 'Sustainable System' aims to analyse the physical system that will perform a projects mission. For this, a lot of factors have to be taken into account that all play a role in acquiring a bigger picture of sustainability for the entire system. Different 'subindicators' have been established within the ELSSI, but as technology evolves and different new techniques immerse, this list may be updated accordingly.

In Situ Resource Utilization

In situ resource utilization, or ISRU for short, is the using, collecting, storing and processing of local materials and resources. As these would otherwise need to be brought from Earth, this is a useful practice to reduce the amount of payload that must be launched. A good example of the use of ISRU are solar panels that provide energy to space systems by using the sunlight captured in orbit and hence reduce the need of additional batteries taken from Earth. ISRU could also provide building materials, materials for life support and propellants to space systems or space exploration crews.

In Orbit Computing

For communication bottlenecks and latency issues, in orbit computing, fast data processing, and decision making could pose a solution. Here the application of artificial intelligence and data processing could benefit the flexibility and data management of the mission, while making smart use of- and minimizing available resources.

Orbital Maintenance

Earth orbiting satellites experience decay. Meaning that the altitude of their orbit decreases over time. For long running missions this means that systems have to actively keep the satellite in the preferred orbit for the duration of their mission. The ISS, for example, uses about 8,000 pounds of propellant a year to maintain a consistent orbit [1]

Agile Space Navigation

Agile Space navigation includes docking and autonomy of space systems and missions. This is tightly correlated with 'In Orbit Computing' but also includes the application of autonomy with respect to manoeuvres and operations.

Space Environment

When designing for a space mission, different effects of the space environment should be taken into account and their effects should be noted and optimized for. Examples include Mitigation techniques for the radiation environment such as the application of radiation hardened or tolerant subsystems. Other factors are vacuum, space debris and meteoroid impact, electrostatic charging and upper atmospheric drag.

Sustainable Engineering

Sustainable Engineering is a broad term that includes an efficient design and use of available resources. Examples could be use of design topology optimization or other subsystems that improve power and data usage. Another part of Sustainable Engineering is the minimization of mission failure. This can be done by elaborate testing, using parts that have mission heritage and the redundancy of subsystems. Other implementations of Sustainable Engineering could be the selection of a propulsion system that makes use of green propellant.

[1] https://www.nasa.gov/mission_pages/station/expeditions/expedition26/issaltitude.html [cited 12 November 2021]

Self Awareness & Repair of systems

The ability of a space system to be self aware of possible damaged or malfunctioning parts/systems can help with analysing mitigation measures. If redundancy measures have been put into place, these can be used. Alternatives would also include having self repairing systems or even self healing materials.

Re-usability

Not just making new systems from scratch but actually reusing the materials and systems that are either already in orbit or have been previously launched could also play a role in the sustainability of a project. Examples could be refuelling, using finalized missions for other purposes, and reusing rocket-parts.

In Orbit Assembly

To make efficient use of the available volume different methods of 'In Orbit Assembly' can be used. Classic examples of In Orbit Assembly are (origami inspired) fold-able solarpanels, but recently strides have been made to 3D print satellites structures while in space.

17.2.2. Manufacturing

The category 'Manufacturing' refers to the sustainability of the mission during the production phase, including the acquisition of raw materials. Due to the many aspects that play during manufacturing, finding a proper measure of sustainability for manufacturing is very difficult. The ELSSI tackles it by dividing the manufacturing into Sustainable Production/Process and Sustainable Materials.

Sustainable Production/Process

The manufacturing of the components and the satellite should also be looked at when wanting to create a sustainable system. Throughout the manufacturing process, energy consumption should be reduced while limiting energy sources to renewable angry. Water consumption and air pollution should be limited. The expulsion of hazardous or poisonous should be prevented. Land use and damage to bio-diversity should be looked at and dealt with.

Sustainable Materials

While the selection and usage of materials is of vital importance to any space mission it is also a great source of pollution. The creation and processing of space-grade materials require a lot of resources and energy. Additionally, in the production process a lot of water is required (eg. for cooling during processing), which is extremely demanding for the environment. It should also not be forgotten that mining for the materials is extremely damaging to the environment, from an emissions and resources point of view, but also from a bio-diversity point of view. Lastly, the use of materials that are hazardous should be avoided, while the use of materials that are recycled or renewable should be encouraged. The selection of materials should thus be looked into when designing a sustainable Satellite (or any space mission for that matter). However, due to needing to reduce risks of losing the satellite and/or mission to near-zero, using alternative, more sustainable materials proves to be quite a challenge.

17.2.3. Transparency

Transparency regarding space missions is critical to ensure a sustainable future of the space industry. Only through transparency the community as whole can grow. Things such as data sharing and identification & detectability are critical to ensure a healthy exchange of information to improve the industry.

Data Sharing

To enhance long term sustainability for the space community, space data sharing is vital. The aspects that are being looked at for the indicator: Data Sharing, are: Payload Data and Design Data. Sharing Payload Data is critical enhance scientific research in the field of space and engineering, but also any other scientific field. Sharing Design Data helps improve the overall engineering of space missions, leading to more advanced and more sustainable designs in the future. It should also be noted that it is not only important to share the appropriate data but also to share accurate data.

Identification & Detectability

Under Identification & Detectability one can consider two main aspects. Transparency on satellite location information, making it easier for others to track satellites and possible space debris. The second aspect is effort to improve trackability/detectability. This includes installing LEDs for example. Efforts to reduce identification & detectability such as scramblers and other technologies (such as those by military satellites for example) are considered extremely unsustainable.

17.2.4. Orbital Debris Prevention

Orbital debris is a threat for space sustainability as it increases the risk of in-orbit collisions for future missions. Due to intentional destructive events, routine operations or accidents large quantities of orbital debris can be produced that remain a threat for spacecraft, satellite and astronaut operations for years or centuries. Scientists estimate that there are many millions pieces of debris orbit Earth. Because these objects can travel at extremely high velocities, even small pieces pose a serious hazard, as could be seen on the 23rd of August 2016 when the Copernicus Sentinel-1A satellite was struck by a millimeter-sized particle which left a severe dent in the solar panel.

Collision Avoidance

In-orbit collisions are a potential major source of orbital debris. The capacity to perform a diversion to avoid collisions with known, and possibly unknown, orbiting objects is thus fundamental for the sustainability of space operations in highly populated orbital regions such as LEO. The design of capable potential threat detection, flexible trajectory generation and a control system with relatively quick reaction times is thus a necessity for the mission.

End of Life processes

Identifying an End of Life process, EOL for short, is essential for preventing orbital debris and having a more sustainable mission. Satellite operations have a responsibility to identify and put an EOL into place. In LEO, satellites could re-enter and burn up in the Earth's atmosphere because of the orbital altitude and atmospheric drag. In GEO, satellites can be re-orbited to ensure that the satellite does not return to the protected zone. Other EOL strategies could include drag-enhancing orbit devices or actively changing the orbit to burn up in the atmosphere. However, before de-orbiting, sources of stored energy need to be removed as much as possible, as this otherwise could result in an accidental explosion or break-up.

17.2.5. Overcrowding

In 2020 alone, over 1000 satellites have been launched from Earth. And this number seems to be increasing over time. With this increasing growth in active satellites, the concern for space-safety grows as well. Three major reasons for this concern will be explained in the following section. [2]

Radio Frequency

Satellites receive commands from their uplink and beam down acquired data and status reports through their downlink. For the uplink and the downlink an assigned radio frequency is used. Because of the increased use and number of satellites, congestion' is currently a serious problem in the lower frequency bands.Next to this, the geostationary satellite orbit above the equator is getting crowded, which can pose a problem for interference between the different transmissions. (Finch, 1986) (Frenzel, 2012)

Light pollution

Light pollution, where the sunlight is reflected by satellites and space debris poses a challenge for ground-based optical astronomy. The current and future deployment of so called 'mega-constellations' raise significant concerns, and while the exact effects are still under investigation, mitigation techniques should be taken into account (Kocifaj et al., 2021). While it wont be as important for this mission it should be mentioned within the frame of sustainability.

Complexity of Space Operations

Due to the increase in number of objects that orbit our Earth, the risk and complexity of space operations might increase. Examples would be orbital debris that needs to be actively avoided, satellites that can not be placed in the preferred orbits due to overcrowding etc.

17.2.6. Sustainable Mission

With the indicator 'Sustainable Mission' the entire mission, mindset and concept of the mission is taken into account. Using space and data acquired by space missions to counteract destructive or irresponsible practices or improving knowledge to be used for environmental or sustainable methods.

Tackling global challenges

High ranking 'Sustainable Missions' could include a broad spectrum of project aims and goals, ranging from detecting pollution and emissions to raising awareness of climate change to using data to preserve national monuments. Satellites and space missions have a plethora of applications and can be used to tackle major environmental, societal and socioeconomic challenges.

[2] https://www.ucsusa.org/resources/satellite-database [cited 12 November 2021]

Awareness
Being aware of a projects sustainability and taking the effects into serious considerations during the different phases of the design and implementation of the mission is important. The Awareness of sustainability issues includes understanding the importance of protecting the environment and being conscious towards the bio-physical environment and its problems and challenges. An organisation working on a space mission can show Awareness by actively trying to tackle any of discussed indicators in this section, or by using other indexes such as the Space Sustainability Rating (SSR). (“Space Sustainability Rating”, n.d.)

17.2.7. Ground Operations
To support and sustain a space mission, ground operations are crucial. But as one can imagine the ground station plays a role within the sustainability of the mission. One of the main factors when looking at sustainability of ground stations is the size of the operation. A small mission which only needs an antenna on ground to complete the mission is far more sustainable than a large mission sustaining a constellation of satellites, with many locations and buildings on earth. Usually, the larger the scale of the ground operations the least sustainable the mission is.

To name a few factors that reduce the sustainability of the ground operations in case of a large mission: building multiple buildings/offices/antennas, maintaining the buildings/offices/antennas (e.g. energy usage, resources usage, water usage) and transportation of personnel. Additionally, the processing of data acquired can be a great burden to the environment. Especially more complex computations require a great amount of energy and water for cooling, which greatly reduces the sustainability of the ground operations.

17.2.8. Standards and Regulations
To ensure that all nations can make use of space and to avoid conflicts it is important to address space sustainability and security challenges through Standards and Regulations. Applications of Standards and Regulations should be researched and implemented. Within the UN the UN General Assembly(UNGA) works on global issues and has two committees that deal with space matters. The UN also has founded an ’Office for Outer Space Affairs’ that has established a working group on the ’Long-Term Sustainability of Outer Space Activities’. The European Union has also created a “Draft International Code of Conduct on Outer Space Activities”. It is important to comply with the laws that are implemented in space. Guidelines can also prove advantageous during the project, an example would be the IADC Guidelines for prevention of orbital debris.

17.2.9. Standards and Regulations
Especially in space missions, testing is a big part of the mission. Proper testing avoids surprises down the road. This category is divided into testing methods and testing logistics. Testing methods evaluates the completeness of the testing and ensures testing is done properly and only when necessary. Testing logistics evaluates the way in which testing is done. This incorporates: use of safety equipment, satellite transportation to testing site and re-usability of testing equipment.

17.2.10. Launch
Atmospheric pollution, gaseous and particulate, and especially orbital debris[3] have become a primary concern for the sustainability of space missions. Launch operations are arguably the largest contributor to both, as well as the atmospheric regions affected.

Launch vehicle re-usability has become the golden standard for launcher companies striving for sustainability. Yet, reusable launchers must undergo significant maintenance to become serviceable again, the impact of which must be considered. In the case of non-reusable launch vehicles, debris disposal must be considered: whether spent stages are deorbited, where they land if that is the case, the emissions and orbital debris generated in the reentry process.

Launch operation debris disposal is closely related to the chemicals used in the propulsion systems of space launchers. Liquid rocket engines are used almost universally in space launch vehicles: traditional oxidizer and fuel pairs demand complex ignition systems. Hypergolic mixtures remove this need at the cost of higher environmental impact and health risks for the personnel involved. Solid rocket boosters, widely used in space launchers as well, release large amounts of alumina particulates to the higher regions of the atmosphere.

To minimize the environmental impact of the mission, the impact of launch operations must be researched, quantified and included in the trade-off to choose a launch vehicle and flight profile for the mission.

[3] ESA - About space debris, https://www.esa.int/Safety_Security/Space_Debris/About_space_debris

17.3. Indicator Criteria - Detailed

Every single category, indicator and criterion is assigned a weight. This was done in collaboration in collaboration experts in the field. Figure Figure 17.1 helps visualize the weights of all the categories and indicators. As seen from the figure, certain categories such as Standards and Regulations are far less important than others such as Sustainable System. Other very important categories are sustainable mission, which ensures the satellite is created with sustainable goals in mind and orbital debris prevention.

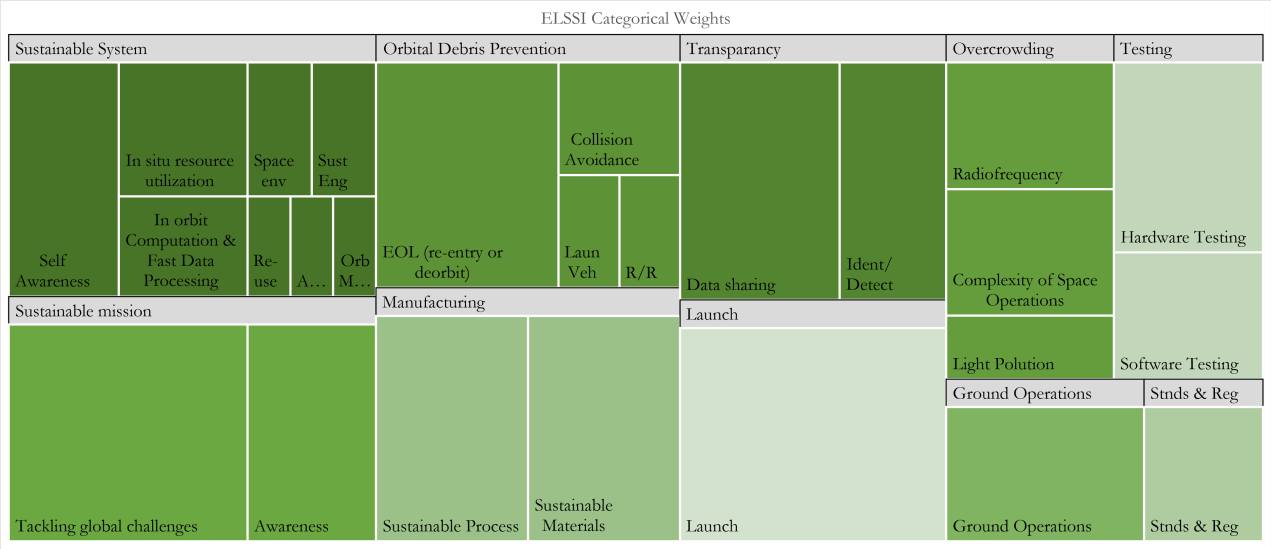

Figure 17.1: ELSSI Categorical Weights

17.4. Implementation of the sustainability strategy

To ensure proper integration of sustainability throughout the project, the ELSSI method of assessing sustainability will be applied at every trade off. In other words, every trade off performed will include a sustainability criterion, which will be directly related to the categories within ELSSI. The criterion relating to sustainability will also have a trade off weight of at least half the maximum weight possible, showing the importance of sustainability at every step of this project. Integrating ELSSI within every trade off not only guarantees that sustainability is considered at every junction, but also ensures that a certain level of quality is upheld for the analysis of sustainability. At the end of the project, the design is exposed for one last time to ELSSI to quantify the amount of sustainability for the entire finished Cube Satellite, this is also incorporated in the requirements, showing that sustainability is a big priority within this project.

To demonstrate the integration of sustainability within our project, a few design decisions are analysed from a sustainability point of view. The mission concept trade off used a reduced version of the ELSSI to evaluate, from a mission perspective, the sustainability of all of the concepts. To emphasize sustainability throughout the mission concept trade off process, the criterion of sustainability was given a weight of 4 out of 5, turning it into the 4th most heavy criterion. When choosing a payload mission, experts such as Michael Rast and Filippo Lodice were contacted to provide information on, from an agency and industry point of view, the most pressing environmental issues that could be tackled with a earth observation CubeSatellite. After consultation and a market analysis, a suitable sustainable mission was found that tackles the problems of fugitive gasses (such as CO2 and CH4) at refineries. Such a mission allowed this project to score a 5/5 for the subcategory: ”Tackling Global Challenges”. The next subsystem that allowed for sustainability submersion within the trade off is astrodynamics. To reduce orbital debris and increase the sustainability of the mission a proper End-of-Life strategy must be defined, as stated in the top-level requirement: AIS-PROP-REQ-24. The conclusions of the initial astrodynamic analysis reveal a maximum orbit time of 5 years before disintegration. The last, but not less critical trade off that involved sustainability is the communication system concept trade off. This trade off allowed for a full ELSSI analysis of the concepts.

An in depth analysis of sustainability throughout the design process performed in this report, using ELSSI, ensures a more reliable and confident approach to sustainability that is able to guarantee costumers, stakeholders and the public a sustainable mission.

17.5. ELSSI Results

Having used the ELSSI to assess the level of sustainability throughout the design process it is time to complete the ELSSI sustainability analysis by giving this mission an ELSSI score. As mentioned before this ELSSI score will be able to give an indication of the amount of sustainability for this mission. Collaboratively, the SigmaSat team filled in the ELSSI indicator. This led to a score of: 4.05. This score corresponds to: ”Good”. The justification for each criterion is given in Table Table 17.1. This positive result allows SigmaSat to conclude that their mission is sustainability in a quantitative manner. This is not a surprise, as sustainability and the ELSSI were incorporated throughout the design. Such an immersion of sustainability from the start of the design phase enable greater sustainability results and greater confidence in a sustainable mission.

Because ELSSI was just developed, this mission is the first mission to use it to quantify their sustainability. The effect of this is that there are no other missions to compare it with. To overcome this issue, the SigmaSat team, with help from external sources, filled in the ELSSI for other, similar, space missions. This allows SigmaSat to compare it’s sustainability compared with other missions.

Table 17.1: ELSSI Grading Justification

Nmbr	Justification	Nmbr	Justification
1.1.1	Not using any mission specific equipment	1.1.2	Not using any mission specific (design) software
1.1.3	Mission not re-usable at end of mission life, mission can be altered however		
1.2.1	Level of self diagnostic is low		
1.3.1	Payload level is very high, bus lower however	1.3.2	Up to a week of inputless operation
1.3.3	Payload completely autonomous	1.3.4	Fully autonomous, expect in emergency situations
1.3.5	Besides common faults, needs ground station input	1.3.6	N/A
1.4.1	Very good due to high usage of AI	1.4.2	Good, due to low amount of computation to be solved
1.4.3	High resource allocation due to AI, but average for similar missions		
1.5.1	The usage of solar panels makes it so that less on board batteries are required		
1.6.1	The radiation never exceeds any of the components their maximum tolerance value	1.6.2	All the components are created for space and can therefor withstand the vacuum space environment
1.6.3	Due to the very low earth orbit collisions are very unlikely	1.6.4	Due to the very low earth orbit collisions are very unlikely
1.6.5	This is considered in the structures section, however not very much in depth	1.6.6	The propulsion system is capable of counteracting the atmospheric drag.
1.6.7	Not all solutions for the space environment go fully in depth.		
1.7.1	Incorporation of sustainability considerations throughout design	1.7.2	Power consumption has played a significant role in almost all trade-offs.
1.7.3	AI usage leads to great optimization measures	1.7.4	Extensive Safe Mode protocols ensure complete failure measures
1.7.5	A very general testing strategy has been set up	1.7.6	Some system still contain single point failure possibilities (such as the camera). However, these systems are very unlikely to fail.
1.8.1	High for similar types of missions (propulsion system is constantly firing)	1.8.2	Mission lifetime extended to 2 years
1.8.3	Low amount of propellant needed, but propellant is not the greenest		

2.1.1	All data will be available to paying costumers	2.1.2	Published through university
2.2.1	No LEDS used	2.2.2	None
2.2.3	All available		
3.1.1	The satellite has no collision avoidance		
3.2.1	An EOL strategy has been created		
3.3.1	TBD		
3.4.1	Satellite is burned up on re-entry	3.4.2	TBD
4.1.1	Radiofrequency so not good	4.1.2	Usage of UHF & S , extremely popular
4.1.3	only 0.3 so very good		
4.2.1	Small solar panels	4.2.2	black paint on body
4.2.3	No significant other sources of light pollution		
4.3.1	no constellation		
5.1.1	Environmental Mission	5.1.2	Energy producers can be checked by government
5.1.3	Can help safe customers money while doing good for environment		
5.2.1	Incorporated into design from start of design phase		
6.1.1	AI reduces need for extensive ground segment	6.1.2	Usage of ground segment provider very sustainable
6.1.3	TBD	6.1.4	All operations from university
7.1.1	TBD	7.1.2	Due to the use of aluminium the energy intensity is pretty high
7.1.3	Usage of dutch energy grid	7.1.4	TBD
7.1.5	TBD	7.1.6	TBD
7.1.7	TBD	7.1.8	Design & manufacturing locations are space efficient
7.2.1	TBD	7.2.2	TBD
7.2.3	TBD	7.2.4	TBD
7.2.5	TBD	7.2.6	TBD
8.1.1	All regulations followed	8.1.2	All regulations followed
8.1.3	All regulations followed		
9.1.1	Experience from university missions	9.1.2	Experience from university missions
9.1.3	In-house experience, but new challenges present due to inclusion of AI	9.1.4	Regular energy consumption for small mission
10.1.1	Launch used for multiple missions, mission is rather large however	10.1.2	TBD
10.1.3	TBD		

17.6. Verification & Validation of ELSSI

Validation of an indicator such as ELSSI can be quite difficult. Luckily, ELSSI is just an indicator and a way of giving a number of sustainability to a design. As it is only an indicator, and only gives an indication of the level of sustainability, it is not a critical tool used in the design of the satellite. This not not mean the model does not need to be verified and validated however. To verify and validate the ELSSI, many experts have been contacted. With these experts the model was discussed, including the different categories, their weights, and the execution. Through the feedback received from these experts the indicator has evolved. Categories have been added and categories have been removed. Through their help, the ELSSI has been created to be as inclusive as possible. As mentioned before, other missions have also been analysed using the ELSSI. This was also done to verify and validate the indicator. Inputting a mission of which one knows is less sustainable should yield a lower ELSSI score. Fortunately, this was also the case, verifying (to a certain extend) the indicator. The verification and validation efforts needed to fully verify and validate the indicator extend the time span provided in this DSE. However, for this particular use-case, it has been verified and validated enough.

17.7. Sustainability conclusion

From the start of the design phase, it was vital for SigmaSat to ensure this mission is as sustainable as possible. Especially today, creating sustainable products is as important as ever. Sustainability is a very difficult concept to judge quantitatively, however to properly analyse the level of sustainability of a mission, a quantitative approach is required. To quantitatively analyze sustainability, SigmaSat made use of the ELSSI. The ELSSI is an easy to use indicator that determines the level of sustainability in a satellite mission. The indicator is comprised of a variety of categories, sub-indicators and criteria that need to be filled in. Each of these categories and sub-indicators have a weight attached to them and are judged on a scale of 1-5, with 1 corresponding to ”Very Bad” and 5 to ”Very Good”. This indicator was developed in corporation with experts in the field. SigmaSat has made use of this indicator throughout the design phase, ensuring a sustainability immersion throughout the design. Incorporating ELSSI also allowed sustainability evaluations throughout the process of the design rather than at the end when making changes is more difficult. At the end of the design phase, the satellite was once again subjected to the ELSII and given a final score. This score is 4.05, which is a very good result and ensures that SigmaSat can call its mission sustainable.

18 Risk

The following chapter will outline the technical risks including the rationale of their management.

18.1. Management

The technical risks of this project are very specific to each concept. Nevertheless, each subsystem can face general risks based on its functionality. These risks will be labelled with an identifier of the following code: RK-xx with the first spacer denoting TR as technical risk. The second spacer will mark the risks with a number. Each risk as to be deduced from the threats of the SWOT analysis will be assigned a probability and severity with its risk resulting from their multiplication, using the following criteria:

Table 18.1: Constants calculated from stationary measurements, compared to provided data.

Probability	Technical Risks
1	Everyday mission occurrence
2	Every-week mission occurrence
3	Every-month mission occurrence
4	Every-year mission occurrence
5	One time mission occurrence

Severity	Technical Risks
1: Negligible	Inconvenience or non-operational impact
2: Marginal	Degradation of secondary mission or small reduction in technical performance
3: Critical	Mission success is questionable or some reduction in technical performance
4: Catastrophic	Mission failure or significant non-achievement of performance

Code	Mitigation Strategy
SF	Using a safety factor when designing or planning
MIS	Have multiple independent systems
AR	Accept risk

Table 18.2: SWOT Analysis

	Helpful	Harmful
Internal	No limit to launcher cost CubeSats are widely used and have a lot of documentation	300-450km orbit so orbit maintenance is needed Limited power available Not a lot of space for the payload
External	AI in space is novel and innovative Low orbit allows for high revisit time CubeSat are good for niche uses	AI in space is an untested technology

In Table 18.3 the mitigated risks are marked with brackets.

Table 18.3: Risks

Code	Description	Result	Probability	Severity	Risk	Mitigation Strategy
RK-01	Failure of structure during launch	Satellite is lost	2(1)	4	8(4)	SF
RK-02	Failure of structure in orbit	Satellite is lost	2(1)	4	8(4)	SF
RK-03	Manufacturing delays	Delay in mission timeline, miss launch window	3	3(2)	9(6)	SF
RK-04	Assembly delays	Delay in mission timeline, miss launch window	3	3(2)	9(6)	SF
RK-05	Material defects	Material is sent back and ordered again or from another supplier	2	2(1)	4(2)	SF
RK-06	Production defects	Part is remade	2	2(1)	4(2)	SF
RK-07	Loss of contact	Possible loss of mission	1	4(2)	4	MIS
RK-08	Environmental Degradation Hardware Components	Possible loss of mission	2(1)	1	2(1)	MIS
RK-09	Obsolescence Hardware components	Possible loss of mission	1	2(1)	2(1)	MIS
RK-10	Obsolescence Software components	Possible loss of mission	1	2(1)	2(1)	MIS
RK-11	Power outage	Possible temporary loss of mission	2(1)	3(2)	6(2)	MIS
RK-12	Connection Loss of any of the subsystems	Possible loss of mission	1	4(3)	4(3)	MIS
RK-13	Cyberattack	Possible loss of mission	4	2(1)	8(4)	MIS
RK-14	Deployment switch does not start EPS initiation.	EPS does not turn on, the satellite is inoperable	1	4	4	AR
RK-15	EPS power lines disconnect from the bus.	The satellite bus is no longer operable	2	2	4	AR
RK-16	EPS power lines disconnect from the payload	The payload is no longer functionable	2	3	6	AR
RK-17	EPS data line to CHDS is compromised	The EPS cannot receive commands to go into other modes of operations.	2	3	6	AR
RK-18	Electrical power generation malfunctions	The satellite can no longer charge batteries and will have limited time before power off.	3	3(1)	9(3)	SF
RK-19	Electrical storage malfunctions	The satellite can no longer work without generating power	3	2	6	AR
RK-20	EPS cannot provide full power to all subsystems	The operations of the satellite will have to be adjusted, power will have to be allocated to critical systems	2	2	4	AR
RK-21	EPS current sensors malfunction	The EPS can no longer accurately distribute power safely to all subsystems.	2	2	4	AR

RK-22	The EPS overheats	The EPS internal resistance increases and potentially compromises components on the PCDs.	2	1	2	AR
RK-23	Insufficient/wrongly fastening OBC onto databoard	Loss of connection, no way to communicate or do other functions of the CDHS	1	4	4	AR
RK-24	Wires or connections getting loose	Possible loss of systems	1	4	4	AR
RK-25	Short circuit of the connections of the databoard/harness	Possible loss of systems	2	3	6	AR
RK-26	Deadlocks in software	A loop in the obc, the obc reboots after a while if its watchdog reset does not reset after a certain period of time	2	2	4	AR
RK-27	Watchdog malfunction	Possible loop of restarting the OBC	1	4	4	AR
RK-28	Transceiver readouts are incorrectly converted	Formulas used to translate telemetry to actual understandable value malfunction and data can not be used	1	4	4	AR
RK-29	General fault in the code	Dependent on the place in the code	1	4	4	AR
RK-30	Latchups	Short circuiting of an integrated system typically occurring because of heavy ions or protons from cosmic rays or solar flares	1	4	4	AR
RK-31	Single Event Upsets or Single Event Effects	Soft error, not considered permanently damaging	2	2	4	AR
RK-32	Transmission replay attack	Hacker attack, loss of communication	1	3	3	AR
RK-33	Unauthorized transmission	Hacker attack, system lockup	1	3	3	AR
RK-34	Thermal sensors fail	Could overheat or under cool	1	4(2)	4(2)	MIS

18.1.1. Contingencies

Several contingencies are considered in the event that a risk actualises, in the event of a partial failure of the satellite new operational modes will be considered such that the SC may still be used. In the event of a full failure of the SC the SC will be tracked and its trajectory predicted so that proper measures can be taken to avoid the SC re-entering the atmosphere and causing harm to anyone.

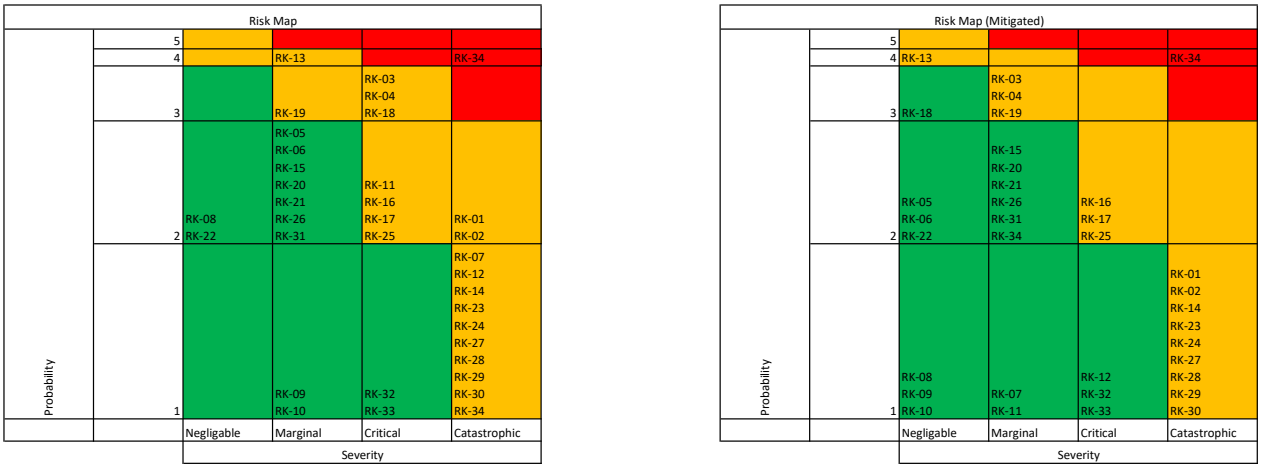

Figure 18.1: Risk maps.

19 Cost Analysis

Top level requirements requires the total cost of the mission not to exceed 5 million euros (excluding the launch). This means creating a detailed cost breakdown analysing the costs made from the start of the design until the end of the mission. The costs have been divided up into three categories, materials/parts, man-hours and MISC. These categories have then been divided into subsystems to ease the analysis. Due to the great amount of uncertainties present at this phase of the design, costs are mentioned either in full costs or ranges of costs. Table Figure 19.1 identifies all costs for materials and parts necessary for this mission. The total material/parts costs mount up to a range of €1,100,400 to €1,160,000, where the most expensive subsystems are payload and propulsion. The expensive items in these subsystems are the off-the-shelf crucial components such as the hyperspectral imager and propulsion unit. The subsystem cost proportion can be shown in Figure Figure 19.4. This figure identifies the great disparities between subsystem costs. From a cost point of view only propulsion, payload and ADCS are truly significant. This means that if savings are necessary at any further stage in the design, these would be the first subsystems to be looked at.

The costs related to the man-hours are presented in Table Figure 19.2. Due to the extensive amount of testing and integrating left the costs for the man-hour add up to be more than those of the materials/parts. The man-hours will cost between €1,616,000 and €1,749,000. These costs are subject to change as further development might lead to a better picture of the remaining work necessary. To calculate the man-hour costs, a hourly rate of €150 is assumed, which is an appropriate amount for this type of mission.The most expensive category within the man-hours costs is the systems engineering category. This is mainly due to the fact that the DSE hours are added to this category.

The last category is the MISC category, as shown in Table Figure 19.3. This category, as of now, is only composed out of two costs. The first is the rent for the propulsion testing facility. The second is the premium that has to be paid to use satellite data for training the AI. Both of these costs have wide ranges due to many uncertainties still present at this design phase. Added up, the cost range for the MISC category is: €50,000 to €315,000.

A cost breakdown ahs also been presented in tree form. To create this figure, averages of ranges are taken. The red symbol present at some of the ground station costs indicate operational costs rather than one-time costs. As visible from this breakdown, there are very few running costs. Most of the incurred costs are capital expenditures. SigmaSat was able to reduce operational costs by opting for a ground station service provider. Through this service any maintenance cost would be avoided. Similarly, there would be no employees that need to be paid to run the ground station. The only running cost left would be incidental data monitoring. Of course, if SigmaSat will opt for a data platform to communicate the data with to customers, the operational costs would increase to also cover for the database and platform.

Overall the mission is projected to cost from €2,766,000 to €3,224,000. The average of this range equals €2,955,000 and gives a good indication of the overall mission cost. The projected total mission cost is far below the requirement of €5 million, and therefore allows room unexpected costs. Especially at this stage of the design the accuracy of the cost breakdown is not high. There are still a lot of uncertainties when it comes to man-hour calculations and unexpected costs that fall within the MISC category. This is also visible by the range of €458,100, which is roughly 15% of the total mission cost. It should be noted that any possible income is not mentioned in this section and report. This is out of the scope of this DSE exercise and requires more market and mission information to determine.

Table 19.1: Total Mission Costs

Total Mission Costs			
	Low Estimate	Avg Estimate	High Estimate
Material Parts	**€ 1,100,400.00**	**€ 1,130,350.00**	**€ 1,160,300.00**
Manhours	**€ 1,615,800.00**	**€ 1,682,400.00**	**€ 1,749,000.00**
MISC	**€ 50,000.00**	**€ 182,500.00**	**€ 315,000.00**
Total	**€ 2,766,200.00**	**€ 2,995,250.00**	**€ 3,224,300.00**

Material/Parts						
Subsystem	Part	Cost	OR	Cost from		Cost to
Payload		€ 328,000.00		0		0
	2 * Chameleon Imager	€ 288,000.00				
	CogniSat	€ 20,000.00				
	CVAI Toolkit Licence	€ 20,000.00				
Communications		€ 27,650.00		0		0
	DP-CRF-5615 S-Band Transmitter	€ 10,000.00				
	CubeSat S-band patch antenna	€ 2,150.00				
	NanoCom AX100	€ 8,000.00				
	ISIS Deployable Antenna System for 6U/12U CubeSats	€ 7,500.00				
ADCS		€ 161,850.00		0		0
	Hyperion T. IU	€ 150,000.00				
	Hyperion T. GPSR	€ 10,000.00				
	ISISPACE GPSA	€ 1,850.00				
EPS		€ 40,000.00	€	28,000.00	€	56,000.00
	NanoPower P110 x32	€ 40,000.00				
	NanoAvionics EPS 2S7P Configuration		€	28,000.00	€	56,000.00
GS		€ 0.00		€ 13,000.00		€ 43,500.00
	Cost Antenna coverage Ground Station Service Provider			€ 13,000.00		€ 43,500.00
Propulsion		€ 450,000.00		0		0
	Entire unit (ROM) x3	€ 450,000.00				
CDHS		€ 43,000.00		0		0
	Antelope (OBC+DPU)	€ 19,000.00				
	Oryx(software)	€ 11,000.00				
	Oasis(ground software)	€ 3,000.00				
	The Herd(Algorithms)	€ 10,000.00				
Structures		€ 8,100.00		0		0
	Aluminium Sheets	€ 500.00				
	Aluminium L-Beams	€ 600.00				
	Solar Panel Tilt Motor	€ 2,000.00				
	Torsion Springs	€ 300.00				
	Hinges	€ 1,000.00				
	Mounting Jig	€ 3,000.00				
	Bolts	€ 300.00				
	Silicone shielding	€ 400.00				
Thermal Control		€ 0.00	€	800.00	€	2,200.00
	20 temp sensors		€	100.00	€	400.00
	Epoxy black paint		€	200.00	€	800.00
	MLI		€	500.00	€	1,000.00
		€ 1,058,600.00	**+**	**€ 41,800.00**		**€ 101,700.00**

Figure 19.1: Material/Parts Costs

Man-hours								
Subsystem/Department	Task/Description	Hours	Cost	OR	Hours from	Hours to	Cost from	Cost to
Systems Engineering			**€ 600,000.00**				**€ 0.00**	**€ 0.00**
	Fulfilled DSE Hours	4000	€ 600,000.00					
	Integration testing	100	€ 15,000.00					
Payload			**€ 18,000.00**				**€ 6,300.00**	**€ 37,500.00**
	Algorithm Training				2	50	€ 300.00	€ 7,500.00
	Payload Testing				40	200	€ 6,000.00	€ 30,000.00
	Writing algorithms	40	€ 6,000.00					
	Algorithm Testing	40	€ 6,000.00					
	Processor testing	40	€ 6,000.00					
Communications			**€ 180,000.00**				**€ 0.00**	**€ 0.00**
	COMMS Integration	200	€ 30,000.00					
	COMMS Testing	400	€ 60,000.00					
	COMMS Qualification	600	€ 90,000.00					
ADCS			**€ 112,500.00**				**€ 0.00**	**€ 0.00**
	GPS Integration	50	€ 7,500.00					
	Assembly	100	€ 15,000.00					
	Qualification	600	€ 90,000.00					
EPS			**€ 165,000.00**				**€ 0.00**	**€ 0.00**
	EPS Integration	100	€ 15,000.00					
	COMMS Testing	400	€ 60,000.00					
	EPS Qualification	600	€ 90,000.00					
GS			**€ 75,000.00**				**€ 0.00**	**€ 0.00**
	Seeting up contracts & data streams	100	€ 15,000.00					
	Data Monitoring	400	€ 60,000.00					
Propulsion			**€ 0.00**				**€ 12,000.00**	**€ 30,000.00**
	Proto flight test model				80	200	€ 12,000.00	€ 30,000.00
Astodynamics			**€ 0.00**				**€ 15,000.00**	**€ 45,000.00**
	Validation time				100	300	€ 15,000.00	€ 45,000.00
CDHS			**€ 105,000.00**				**€ 0.00**	**€ 0.00**
	Antelope (OBC+DPU)	100	€ 15,000.00					
	Oryx(software)	200	€ 30,000.00					
	Oasis(ground software)	100	€ 15,000.00					
	The Herd(Algorithms)	300	€ 45,000.00					
Structures			**€ 165,000.00**				**€ 0.00**	**€ 0.00**
	Machining	100	€ 15,000.00					
	Design	400	€ 60,000.00					
	Assembily	100	€ 15,000.00					
	Quality Control	300	€ 45,000.00					
	Launch Preparations	200	€ 30,000.00					
Thermal Control			**€ 66,000.00**				**€ 96,000.00**	**€ 150,000.00**
	Testing				640	1000	€ 96,000.00	€ 150,000.00
	Detailed analysis	320	€ 48,000.00					
	Verification of model	120	€ 18,000.00					
		10010	**€ 1,486,500.00**	**+**	**862**	**1750**	**€ 129,300.00**	**€ 262,500.00**

Figure 19.2: Man-hour Costs

MISC				
Description	Cost	OR	Cost from	Cost to
Propulsion testing facility			€ 40,000.00	€ 100,000.00
Access to satellite orbital data			€ 10,000.00	€ 215,000.00
	€ 0.00	**+**	**€ 50,000.00**	**€ 315,000.00**

Figure 19.3: MISC Costs

Figure 19.4: Materials/Parts Cost Breakdown

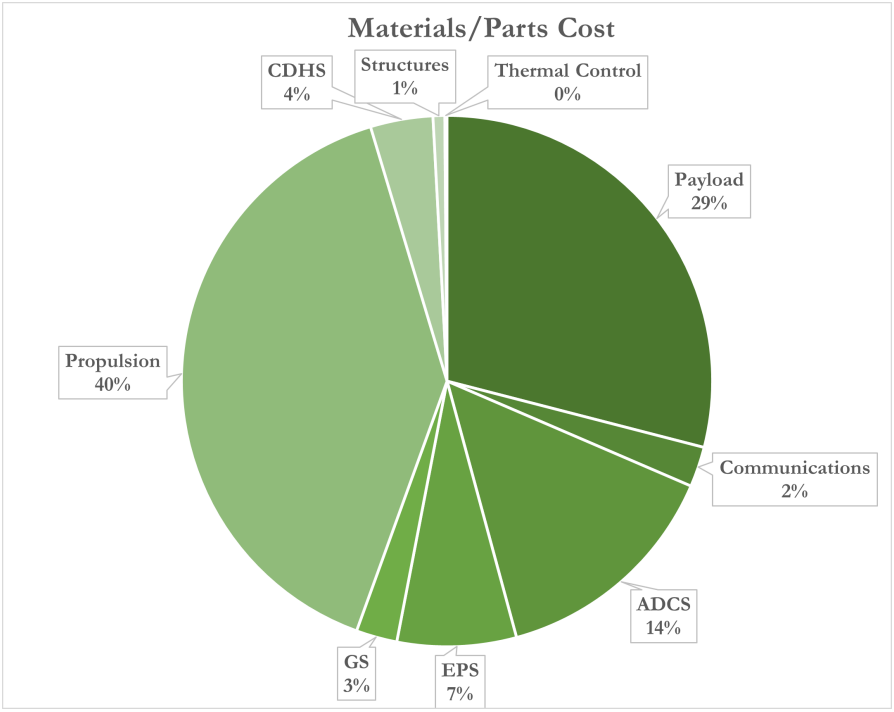

Figure 19.5: Man-hour Cost Breakdown

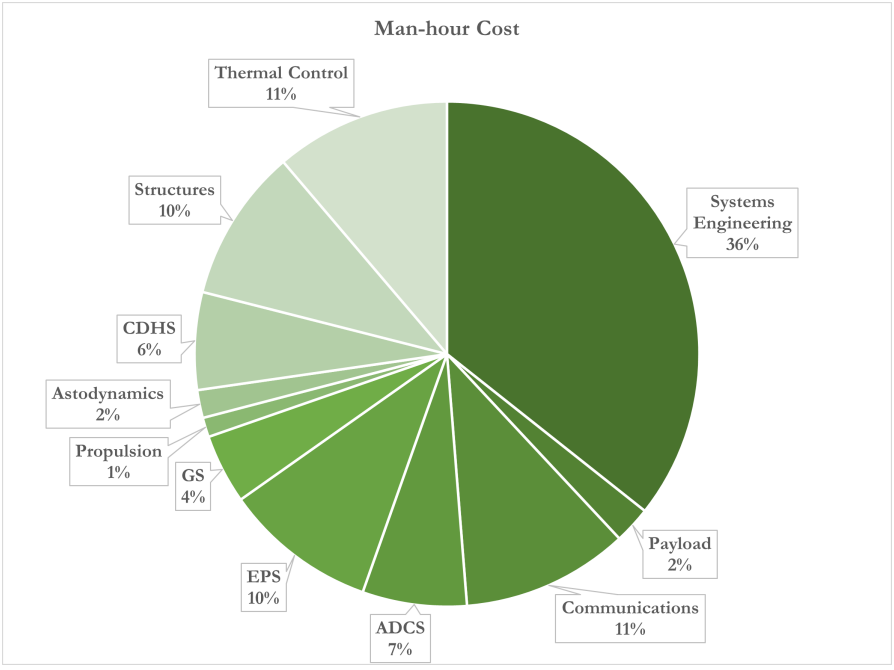

- Total Mission Cost — €2,995,250
  - Materials/Parts — €1,130,350
    - Payload — €328,000
      - Chameleon Imager x2 — €288,000
      - CogniSat — €20,000
      - CVAT Toolkit Licence — €20,000
    - Communications — €27,650
      - DP-CRF-5615 S-Band — €10,000
      - S-Band Patch Antenna — €2,150
      - NanoCom AX100 — €8,000
      - ISIS Deployable Antenna — €7,500
    - ADCS — €161,850
      - Hyperion T. IU — €150,000
      - Hyperion T. GPSR — €10,000
      - ISIS GPSA — €1,850
    - EPS — €82,000
      - NanoPower P110 x32 — €40,000
      - NanoAvionics EPS 2S7P — €42,000
    - Ground Segment — €28,250
      - KSAT GSaaS — €28,250
    - Propulsion — €450,000
      - ROM Unit x3 — €450,000
    - CDHS — €43,000
      - Antelope — €19,000
      - Oryx — €11,000
      - Oasis — €3,000
      - The Herd — €10,000
    - Structures — €8,100
      - Aluminium Sheets — €500
      - Aluminium L-Beams — €600
      - Solar Panel Tilt Motor — €2,000
      - Torsion Springs — €300
      - Hinges — €1,000
      - Mounting Jig — €3,000
      - Bolts — €300
      - Silicone Shielding — €400
    - Thermal Control — €1,500
      - Temperature Sensors x20 — €250
      - Epoxy Black Paint — €500
      - MLI — €750
  - Man-hours — €1,682,400
    - Systems Engineering — €600,000
      - DSE Hours — €600,000 [4000hrs]
      - Integration Testing — €15,000 [100hrs]
    - Payload — €39,900
      - Alogorithm Training — €3,900 [26hrs]
      - Payload Testing — €18,000 [120hrs]
      - Writing Algorithms — €6,000 [40hrs]
      - Algoritm Testing — €6,000 [40hrs]
      - Processor Testing — €6,000 [40hrs]
    - Communications — €180,000
      - Integration — €30,000 [200hrs]
      - Testing — €60,000 [400hrs]
      - Qualification — €90,000 [600hrs]
    - ADCS — €112,500
      - GPS Integration — €7,500 [50hrs]
      - Assembly — €15,000 [100hrs]
      - Qualification — €90,000 [600]
    - EPS — €82,000
      - EPS Integration — €15,000 [100hrs]
      - COMMS Testing — €60,000 [400hrs]
      - EPS Qualification — €90,000 [600]
    - Propulsion — €21,000
      - Testing — €21,000 [140hrs]
    - Astrodynamics — €30,000
      - Validation — €30,000 [200hrs]
    - CDHS — €105,000
      - Antelope — €15,000 [100hrs]
      - Oryx — €30,000 [200hrs]
      - Oasis — €15,000 [100hrs]
      - The Herd — €45,000 [300]
    - Structures — €165,000
      - Machining — €15,000 [100hrs]
      - Design — €60,000 [400hrs]
      - Assembly — €15,000 [100hrs]
      - Quality Control — €45,000 [300hrs]
      - Launch Preparations — €30,000 [200hrs]
    - Thermal Control — €189,000
      - Testing — €123,000 [820hrs]
      - Detailed Analysis — €48,000 [320hrs]
      - Verification of Model — €18,000 [120hrs]
    - Ground Segment — €75,000
      - Data Streams Set Up — €15,000 [100hrs]
      - Data Monitoring — €60,000 [400hrs]
  - MISC — €182,500
    - Propulsion Testing Facility — €70,000
    - Satellite Data — €112,500

20 Post-DSE Project Planning

Upon the DSE finishing, there will be further steps necessary to bring the satellite into space. To evaluate the steps that are necessary up until launch (Gillette & Varga, 1970) was consulted. The launch date was set for 01.01.2025, since the astrodynamics department chose that date for launch, but the project can be extended up until the end of that year to comply with the requirement of launching no later than 2025. The DSE can be seen as the preliminary design phase and further phases are taken from the reference. A preliminary Gantt chart can be seen in Figure 20.1 and the respective project design & development logic graph can be found on the next page.

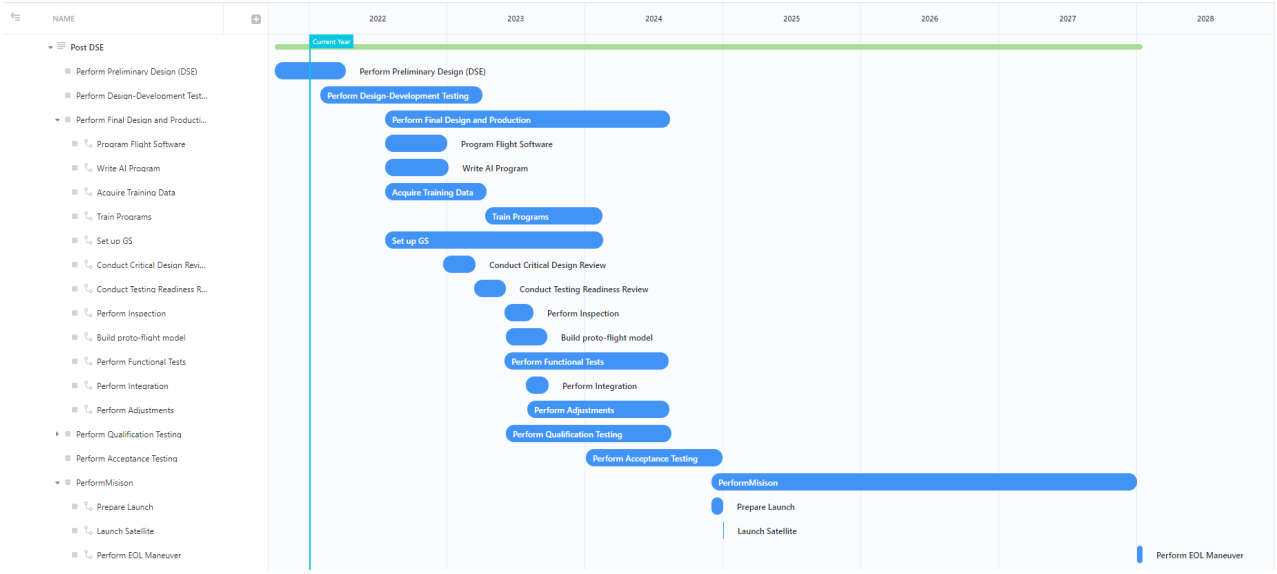

Figure 20.1: Project Gantt Chart

Test-program Phases

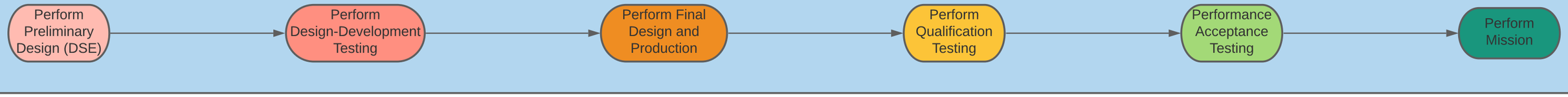

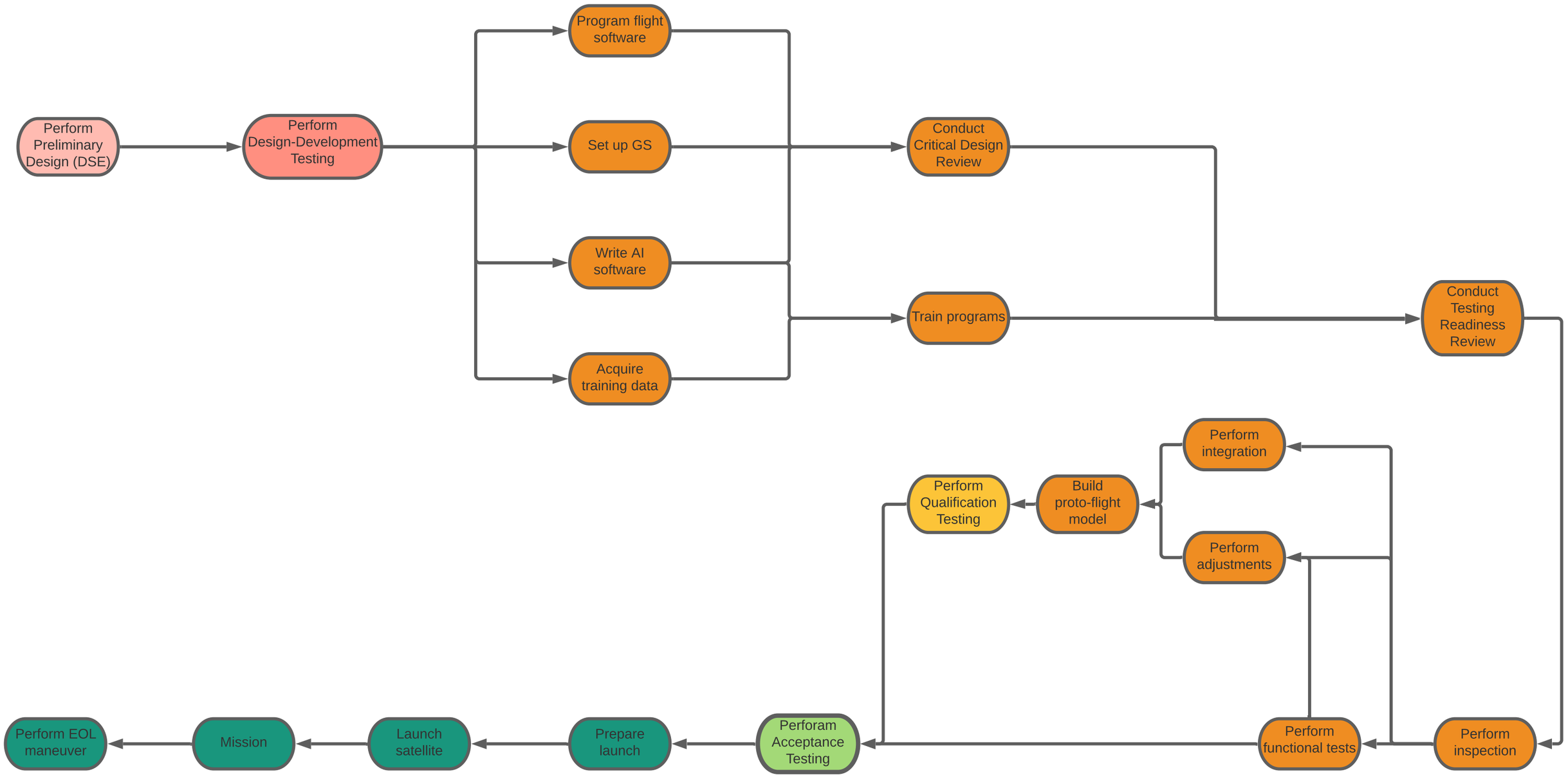

21 Conclusion

The aim of this report was to present the detailed design for the satellite as well as the respective approach towards it. Additionally, a market and functional analysis were presented. The sustainability of the different aspects of the project were evaluated followed by a risk and cost analysis. Finally, the project planning after this DSE are outlined summarizing future prospects of each subsystem within the respective chapter. This report is based on prerequisite work presented in the Baseline Report (Canosa et al., 2021a) and Midterm Report (Canosa et al., 2021a).

Based on the mission, being 'To demonstrate the latest advance in Artificial Intelligence with an Earth Observation CubeSat mission', a thorough market analysis was administered. The analysis defined the niché the project would be situated in for the inspection of methane leaks. Different mission guidelines were established that would guide the requirements on the hyperspectral instrument and the subsequent design.
Then the functional analysis was performed by utilising the FBS and FDD which was followed by the description of the modes of operations.
With this foundation set, the detailed design of the satellite can be established: the payload used the Chameleon camera to obtain hyperspectral data. This data will be pre-processed in order to reduce the noise. After this step clouded scenes will be filtered and the data is ready for the AI that will recognize methane and carbon dioxide leaks. For this the Myriad 2 will be used as processor allowing for a quick and low power consuming processing
In contrast to the preliminary design a new obit was chosen as the old orbit was not feasible from market analysis; it would have been required for the satellite to pass by more often. The new orbit is earth repeat and sun-synchronous at very low earth orbit (VLEO). The delta-V was calculated for orbit maintenance, serving as an input to propulsion. The satellite will de-orbit naturally if propulsion runs out as EOL maneuver. The first recommendation in case of more time, the RAAN can be optimized.
The propulsion system was initially deemed not necessary at the preliminary design phase, but due to new orbit, it was re-entertained. The new propulsion system had to be electric since it has to fire constantly to compensate for drag. Enpulsion NANO was selected after a trade-off as it can compensate for drag and is the most efficient for the mission. HPGP was deemed infeasible and also "less green" since the thrust is too high and it uses almost 24 times as much propellant.
For the ground station, a ground segment provider was chosen to allow access to ground stations all over the earth at a fraction of the cost of building and manning a ground station (cost range: EUR 13,025 to EUR 43,417). The chosen ground station provider is KSAT, using their ground stations in Troll and Svalbard. A fugitive emissions database and platform have been explored to overcome complications present in data streams today. Additionally, a possible revenue model has been discussed for the proposed database and platform.
The communications system is separated into two systems, one for TT&C (tracking, telemetry, and control) in UHF and one for the payload data in S-Band. Reason for this is the following; firstly, UHF antennas are omni-directional and highly reliable which is translated into a practical sense to the possibility of not sending down a lot of data for TT&C; secondly, the S-Band was chosen for comms because a higher data rate is needed. From this the link budget for both of the comms systems to enable contact was determined, of which a very high and stable link is attained as the ground stations was chosen to have excellent gain.
For the selection of the OBC over 20 possible On Board Computers were compared and 5 potential candidates were selected based on applicability of AI algorithms on the subsystem. From here, a more in depth analyses has been performed with the help of experts. The Antelope by KP Labs was found to be the best choice, and together with the additional services provided by KP labs and the Payload Processor from Ubotica, a CDHS integrated setup has been created. The six different implementations for AI on the CDH system have been analysed and elaborated upon. Through a more in-depth analysis of the compatible electrical interfaces a block diagram has been created that shows the connections between all subsystems of the satellite.
For the design of the Electrical Power system the modes of operation were used to determine the busiest orbit, the power required during the eclipse and the sunlit period. This enabled the sizing of the solar panels using the time spent in the sun, and the battery size from the time spent in eclipse. As the satellite is in a sun-synchronous orbit, one degree of freedom on the solar panels was applied to provide a maximum power

generation throughout the charge cycle. The final solar array size is 8x2U or 4x2U on both sides. Due to the large solar power input, the batteries are increased in size to accommodate for the required capacity which is more than originally estimated.
The ADCS was analysed and the Hyperion Technologies iADCS400-50 was chosen, with attitude determination and control accuracies of 30 and 360 arcseconds respectively and high specific maximum torque and momentum storage capacity. Its lack of an integrated ADCS receiver prompted a similar search and trade-off, resulting in the choice for the Hyperion Technologies GNSS200 GPS receiver and the ISISPACE ISIS-GAPA-DSH-0001 antenna. Integration of the GPS receiver and antenna into the iADCS400-50 was discussed with Hyperion Technologies representatives and positively assessed. The choice for an integrated ADCS unit, and for the integration of the GPS receiver and antenna in it offloads significant design, integration and testing effort to a company with extensive expertise and facilities, increasing the reliability of the final assembly and reducing engineering and logistics costs for the mission. Target acquisition algorithm was discussed afterwards. Thanks to the on-board controller of the iADCS400-50 and the target acquisition algorithm, SigmaSat is capable of independently identifying, planning and executing all possible target acquisition manoeuvres, in each and every orbit, enabling it to fulfill its Earth observation mission.
The structure of a CubeSat was designed to be 2x2x2U using an OTS solution. THis was deemed not possible considering the fundamentally different design of the satellite. A CAD model was set up to aid the analysis. From the final CAD of the spacecraft it was found that the is a 2U column in the structure that is empty, although this is not necessarily a drawback it does mean that the spacecraft could be changed into a 6U satellite or more components could be added to improve the mission. For the continuation of the project, the integration is a vital part of a more detailed design of the structure. As the possibility of designing an own structure, the continuation must focus on the finite element analysis, topology optimization and coating and material finish.
The design of the thermal control system comprises of 2 main analyses: a single and multi-node thermal model. Due to the stringent power budget, all active systems were disregarded for the detailed design. Within the passive systems, the focal point was directed to surface finishes and coatings. With a thermal model developed in ESATAN, several radiative cases were analysed. However, due to time constraint and licensing issues, the boundary conditions stemming from the power dissipation of the subsystems were unable to be included in the runned analyses. Instead a smaller evaluation of the highest resulting temperature from the components' dissipating heat was performed yielding the necessity for insulation. From this, a black epoxy paint was chosen for the side panels of the satellite while a trade-off on different OTS MLI options was executed. For future work, the inclusion of the components in the ESATAN thermal case is important while applying the chosen clean MLI by RUAG.

For each component, the reliability, availability, maintainability, and safety was analysed, as well as the verification and validation. Additionally, a plan for the full satellite verification was outlined, where the test approach at later stages of the project is described.
To quantitatively analyze sustainability, SigmaSat made use of the ELSSI. SigmaSat has made use of this indicator throughout the design phase, ensuring a sustainability immersion throughout the design. Incorporating ELSSI also allowed sustainability evaluations throughout the process of the design rather than at the end when making changes is more difficult. At the end of the design phase, the satellite was once again subjected to the ELSII and given a final score. This score is 4.05, which is a very good result and ensures that SigmaSat can call its mission sustainable.
Lastly, the project planning for the continuation of SigmaSat is outlined using a project gantt chart and the project design and development logic. Main recommendations to be highlighted for the continuation of the project are the following: the analytical tools used in this report will need to be refined and expanded upon optimizing properties such as the RAAN, the revaluation of possible constellations, testing for the bandwidth of the hyperspectral camera. Furthermore, more extensive verification and validation is required, for which extensive testing, amongst others, development testing, will be performed.

21 Bibliography

Anomaly detection. (2022). http://www.profitana.cz/en/anomaly-detection/

Arechiga, A. P., Michaels, A. J., & Black, J. T. (2018). Onboard image processing for small satellites. *NAECON 2018 - IEEE National Aerospace and Electronics Conference*. https://doi.org/10.1109/naecon.2018.8556744

Auch, T. (2017). Tracking global oil refineries and their emissions: Fractracker. https://www.fractracker.org/2017/12/global-oil-refineries-emissions/

Baumann, R., & Kruckmeyer, K. (2013). *Radiation handbook for electronics*. Texas Instruments.

Bock, D., Rößler, F., Kößling, M., & Tajmar, M. (2014). Development and testing of a cubesat with highly miniaturised feep thrusters on a thrust balance with sub-nanonewton resolution.

Boley, A. C., & Byers, M. (2021). Satellite mega-constellations create risks in low earth orbit, the atmosphere and on earth. *Scientific Reports*, *11*(1). https://doi.org/10.1038/s41598-021-89909-7

Bouwmeester, J. (2017). Testing of an optimised data bus for pico- and nanosatellites.

Braeunig, R. A. (2014). Atmospheric models. http://www.braeunig.us/space/atmmodel.htm

Can application programming interface. (2010).

Can bus explained - a simple intro. (2022). https://www.csselectronics.com/pages/can-bus-simple-intro-tutorial

Canosa, D., Janisch, K., Kalis, N., Lentschig, D., Lopez Rivera, A., Manieri, M., Regnery, K., & van der Wal, T. (2021a). Baseline report.

Canosa, D., Janisch, K., Kalis, N., Lentschig, D., Lopez Rivera, A., Manieri, M., Regnery, K., & van der Wal, T. (2021b). Midterm report.

Cappiello, A. (2019). Design, implementation, and analysis of electrical system architecture for cubesat to ground communications. https://doi.org/10.25777/w5cz-pa62

Cook, R., Swan, L., & Plucknett, K. (2020). Uart: A hardware communication protocol understanding universal asynchronous receiver/transmitter. *Batteries*, *54*(4).

Cook, R., Swan, L., & Plucknett, K. (2021). Impact of test conditions while screening lithium-ion batteries for capacity degradation in low earth orbit cubesat space applications. *Batteries*, *7*(1), 20. https://doi.org/10.3390/batteries7010020

Curtis, H. (2020). Spotlight: How to secure a license for your space mission ground segment, with leaf space. https://blog.satsearch.co/2020-07-30-how-to-secure-a-license-for-your-space-mission-ground-segment

Ehren, J. T. (2019). Energy analysis and orbit simulation of actuating cubesat solar arrays. *Honors Thesis*.

Enpulsion. (n.d.). Enpulsion nano. https://www.enpulsion.com/order/enpulsion-nano/

Enpulsion. (2018). Enpulsionnano data sheet.

ESA. (2008). Ecss: Space engineering; thermal control general requirements.

ESA. (2020). Newcomers earth observation guide. https://business.esa.int/newcomers-earth-observation-guide

Finch, M. J. (1986). Limited space: Allocating the geostationary orbit. *Northwestern Journal of International Law and Business*, *7*(4).

Fischer, K. W., Witiw, M. R., Baars, J. A., & Oke, T. R. (2004). Atmospheric laser communication new challenges for applied meteorology. *Bulletin of the American Meteorological Society*, *85*(5), 725–732. https://doi.org/10.1175/bams-85-5-725

Fletcher, R. (1987). *Practical methods of optimization* (Second). John Wiley & Sons.

Frenzel, L. (2012). Understanding solutions for the crowded electromagnetic frequency spectrum. https://www.electronicdesign.com/technologies/communications/article/21799723/understanding-solutions-for-the-crowded-electromagnetic-frequency-spectrum

Gillette, L., & Varga, R. (1970). Acceptance testing.

GlobalPetrolPrices. (2021). Methane prices around the world, 06-dec-2021. https://www.globalpetrolprices.com/methane_prices/

Guanter, L., Irakulis-Loitxate, I., Gorroño, J., Sánchez-García, E., Cusworth, D., Cogliati, S., & Colombo, R. (2021). Mapping methane point emissions with the prisma spaceborne imaging spectrometer. *Remote Sensing of Environment*. https://doi.org/10.31223/x5vc9c

Hamilton, I. A. (2020). The first satellite with ai onboard is now in orbit, and its tech could completely change how we respond to wildfires. https://www.businessinsider.com/intel-esa-launch-ai-satellite-phisat-1-2020-10?international=true&r=US&IR=T

Heikkinen, N. (2017). Epa revises the social cost of a potent greenhouse gas. *Sceintific American*.

Hughes, S. P., Qureshi, R. H., Cooley, D. S., & Parker, J. J. (n.d.). Aiaa technical conference. In T. G. Grubb (Ed.), *Nasa.gov*. NASA. https://ntrs.nasa.gov/api/citations/20140017798/downloads/20140017798.pdf

Hutchins, M. (2021). Ultrathin gallium-arsenide solar cell with light management architecture. https://www.pv-magazine.com/2021/10/06/ultrathin-gallium-arsenide-solar-cell-with-light-management-architecture/

Iadcs-400 [V2.1]. (2019). Hyperion Technologies, Berlin Space Technologies.

IEA. (2021). Methane tracker database. https://www.iea.org/articles/methane-tracker-database?utm_content=buffer28224&utm_medium=social&utm_source=linkedin-Birol&utm_campaign=buffer

Intelligence, M. (2020). Global satellite-based earth observation market: 2021 - 26: Industry share, size, growth - mordor intelligence. https://www.mordorintelligence.com/industry-reports/global-satellite-based-earth-observation-market-industry

Itu-r p.838-3. (2013).

Itu-r p.839-4. (2019).

J. Meseguer, A. S.-A., I. Pérez-Grande. (2012). *Spacecraft thermal control*. Woodhead Publishing.

Jacchia, L. G., & NASA. (1964). Standard jacchia reference atmosphere 1977. https://ccmc.gsfc.nasa.gov/modelweb/atmos/jacchia.html

Jervis, D., McKeever, J., Durak, B. O. A., Sloan, J. J., Gains, D., Varon, D. J., Ramier, A., Strupler, M., & Tarrant, E. (2021). The ghgsat-d imaging spectrometer. *Atmospheric Measurement Techniques*, *14*(3), 2127–2140. https://doi.org/10.5194/amt-14-2127-2021

Kocifaj, M., Kundracik, F., Barentine, J. C., & Bará, S. (2021). The proliferation of space objects is a rapidly increasing source of artificial night sky brightness. *Monthly Notices of the Royal Astronomical Society: Letters*, *504*(1). https://doi.org/10.1093/mnrasl/slab030

Kyle, M. (2022). Can bus explained - a simple intro. https://audiouniversityonline.com/twisted-pairs/

Ltd., I. E. U. (2017). Esatan-tms workbench user manual.

Mingle, J. (2019). Methane detectives: Can a wave of new technology slash natural gas leaks? *Yale School of the Environment*.

Miyakita, H. R., T., & H., S. (2015). Evaluation of thermal insulation performance of a new multi-layer insulation with non-interlayer-contact spacer.

M.M. Finckenor, R. C. (2014). Optical properties of nanosatellite hardware.

NASA. (n.d.). Thermal management systems. *Nasa technology roadmaps*.

NASA. (2021). Thermal control. In S. Weston (Ed.), *State-of-the-art small spacecraft technology*. NASA Ames Research Center, Small Spacecraft Systems Virtual Institute.

Noomen, R. (n.d.). Ae2230-i lecture 1: Kepler orbit, specialized orbit.

Noomen, R. (2022). Ae2-104: Eclipse, maneuvers.

Nuñez-Lopez, V., Gil-Egui, R., Hosseininoosheri, P., Hovorka, S. D., & Lake, L. W. (2019). Carbon life cycle analysis of co2-eor for net carbon negative oil (ncno) classification (final report). *U.S. Department of Energy*. https://doi.org/10.2172/1525864

Nwankwo, V. U. J., Jibiri, N. N., & Kio, M. T. (2020). The impact of space radiation environment on satellites operation in near-earth space. *Satellites Missions and Technologies for Geosciences*. https://doi.org/10.5772/intechopen.90115

Observations, K. R. S. (n.d.). http://www.tropomi.eu/

Oltrogge, D. L., & Leveque, K. (n.d.). An evaluation of cubesat orbital decay. https://digitalcommons.usu.edu/cgi/viewcontent.cgi?article=1144&context=smallsat

Panwar, R. (1999). https://www.sws.bom.gov.au/Category/Educational/Space%20Weather/Space%20Weather%20Effects/SatelliteOrbitalDecayCalculations.pdf

pwc. (2020). Market perspectives of ground segment as a service (gsaas. *International Astronautical Congress (IAC)*, *71*.

Regnery, K. S. C. N. A., & Manieri, M. (2021). Elaborate life cycle space sustainability indicator [Unpublished internal company document].

Rennert, K., Prest, B. c., Pizer, W. A., Newell, R. G., Anthoff, D., Kingdon, C., Rennels, L., Cooke, R., Raftery, A. E., Sevcikova, H., & et al. (2021). The social cost of carbon. *Brookings*.

Roddy, D. (2011). *Satellite communications*. McGraw-Hill.

RUAG. (2020). Thermal insulation products.

Scripts, M. T. (2019). Calculate distance, bearing and more between latitude/longitude points. https://www.movable-type.co.uk/scripts/latlong.html

Secretariat, E. (2019). Space engineering testing.

Sheldahl. (2020). *The red book*. Sheldahl.

Shell. (n.d.). Shell methane case study - shell global | shell global. https://www.shell.com/energy-and-innovation/natural-gas/methane-emissions/_jcr_content/par/textimage_438437728.stream/1587995196996/53beef2f8ba2e90560c074f56552e2acfe30582b/shell-methane-case-study.pdf

Space sustainability a practical guide. (n.d.).

Space sustainability rating. (n.d.). https://espace.epfl.ch/research/space-sustainability-rating/

Spaceworks. (2020). https://www.spaceworks.aero/nano-microsatellite-forecast-10th-edition-2020/

Thomas, J. W. (1998). Numerical partial differential equations.

Timmermans, R. (2021). Detecting methane leaks from space. https://www.groundstation.space/detecting-methane-leaks-from-space/?utm_source=rss&utm_medium=rss&utm_campaign=detecting-methane-leaks-from-space

UGCS. (n.d.). Detecting a methane leak faster and more safely. https://www.ugcs.com/news-entry/detecting-a-methane-leak-faster-and-more-safely

Varon, D. J., Jacob, D. J., Jervis, D., & McKeever, J. (2020). Quantifying time-averaged methane emissions from individual coal mine vents with ghgsat-d satellite observations. *Environmental Science amp; Technology*, *54*(16), 10246–10253. https://doi.org/10.1021/acs.est.0c01213

Vetter, J. R. (n.d.).

Virtanen, P., Gommers, R., Oliphant, T. E., Haberland, M., Reddy, T., Cournapeau, D., Burovski, E., Peterson, P., Weckesser, W., Bright, J., van der Walt, S. J., Brett, M., Wilson, J., Millman, K. J., Mayorov, N., Nelson, A. R. J., Jones, E., Kern, R., Larson, E., … SciPy 1.0 Contributors. (2020). SciPy 1.0: Fundamental Algorithms for Scientific Computing in Python. *Nature Methods*, *17*, 261–272. https://doi.org/10.1038/s41592-019-0686-2

Wertz, J. R., Everett, D. F., & Puschell, J. J. (2011). *Space mission engineering: The new smad*. Microcosm Press.

Yida. (2022). Uart vs i2c vs spi – communication protocols and uses. https://www.seeedstudio.com/blog/2019/09/25/uart-vs-i2c-vs-spi-communication-protocols-and-uses/?sfw=pass1643368069

Yongjian, N., Ke, X., Jianwei, W., Ling, W., & Mi, H. (2016). Block-based klt compression for multispectral images. https://doi.org/10.1142/S0219691316500296

Yost, B., & Weston, S. (2021).

*[title=References]

22 Appendix A: Scripts

```python
from math import pi, ceil

"""
Preliminary structure designer:
1. Set values
2. Define basic area and moment of inertia functions
3. Start with weakest structure with a set thickness and increase the flanges of
    the L-beam until the structure just does not fail

Area verification:
A_member                    - Verified using CATIA V5 to 3 s.f.
A_struct                    - Verified using CATIA V5 to 3 s.f.
Moment of inertia verification:
I_member                    - Verified using CATIA V5 to 3 s.f.
I_member_around_struct_np   - Verified using CATIA V5 to 3 s.f.
I_struct                    - Verified using CATIA V5 to 3 s.f.

Output:
Set thickness 1 d.p.
Flange length required 0 d.p.
"""

Launcher_Data = {"Vega_External": [[35, 90], [3.4, 5.75]]}
Material_Data = {"AL7075-T6": [70 * 10 ** 9, 3000, 120 * 10 ** 6]}
U = 0.1
# Length of the unclamped axis
L = 3 * U
# Shortest width of the clamped face
width = 1 * U
m = 10
SF = 3

# Launcher and Material choices
Launcher = "Vega_External"
Material = "AL7075-T6"


def check_required_properties(Launcher, SF = SF, m = m, L = L, Material = Material):
    I_f = ((((Launcher_Data[Launcher][0][0] * SF) / 0.56) ** 2) * m * L ** 3) /
    ↪  Material_Data[Material][0]
    A_f = ((((Launcher_Data[Launcher][0][1] * SF) / 0.25) ** 2) * m * L) /
    ↪  Material_Data[Material][0]
    I_Bu = ((Launcher_Data[Launcher][1][1] * 9.81 * SF * m) * (L * L) / pi ** 2) /
    ↪  Material_Data[Material][0]
    I_Be = (Launcher_Data[Launcher][1][0] * 9.81 * SF * m * L) * (width / 2) /
    ↪  Material_Data[Material][2]
    return I_f, A_f, I_Bu, I_Be


def A_member(a, t):
```

```
    return (2 * a - t) * t


def A_struct(a, t):
    return A_member(a, t) * 4


def I_member(a, t):
    return (1 / 3) * (t * ((t * (2 * (a - t) + a) + (a - t) ** 2) / (2 * (2 * a - t))) ** 3 + a * (
            a - ((t * (2 * (a - t) + a) + (a - t) ** 2) / (2 * (2 * a - t)))) ** 3 - (a - t) * (
                                a - ((t * (2 * (a - t) + a) + (a - t) ** 2) / (2 * (2 * a - t))) - t) ** 3)


def I_member_around_struct_np(a, t):
    return I_member(a, t) + (2 * a - t) * t * (width / 2) ** 2


def I_struct(a, t):
    return I_member_around_struct_np(a, t) * 4


I_f, A_f, I_Bu, I_Be = check_required_properties(Launcher)

t = 0.0015
Failed = True
a = 0.001
# Beam design
while Failed:
    # Check if structure has failed
    if I_Bu < I_member(a, t) and \
            I_f < I_struct(a, t) and \
            A_f < A_struct(a, t) and \
            (Launcher_Data[Launcher][1][1] * 9.81 * SF * m) / A_struct(a, t) < Material_Data[Material][2] and \
            I_Be < I_struct(a, t):
        Failed = False
        a_final = a
    # If it has failed, make the beams thicker
    a = a + 0.001
# Mass of the beams
mass = (2 * a_final - t) * t * L * Material_Data[Material][1] * 4
print("==========================")
print(f"Set thickness\t\t\t\t=\t{ceil(t * 10000) / 10} mm")
print(f"Flange length required\t\t=\t{ceil(a * 1000)} mm")
print("==========================")
```